Kinematic Behaviour of Cross Laminated Timber (CLT) Shearwalls with Openings

By

Mohammed MESTAR

Thesis submitted to the University of Ottawa

in partial Fulfillment of the requirements for the Doctorate in Philosophy degree

Department of Civil Engineering

Faculty of Engineering

University of Ottawa

BOARD OF EXAMINERS

THIS THESIS HAS BEEN EVALUATED

BY THE FOLLOWING BOARD OF EXAMINERS

Dr. Ghasan Doudak, supervisor of the thesis

Department of Civil Engineering at the University of Ottawa

Dr. Murat Saatcioglu, member of the jury

Department of Civil Engineering at the University of Ottawa

Dr. Elena Dragomirescu, member of the jury

Department of Civil Engineering at the University of Ottawa

Dr. Heng-Aik Khoo, external member of the jury

Department of Civil Engineering at Carleton University

Dr. Sam Salem, external member of the jury

Department of Civil Engineering at Lakehead University

THIS THESIS WAS PRESENTED

IN THE PRESENCE OF A BOARD OF THE EXAMINERS

July 16, 2020

AT UNIVERSITY OF OTTAWA

Abstract

An integrated experimental and numerical research program investigating the elastic and inelastic performance as well as the kinematic behaviour of shearwalls with openings is presented in this study. The influence of the geometrical dimensions of the wall configurations and the mechanical properties and configurations of hold-downs on both elastic and inelastic behaviours including the possible kinematic modes of the shearwalls are investigated. The research also proposes the concept of equivalent-frame-model applicable for shearwalls where openings are cut out from CLT panels. Are also presented, five racking tests performed on full scale CLT walls in order to validate the numerical models as well as the equivalent frame model.

From a review of the available literature emerges that for CLT shearwalls with openings, studies are not at the same level of abundance in research compared to walls without openings, due to the simple reason that SSW is generally a widespread technique. Thus, the kinematic behaviour and the coupling effect are inexistent and presented here.

The investigations of the wall's behaviour in the elastic and inelastic ranges demonstrate the important effect of the lintel and wall segment slenderness as well as the hold-down stiffness effect on the mechanical behaviour and the global kinematic behaviour as well. It is found that the kinematic modes can change when the walls are stressed beyond their elasticity limit. The failure mode and the global ductility are highly dependent on the hold-down configurations particularly for walls with door openings. The degree of coupling decrease with increased hold-down stiffness and the wall segment width.

With regard to the equivalent frame model, a reasonable fit is found between the proposed EFM and a detailed 2D area element model when the global elastic stiffness and tensile load in the hold-down were compared. The model is successfully validated through five full-scale tests on CLT shearwalls with door or window opening as well as two published studies on walls with door openings. The EFM is capable of predicting the behaviour in the wall with reasonable accuracy, especially for walls whose behaviour was dominated by the hold-down behaviour.

Acknowledgements

I would like to honestly thank my supervisor Ghasan Doudak for encouraging me during these past five years. He has been supportive and has given me the freedom for various projects without objection. I am thanking him for his insightful discussions about the research project. I especially appreciate his guidance and constant encouragement throughout this research.

Sincere thanks are also extended to Daniele Casagrande from CNR-IVALSA (Trento, Italy), who provided me technical advice and expertise. Daniele has been supportive to this project well beyond his obligation. Again, I am thanking him for his availability during this project.

I would like to thank sincerely Giovanna Bochicchio, manager of the CNR-IVALSA Institute at Trento, for hosting me during my international research experience.

The valuable input of Andrea Polastri from CNR-IVALSA (Trento, Italy) gratefully acknowledged. I appreciate his availability regarding the experimental testing program and his guidance. The assistance of Mario Pinna and Diego Magnago throughout the testing program conducted at CNR-IVALSA (Trento) is also greatly appreciated.

The author gratefully acknowledges Luc Cloutier from the Civil Engineering Department for his administrative support and his extraordinary good mood during the last 5 years I worked with him.

Special thanks to my parents for their unconditional love and support. Thank you, my wife, my brothers and sisters, for your patience and support.

Thanks to each person who helped with the accomplishment of this project and of which I am not aware.

Thanks God.

Table of contents

List of figures

List of tables

Notation

1. List of abbreviations

APA Engineered Wood Association

ASCE American Society of Civil Engineers

ASTM American Society for Testing and Materials

CLT Cross Laminated Timber

CSA Canadian Standards Association

DC degree of coupling

DH single hold-down configuration

EEEP Equivalent Energy Elastic Plastic

EFM Equivalent Frame Model

ETA European Technical Approvals

EWP Engineered Wood Products

FEM Finite Element Method

LVDT Linear Variable Differential Transducer

MSW Monolithic Shear-Wall

NBCC National Building Code of Canada

NDS National Design Specification for Wood Construction

PWM Perforated Wall Method

RMD residual mean deviance

RVE Representative Volume Element

RVSE Representative Volume Sub-Element

SH single hold-down configuration

SSW Segmented Shear-Wall

X − LEF X-Lam Equivalent Frame

2. List of symbols

2.1 Roman

A area under the capacity curve

a dimension of the gluing interface (= board width)

b length of the wall segments

d_1 lateral displacement at the top of the wall segments for load method #1

d_2 lateral displacement at the top of the wall segments for the EFM in load method #2

$E_{ef,L}$ Effective modulus of elasticity for frame elements representing lintels

$E_{ef,W}$ Effective modulus of elasticity for frame elements representing vertical wall segments

$E_{ef,2D,v}$ effective modulus of elasticity of the homogenous shell elements along the vertical direction

$E_{ef,2D,h}$ effective modulus of elasticity of the homogenous shell elements along the horizontal direction

E_0 the elastic modulus of the laminations in the direction parallel to the grain

E_{90} the elastic modulus of the laminations in the direction perpendicular to the grain

$f_{c,0}$ average compressive strength of CLT panel

$F_{failure}$ maximum load in capacity curve

F_{max} maximum strength of connection

f_R rolling strenght

$f_{t,0}$ tensile strength

$f_{v,tor}$ torsional strength

F_{yield} load corresponding to the yielding of hold-down

G^* effective shear modulus of CLT panel

G_{ef} effective shear modulus of frame elements

$G_{0,mean}$ in-plane shear modulus of laminations

G_{2D} effective shear modulus of homogenous shell elements

H height of the wall

h' distance between the midpoints of the lines connecting the corners of the opening to the wall vertical edges

h_C height of the segment below the window openings

h_{eff} effective height of the wall segments

h_L height of the top lintels

$h_{O,d}$ height of wall segments for walls with door openings

$h_{O,w}$ height of window openings

$K_{A,w}$ axial stiffness of CLT cross-section of vertical wall segments

$K_{B,w}$ in-plane bending stiffness of CLT cross-section of vertical wall segments

$K_{A,CLT,h}$ axial stiffness per unit length of the CLT panel along the horizontal direction

$K_{A,CLT,v}$ axial stiffness per unit length of the CLT panel along the vertical direction

$K_{A,frame,l}$ axial stiffness of rectangular cross-sections of the frame elements representing lintels

$K_{B,frame,l}$ bending stiffness of rectangular cross-sections of the frame elements representing lintels

$K_{A,l}$ axial stiffness of CLT cross-section of lintels

$K_{B,l}$ in-plane bending stiffness of CLT cross-section of lintels

$K_{A,2D,h}$ axial stiffness per unit length of homogenous shell elements along the horizontal direction

$K_{A,2D,v}$ axial stiffness per unit length of homogenous shell elements along the vertical direction

$K_{A,frame,w}$ axial stiffness of rectangular cross-sections of the frame elements representing wall segments

$K_{B,frame,w}$ bending stiffness of rectangular cross-sections of the frame elements representing wall segments

K_e elastic stiffness determined from capacity curve

k_h horizontal stiffness of a generic mechanical anchors

$k_{h,a}$ horizontal stiffness of angle brackets

$k_{h,hd}$ horizontal stiffness of hold down

k_{ser} elastic stiffness of connection

k_v vertical stiffness of a generic mechanical anchors

$k_{v,c}$ vertical compressive stiffness of a generic mechanical anchors

$k_{v,t}$ vertical tensile stiffness of a generic mechanical anchors

$k_{v,t,a}$ vertical tensile stiffness of angle brackets

$k_{v,t,hd}$ vertical tensile stiffness of hold-down

l length of lintels

l_{la} lever arm of coupling moment

l_{eff} flexible length of lintels

M_i bending moment at the base of i^{th} wall segment

M_o global overturning moment acting on the shearwall

N number of layers in the CLT panel

T axial force in vertical wall segments

t thickness of CLT panel

$t_{h,j}$ $t$hickness of the j^{th} horizontal laminate in a CLT panel

t_i^* ideal thickness of i^{th} RVSE

$t_{v,i}$ $t$hickness of the i^{th} vertical laminate in a CLT panel

$V_{b,EFM}$ base shear load of the equivalent frame model

$V_{b,2D}$ base shear load of the 2D model

V_u maximum displacement of connection

V_y yield displacement of connection

w average of the board width and spacing or edge distance of reliefs.

2.2 Greek

α number considering the effective distance of a connector relative to the centre of rotation

Δ_{BS} difference between the base shear of shear-walls with and without openings

$\Delta_{failure}$ maximum displacement in capacity curve

Δ_{yield} yielding displacement in capacity curve

ϵ discrepancy between EFM and 2D model

$|\varepsilon_{BS}|_{max}$ maximum of the absolute values of discrepancies for base shear load

$|\varepsilon_{BS}|_{mean}$ mean of the absolute values of discrepancies for base shear load

$|\varepsilon_{Th}|_{max}$ maximum of the absolute values of discrepancies for tensile load in the hold-down

$|\varepsilon_{Th}|_{mean}$ mean of the absolute values of discrepancies for tensile load in the hold-down

$|\varepsilon_{Vl}|_{max}$ maximum of the absolute values of discrepancies for shear load in the end section of lintel

$|\varepsilon_{Vl}|_{mean}$ mean of the absolute values of discrepancies for shear load in the end section of lintel

$|\varepsilon_{Ml}|_{max}$ maximum of the absolute values of discrepancies for bending moment in the end section of lintel

$|\varepsilon_{Ml}|_{mean}$ mean of the absolute values of discrepancies for bending moment in the end section of lintel

η maximum shear force per unit length

λ_l slenderness of lintels

$\lambda_{w,d}$ slenderness of wall segments in case of door openings

$\lambda_{w,o}$ slenderness of wall segments in case of window openings

μ ductility ratio

σ_{11} tensile or compressive stress in the lintel

τ_0^* nominal shear stress

τ_M torsional shear stress

τ_{tor} torsional shear in the crossing area

τ_v real shear stress

τ_{xz} longitudinal shear in the crossing area

τ_{yz} transversal shear in the crossing area

ψ *openings' ratio*

CHAPTER 1

Introduction

1.1 General

Sustainable construction has been the primary driver in positioning timber and timber-hybrid structure to play a significant role in enabling wood to be used in mid-rise and tall wood applications. Intensive research efforts in the last decade has been instrumental in establishing knowledge related to engineered wood products in general, but with much greater emphasis on panel-type structural elements, particularly cross laminated timber (CLT) panels. The need to use this material in projects has not arrived at the same rate as the development of technical guidelines and design provisions. Although the Canadian wood design standard (CSA 2019) contains extensive and significant provisions on the design and detailing of CLT buildings, compared to almost any other design code, it still lacks in translating the collective research effort in the area of CLT shearwalls and diaphragms into design rules. This is particularly the truth in the case of CLT shearwalls with windows or door openings. The current study attempts to provide a tangible contribution to this important field of knowledge through experimental testing, analytical development as well as numerical modeling. The aim is to establish some fundamental understanding of the behaviour of assemblies consisting of shearwalls with openings, on which further knowledge can be built.

1.2 Cross Laminated Timber (CLT)

1.2.1 Overview

Cross-laminated timber (CLT) is an innovative engineered wood product that originated in Europe and has since been used in many different types of building project all over the globe. CLT panels consist of multiple layers of dimension lumber that are glued on their wide face and glued orthogonally to one another, as illustrated in Figure 1-1. The narrow side of the boards may also be glued together but this is not frequently done to allow some dimensional movement in the boards in the direction perpendicular to the wood grain. The panels can be utilized for as walls, floors, or roofs, presenting an advantageous alternative in North America to the use of light-frame and post-and-beam constructions. CLT presents many advantages, including ease of handling, quick and cost effective erection time, in addition to thermal, acoustic, fire, and seismic properties.

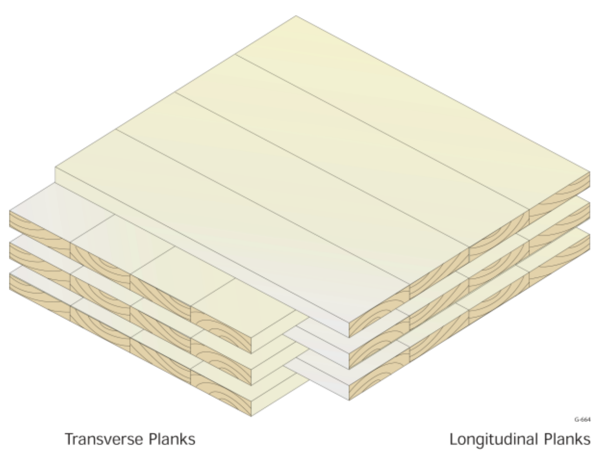

Figure 1-1. Cross Laminated Timber product, adapted from Karacabeyli and Gagnon (2019)

CLT panels are usually constructed with an odd number of layers (in principle similar to the concept used in plywood), thereby defining the major and minor axes, as shown in Figure 1-2. The outer laminations are generally oriented in the direction that is parallel to the load in order to maximize the resistance of the system.

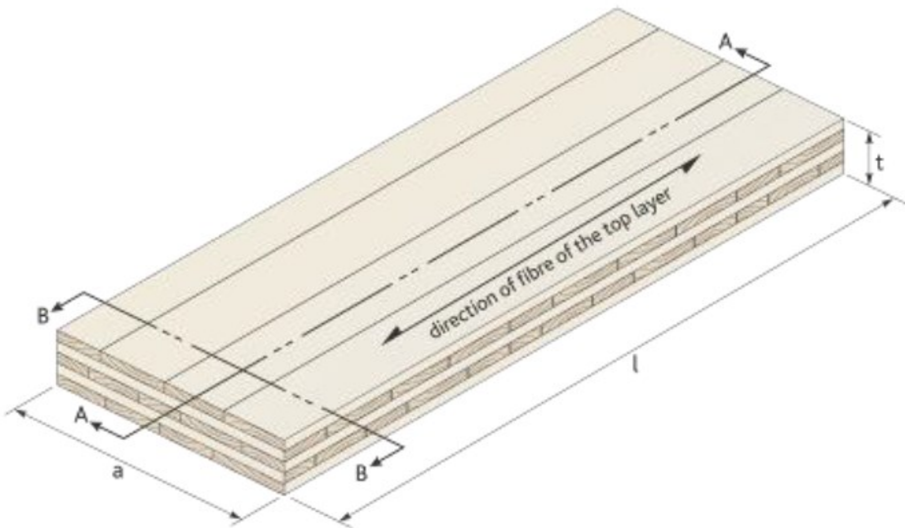

Figure 1-2. Major and minor axes direction and orientation of the outer fibers, adapted from Karacabeyli and Gagnon (2019)

The minimum number of layers used is three, with the standard layup consisting of simply adding two layers to the basic configuration, generating five-, seven-, nine- and in some rare cases eleven layers. Consecutive layers, or ‘double layers’, may also be placed in the same direction in order to achieve a desired capacity or stiffness. Examples of these configurations are shown in Figure 1-3. In general, CLT panels are fabricated in widths that generally range between 0.6 – 3 m. Wider panels can be obtained depending on construction requirements. The length of the panels can reach 18 m, and a maximum of

400 mm in depth can be obtained. Transportation may impose limitations on the dimensions of the panels produced.

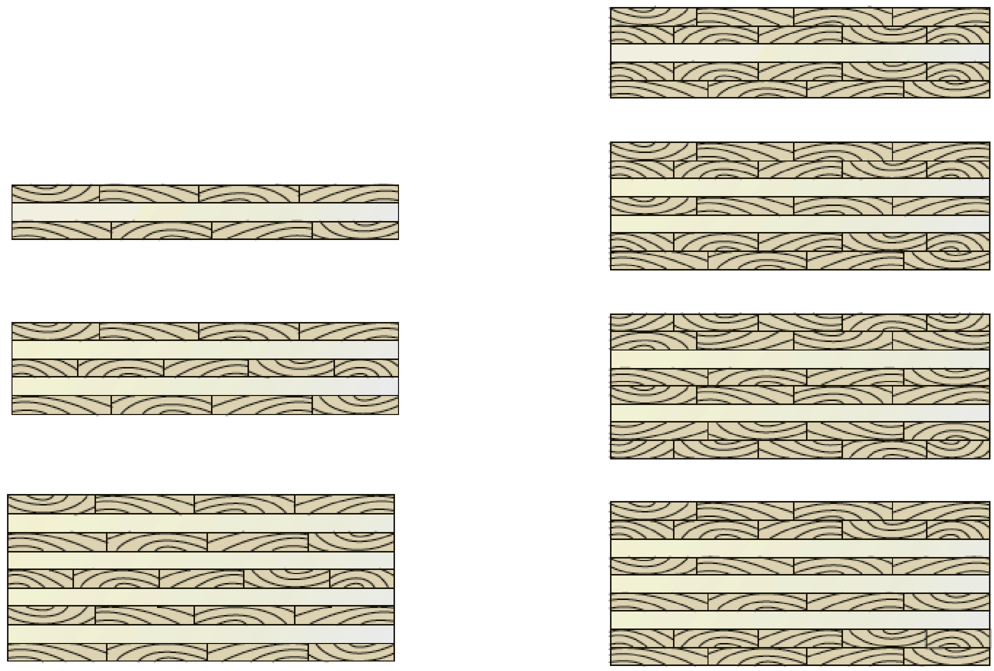

(a) 3, 5, and 9-ply

(b) 'Double Layer' Sections

Figure 1-3. Typical CLT Cross-Sections, adapted from Karacabeyli and Gagnon (2019)

Due to their relatively high stiffness, CLT panels are well suited to be used as a lateral load resisting system to resist seismic and wind loads. The behaviour changes significantly, however, when openings are introduced in the wall. As will be discussed later, the flexibility of various panel components becomes crucially influential in the overall behaviour of the wall assembly.

1.2.2 The Standardization Process of CLT in Canada

There has been considerable progress in the development of the regulatory frame work around the design of CLT structures since their initial publication in the Canadian timber design standard (CSA 2014). The standard governing the manufacturing of CLT panels is the ANSI/APA PRG 320 (ANSI/APA, 2018). The standard includes performance requirements for MSR (Machine Stress-Rated) lumber and visually-graded lumber in longitudinal layers. The transverse layers typically consist of visually graded lumber only and of an inferior grade to the longitudinal laminates. It also includes provisions for custom lay-ups and contains options for use of structural composite lumber (SCL) in the laminations. The CSA O86 Standard references the PRG 320 product standard, and provides design provisions related to structural as well as fire (CSA 2016). The CSA O86 standard is referenced in the National Building Code of Canada (NBC 2015). For seismic design, the detailing provided in the Standard corresponds to the behavioural factors assigned to various structural systems in the NBC code. Currently, the only recognized system for CLT shearwall assemblies is the platform type construction, limited in height depending on the severity in seismicity. Platform-type CLT construction consists of shearwalls that are only one storey high, and where the floor platform of each storey is used as a base for erecting the CLT walls of the next storey.

1.3 Lateral Stability of CLT Shear Walls with Openings

The lateral stability of CLT structures is usually ensured using shearwall panels which are connected to the foundation or the lower floor through mechanical anchors, such as hold-downs and angle brackets. Several research projects, conducted in various countries, have investigated CLT buildings subjected to seismic action through full-scale testing (Ceccotti et al., 2013; Flatscher & Schickhofer, 2015; Popovski & Gavric, 2016; Yasumura et al., 2016). In general, it was reported that the high strength-to-weight ratio of CLT and its ability to dissipate energy through ductile mechanical connections have considerably contributed to the reported good performance under seismic action (Izzi, Casagrande, et al., 2018; Pei et al., 2016). At the wall assembly level, testing programs have been undertaken in Europe (Dujic et al., 2005; Dujic et al., 2006; Gavric et al., 2015; Hristovski et al., 2005; Hummel et al., 2013; Pozza et al., 2014), Canada (Popovski et al., 2010) and Japan (Okabe et al., 2012) to determine the racking behaviour of CLT shear-walls without openings and using various mechanical devices.

Of particular interest to the current study is the behaviour of CLT shear-walls with openings. In such structural systems, the mechanical behaviour may be significantly affected by the construction layout and the size of the lintel, especially relative to the vertical wall segments. The fabrication process generally leads to either the lintel beam being integrated into the shear-wall system (the opening is cut out of the wall) or as an independent element connected to the vertical wall segments, subsequent to their installation. The walls could, therefore, be analyzed as segmented shearwalls (SSW) or monolithic shearwalls (MSW), as illustrated in Figure 1-4a and Figure 1-4b, respectively.

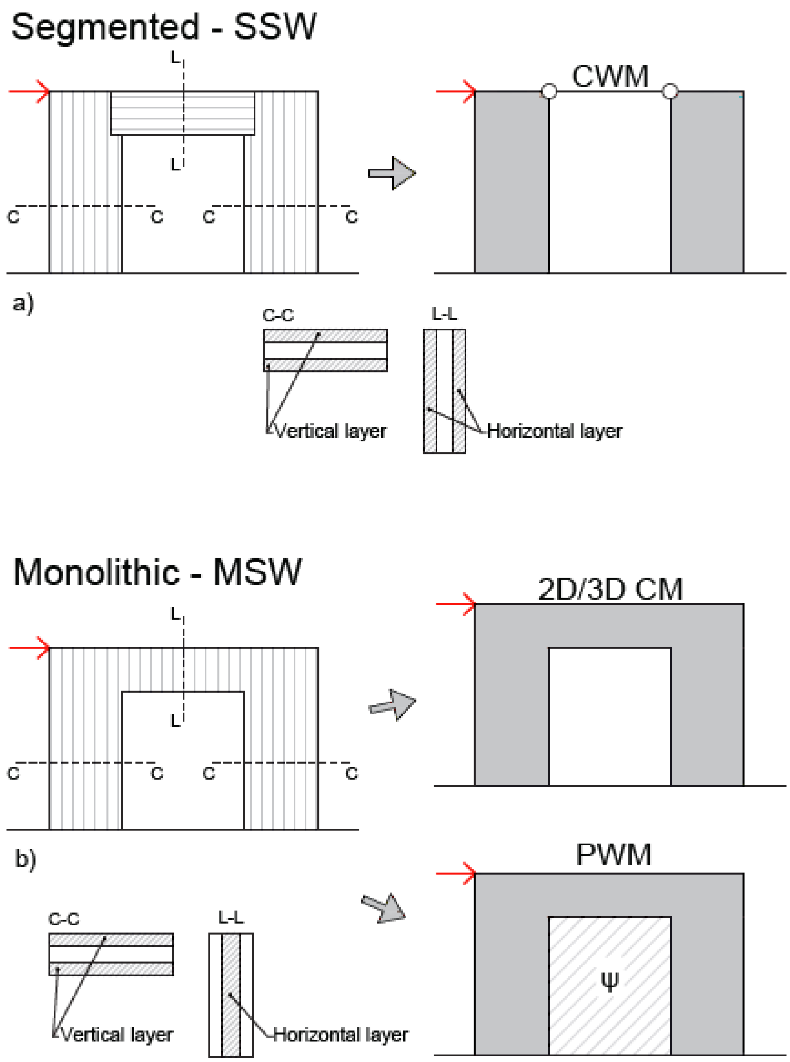

Figure 1-4. Categories of shearwalls in CLT. Example of shearwalls with door openings: a) segmented and b) monolithic

A SSW is considered to contain a lintel acting as an independent element and could, therefore, be assumed to behave as two separate cantilever walls. In this case, no bending moment is anticipated to be transmitted between the lintel and the two vertical wall segments. Alternatively, in an MSW, structural continuity between the lintel beam and the vertical wall segments is assumed, and the influence of the elements below and above openings ought to be taken into account in the analysis. In this case, the influence of openings could be considered in the analysis by either using stiffness and strength reduction coefficients that take into account the opening dimensions leading to what is called Perforated Wall Method (PWM) or by adopting a 2-D (or 3-D) continuous model, which considers the interaction between vertical wall segments and lintels. Such an approach has been used by several researchers (Moosbrugger et al., 2006; Shahnewaz et al., 2016) in order to investigate the behaviour of CLT shearwalls with openings and to assess the value of the reduction factors due to geometrical dimensions of the opening.

Although the segmented wall assumption is widely used by designers, due to its simplicity, the behaviour between segmented and monolithic layouts could be significantly different and requires more investigation, especially regarding the global kinematic behaviour of the wall assembly, object of the following section.

1.4 Kinematic modes

Due to the high in-plane stiffness of CLT panels without openings, rigid body behaviour is generally assumed, where shear and bending deformations within the panel are considered insignificant, compared to those obtained in the mechanical anchors (Casagrande et al., 2016; Flatscher & Schickhofer, 2016; Gavric et al., 2015; Hummel et al., 2016; Wallner-Novak et al., 2013). Rocking behaviour is typically achieved when the wall is composed of multiple segments while maintaining a relatively high (typically between 2:1 and 4:1) segment height-to-width aspect ratio (Nolet et al., 2019), while sliding deformation in the angle brackets is dominant in CLT panels with low aspect ratio (Deng et al., 2019). Walls with rocking behaviour were found to have higher ductility and ability to dissipate energy, especially in the connections between wall panels, however lower stiffness and strength have been observed when compared to monolithic walls of the same dimension (Gavric et al., 2015).

For segmented CLT shearwalls with lintels, assuming that the wall behaves as a rigid body may no longer be valid and the kinematic behaviour of the wall is expected to also depend on the shear and bending deformations of the lintel, which in turn affect the overall behaviour of the wall. The rocking behaviour of the walls with openings consists of two distinct kinematic modes, where i) one centre of rotation for the entire wall (Figure 1-5a) or ii) one centre of rotation for each segment (Figure 1-5b), is attained.

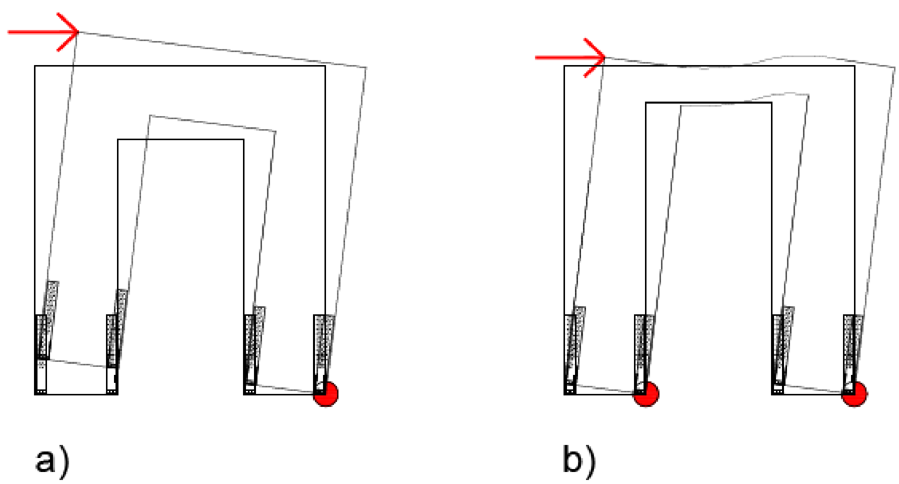

Figure 1-5. Kinematic modes or CLT shearwall with opening ; a) one centre of rotation for the entire wall – b) one centre of rotation for each segment

The layout of the hold-downs also plays a significant role in the mechanical behaviour of CLT shearwalls with openings. For example, in a shearwall consisting of two segments (i.e. single opening) connected together by a lintel beam, hold-downs are typically placed at the extremities of each wall segment, creating a double hold-down (DH) configuration or at the two ends of the wall in a single hold-down (SH) configuration, as shown in Figure 1-6.

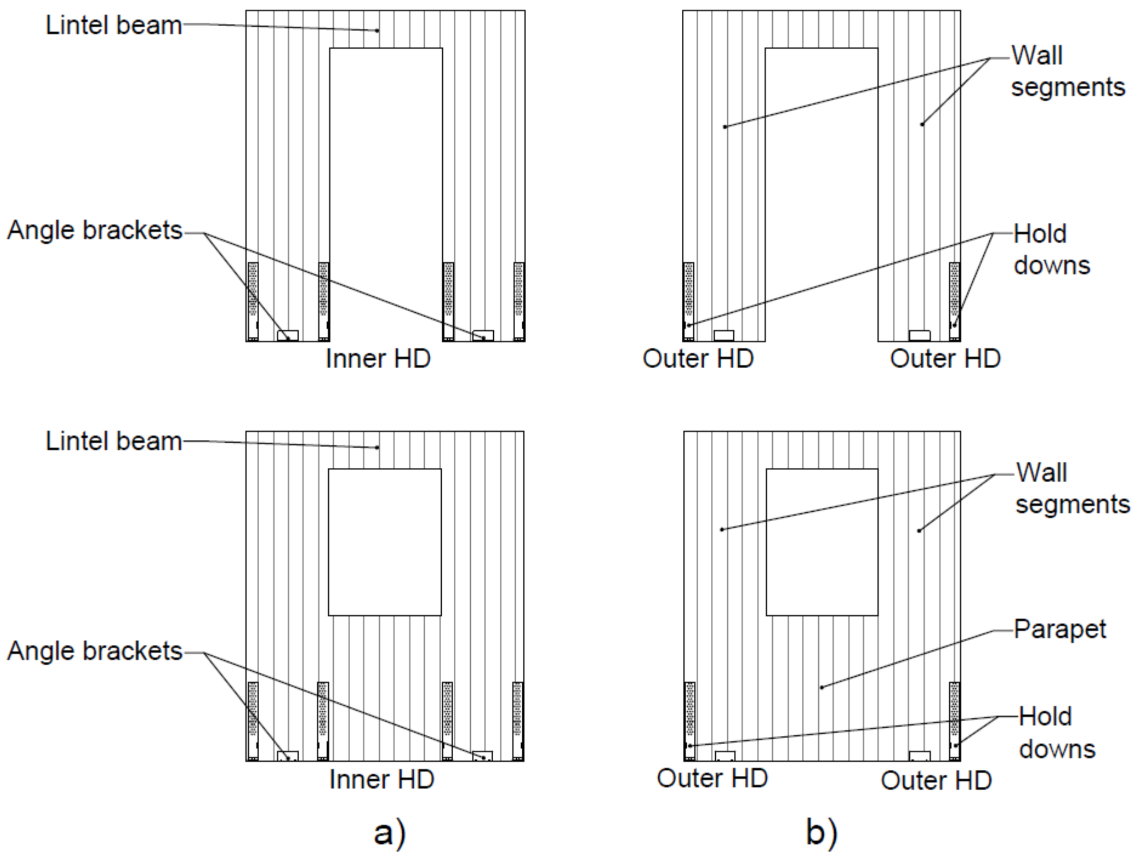

Figure 1-6. Hold-down configurations for CLT shearwall with opening ; a) Double Hold-down (DH) configuration – b) Single Hold-down (SH) configuration

Despite the fact that substantial research has been undertaken on the behaviour of monolithic and segmented CLT shearwalls without openings, the research reported on the mechanical behaviour of CLT shearwalls with openings, especially regarding their kinematic behaviour and the influence of hold-down configuration, has been very limited. The objective of the current study is to investigate the conditions for which different kinematic modes can be attained in the CLT shearwalls with openings and the effect of different hold-down configurations on the behaviour of the shearwall in terms of base shear and tensile load in the hold-down.

Dimensionless analysis is performed to determine the main influencing parameters in the global kinematic behaviour. In order to evaluate the effectiveness of using one or two hold-downs for the CLT panels, results from the numerical analyses of degree of coupling (DC) in the elastic range are also presented. A correlation between the two concepts (i-e: number of centres of rotation and degree of coupling, DC) is found and its validation is performed via experimental testing of CLT shearwalls with either door or window openings. The test's results were also used to validate a finite element model used in the kinematic behaviour investigation in the inelastic range. A method to help with preliminary design and classification of the failure mode in the wall in terms of CLT or hold-down failure is proposed.

One of the objectives of the current study is to propose a classification based on the kinematic behaviour of CLT shearwalls with openings (number of centres of rotation) both in the elastic and the inelastic ranges by investigating cases with different opening types and dimensions, hold-down stiffness, gravity load, and hold-down configuration. The concept of degree of coupling (DC) is introduced to provide a tool to structural engineers to optimize the use of hold-downs in CLT walls such that in case of single-wall behaviour (one centre of rotation), single hold-down layout may be used for wall segments that are fully coupled, while double hold-down layout may be more suitable in case of partially coupled or uncoupled behaviour. The current study applies to monolithic CLT walls and takes into account the mechanical interaction between wall segments and lintels.

1.5 Modelling of CLT Structures

Numerical models have gained acceptance in both research and some design practices due to the cost and limitations associated with the implementation of full-scale tests. For CLT structures, several numerical analysis methods have been proposed in the literature with focus on the deformation contribution of the connections. In most cases, the CLT shearwalls are modelled using multi-layered shell elements (Rinaldin & Fragiacomo, 2016; Sustersic et al., 2016), which take into account the orthotropic nature of the CLT panels. Alternatively, homogenous shell elements can be adopted using an effective orthotropic approach (e.g. Blass and Fellmoser (2004). The mechanical connections are usually modelled employing spring elements, considering uniaxial (Casagrande et al., 2018; Pozza et al., 2016) or biaxial (Izzi, Polastri, et al., 2018; Pozza et al., 2017; Rinaldin et al., 2013) behaviour, depending on whether the connections act in one direction or represent a coupled behaviour in multiple directions. Despite the contributions and advancement in complex numerical analysis methods, the appropriateness of such methods is limited, when considering their use in design practice. Furthermore, the applicability of such complex analysis for multi-storey buildings is also hindered by the high number of degrees of freedom and the complex post-processing analysis. The following sections describe an approach proposed to simplify the analysis and enable reasonably simple yet accurate modeling of CLT shearwalls with openings.

1.5.1 Equivalent Frame Model for CLT Shear Walls

The applicability of an equivalent frame model (EFM) as an alternative analysis approach for CLT shearwalls with openings when subjected to lateral loads is investigated. This approach has been successfully used for modelling other structural materials, such as concrete and masonry (Brencich et al., 1998; Magenes & Della Fontana, 1998; Tomaževič, 1978), but its application to CLT is novel. The EFM approach used in masonry represents the vertical wall segments (also known as piers) and lintel using one-dimensional frame elements, connected by rigid end-offsets. The deformability of the wall is assumed to be reflected in the frame elements, whereas the intersection zones (also known as nodes) are characterized by high stiffness. Recent studies have shown that the assumptions related to the flexible length of the wall segments and lintels, as well as the dimension of nodes, have a significant effect on the results of the analyses (Siano et al., 2017). The proposed *X-Lam Equivalent Frame* model (i.e. X-LEF Model) is developed specifically to aid in the analyses of the behaviour of CLT shearwalls with openings. The X-LEF model applies to monolithic CLT walls and takes into account the mechanical interaction between wall segments and lintels.

1.6 Research Objectives

The overall objective of this study is to investigate the kinematic and mechanical behaviours of CLT shearwalls with openings. More specifically, the study aims to:

1- Investigate the influence of the geometrical dimensions and the mechanical properties and configurations of hold-downs on the elastic and the inelastic behaviours of CLT shearwalls with openings
2- Validate the numerical model using full-scale test results of CLT shearwalls with different configurations

3- Develop a simplified numerical approach for the anlysis of CLT shearwalls with openings by means of an Equivalent Frame Model

1.7 Research Methodology

To achieve the proposed objectives, the following research methodology is adopted:

1. Review of existing research studies and construction techniques;
2. Selection of typical geometric configurations of CLT shearwalls;
3. Development of finite element numerical models with 2D elements in elastic and inelastic ranges;
4. Conduct monotonic experimental tests on five full scale shearwalls with door and window openings;
5. Develop a simplified finite element numerical model with equivalent frame elements;

1.8 Limitations of the current study

The current study deals with CLT shearwalls where openings are created by means of cutting out sections of the CLT panel, and where complete structural continuity between the lintel beam and the vertical wall segments is obtained. Lintels and parapets are assumed integrated in the shearwalls and as such, no mechanical connectors are required to connect lintels to wall segments. It is also important to note that the current research study does not attempt to demonstrate the effect of openings on the strength and stiffness of CLT shearwalls, but rather establishes the relationship between the coupling effect and the kinematic behaviour as a function of the wall aspect ratio. Furthermore, non-symmetrical openings and the presence of both opening types (doors and windows) in the same shearwall are outside the scope of the current research work. The findings in this study are assumed limited in their application to platform type CLT buildings only.

The proposed equivalent frame model is limited in scope to a single storey, where the opening is centred, and elastic behaviour of CLT panel and inelastic mechanical anchors is assumed. It is suggested that future work includes validation of the proposed model through a more extensive experimental campaign than that presented in the current study, potentially extending the model applicability to multiple storey. Further investigations regarding the evaluation of the internal distribution of stresses in CLT elements and the influence of the non-linear behaviour of mechanical anchors on the behaviour of the shearwalls are also subject to future research efforts.

1.9 Organization of the Thesis

This research work is organized into 8 chapters.

Chapter 1 introduces the problem statement with the study objectives and provides a summary of the scope and the methodology adopted to meet the objectives.

Chapter 2 presents a detailed literature review.

Chapter 3 discusses the kinematic behaviour of the walls and the corresponding degree of coupling (DC) in the elastic range.

Chapter 4 deals with the inelastic range where the kinematic behaviour and the failure mechanisms are investigated.

Chapter 5 discusses the proposed equivalent frame model.

Chapter 6 presents the results obtained from the experimental testing and validation of the numerical models.

Chapter 7 Provides key conclusions and proposes recommendations for future investigations.

References of Chapter 1

Blass, Hans Joachim, & Fellmoser, Peter. (2004). *Design of solid wood panels with cross layers*.

Brencich, Antonio, Gambarotta, Luigi, & Lagomarsino, Sergio. (1998). *A macroelement approach to the three-dimensional seismic analysis of masonry buildings*.

Casagrande, Daniele, Doudak, Ghasan, Mauro, Luigi, & Polastri, Andrea. (2018). Analytical Approach to Establishing the Elastic Behavior of Multipanel CLT Shear Walls Subjected to Lateral Loads. *Journal of Structural Engineering, 144*(2), 04017193. doi:doi:10.1061/(ASCE)ST.1943-541X.0001948

Casagrande, Daniele, Rossi, Simone, Sartori, Tiziano, & Tomasi, Roberto. (2016). Proposal of an analytical procedure and a simplified numerical model for elastic response of single-storey timber shear-walls. *Construction and Building Materials, 102*, 1101-1112. doi:https://doi.org/10.1016/j.conbuildmat.2014.12.114

Ceccotti, Ario, Sandhaas, Carmen, Okabe, Minoru, Yasumura, Motoi, Minowa, Chikahiro, & Kawai, Naohito. (2013). SOFIE project – 3D shaking table test on a seven-storey full-scale cross-laminated timber building. *Earthquake Engineering & Structural Dynamics, 42*(13), 2003-2021. doi:doi:10.1002/eqe.2309

CSA. (2014). CSA Standard O86-14, Engineering design in wood: CSA Group.

CSA. (2019). CSA Standard O86-19, Engineering design in wood: CSA Group.

Deng, Peng, Pei, Shiling, van de Lindt, John W., Omar Amini, M., & Liu, Hongyan. (2019). Lateral behaviour of panelized CLT walls: A pushover analysis based on minimal resistance assumption. *Engineering Structures, 191*, 469-478. doi:https://doi.org/10.1016/j.engstruct.2019.04.080

Dujic, Bruno, Aicher, Simon, & Zarnić, Roko. (2005). Investigation on in-plane loaded wooden elements-influence of loading on boundary conditions. *Otto-Graf-Journal, 16*, 259-272.

Dujic, Bruno, Hristovski, Viktor, Stojmanovska, Marta, & Zarnić, Roko. (2006). *Experimental investigation of massive wooden wall panel systems subjected to seismic excitation*.

Flatscher, Georg, & Schickhofer, Gerhard. (2015). Shaking-table test of a cross-laminated timber structure. *Proceedings of the Institution of Civil Engineers - Structures and Buildings, 168*(11), 878-888. doi:10.1680/stbu.13.00086

Flatscher, Georg, & Schickhofer, Gerhard. (2016). *Displacement-Based Determination of Laterally Loaded Cross Laminated Timber (CLT) Wall Systems.* Paper presented at the INTER - International Network on Timber Engineering Research.

Gavric, Igor, Fragiacomo, Massimo, & Ceccotti, Ario. (2015). Cyclic Behavior of CLT Wall Systems: Experimental Tests and Analytical Prediction Models. *Journal of Structural Engineering, 141*(11), 04015034. doi:doi:10.1061/(ASCE)ST.1943-541X.0001246

Hristovski, Viktor, Stojmanovska, Marta, Zarnic, R., & Dujic, Bruno. (2005). *Experimental and analytical evaluation of the racking strength on massive wooden wall panels - Preliminary project phase*.

Hummel, Johannes, Flatscher, Georg, Seim, Werner, & Schickhofer, Gerhard. (2013). *CLT Wall Elements Under Cyclic Loading - Details for Anchorage and Connection*. Paper presented at the COST Action FP1004, Focus solid timber solutions – European Conference on Cross Laminated Timber (CLT), Graz, Austria.

Hummel, Johannes, Seim, Werner, & Otto, Simone. (2016). Steifigkeit und Eigenfrequenzen im mehrgeschossigen Holzbau. *Bautechnik, 93*(11), 781-794. doi:10.1002/bate.201500105

Izzi, Matteo, Casagrande, Daniele, Bezzi, Stefano, Pasca, Dag, Follesa, Maurizio, & Tomasi, Roberto. (2018). Seismic behaviour of Cross-Laminated Timber structures: A state-of-the-art review. *Engineering Structures, 170*, 42-52. doi:https://doi.org/10.1016/j.engstruct.2018.05.060

Izzi, Matteo, Polastri, Andrea, & Fragiacomo, Massimo. (2018). Modelling the mechanical behaviour of typical wall-to-floor connection systems for cross-laminated timber structures. *Engineering Structures, 162*, 270-282. doi:https://doi.org/10.1016/j.engstruct.2018.02.045

Karacabeyli, Erol, & Gagnon, Sylvain. (2019). *CLT handbook : cross-laminated timber*. Québec: FPInnovations.

Magenes, Guido, & Della Fontana, A. (1998). *Simplified non-linear seismic analysis of masonry buildings* (Vol. 8).

Moosbrugger, Thomas, Guggenberger, Werner, & Bogensperger, Thomas. (2006). *Cross-laminated timber wall segments under homogeneous shear - With and without openings.* Paper presented at the 9th World Conference on Timber Engineering 2006, WCTE 2006, August 6, 2006 - August 10, 2006, Portland, OR, United states.

Nolet, Vincent, Casagrande, Daniele, & Doudak, Ghasan. (2019). Multipanel CLT shearwalls: an analytical methodology to predict the elastic-plastic behaviour. *Engineering Structures, 179*, 640-654. doi:https://doi.org/10.1016/j.engstruct.2018.11.017

Okabe, M , Yasumura, M, Kobayashi, K, Haramiishi, T, Nakashima, Y, & Fujita, K. (2012). *Effect of vertical load under cyclic lateral load test for evaluating Sugi CLT wall panel*. Paper presented at the World Conference on Timber Engineering (WCTE), Auckland, New Zealand.

Pei, S., Lindt, J. W. van de, Popovski, M., Berman, J. W., Dolan, J. D., Ricles, J., . . . Rammer, D. R. (2016). Cross-Laminated Timber for Seismic Regions: Progress and Challenges for Research and Implementation. *Journal of Structural Engineering, 142*(4), E2514001. doi:doi:10.1061/(ASCE)ST.1943-541X.0001192

Popovski, Marjan, & Gavric, Igor. (2016). Performance of a 2-Story CLT House Subjected to Lateral Loads. *Journal of Structural Engineering, 142*(4), E4015006. doi:doi:10.1061/(ASCE)ST.1943-541X.0001315

Popovski, Marjan, Schneider, Johannes, & Schweinsteiger, Matthias. (2010). *Lateral load resistance of cross-laminated wood panels*.

Pozza, Luca, Massari, Milena, Ferracuti, Barbara, & Savoia, Marco. (2017). *Experimental cyclic tests on CLT hold-down connections subjected to a combination of shear and tension*.

Pozza, Luca, Scotta, Roberto, Trutalli, Davide, Pinna, Mario, Polastri, Andrea, & Bertoni, Paolo. (2014). Experimental and Numerical Analyses of New Massive Wooden Shear-Wall Systems. *Buildings, 4*(3), 355-374.

Pozza, Luca, Scotta, Roberto, Trutalli, Davide, Polastri, Andrea, & Smith, Ian. (2016). Experimentally based q-factor estimation of cross-laminated timber walls. *Proceedings of the Institution of Civil Engineers - Structures and Buildings, 169*(7), 492-507. doi:10.1680/jstbu.15.00009

Rinaldin, Giovanni, Amadio, Claudio, & Fragiacomo, Massimo. (2013). A component approach for the hysteretic behaviour of connections in cross-laminated wooden structures. *Earthquake Engineering & Structural Dynamics, 42*(13), 2023-2042. doi:doi:10.1002/eqe.2310

Rinaldin, Giovanni, & Fragiacomo, Massimo. (2016). Non-linear simulation of shaking-table tests on 3- and 7-storey X-Lam timber buildings. *Engineering Structures, 113*, 133-148. doi:https://doi.org/10.1016/j.engstruct.2016.01.055

Shahnewaz, Md, Alam, M. Shahria, Tannert, Thomas, & Popovski, Marjan. (2016). *Cross Laminated Timber walls with openings: In-plane stiffness prediction and sensitivity analysis*.

Siano, Rossella, Sepe, Vincenzo, Camata, Guido, Spacone, Enrico, Roca, Pere, & Pelà, Luca. (2017). *Analysis of the performance in the linear field of Equivalent-Frame Models for Regular and Irregular Masonry Walls* (Vol. 145).

Sustersic, Iztok, Fragiacomo, Massimo, & Dujic, Bruno. (2016). Seismic Analysis of Cross-Laminated Multistory Timber Buildings Using Code-Prescribed Methods: Influence of Panel Size, Connection Ductility, and Schematization. *Journal of Structural Engineering, 142*(4), E4015012. doi:doi:10.1061/(ASCE)ST.1943-541X.0001344

Tomaževič, M. (1978). *The computer program POR*. Retrieved from Ljubljana, Slovenia:

Wallner-Novak, Markus, Pock, Kurt, & Koppelhuber, Josef. (2013). *Brettsperrholz | Bemessung*.

Yasumura, Motoi, Kobayashi, Kenji, Okabe, Minoru, Miyake, Tatsuya, & Matsumoto, Kazuyuki. (2016). Full-Scale Tests and Numerical Analysis of Low-Rise CLT

Structures under Lateral Loading. *Journal of Structural Engineering, 142*(4), E4015007. doi:doi:10.1061/(ASCE)ST.1943-541X.0001348

CHAPTER 2

Literature review

2.1 General

The analysis approach to CLT shearwalls has generally followed that of light-frame shearwalls. The segmented wall method (SWM) and the perforated wall method (PWM) have typically been used to analyze and design wood-based shearwalls. SWM has been widely used in design codes and standards in Canada (CSA, 2014) and the US (AWC, 2015). In this method, the role of the lintels is neglected and it is assumed that there is a continuity in the lateral resisting elements over the entire height of the structure, while in PWM, the effects of the elements above and below the openings are incorporated.

2.2 CLT Shearwalls with no Openings

Dujic et al. (2005) investigated the racking behaviour of CLT shearwalls with three cases of boundary conditions and vertical load subjected to cycling loading. The three situations investigated were shear cantilever mechanism (rocking response), restricted rocking mechanism (coupled shear-rocking response), and pure shear mechanism. They pointed out the importance of properly taking into account the boundary conditions, the influence of vertical load, and the type of horizontal loading. They recommended new standards to implement the concept of performance-based earthquake engineering design to obtain experimental data needed for evaluation of the behaviour factor “q”.

Popovski et al. (2010) conducted quasi-static tests to investigate the performance of CLT wall panels with various configurations and connection details. The study varied the wall aspect ratios, and evaluated different types of screws connecting the wall panels to each other. The study also investigated the connections between the wall and the supporting floor or foundation, including fasteners like nails, screws and timber rivets. The study emphasized the adequacy of the CLT walls to perform well when subjected to earthquake loading using nails or screws with the steel brackets. The seismic perfomance was enhanced when the hold-down brackets were connected using nails, mainly due to the ductile behaviour of the nails. Contrarily, diagonally placed screws connecting the wall to the floor below exhibited less ductility and was therefore not recommended in high seismic zones. It was also shown that timber rivet could be used effectively as fasteners in the hold-down joint but it required special detailing of both the connection group and the brackets.

Okabe et al. (2012) studied the lateral performance of Japanese (Sugi) CLT shearwalls using cyclic lateral load tests. The study also investigated the effect of three levels of vertical load. It was observed that rocking mode was the dominant mode of deformation in the Sugi CLT shearwalls. The presence of vertical load was observed to increase the stiffness of the CLT walls. A positive effect on the ultimate strength was also observed but to a lesser degree than that on stiffness.

Hummel et al. (2013) conducted experimental tests of CLT walls under cyclic loading with focus on the influence of different configurations of connections, vertical load and loading protocol. The effect of building physics detailing was found to have an effect on the wall behaviour, especially related to friction between the wall and floor slab, affecting the damping, stiffness and ductility. The wall's kinematic mode was also observed to have a significant effect on the damping capacity of the wall element under cyclic loading. It was also found that multi-panel walls exhibited more ductile behaviour than monolithic walls but did not exhibit an increase in the hysteretic damping.

Rinaldin et al. (2013) introduced a numerical model to describe the behaviour of CLT buildings and to establish an estimate of the building's capacity to dissipate energy. The model incorporated the strength interaction between different degrees of freedom of the hold-downs and angle bracket connections. The connections were modelled using nonlinear springs, while the wood components were modelled using elastic shell elements. The connection behaviour included effects of post-peak strength, pinching and stiffness degradation. The model prediction was compared with the experimental results from cyclic tests on single walls, coupled walls and a single-storey building, with reasonable accuracy. The experimental-numerical comparisons with the single-storey CLT building demonstrated that the model was capable of accurately predicting the cyclic response and total energy with a relatively small error.

Pozza et al. (2015) conducted experimental tests and numerical analysis on four CLT walls, including typical CLT panels with glued interfaces and innovative massive timber panels adopting steel staples or wooden dovetail inserts to connect the layers. The authors performed quasi-static cyclic tests and the results were used to calibrate a non-linear numerical model. The results showed that the examined walls could present viable construction technique in seismic-prone areas. Once calibrated, the model was used to perform non-linear dynamic analyses on a three-storey shearwall building and proposed intrinsic behaviour factor. The authors also discussed the deformability of the CLT panels, especially when evaluating the behavioural factor (q). It was recommended that a q-factor up to 3 can be used for the seismic design of shearwalls with rigid wooden panels, whereas a q-factor of 4 is suitable for wall systems with deformable panel.

Hristovski et al. (2018) conducted full-scale shaking-table tests on CLT panel systems, containing a pair of single- or two-unit principal wall elements. The test specimens had the same geometry, dimensions, and mass, and were both tested using seismic excitations and sinusoidal inputs. Ambient and forced-vibration tests were also conducted to determine the natural periods after each test and to compute the structural damping ratio. For the single panel test, the authors confirmed that the rocking mode behaviour and attributed such behaviour to the mechanical anchors between the panels and the floor or foundation support. The CLT panels and the mechanical anchors remained undamaged after the tests. This was also corroborated through the vibration tests, where the natural periods were unchanged. For the double panel test, the rocking behaviour was governed primarily by the vertical connections between the panels. The results also showed that the two-unit wall specimen exhibited slightly lower displacements and seismic forces compared to the single-wall specimen, mainly due to the slightly higher energy-dissipation mechanism. The results obtained from a proposed 2-D numerical model showed a reasonable correlation with the results obtained from the dynamic tests.

Casagrande et al. (2018) proposed expressions for determination of the elastic stiffness and capacity of multi-panel CLT shearwalls, while taking into account the geometry of the panels and stiffness of hold-down and vertical joint connections. The predicted elastic response was expressed as a function of the ratio between the stiffness of the vertical joints and that of the hold-downs. It was found that this ratio determines the global behaviour such that when the stiffness of the hold-downs is higher than of the vertical joints, where each CLT panel exhibits an absolute center of rotation. Contrarily, in the case of relatively flexible hold-down, a progressive uplift of the panels may occur. An analytical expression to evaluate the elastic strength of an entire wall is presented for different kinematic cases. The proposed analytical model was verified using a detailed numerical model.

Izzi et al. (2018) investigated the hysteretic behaviour and failure mechanism of CLT shearwall systems with varying connection types using a detailed numerical model based on linear-elastic 3-D solid elements and nonlinear springs. The results from the numerical model were compared with test data published in the literature. Parametric analyses were performed to investigate the effect of boundary conditions and panel aspect ratio. The study emphasized the importance of considering the friction between the wall panels and the floor, especially when predicting energy dissipation. The study also found that rocking behaviour dominated the wall behaviour when the segment width to length ration was equal to unity, whereas sliding occurred when the aspect ratio was equal to two.

Shahnewaz et al. (2018) investigated the behaviour of walls with single and coupled CLT panels under lateral loading. Finite element models were used in a parametric study, varying the number and type of connectors to evaluate the capacity, stiffness, ductility and energy dissipation for both single and coupled CLT shear walls. The ductility of the coupled shear walls was found to be higher than in single shear walls.

Nolet et al. (2019) developed an analytical procedure to describe the elastic-plastic behaviour of multi-panel CLT shearwalls. The proposed methodology outlined the sequence of yielding and failure of connectors and provided conditions to attain desired wall behaviour. The study showed that the Coupled-Panel behaviour (i.e. multi-panel wall) was controlled by the yielding of the vertical joints prior the yielding of the hold-down whereas the opposite was valid for the case of Single-Wall behaviour (i.e. monolithic wall). The proposed model was found to be dependent on the panel aspect ratio, connectors' configuration and properties and gravity load. The results from the analytical model in terms of key stiffness and strength properties were compared with those analyzed using a suitable numerical model and it was found that the proposed analytical model was capable of describing the wall behaviour with reasonable accuracy.

2.3 CLT Shear Walls with Openings

Moosbrugger et al. (2006) studied the effect of openings on the behaviour of CLT wall segment under uniform in-plane shear loading, considering the layout of the lamellae in the CLT panel. The authors carried out parametric studies using finite element method on wall models with and without openings. A simplified mechanical model was derived based on the Representative Volume Sub-Element (RVSE) and compared to the detailed 3-D finite element model and reasonable fit between the two models was observed.

Shahnewaz et al. (2017) investigated the stiffness of CLT walls with opening using a finite element analysis model. The model was verified with test results of CLT panels under in-plane loading. A parametric study was undertaken to investigate the effect of varying types and sizes of openings, as well as opening and wall aspect ratios on the overall wall stiffness. It was found that the stiffness results obtained from the finite element model matched the experimental results with reasonable accuracy. A sensitivity analysis undertaken using the verified model showed that important factors affecting the wall stiffness include the ratio of opening area to wall area, maximum aspect ratio of opening and the aspect ratio of opening. The walls with openings were compared to a reference wall without openings, and it was found that the relationship between the removed area and the reduction in stiffness was non-linear, where, for example, about 60% of the wall stiffness was reduced when half of the area of the wall was removed.

Pai et al. (2017) studied the effect of a single symmetrical opening on the force-deformation response of a CLT shearwalls to investigate the applicability of the force transfer around openings (FTAO) method in CLT shearwalls. The transfer force to design necessary reinforcements around the openings were also investigated. A detailed finite element model was developed and the results showed that the shearwall with cut-out openings may experience shear failure around the corners of openings. The study showed that the presence of an opening in a coupled-panel wall decreased the strength and stiffness. Tierods have been suggested as reinforcements at opening corners in coupled-panel CLT shearwalls to resist the transfer force. It was shown that the Diekmann model provided a good alternative to determine the design transfer force for a window-type opening. However, the Diekmann method was not applicable for door openings.

Dujic et al. (2017) studied the racking behaviour of CLT walls with openings, particularly the effect of opening shape and area on the shear capacity and stiffness. Cyclic tests were conducted on two CLT wall configurations, including door and window openings as well as a reference wall without openings. The study confirmed the relatively high stiffness of CLT walls with no openings, leading to the anchors between the wall panel and the foundation being critical elements that govern the wall response to earthquake excitations. For CLT walls with large openings, lower shear stiffness was observed, whereas the load-bearing capacity was not reduced at the same rate. This was attributed to the failure mainly occurring in the anchors areas and in the corners around the openings. The results of the parametric analyses showed that reduction up to 30% in the wall area, caused no significant reduction in the capacity, however, the stiffness was reportedly reduced by about 50% compared to walls with no openings.

2.4 Kinematic behaviour

Gavric et al. (2015) reported on an extensive experimental program on single and coupled CLT shearwalls, where different anchoring systems and types of joints between panels were investigated. Influencing parameters on the structural performance of the wall included the layout and mechanical properties of the connectors and the vertical joints. The deformation of the wall was mainly attributed to the connections, whereas very little deformation was observed in the CLT panels. The authors conducted a parametric study on CLT shearwall assemblies using pushover analysis with varying aspect ratios. The analysis showed that segmentation of CLT walls decreased the wall stiffness and strength, while enhancing their deformation capacity. From cyclic tests it was also found that the kinematic behaviour was characterized by rocking and was strongly affected by the number of screws installed between the adjacent CLT panels. The addition of vertical load had a significant and positive effect on the wall behaviour. The authors recommended that plasticization should preferably occur in the hold-downs and angle brackets loaded in tension, whereas the angle bracket should ideally remain elastic in shear so that there is no residual slip in the wall at the end of the seismic event. It was also reported that ignoring the shear capacity of holddowns and the tension capacity of angle brackets significantly underestimates the CLT wall resistance and displacement capacity.

Reynolds et al. (2017) investigated two buildings each consisting of two-story CLT shearwall systems, subjected to lateral and vertical loading. The authors investigated the kinematic behaviour using discrete transducers and continuous field displacements obtained by digital image correlation and found that the movement of the complete shearwall was dominated by rigid-body movement of the panels. It was also found that some of the simple design calculation methods currently used by structural engineers substantially underestimated the peak load resistance of this system.

Oh et al. (2017) investigated the kinematic behaviour and equivalent shear performance of panelized CLT shearwalls using small panels connected together with panel-to-panel connections. The study found that the kinematic model proposed by the authors showed a good agreement with the envelope curve obtained from the experimental test results. Additional kinematic formulae for panel-to-panel failure was developed. The study also found that the global peak load did not decrease significantly compared with the wall made of a single CLT panel, while the global displacement exhibited a large increase. In all tested walls, failure occurred at the bracket by the uplift force as designed by the kinematic formulae and the predicted envelope curves showed good agreement with the experimental results. Ultimately the study concluded that a large CLT panel can be constructed using small panels without significant loss in strength, but the deformations are anticipated to be larger than in the wall made of a single panel.

Deng et al. (2019) presented a simplified mechanistic model to predict the rocking and sliding lateral response of CLT walls with different boundaries and gravity loading conditions based on an approximation of the principle of virtual work. The analyses showed that the panel aspect ratio was the most influential parameter on the kinematic behaviour, where generally, aspect ratios smaller than unity resulted in an increase of the sliding behaviour. The backbone characterization from the proposed model was compared to the existing test results and results showed some differences that were attributed to a number of material nonlinear characteristics. However, the model was capable of predicting whether sliding or rocking behaviour contributed to the overall drift of the CLT shearwall. The model was used to investigate the effect of wall configurations and boundary conditions using sensitivity analyses.

2.5 Failure Mechanisms of CLT

Due to the high in-plane rigidity and strength of the CLT panels, failure in CLT shearwalls is generally limited to that of the connections. The Canadian timber design standard (CSA 2019) specifically requires that the lateral resistance of CLT shearwalls to be governed by the resistance of connections between the shearwalls and the foundation or floor, and connections between the individual panels, calculated using methods of mechanics. These provisions are adequate and sufficient when the wall does not have any openings that are integrated into the wall panels. In such walls, the CLT panels would govern the failure of the wall and the stresses in the panel, especially those in the lintels are required to be checked. This section presents the existing analytical models for analyzing the state of stress in terms of shear in the panel in order to estimate whether failure is expected to occur in the CLT or the mechanical connectors. Three models are presented herein, namely i) Representative Volume Sub-Element (RVSE), ii) beam model and iii) panel model. Regarding axial stress, this can be verified using classical finding of Resistance of Material. A proposed method consisting to check sections including only lamellae that the load is acting in their grain direction can be found in Bogensperger et al. (2010).

2.5.1 RVSE Model

Moosbrugger et al. (2006) developed a simplified mechanical model allowing for the compact description of the finite element results. The model is based on considering representative volume sub-element, which represents the intersection area of two sets of perpendicular board lamellae. In a subsequent study, Bogensperger et al. (2010) extended the calculations of the shear strength based on the RVSE model and analyzed the shear stresses and shear stiffness based on a representative volume element (RVE) of a CLT-element. This RVE can be simplified further to a representative volume sub-element (RVSE). The RVSE can be used for shear strength verifications with its two main mechanisms, namely shear in a single board and a local torsional moment in the gluing interface between two boards. The shear strength for loads in plane of CLT panel is higher than the corresponding value for glulam. Three failure modes within the thickness of the CLT panel are defined as follows: (i) failure mode I where the parallel to grain shear failure occurs in the gross cross-section between the unglued lamellae with equal shear magnitude in the orthogonal lamellae (Equation 2-1), (ii) failure mode II where the perpendicular to grain shear failure occurs in the net cross-section of the orthogonal lamellae (Equation 2-2) and (iii) failure mode III where the unidirectional and torsional shear stresses, resulting from shear force of adjacent layers, occur in the crossing areas (Equation 2-3).

The nominal shear stress, τ_0^*, can be expressed as follows:

$$\tau_0^* = \frac{\eta \cdot \frac{t_i^*}{\sum_i t_i^*}}{t_i^*} = \frac{\eta}{\sum_i t_i^*} \qquad (2\text{-}1)$$

where η is the maximum shear force per unit length and t_i^* is the ideal thickness.

The ideal thicknesses are determined in a conservative manner that the thinner thickness of two attached boards is the controlling thickness for the ith RVSE when checking the ith gluing interface of the CLT-element. As an example, for a five ply CLT element four RVSE and 4 ideal thicknesses can be determined in accordance to Table 1-1.

Table 2-1. Ideal thickness in the RVSE model

# of RVSE	Ideal thickness t_i^*
1	t_1^* =min (2 t1; t2)
2	t_2^* =min (t2; t3)
3	t_3^* =min (t3; t4)
4	t_4^* =min (t4; 2 t5)

The real shear stress where, τ_v, is defined in Equation (2-2) as follows:

$$\tau_v = 2 \cdot \tau_0^* \qquad (2\text{-}2)$$

where τ_0^* is the nominal shear stress defined in Equation (2-1).

And finally, the torsional shear stress, τ_M, can be calculated using the nominal shear stress,τ_0^*, the ideal thickness, t_i^*, and the dimension of the gluing interface, which is identical to the board width, a , as expressed in Equation (2-3):

$$\tau_M = 3 \cdot \tau_0^* \cdot \frac{t_i^*}{a} \qquad (2\text{-}3)$$

2.5.2 CLT Beams

This model was initially developed by Flaig and Blaß (2013). The authors developed analytical solutions for the calculation of shear stresses and shear deformations in CLT-beams loaded in plane. These solutions were also validated using test results. The failure modes in this model are consistent with those in the RVSE model, considering shear stresses acting parallel and perpendicular to the grain within the lamellae and shear stresses within the crossing areas of orthogonally bonded lamellae. The strength properties and criteria for the verification of shear stresses corresponding to the different failure modes were specified based on experimental results by the authors and those available in the literature. The study showed that the effective shear strength of CLT-beams was strongly dependent on the cross-sectional arrangement and thickness ratio of longitudinal and transversal layers and on the width of lamellae. A closed-form solution for an effective shear modulus of CLT-beams was obtained. For failure mode I and II, the calculations were based on the beam theory, whereas for failure mode III, a composite beam approach is used. Failure mode III is the most complex as it consists of three shear components: (i) a shear stress parallel to the longitudinal axis of the beam, which is a consequence of the differential axial forces due to the change of the bending moments in the case where the longitudinal layers are not bonded; (ii) a shear stress perpendicular to the longitudinal axis of the beam, resulting from loading and boundary conditions and (iii) a torsional shear arising from the eccentricity of the different crossing areas concerning the horizontal plane passing through the centre of the total transversal section of the beam. In this failure mode, the longitudinal shear stress is found to be affected by the number of lamellae within the longitudinal layers and the ratio of the thickness of the individual layers and number of the crossing areas that longitudinal laminations have with the transversal ones. However, in practice, this ratio is constant and consequently, the stress distribution is considered to be constant in the thickness direction. Concerning the torsional shear, it is not only considered constant in the thickness direction but also in the height direction. More specifically, compared to the RVSE model, the torsional stress in the crossing areas takes into account the rolling shear for torsional stress verification based on experimental tests on crossing areas loaded in either uni-axial shear, pure torsion, or a combination of the two. The failure criterion was reported to be as in Equations 2-4 and 2-5.

$$\frac{\tau_{tor}}{f_{v,tor}} = \frac{\tau_{xz}}{f_R} \leq 1.0 \qquad (2\text{-}4)$$

$$\frac{\tau_{tor}}{f_{v,tor}} = \frac{\tau_{yz}}{f_R} \leq 1.0 \qquad (2\text{-}5)$$

where

τ_{tor} is torsional shear in the crossing area, τ_{xz} and τ_{yz} are longitudinal and transversal shear in the crossing area respectively.

and

$f_{v,tor}$ and f_R are the torsional and rolling strengths.

Danielsson and Serrano (2018) noted that although the beam model has appealing properties it contains some inaccuracies related to the assumed distributions of internal forces, based on comparison to finite element analysis. The authors proposed that modified model assumptions regarding the distribution of lamination shear forces be taken into account in design of CLT beams.

The study concluded that the relative widths of the longitudinal layers have a significant influence on the predicted stresses, and found difference in maximum predicted stress up to 60% for CLT element lay-ups which are commonly used in practice. The study also found that the assumption of equal torsional moments for all crossing areas in the beam height direction was inaccurate. The study proposed a new model showing that the lamination shear forces, the torsional moments and the torsional shear stresses have maximum values at the lamination/laminations closest to the beam centreline.

Danielsson et al. (2019) further developed on the model proposed by Flaig and Blaß (2013) especially related to the assumptions relating to the internal force distribution. Comparison between the two models was made using FE-analyses regarding magnitude and distribution of internal forces, especially as it pertains to the forces and torsional moments acting in the crossing areas between longitudinal and transversal laminations. The results showed that the analytical model by Danielsson and Serrano (2018) yielded predictions that were much closer to the predictions of the FE model compared with the analytical model by Flaig and Blaß (2013).

2.5.3 CLT Panels

Compared to the available knowledge associated with RVSE and beam theory, knowledge about CLT panels similar to those found in a CLT wall with openings is still limited. This is mainly attributed to the complexity associated with the panel's boundary conditions. As such, the work established based on the beam theory is not considered adequate to determine the shear stiffness and strength in the CLT panel. Kreuzinger and Sieder (2013) proposed an analytical approach for the CLT panels based on plane stress analysis, and assuming gross shear failure in the CLT panels. The work was later further developed by Brandner et al. (2017), where the shear distribution was analyzed, including the net shear failure in the CLT elements. The authors evaluated the net- and gross-shear strength and stiffness using an experimental study where CLT panels were subjected to a simple compression force on the top. Parametric analysis was executed by varying gap, layer width and thickness, number of layers, and laminate layup. It was found that the gap execution and layer thickness were the main parameters significantly influencing in-plane shear properties. The proposed analytical model was deemed suitable for beam elements taking additionally into account a reduced resistance of external layers due to shrinkage cracks.

2.5.4 Experimental investigations of CLT beams

Bejtka (2011) investigated the performance of CLT beams loaded in bending and by tensile stresses perpendicular to the grain direction. A new beam element with crosswise diagonally orientated elements (DLT) was investigated. To promote shear failure, short CLT and DLT beams were tested, while long beams were used to enforce bending failure. A finite element analysis was performed. It was demonstrated that DLT elements provide a higher performance than CLT elements for beams loaded in bending. The study did not provide general equations to calculate the strength and stiffness properties for CLT and DLT beams loaded in bending, but provided some insight to the use of finite element analysis to obatin reasonable representation of the beam behaviour.

To validate their analytical model, described in Section 1.5.2, Flaig and Blaß (2013) conducted tests and used experimental data of other researchers to determine the shear design of CLT-members loaded in-plane. The experimental results were compared with the proposed model and showed reasonable agreement. The tests confirmed that the effective shear strength of CLT-beams is strongly dependent on the cross-sectional arrangement and thickness ratio of longitudinal and transversal layers and on the width of lamellae. Further, tests validated the analytical expression showing that the effective shear stiffness of CLT-beams, like the effective shear strength, strongly depends on the width of lamellae and their cross-sectional arrangement.

Gagnon et al. (2014) conducted testing on 3- and 5-ply CLT beam elements to evaluate their in-plane shear strength using a testing method for structural composite lumber (SCL) elements. Span to depth ratio of 3:1 was used in order to promote shear failure mode. The results indicate that the existing test methods applicable to SCL may be suitable for evaluation of in-plane shear strength of CLT elements. The study also concluded that the in-plane shear strength could be determined using existing North American testing methods applicable to other wood products.

Katona et al. (2016) performed four-point bending tests on deep CLT beams to investigate the influence in the stresses at crossing areas of the lamellae direction and the corresponding thickness. The change in orientation of the outer and inner layers were investigated. The study found that the failure type was related to the internal geometry of the specimens. The results also showed that the governing failure modes were bending and shear. The bending failure typically initiated at a finger joint or knot.

2.6 Background Information on the Equivalent Frame Model Used in Masonry Structures

In the current study, an equivalent frame model is proposed for CLT shearwalls with openings, as described in detail in Chapter 5. The concept on EFM is not novel, as it has been used to analyze structural elements like masonry and concrete with similar geometrical layout as the CLT walls investigated as part of the current study. The main difference is the flexibility of the hold-down, which affects the behaviour significantly. This section provides a brief overview of the current state of knowledge on the EFM approach used in masonry structures.

The basic concept in the EFM is to represent the vertical wall segments (also known as piers) and lintel with one-dimensional frame elements, connected by rigid end-offsets. The deformability of the wall is assumed to be reflected in the frame elements, whereas the intersection zones (also known as nodes) are characterized by high stiffness. Augenti (2006) and Parisi and Augenti (2013) assumed that the height of the wall segments is equal to the opening height, whereas Dolce (1991) presented a criterion to define the flexible (or effective) height taking into account the interaction between the wall segments, lintel, and the nodes. Recent studies have shown that the assumptions related to the flexible length of the wall segments and lintels, as well as the dimension of nodes, have a significant effect on the results of the analyses (Siano et al. 2017). A threshold of the discrepancy of 15% between the EFM applied for masonry multi-storey shearwalls and corresponding detailed finite element models was considered to estimate the efficiency of the EFM (Siano et al., 2017).

References of Chapter 2

AWC. (2015). National Design Specification for Wood Construction American Wood Coucil.

Bejtka, Ireneusz. (2011). *Cross (CLT) and diagonal (DLT) laminated timber as innovative ma-terial for beam elements*. Retrieved from http://dx.doi.org/10.5445/KSP/1000021129

Bogensperger, Thomas, Moosbrugger, Thomas, & Silly, Gregor. (2010). *Verification of CLT-plates under loads in plane.* Paper presented at the 11th World Conference on Timber Engineering 2010, WCTE 2010, June 20, 2010 - June 24, 2010, Trentino, Italy.

Brandner, Reinhard, Dietsch, Philipp, Dröscher, Julia, Schulte-Wrede, Michael, Kreuzinger, Heinrich, & Sieder, Mike. (2017). Cross laminated timber (CLT) diaphragms under shear: Test configuration, properties and design. *Construction and Building Materials, 147*, 312-327. doi:https://doi.org/10.1016/j.conbuildmat.2017.04.153

Casagrande, Daniele, Doudak, Ghasan, Mauro, Luigi, & Polastri, Andrea. (2018). Analytical Approach to Establishing the Elastic Behavior of Multipanel CLT Shear Walls Subjected to Lateral Loads. *Journal of Structural Engineering, 144*(2), 04017193. doi:doi:10.1061/(ASCE)ST.1943-541X.0001948

CSA. (2014). CSA Standard O86-14, Engineering design in wood: CSA Group.

Danielsson, Henrik, Jeleč, Mario, Serrano, Erik, & Rajčić, Vlatka. (2019). Cross laminated timber at in-plane beam loading – Comparison of model predictions and FE-analyses. *Engineering Structures, 179*, 246-254. doi:https://doi.org/10.1016/j.engstruct.2018.10.068

Danielsson, Henrik, & Serrano, Erik. (2018). Cross laminated timber at in-plane beam loading – Prediction of shear stresses in crossing areas. *Engineering Structures, 171*, 921-927. doi:https://doi.org/10.1016/j.engstruct.2018.03.018

Deng, Peng, Pei, Shiling, van de Lindt, John W., Omar Amini, M., & Liu, Hongyan. (2019). Lateral behaviour of panelized CLT walls: A pushover analysis based on minimal resistance assumption. *Engineering Structures, 191*, 469-478. doi:https://doi.org/10.1016/j.engstruct.2019.04.080

Dujic, Bruno, Aicher, Simon, & Zarnić, Roko. (2005). Investigation on in-plane loaded wooden elements-influence of loading on boundary conditions. *Otto-Graf-Journal, 16*, 259-272.

Dujic, Bruno, Klobcar, Simona , & Zarnić, Roko. (2017). *Shear Capacity of Cross-Laminated Wooden Walls*.

Flaig, Marcus, & Blaß, Hans Joachim. (2013). *Shear strength and shear stiffness of CLT-beams loaded in plane.* Paper presented at the Proceedings of the International Council for Research and Innovation in Building and Construction, Working Commission W18 - Timber Structures, Meeting 46, Vancouver, Canada, 26 August - 29 August 2013. Ed.: R. Görlacher.

Gagnon, Sylvain, Mohammad, Mohammad, Toro, Williams Munoz, & Popovski, Marjan. (2014). *Evaluation of the in-plane shear strength of CLT.* Paper presented at the World Conference on Timber Engineering: Renaissance of Timber Construction, WCTE 2014, August 10, 2014 - August 14, 2014, Quebec City, QC, Canada.

Gavric, Igor, Fragiacomo, Massimo, & Ceccotti, Ario. (2015). Cyclic Behavior of CLT Wall Systems: Experimental Tests and Analytical Prediction Models. *Journal of Structural Engineering, 141*(11), 04015034. doi:doi:10.1061/(ASCE)ST.1943-541X.0001246

Hristovski, Viktor, Mircevska, Violeta, Dujic, Bruno, & Garevski, Mihail. (2018). Comparative dynamic investigation of cross-laminated wooden panel systems: Shaking-table tests and analysis. *Advances in Structural Engineering, 21*(10), 1421-1436. doi:10.1177/1369433217749766

Hummel, Johannes, Flatscher, Georg, Seim, Werner, & Schickhofer, Gerhard. (2013). *CLT Wall Elements Under Cyclic Loading - Details for Anchorage and Connection*. Paper presented at the COST Action FP1004, Focus solid timber solutions – European Conference on Cross Laminated Timber (CLT), Graz, Austria.

Izzi, Matteo, Polastri, Andrea, & Fragiacomo, Massimo. (2018). Investigating the Hysteretic Behavior of Cross-Laminated Timber Wall Systems due to Connections. *Journal of Structural Engineering, 144*(5), 04018035. doi:doi:10.1061/(ASCE)ST.1943-541X.0002022

Katona, O., Klas, Tomáš, Duchoň, V., Brodniansky, Ján, Balcierák, Ľ, & Sandanus, Jaroslav. (2016). *Experimental study of a four-point bending test on CLT deep beams*.

Kreuzinger, Heinrich, & Sieder, Mike. (2013). Einfaches Prüfverfahren zur Bewertung der Schubfestigkeit von Kreuzlagenholz/Brettsperrholz. *Bautechnik, 90*(5), 314-316. doi:doi:10.1002/bate.201300024

Moosbrugger, Thomas, Guggenberger, Werner, & Bogensperger, Thomas. (2006). *Cross-laminated timber wall segments under homogeneous shear - With and without openings*. Paper presented at the 9th World Conference on Timber Engineering 2006, WCTE 2006, August 6, 2006 - August 10, 2006, Portland, OR, United states.

Nolet, Vincent, Casagrande, Daniele, & Doudak, Ghasan. (2019). Multipanel CLT shearwalls: an analytical methodology to predict the elastic-plastic behaviour. *Engineering Structures, 179*, 640-654. doi:https://doi.org/10.1016/j.engstruct.2018.11.017

Oh, Jung-Kwon, Hong, Jung-Pyo, Kim, Chul-Ki, Pang, Sung-Jun, Lee, Sang-Joon, & Lee, Jun-Jae. (2017). Shear behaviour of cross-laminated timber wall consisting of small panels. *Journal of Wood Science, 63*(1), 45-55. doi:10.1007/s10086-016-1591-2

Okabe, M , Yasumura, M, Kobayashi, K, Haramiishi, T, Nakashima, Y, & Fujita, K. (2012). *Effect of vertical load under cyclic lateral load test for evaluating Sugi CLT wall panel*. Paper presented at the World Conference on Timber Engineering (WCTE), Auckland, New Zealand.

Pai, Sai Ganesh S., Lam, Frank, & Haukaas, Terje. (2017). Force Transfer around Openings in Cross-Laminated Timber Shear Walls. *Journal of Structural Engineering, 143*(4), 04016215. doi:doi:10.1061/(ASCE)ST.1943-541X.0001674

Popovski, Marjan, Schneider, Johannes, & Schweinsteiger, Matthias. (2010). *Lateral load resistance of cross-laminated wood panels*.

Pozza, Luca, Scotta, Roberto, Trutalli, Davide, & Polastri, Andrea. (2015). Behaviour factor for innovative massive timber shear walls. *Bulletin of Earthquake Engineering, 13*(11), 3449-3469. doi:10.1007/s10518-015-9765-7

Reynolds, Thomas, Foster, Robert, Bregulla, Julie, Chang, Wen-Shao, Harris, Richard, & Ramage, Michael. (2017). Lateral-Load Resistance of Cross-Laminated Timber Shear Walls. *Journal of Structural Engineering, 143*(12), 06017006. doi:doi:10.1061/(ASCE)ST.1943-541X.0001912

Rinaldin, Giovanni, Amadio, Claudio, & Fragiacomo, Massimo. (2013). A component approach for the hysteretic behaviour of connections in cross-laminated wooden structures. *Earthquake Engineering & Structural Dynamics, 42*(13), 2023-2042. doi:doi:10.1002/eqe.2310

Shahnewaz, Ida, Tannert, Thomas, Shahria Alam, M., & Popovski, Marjan. (2017). In-Plane Stiffness of Cross-Laminated Timber Panels with Openings. *Structural Engineering International, 27*(2), 217-223. doi:10.2749/101686617X14881932436131

Shahnewaz, Md, Alam, Shahria, Tannert, Thomas . In-Plane Strength and Stiffness of Cross-Laminated Timber Shear Walls. Buildings. 2018;8:100.

Siano, Rossella, Sepe, Vincenzo, Camata, Guido, Spacone, Enrico, Roca, Pere, & Pelà, Luca. (2017). *Analysis of the performance in the linear field of Equivalent-Frame Models for Regular and Irregular Masonry Walls* (Vol. 145).

CHAPTER 3

Elastic analysis

3.1 General

This chapter presents the methodology and results from an elastic analysis to investigate the key parameters affecting the behaviour of CLT walls with window or door openings, centrally placed within the wall.

Based on the review of the available literature, it was found that rocking mode typically dominate the response of CLT shearwalls subjected to lateral loading, and that the kinematic behaviour of the wall depends primarily on the behaviour of the mechanical anchors. Limited studies have focussed on the kinematic behaviour of CLT shearwalls with openings, and no study, to the author's knowledge has investigated the coupling effect due to the presence of the lintel beam connecting the vertical wall segments.

The current study aims to investigate the influence of geometrical dimensions of the lintel, wall segments, lamella layup and hold-down stiffness and configuration on the elastic behaviour of the wall assembly. Also, the effect of hold-down on the kinematic behaviour of the walls will be investigated and discussed.

3.2 Description of the Numerical Model and Analyses

The elastic behaviour of CLT shearwalls with openings was investigated using finite element (FE) models developed with the commercially available software SAP2000 (CSI, 2017). The CLT panels were modelled using four-node quadrilateral area elements, and multi-linear links (spring elements) were used to model the mechanical anchors with unidirectional tension-compression properties.

The geometry and panel dimensions were selected based on practical sizes used in construction. In total, one hundred twenty-six (126) wall configurations with different height-to-length aspect ratios were investigated (Figure 3-1). For configurations with door openings, $2.8\,m$ was used as the height of the wall segments (h_O). For layout configurations with window openings, the height of wall segments (h_O) were equal to $1.8\,m$ and the height of the parapet (h_C) was set to $1.0\,m$. Lintel length (l) values of $[0.8;\ 1.2;\ 1.6;\ 2; 2.4;\ 2.8; 3.2]$ m were considered, while the values of the lintel height (h_L) were equal to $[0.4;\ 0.8;\ 1.2]$ m. The vertical wall segment's width (b) was assigned values of $[0.8;\ 1.4;\ 2.8]$ m.

One CLT panel thickness of 100 mm is included in this chapter. The same analysis was conducted on CLT panels with 150 mm with the same transversal to longitudinal thickness ratio equal to 0.67 and generally it was found that the total wall thickness affects the kinematic behaviour of the shearwalls. The most significant results are presented in this chapter, however the detailed results from this analysis are included in Appendix A.

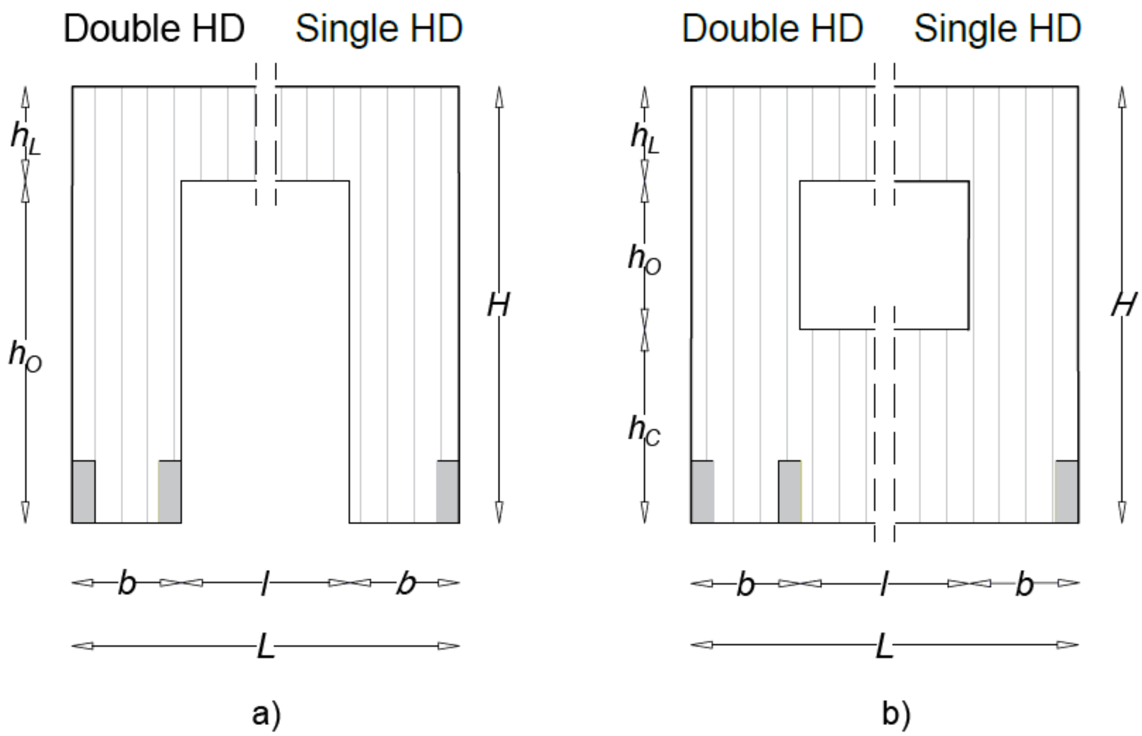

Figure 3-1. Geometric configuration of the analyzed shearwalls for a) walls with door openings and b) walls with window openings

The major direction of the CLT panels was assumed to be in the vertical direction. Values for the modulus of elasticity (MOE) in the directions parallel and perpendicular to grain, E_0, and E_{90}, of 12000 MPa and 500 MPa, respectively were selected according to ETA-12/0347 (2017). An equivalent orthotropic material model was adopted to obtain equivalent moduli of elasticity, used as inputs in the model for the area elements, based on the work developed by (Blass & Fellmoser, 2004; Mestar et al., 2020). A value of $E_{eq,v} = 7200MPa$ was obtained in the vertical direction, while $E_{eq,h} = 4800\ MPa$ was obtained in the horizontal direction. An equivalent shear modulus of $G_{eq} = 500MPa$ was used to take into account the in-plane shear and torsional deformability of the CLT lamellae (Brandner et al., 2017).

The mechanical anchors were modelled using uniaxial link elements. The hold-downs were represented by vertical link elements located at the ends of the wall segments, while the angle brackets were represented by a horizontal link element located at the centre of each wall segment. The vertical stiffness of the angle brackets is assumed to be included in the hold-down stiffness, and therefore, their effect on the kinematic modes and degrees of coupling is considered. Figure 3-2 illustrates the mechanical parameters used in the proposed model.

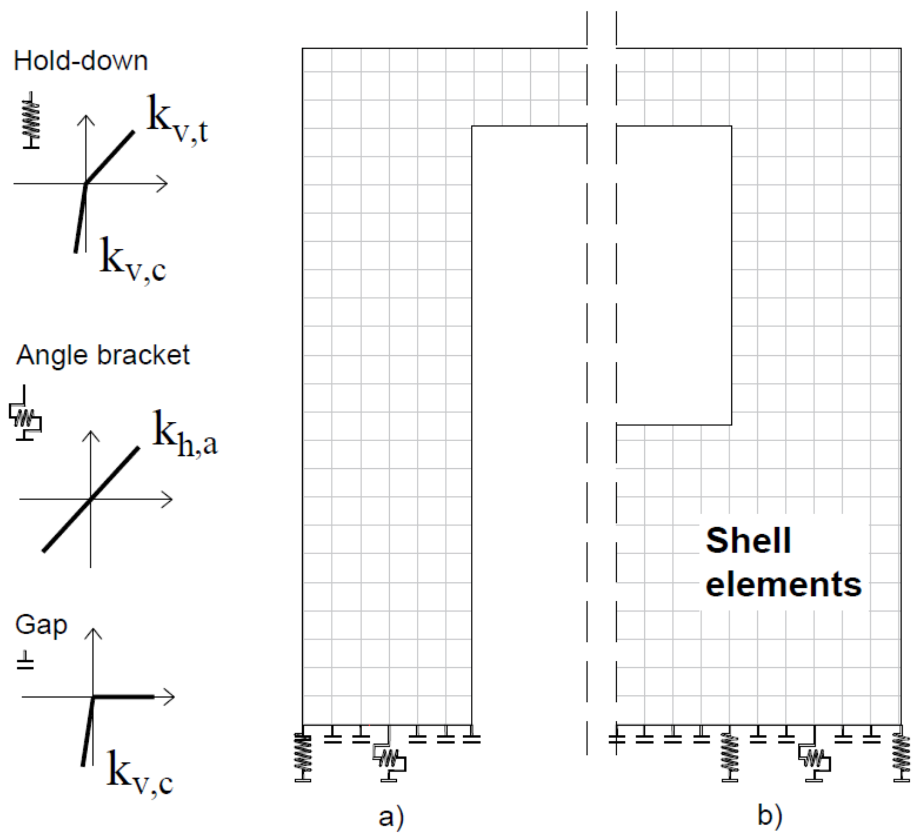

Figure 3-2. FE model for CLT shearwalls with door (a) and window (b) openings

The stiffness of the link elements representing the hold-down and the angle brackets in the vertical and horizontal directions are denoted k_v and k_h, respectively. The stiffness of hold-down along the vertical direction is non-linear even in the elastic phase, due to the contact between the wall panels and the base. The compressive and tensile stiffness in the hold-down are defined as $k_{v,c}$ and $k_{v,t}$, respectively. Three values are considered for the tensile stiffness of the hold-downs, namely $k_{v,t} = 8, 14$ and $20\ kN/mm$ whereas an arbitrarily high value equal to $k_{v,c} = 10^6\ kN/mm$ was assigned to the compressive stiffness, to represent contact with the base. The stiffness values for the tensile stiffness reflect the range observed during experimental testing (Gavric et al., 2015). The prediction curves for the hold-downs from Casagrande et al. (2016) are used.

The tensile vertical stiffness of the angle brackets $k_{v,t,a}$ is assumed to be included in the equivalent hold-down tensile stiffness $k_{v,t}$, and therefore the effect of angle brackets on the kinematic modes and degrees of coupling is considered. The mathematical expression to determine the equivalent vertical stiffness $k_{v,t}$, which includes the vertical stiffness of the hold-down $k_{v,t,hd}$ and angle brackets $k_{v,t,a}$ is presented next.

Assuming a series of *N* angle brackets a_1, a_2, a_3, N located at a distance $\alpha \cdot x_1, \alpha \cdot x_2, \alpha \cdot x_3, N$ from the centre of rotation and assuming that the hold-down is located at a distance $\alpha \cdot l$, as shown in Figure 3-3, where α, takes into account the effective distance of the connectors relative to the centre of rotation.

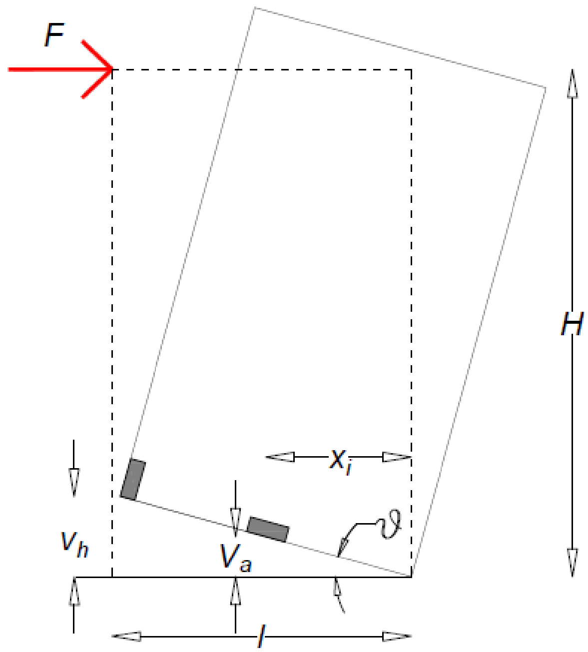

Figure 3-3. Equivalent vertical stiffness of the connectors

The condition of equilibrium under the resulting forces can be expressed by the sum of the moments about (O) as reported in Equation 3-1:

$$F \cdot H = T_H \cdot (\alpha \cdot l) + \sum_{i=1}^{N} T_{a_i} \cdot \alpha \cdot x_i \qquad (3\text{-}1)$$

where T_H is the tensile force in hold-down and T_{a_i} is the tensile force in the angle bracket.

Assuming an angle of rotation ϑ of the wall and a triangular distribution of the tensile load in the angle brackets, the vertical displacement in the i^{th} angle bracket $v_{a,i}$ and in the hold-down v_h can be expressed as:

$$v_{a,i} = \vartheta \cdot \alpha \cdot x_i \; ; \; v_h = \vartheta \cdot \alpha \cdot l \qquad (3\text{-}2)$$

Substituting Equation 3-2 in Equation 3-1, one obtains:

$$F \cdot H = k_{v,t,hd} \cdot \vartheta \cdot (\alpha \cdot l)^2 + \sum_{i=1}^{N} k_{v,t,a,i} \cdot (\alpha \cdot x_i)^2 \cdot \vartheta \qquad (3\text{-}3)$$

The rotation of the wall can hence be calculated as:

$$\vartheta = \frac{F \cdot H}{(\alpha \cdot l)^2 \cdot k_{v,t}} \quad (3\text{-}4)$$

where the equivalent vertical stiffness of the hold-down $k_{v,t}$ is:

$$k_{v,t} = k_{v,t,hd} + \sum_{i=1}^{N} \frac{k_{v,t,a,i} \cdot x_i^2}{l^2} \qquad (3\text{-}5)$$

Where an anchor is omitted, the equivalent spring is replaced with a contact element (i.e. gap element) with zero-stiffness in tension and a stiffness equal to $k_{v,c}$ in compression. For the horizontal stiffness of the spring representing the angle brackets, a value of $k_h = 15\ kN/mm$ was adopted. The gravity effect was also considered in the analyses with a uniform line load of $20\ kN/m$.

A displacement control method was used in the FE analyses, where a lateral displacement of 10 mm was applied to the joints of the area elements at the top of the walls following the application of the vertical load.

3.3 Results and discussions

3.3.1 Kinematic modes

The slenderness of the wall segments and lintel beam denoted λ_w and λ_l, respectively, are defined in Equation 3-6 for walls with door openings and Equations 3-7 to 3-8 for walls with window openings, based on notations found in Figure 3-1.

$$\lambda_w = \frac{h_O}{b} \tag{3-6}$$

$$\lambda_w = \frac{h_O + h_C}{b} \tag{3-7}$$

$$\lambda_l = \frac{l}{h_L} \tag{3-8}$$

The methodology adopted to represent the two possible kinematic behaviours, i.e *i)* one centre of rotation for the entire wall or *ii)* one centre of rotation for each segment, is shown in Figure 3-4. In this figure, the slenderness of the wall segment is plotted as a function of lintel slenderness representing the kinematic behaviour found for each wall configuration. For each hold-down stiffness, the two possible kinematic behaviour were represented by the two slenderness. In doing so, two different zones representing cases i) and ii) can be used in order to predict the kinematic behaviour of CLT shearwalls. The delineation between the two zones is indicated by a bilinear curve.

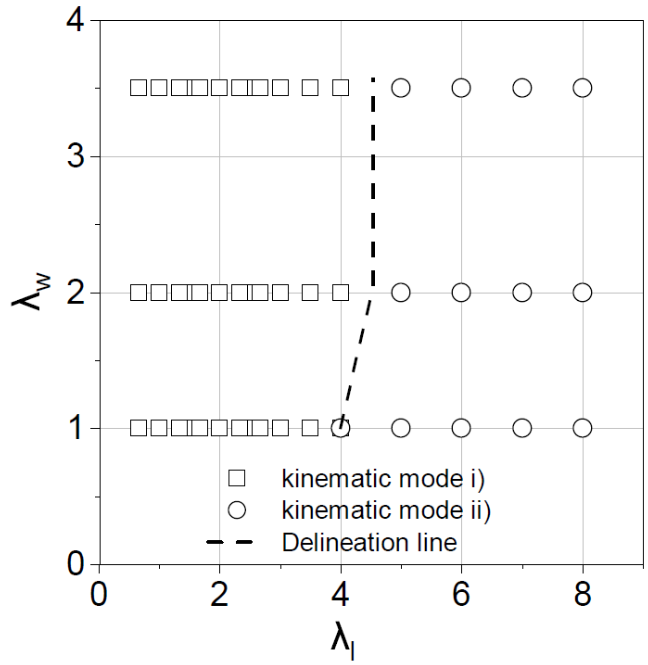

Figure 3-4. Methodology adopted to represent the two possible kinematic behaviours

Based on the methodology outlined in Figure 3-4, the global kinematic behaviour for the single and double hold-down configurations is presented in Figure 3-5 for case without vertical load, for 100 mm wall thickness.

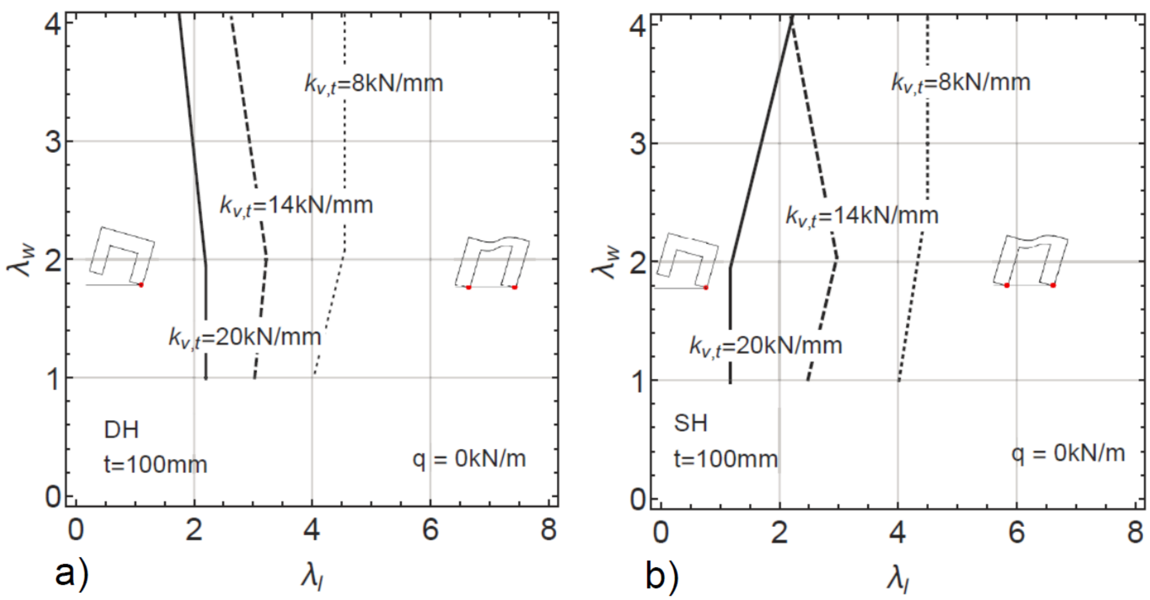

Figure 3-5. Kinematic behaviours for CLT shearwalls without vertical load effect using (a) DH and (b) SH configuration

In general, it is observed that the wall segment slenderness (λ_w) has little to moderate effect, whereas the lintel slenderness (λ_l) has relatively a very significant effect on global kinematic behaviour. The hold-down stiffness appears to play a significant role in the global kinematic behaviour, where it can be observed that higher hold-down stiffness leads to a greater number of cases with one centre of rotation for each segment, i.e. shifting the delineation lines to the left in Figures 3-5.

The results also show that the hold-down layout configuration (i.e. SH or DH) has no significant effect on the global kinematic behaviour for low values of hold-downs stiffness encountered in practice ($k_{v,t} = 8\ kN/mm$). A small effect is observed for higher hold-downs stiffness ($k_{v,t} = 14kN/mm\ and\ 20\ kN/mm$) as more cases with one centre of rotation for each segment are observed.

The results from the analysis also show that the wall thickness has a significant effect on the kinematic behaviour of the walls. More cases of kinematic mode 1 (i-e: 1 centre of rotation) were observed for walls with 150 mm thickness, which can mainly be attributed to the increase in the effective thickness of the horizontal lamellae in the lintel beam. It can be noted that the influence of the wall thickness on the kinematic behaviour is decreasing with increasing hold-down stiffness, as shown in Figure 3-6.

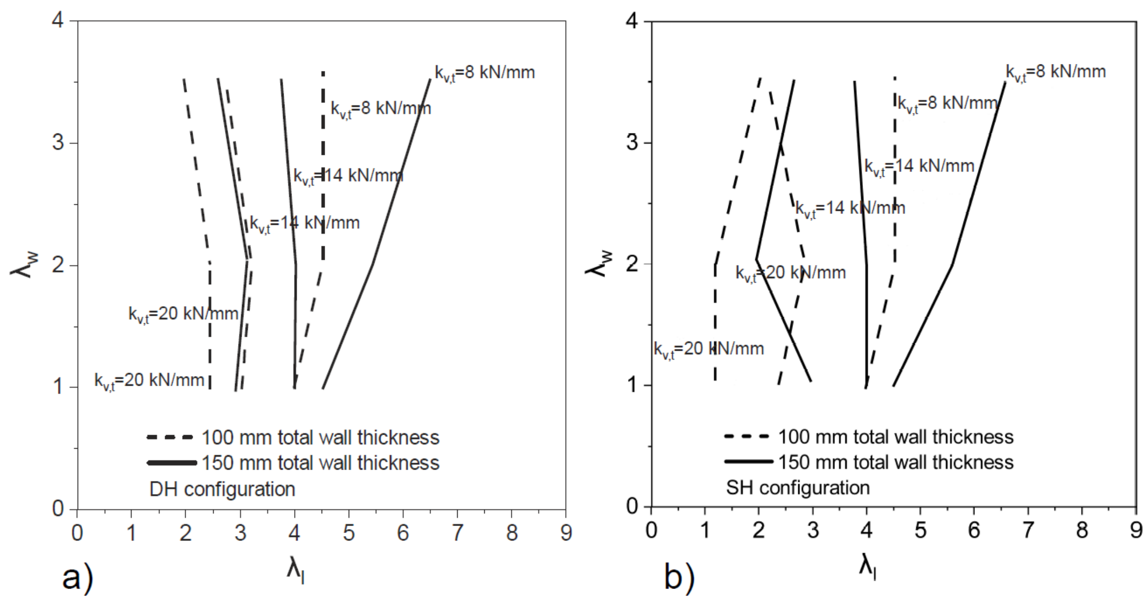

Figure 3-6. Effect of wall thickness in the kinematic behaviour

As expected, the region containing the cases with one centre of rotation for each segment considerably increased, for both SH and DH configurations, when vertical load was applied, which can be attributed to the stabilizing effect of the vertical load. The effect of vertical load was much less significant for walls with 150 mm thickness, and therefore only results for 100 mm wall thickness are presented in Figure 3-7. The application of the vertical load caused the delineation curves to shift to a lintel slenderness value approximately equal to unity ($\lambda_l = 1$).

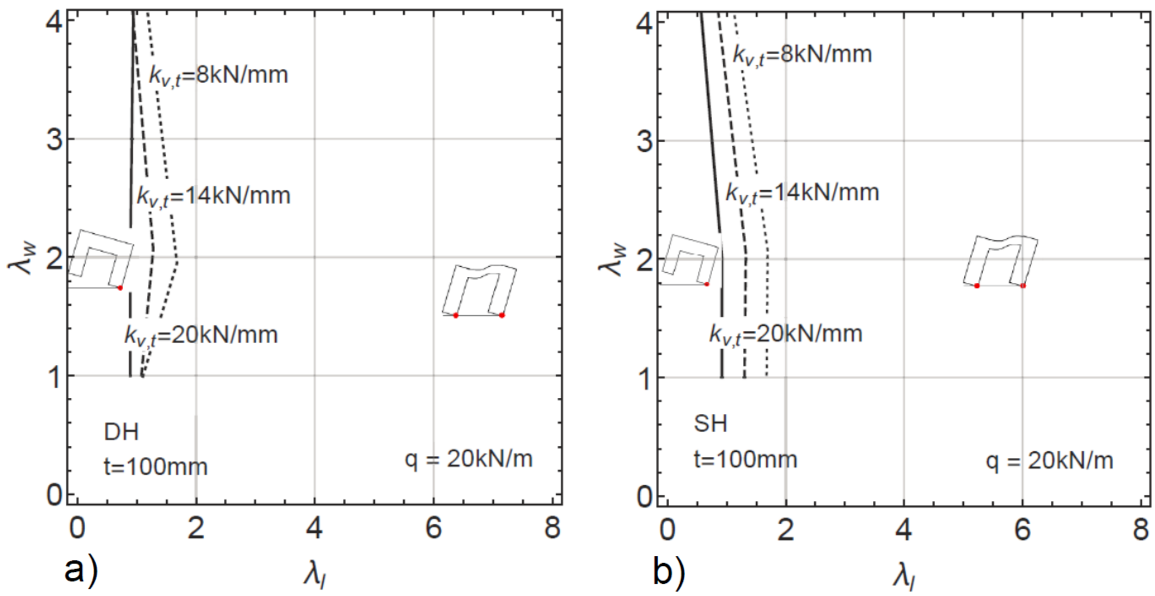

Figure 3-7. Kinematic behaviours for CLT shearwalls with vertical load effect using DH (a) and SH (b)

For all analyzed cases with window opening, only one global kinematic behaviour, consisting of walls with one centre of rotation for the entire wall (*case i*), was observed. This is due to the strong effect of the bottom lintel on the overall stiffness of the walls.

3.3.2 Effect of double and single hold-down configuration on the hold-down tensile load and on the base shear

The results from numerical models introduced in section 3.2 are used to determine the effect of double and single hold-down configurations on the base shear and the hold-down tensile load, for shearwalls with both window and door openings. The discussion in this section is limited to walls with 100 mm thickness only.

3.3.2.1 Effect on the tensile load in the hold-down

The ratio of the tensile load in the outermost hold-down resulting from single and double hold-down configurations, T_{SH}/T_{DH}, is presented as a function of the lintel length, l, in Figure 3-8 and Figure 3-9 for walls with door and window openings, respectively. For all cases, the range of T_{SH}/T_{DH} ratios are observed to be between 1.00 and 1.20 for shearwall with door openings and between 1.10 and 1.40 for shearwalls with window openings.

Generally, the magnitude of the ratio is decreasing with hold-down stiffness and increasing with the lintel height. However, the shape of the curves representing the trends is different for different values of the lintel height h_L. For lintels with height equal to $0.4\,\mathrm{m}$ and stiffness of the hold-down of $8\mathrm{kN/mm}$, the ratio is decreasing with the lintel length until reaching an aspect ratio of about 0.4 (h_L of 2m), where it remains relatively constant (Figure 3-8a). When the hold-down stiffness is increased to $14\mathrm{kN/mm}$ (Figure 3-8d), the ratio decreases with lintel length until reaching an aspect ratio of about 0.5 (h_L of 1.2m). For stiffer hold-downs ($20\mathrm{kN/mm}$), the ratio is relatively constant for any value of lintel length (Figure 3-8g). For lintels with height equal to 0.8m, the T_{SH}/T_{DH} ratio follows, in general, similar trends to that described for lintel beams with height equal to 0.4 m (Figure 3-8b, e, and h), especially when the hold-down stiffness is relatively high.

The results from the lintels with height equal to 1.2m show that the ratio increases until reaching an aspect ratio of about 0.4 to 0.5 (h_L of $1.5\ to\ 2.5m$) and then decreases with lintel length for low and moderate hold-down stiffness ($8\ and\ 14kN/mm$) (Figures 3-8c and 8f). However, the results only show a descending pattern for high hold-down stiffness ($20kN/mm$) (Figure 3-8i). Interestingly, the sudden changes in the behaviour could be attributed to change in the kinematic modes as shown in Figure 3-8, where “1” indicates one-centre of rotation and “2” indicates two-centre of rotations.

For walls with window openings (Figure 3-9), the ratio T_{SH}/T_{DH} increases with lintel length, except for the case with lintel height equal to 0.4 m, hold-down stiffness equal to 20 kN/mm and width of wall segment equal to 2.8 m (Figure 3-9g).

The results show that hold-down configuration is more significant for cases of shearwalls with window openings than with door openings.

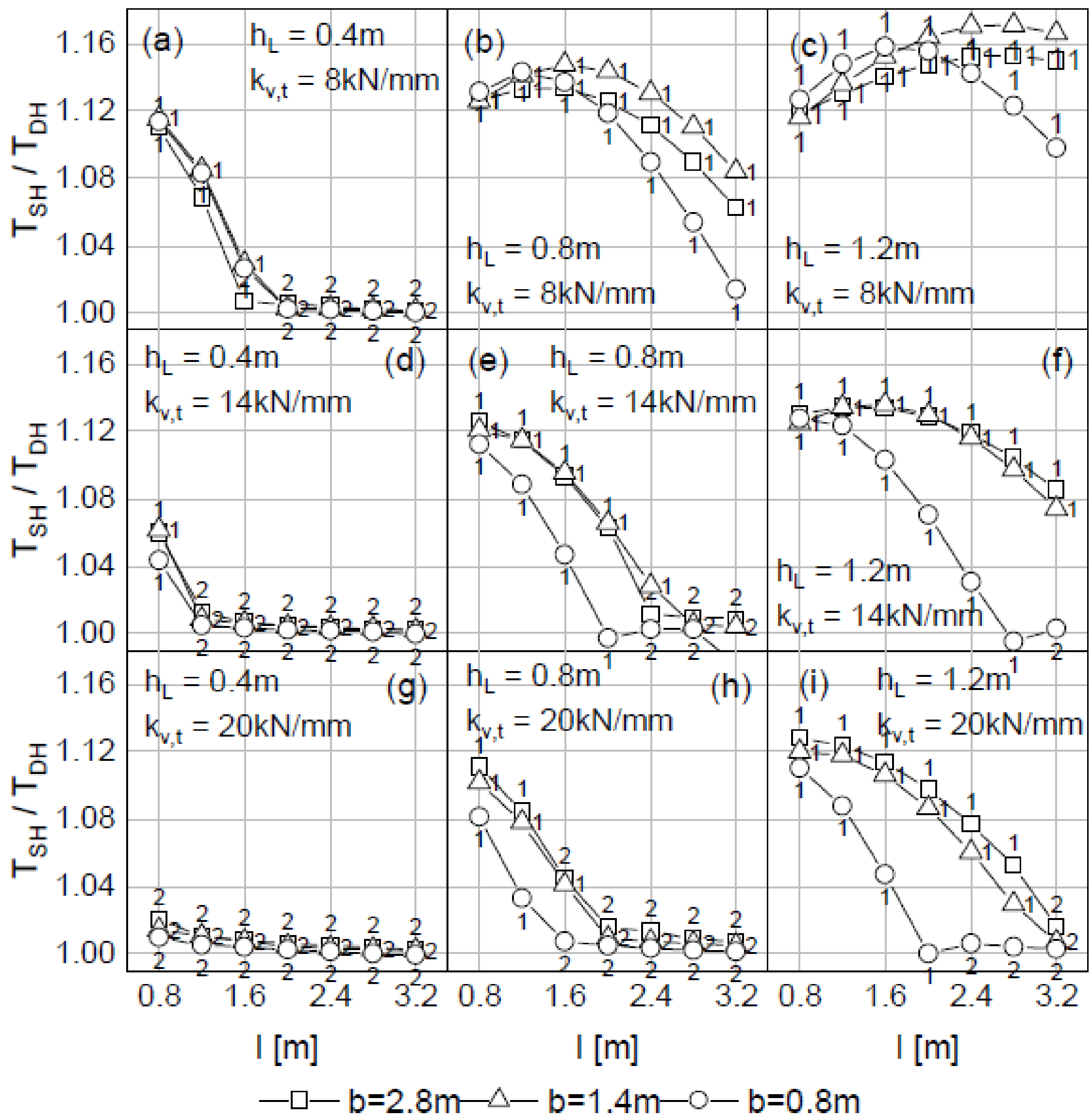

Figure 3-8. Ratio of the tensile load in the outermost hold-down between SH and DH configuration for shearwalls with door openings

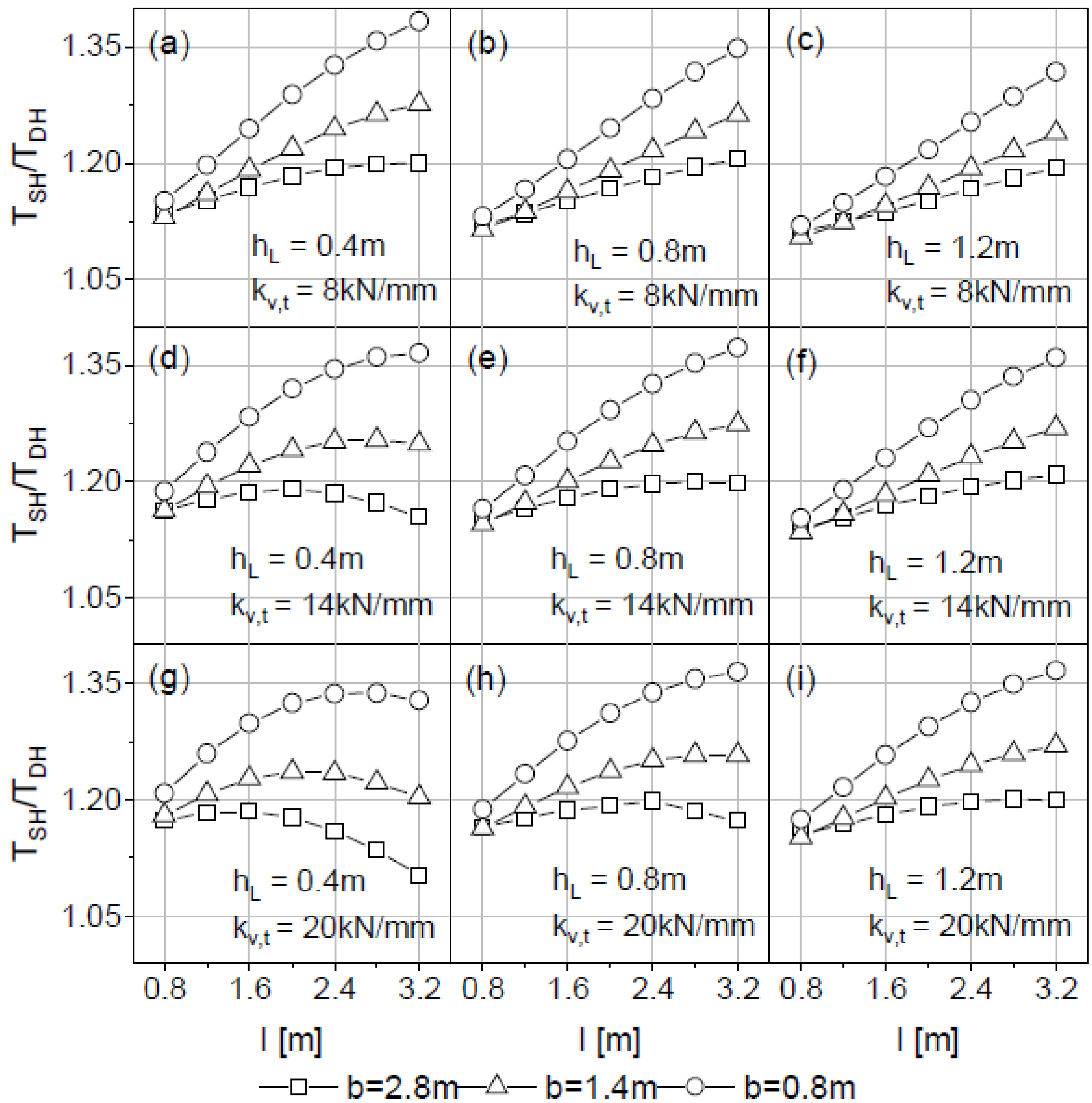

Figure 3-9. Ratio of the tensile load in the outermost hold-down between SH and DH configuration for shearwalls with window openings

3.3.2.2 Effect on the base shear of shearwalls

The ratio, V_{SH}/V_{DH}, between the base shear resulting from single and double hold-down configuration is presented in Figure 3-10 and 3-11 for walls with door and window openings, respectively.

For lintel beams with height equal to 0.4m the ratio is decreasing with lintel length within a range of 0.6 and 0.9 depending on the hold-down stiffness and the wall segment length (Figures 3-10a, d and g). For lintel beams with height equal to 0.8 m and 1.2m, the range is between 0.8 and 0.9. The reduction of the ratio in base shear appears insensitive to the hold-down stiffness, lintel length and wall segment length (Figures 3-10b, c, e, f, h and i).

For shearwalls with window openings, the ratio of V_{SH}/V_{DH} is linearly increasing between values of 0.8 and 0.9 in the range of lintel lengths investigated. The wall segment length appears to have no significant effect on the base shear (Figure 3-11).

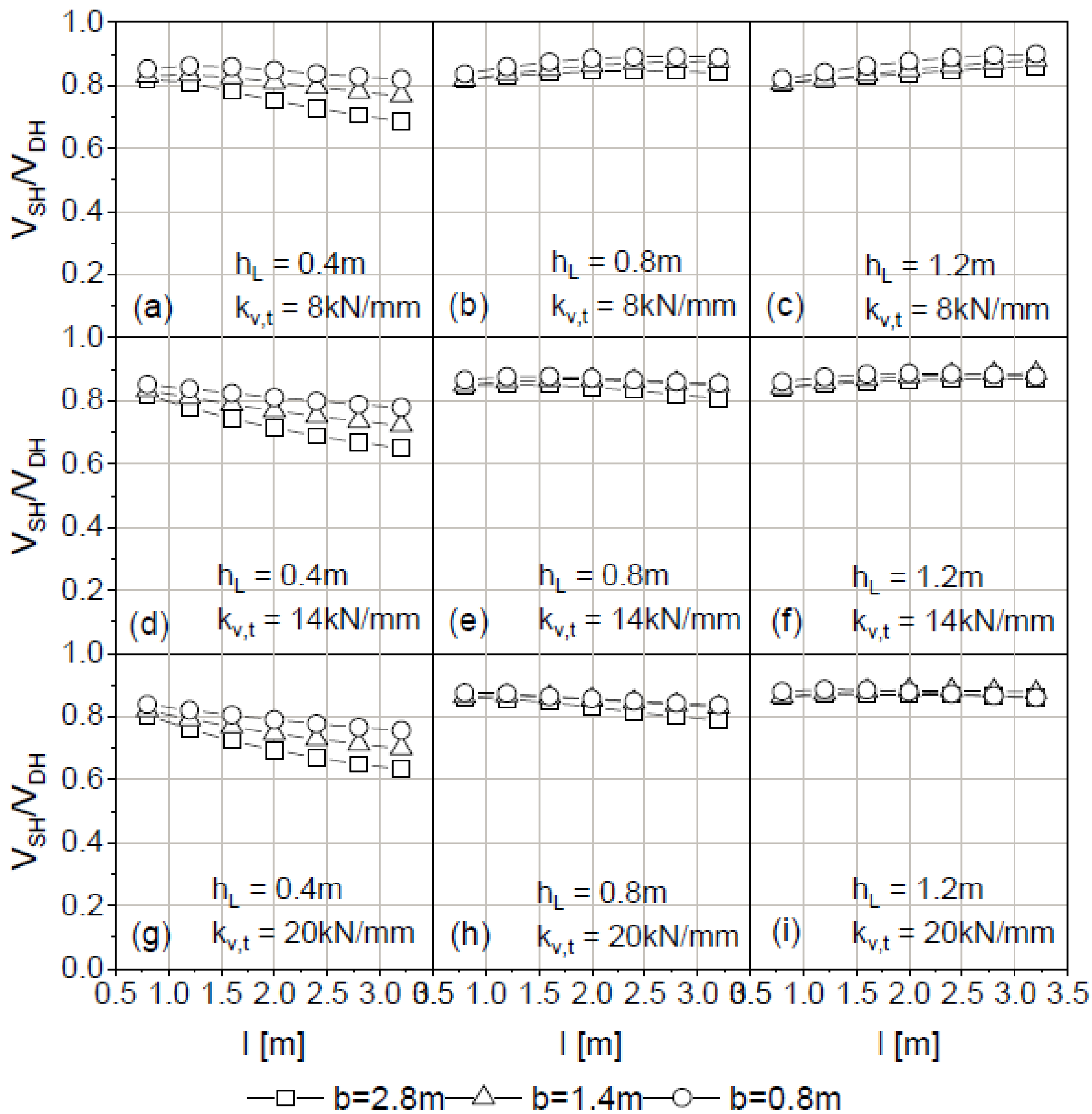

Figure 3-10. Ratio of the base shear for shearwalls with door openings

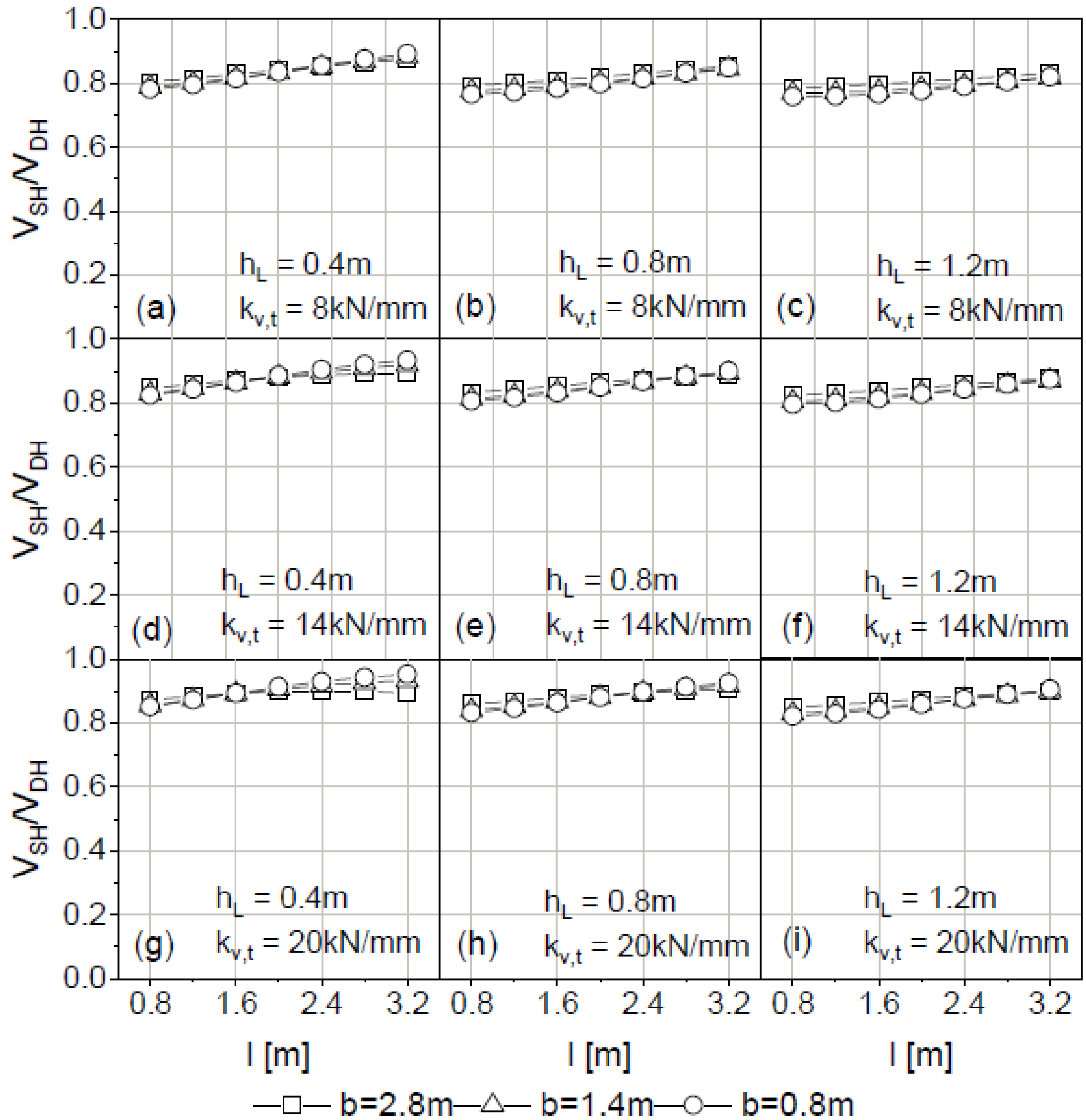

Figure 3-11. Ratio of the base shear for shearwalls with window openings

3.4 Degree of coupling (DC)

The degree of coupling (DC) is defined as ratio of the coupling moment ($T \cdot l_{l,a}$), which is produced by the axial forces T in the vertical wall segments, and the global overturning moment (M_o) acting on the shearwall (Paulay, 1972), as presented in Equation 3-9.

$$DC = \frac{T \cdot l_{l,a}}{M_O} = \frac{T \cdot l_{l,a}}{T \cdot l_{l,a} + M_1 + M_2} \quad (3\text{-}9)$$

where M_1 and M_2 are the bending moment at the base of each wall segment, as shown in Figure 3-12.

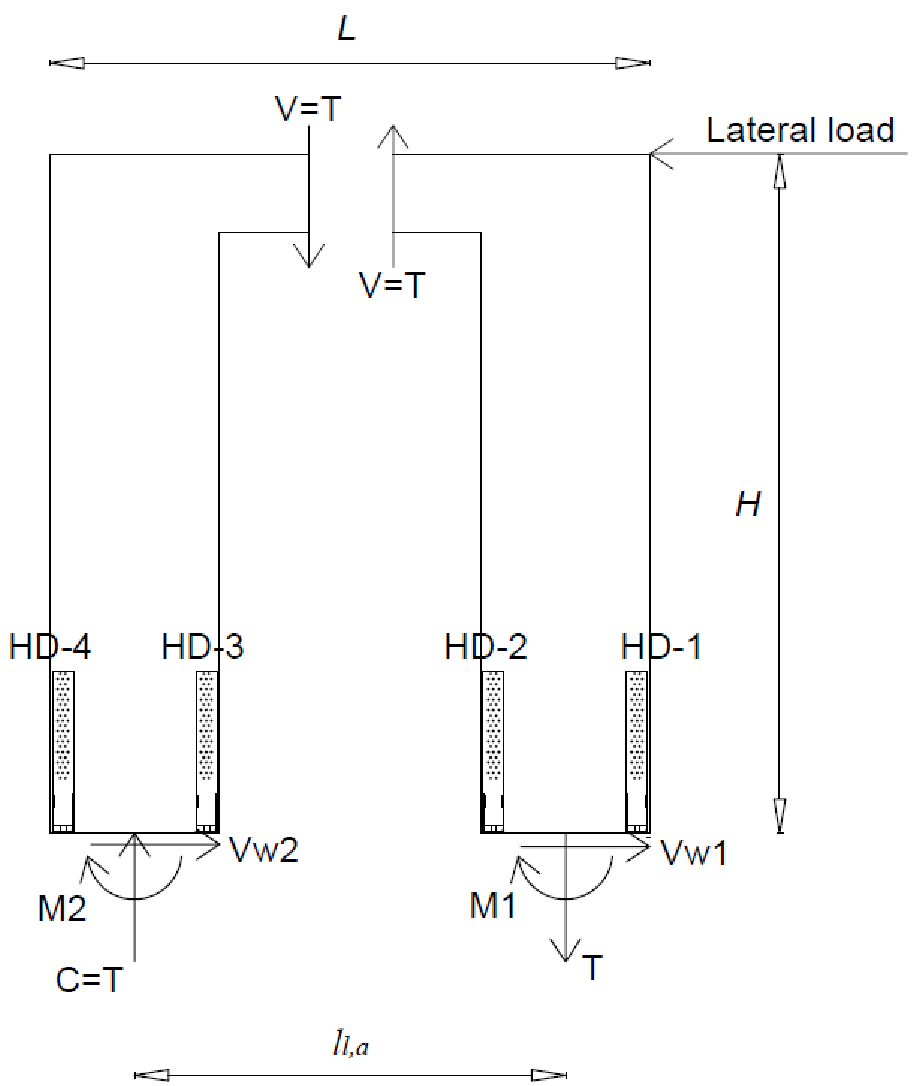

Figure 3-12. Principle of coupling effect in CLT shearwalls with openings

The degree of coupling of the sixty-three (63) cases was investigated for walls with 100 mm thickness, lintel beam height of 0.4, 0.8 and 1.2m and hold-down stiffness of 8, 14 and 20 kN/mm, and plotted in Figure 3-13 as a function of the lintel slenderness. The axial forces, T, in the vertical wall segments and the global overturning moment, M_o, were obtained from the FE model by means of the 'section cut' function available in SAP2000. This allows the integration of the internal forces per unit length of the area elements for a given cross section.

Figure 3-13 shows that the DC decreases with increased hold-down stiffness, $k_{v,t}$, and wall segment width, b. The higher the hold-down stiffness, the higher is the ratio of relative stiffness between the wall segments and lintel.

Two distinct zones, delineated by a transition line, can be observed in Figure 3-13. These represent the two global kinematic behaviours discussed in Section 3.3.1. The transition limit occurs at $\lambda_l = 4,$ 3 and 2 for hold-down stiffness of 8, 14 and 20 kN/mm, respectively. In the zone containing one centre rotation for the entire wall, the DC increases with the lintel slenderness due to resulting increase in the lintel length. This implies that the contribution from the coupling moment, $T \cdot l$, is more dominant than the overturning moment on each wall segment. In the zone containing one centre rotation for each wall segment, the results show, as expected, a decreasing tendency of the DC with increased lintel beam slenderness.

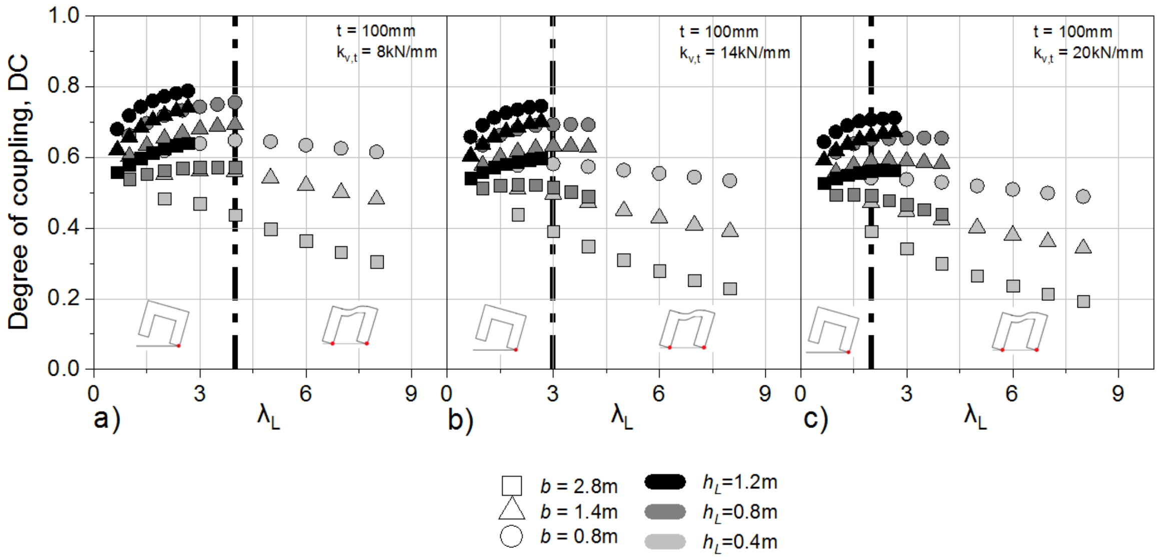

Figure 3-13. Degree of coupling DC for shearwall of 100 mm thickness (5x20mm) and different HD stiffness

3.5 Effect of Opening on the Base Shear Load

Introducing an opening in a CLT wall is expected to influence the overall wall behaviour. Results from the developed model were used to investigate the effect of openings and compare them to the case with no opening for all studied cases. Figure 3-14 shows an example of the percentage difference between the two cases (Δ_{BS}) for cases with double hold-down and hold-down stiffness equal to 6609 kN/m. As expected, the difference is more significant in the case of walls with door openings (up to -64%) compared to those with window openings (up to -26%). The results also show that the reduction in base shear becomes greater the higher the slenderness ratios are for both the wall segment and the lintel.

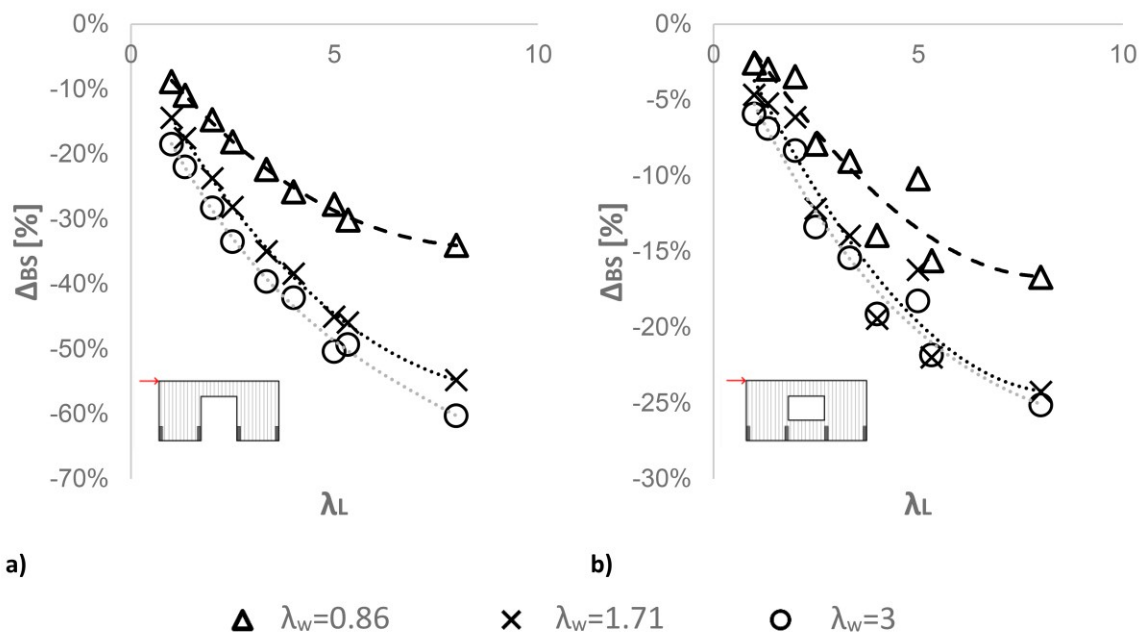

Figure 3-14. Ratio of the base shear for shearwalls with door openings

Table 3-1 presents the percentage reduction values for lintel slenderness 2, 5 and 8, for both single and double hold-down configurations. The results for the walls with window openings show that there is no significant difference between using single and double hold-down. The difference is slightly more significant for walls with door openings, where there is more reduction when the hold-down stiffness increases (from 6609 kN/m to 13247 kN/m).

Table 3-1. Difference in Base shear load between shear-walls with and without openings

			λ_w=0.86			λ_w=1.71			λ_w=3		
Opening	**H-d**	$\mathbf{k_{v,t,hd}}$	λL=2	λL=5	λL=8	λL=2	λL=5	λL=8	λL=2	λL=5	λL=8
[-]	[-]	[kN/m]	[%]	[%]	[%]	[%]	[%]	[%]	[%]	[%]	[%]
Door	Double	13247	-13	-22	-27	-23	-40	-48	-29	-47	-55
Door	Double	6609	-15	-28	-34	-24	-45	-55	-28	-50	-60
Door	Single	13247	-14	-32	-41	-24	-48	-58	-28	-51	-62
Door	Single	6609	-15	-34	-44	-23	-49	-61	-25	-52	-64
Window	Double	13247	-3	-10	-15	-7	-17	-24	-10	-19	-26
Window	Double	6609	-3	-10	-17	-6	-16	-24	-8	-18	-25
Window	Single	13247	-3	-10	-17	-6	-16	-24	-8	-18	-24
Window	Single	6609	-3	-10	-18	-5	-15	-23	-7	-16	-24

References of Chapter 3

Blass, Hans Joachim, & Fellmoser, Peter. (2004). *Design of solid wood panels with cross layers*.

Brandner, Reinhard, Dietsch, Philipp, Dröscher, Julia, Schulte-Wrede, Michael, Kreuzinger, Heinrich, & Sieder, Mike. (2017). Cross laminated timber (CLT) diaphragms under shear: Test configuration, properties and design. *Construction and Building Materials, 147*, 312-327. doi:https://doi.org/10.1016/j.conbuildmat.2017.04.153

Casagrande, Daniele, Polastri, Andrea, Sartori, Tiziano, Loss, Cristiano, Chiodega, Manuela. (2016). Experimental tests for mechanical characterization of timber buildings connections World Conference on Timber Engineering (14WCTE). Vienna, Austria

CSI. (2017). SAP2000 Integrated Software for Structural Analysis and Design. Berkeley, California: Computers and Structures Inc.

ETA-12/0347. (2017). European Technical Approval - XLam Dolomiti - CLT. EOTA.

Gavric, Igor, Fragiacomo, Massimo, & Ceccotti, Ario. (2015). Cyclic behaviour of typical metal connectors for cross-laminated (CLT) structures. *Materials and Structures, 48*(6), 1841-1857. doi:10.1617/s11527-014-0278-7

Mestar, Mohammed, Doudak, Ghasan, Caola, Maurizio, & Casagrande, Daniele. (2020). Equivalent-frame model for elastic behaviour of cross-laminated timber walls with openings. *Proceedings of the Institution of Civil Engineers - Structures and Buildings, 0*(0), 1-16. doi:10.1680/jstbu.19.00057

Paulay, T. (1972). *Some aspects of shear wall design* (Vol. 5): NZSEE – New Zealand Society for Earthquake Engineering.

CHAPTER 4

Inelastic analysis

4.1 General

In this chapter, analysis is performed in order to investigate the influence of geometrical dimensions of the lintel, wall segment, lamella layup and the mechanical behaviour of hold-down on the inelastic behaviour of the wall assembly. The study also aims at investigating the effect of hold-down configuration, including the kinematic behvaiour in the inelastic range as it may differ from that of the elastic range.

The Equivalent Energy Elastic Plastic method, as outlined in the ASTM E2126 standard (ASTM, 2007) was used to derive the properties of the tested wall specimens, for the purpose of comparring them with analysis results in subsequent chapters. The verification of failure in the CLT panels is done using the RVSE model, reviewed in Chapter 2 (Bogensperger et al., 2010).

Based on the obervation that door openings had significantly more effect on the behaviour of the shearwalls than window openings, more emphasis was put on investigating walls with door openings in the inelastic range. A total of 72 numerical analyses were performed, of which 64 runs were dedicated to walls with door openings.

4.2 Geometrical and Mechanical Properties of the Walls

In order to investigate the nonlinear behaviour of the shearwalls, four configurations of walls with door openings, identical to those used in Chapter 3 were investigated. Similarily, two wall configurations with window openings were investigated in this study. These walls are chosen to be representative of the most probable practical cases, while being different enough to yield significantly different behaviours. The geometrical dimensions of the walls used in the current study are provided in table 4-1, where the wall segment and lintel slendernesses are based on the notations presented in Equations 3-6 to 3-8 of Chapter 3. The geometrical configurations of the walls are consistent with those presented in Figure 3-1 in Chapter 3.

Table 4-1. Geometrical configurations of the analyzed CLT walls

	Wall 1	**Wall 2**	**Wall 3**	**Wall 4**
Door segment height	2.8	2.8	2.8	2.8
Door segment length	1.4	1.4	0.8	0.7
Door segment slenderness (λ_w)	**2.00**	**2.00**	**3.50**	**4.00**
Door lintel height	0.4	0.4	0.8	0.8
Door lintel length	0.8	2.4	0.8	3.2
Door lintel slenderness (λ_l)	**2.00**	**6.00**	**1.00**	**4.00**
Window segment height	-	2.8	-	2.8
Window segment length	-	1.4	-	0.7
Window segment slenderness (λ_w)	-	**2.00**	-	**4.00**
Window lintel height	-	0.4	-	0.8
Window lintel length (λ_l)	-	2.4	-	3.2
Window lintel slenderness (λ_l)	-	**6.00**	-	**4.00**

The choice of the WHT440 and WHT620 hold-downs (EOTA, 2015) was motivated by the fact that they represent values of low and high capacity mechanical connectors that are commonly used in design (Casagrande et al., 2016). The mechanical properties of the hold downs are summarized in Table 4-2. In this table, F_{max} represents the maximum strength of the connector, as obtained from tests and k_{ser} is the elastic stiffness corresponding to the slip modulus, represented by the slope of straight line connecting the points at10% and 40% of F_{max}, as provided in Eurocode 5 (EN1995-1-1, 2004). V_y is the yield displacement and V_u is the maximum displacement. μ is the ductility of the connection, defined by the ratio of yield and maximum displacements.

Table 4-2. Mechanical properties of the connections, obtained from Casagrande et al. (2016)

Test ID	Fmax [kN]	Kser [N/mm]	Vy [mm]	Vu [mm]	μ [-]
WHT440	*78.14*	*6609*	*11. 80*	*28.47*	*3.07*
WHT620	*107.32*	*13247*	*8.10*	*20.70*	*3.24*

The selected wall configurations represent different cases encountered in design, including: 1) Configuration 1 representing the case where the slenderness of the wall segment and the slenderness of the lintel are both considered low and equal to each other, 2) Configuration 2 represents a case where the wall segment slenderness is relatively lower than the lintel slenderness, 3) Configuration 3 represents the case where the wall segment slenderness is relatively higher than the lintel slenderness, and finally 4) Configuration 4 represents the case where the wall segment slenderness and the lintel slenderness are both considered high and equal to each other. Figure 4-1 shows the difference in the geometrical properties of each of the four configurations investigated.

For walls with window openings, two geometrical configurations were selected given that, as mentioned earlier, for these walls the variations observed in the elastic range were relatively small compared to walls with door openings. The configurations 5 and 6, with window openings, were based on the geometry of the walls with configurations 2 and 4, by adding a bottom parapet of 1 m. These two configurations of walls with windows were expected to display a relatively higher effect on the wall behaviour due to the high bottom lintel slenderness.

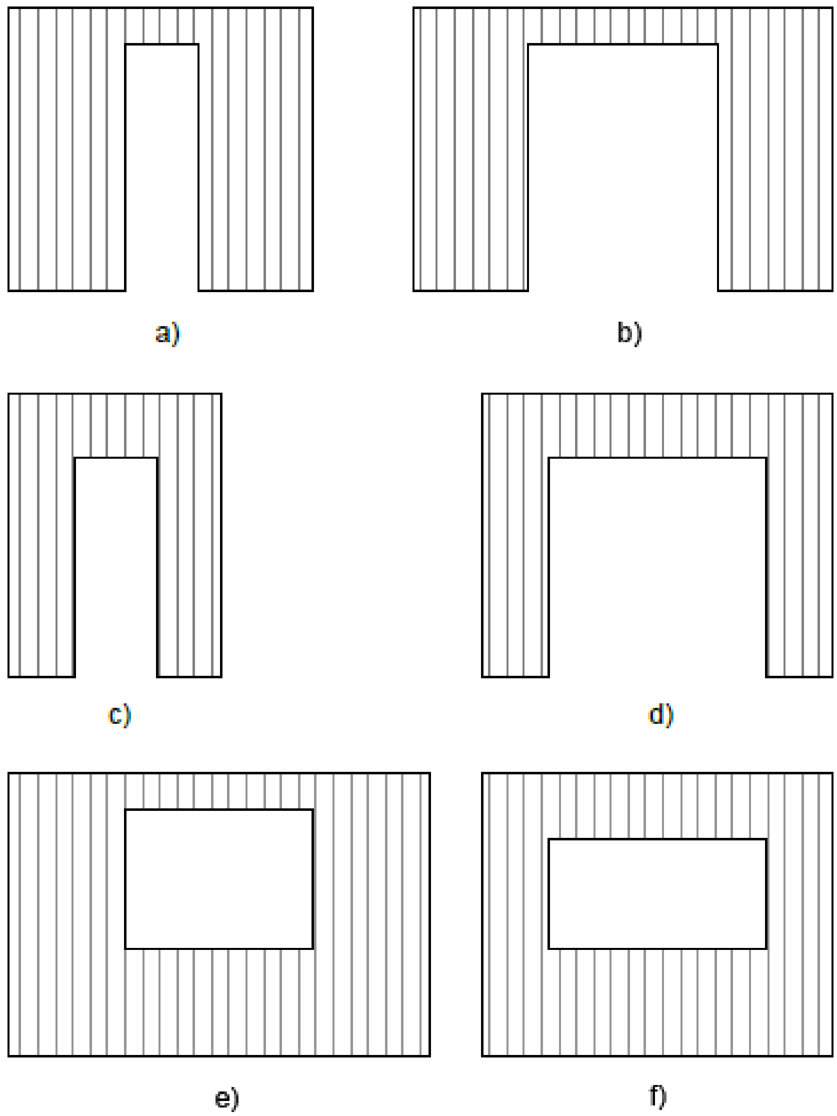

Figure 4-1. Selected shearwalls for the inelastic analyses, a) configuration 1, b) configuration 2, c) configuration 3, d) configuration 4, e) configuration 5 and f) configuration 6

For the walls with door openings, the numerical analyses were performed by varying the hold-down stiffness, hold-down configuration (i.e. SH or DH), lamella layup, as well as wall thickness. For walls with window openings, only one wall thickness and one lamella layup were investigated because, as mentioned earlier, the observed variations in the elastic range were relatively small .

Tables 4-3 and 4-4 summarize the mechanical and geometrical parameters of the walls with door and window openings, respectively. Also included in the tables is the predicted kinematic mode obtained in the elastic range (Chapter 3). The numbers indicated in the column depicting the kinematic mode (i.e. 1 or 2) correspond to one or two centres of rotation, respectively.

Table 4-3. Mechanical and geometrical properties of the CLT wall's configuration with door openings

Wall config.	Wall id	Connection stiffness [N/mm]	Total wall thickness [mm]	Layup configuration	Predicted # of centre of rotation	Hold down configuration
1	W1-1	6609	100	16+25+18+25+16	1	SH or DH
1	W1-2	6609	100	20+20+20+20+20	1	SH or DH
1	W1-3	6609	150	25+37.5+25+37.5+25	1	SH or DH
1	W1-4	6609	150	30+30+30+30+30	1	SH or DH
1	W1-5	13247	100	16+25+18+25+16	1	SH or DH
1	W1-6	13247	100	20+20+20+20+20	1	SH or DH
1	W1-7	13247	150	25+37.5+25+37.5+25	1	SH or DH
1	W1-8	13247	150	30+30+30+30+30	1	SH or DH
2	W2-1	6609	100	16+25+18+25+16	2	SH or DH
2	W2-2	6609	100	20+20+20+20+20	2	SH or DH
2	W2-3	6609	150	25+37.5+25+37.5+25	1	SH or DH
2	W2-4	6609	150	30+30+30+30+30	1	SH or DH
2	W2-5	13247	100	16+25+18+25+16	2	SH or DH
2	W2-6	13247	100	20+20+20+20+20	2	SH or DH
2	W2-7	13247	150	25+37.5+25+37.5+25	2	SH or DH
2	W2-8	13247	150	30+30+30+30+30	2	SH or DH
3	W3-1	6609	100	16+25+18+25+16	1	SH or DH
3	W3-2	6609	100	20+20+20+20+20	1	SH or DH
3	W3-3	6609	150	25+37.5+25+37.5+25	1	SH or DH
3	W3-4	6609	150	30+30+30+30+30	1	SH or DH
3	W3-5	13247	100	16+25+18+25+16	1	SH or DH
3	W3-6	13247	100	20+20+20+20+20	1	SH or DH
3	W3-7	13247	150	25+37.5+25+37.5+25	1	SH or DH
3	W3-8	13247	150	30+30+30+30+30	1	SH or DH
4	W4-1	6609	100	16+25+18+25+16	1	SH or DH

4	W4-2	6609	100	20+20+20+20+20	1	SH or DH
4	W4-3	6609	150	25+37.5+25+37.5+25	1	SH or DH
4	W4-4	6609	150	30+30+30+30+30	1	SH or DH
4	W4-5	13247	100	16+25+18+25+16	2	SH or DH
4	W4-6	13247	100	20+20+20+20+20	2	SH or DH
4	W4-7	13247	150	25+37.5+25+37.5+25	2	SH or DH
4	W4-8	13247	150	30+30+30+30+30	2	SH or DH

Table 4-4. Mechanical and geometrical properties of the CLT wall's configuration with window openings

Wall config.	Wall id	Connection stiffness [N/mm]	Total wall thickness [mm]	Layup configuration	Predicted # of centre of rotation	Hold down configuration
5	W5-1	6609	100	16+25+18+25+16	1	SH or DH
5	W5-2	13247	100	16+25+18+25+16	1	SH or DH
6	W6-1	6609	100	16+25+18+25+16	1	SH or DH
6	W6-2	13247	100	16+25+18+25+16	1	SH or DH

4.3 Verification of the failure mechanisms

4.3.1 CLT failure

As presented in Chapter 2, failure in the CLT panel can be governed by either net shear, shear due to the torsion of laminations or axial forces. In this section, a numerical example is presented to show how the stress in the lintel was verified. Wall W1-1 with properties as summarized in Table 4-5, is used to demonstrate this check.

Table 4-5. Geometrical and mechanical properties of wall W1-1

Hold-sown stiffness [N/mm]	*6609*
Total wall thickness [mm]	*100*
Lamella Layup configuration	*16+25+18+25+16*
t_h (thickness of horizontal lamellae) [mm]	*25+25 = 50*
t_v (thickness of vertical lamellae) [mm]	*16+18+16 = 50*
a (bord width lamellae) [mm]	*100*
Hold down configuration	*Double Hold down (DH)*

4.3.1.1 Axial stress

When checking the axial stress in the lintel, only lamellae oriented in horizontal direction (t_h) are considered in the analysis since the vertical lamellae do not contribute to the axial resistance.

An example of the axial stress state in the lintel obtained from the analysis in SAP2000 (CSI, 2017), is shown in Figure 4-2, where the maximum stress of 1214.6 N/mm^2 ($\boldsymbol{F_{11}}$) is obtained.

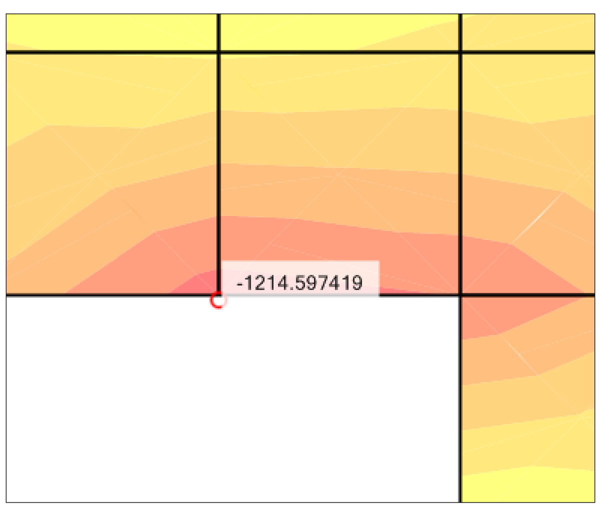

Figure 4-2. Maximum compressive stress in the lintel

The compressive stress (σ_{11}) is calculated as follows:

$$\sigma_{11}(compression) = \frac{F_{11}}{t_h} = \frac{1214.6}{50} = 24.29\ N/mm^2$$

This value is then compared with the average compressive strength ($f_{c,0}$) of 33 N/mm^2 obtained from ETA-12/0347 (2017)

$$\frac{\sigma_{11}}{f_{c,0}} = \frac{24.29}{33.04} = 0.73$$

The result from the axial stress check in this example shows that the lintel is not governed by compression failure.

The stress state for the tension stress in the lintel is provided in Figure 4-3 below, where a maximum tensile stress (F_{11}) of 1117.7 N /mm is obtained.

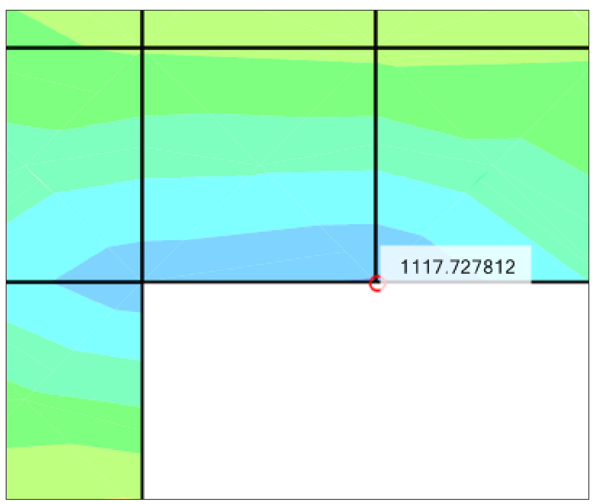

Figure 4-3. Maximum tension in the lintel

Similar to the compression check, the tensile stress (σ_{11}) is calculated considering that only the horizontal lamellae are contributing to the tensile strength.

$$\sigma_{11}(tension) = \frac{F11}{t_h} = \frac{1117.7}{50} = 22.35\ N/mm^2$$

Verifying the stress against the tensile strength ($f_{t,0}$) of 27.85 N/mm^2, one obtains a ratio less than unity, indicating that the lintel is not expected to fail in tension.

$$\frac{\sigma_{11}}{f_{t,0}} = \frac{22.35}{27.85} = 0.80$$

4.3.1.2 Shear stress

The shear stress state at mid-span of the lintel is shown in Figure 4-4, where a maximum shear stress (F_{12}) of 305.4 N /mm is obtained. Although the maximum shear is expected to be at mid-depth of a given beam element, it is observed at the edge of the little in the current study due to horizontal constraints imposed at the top of the wall to represent the in-plane rigidity of the diaphragm. It is noteworthy to mention that the distribution of shear stress does not differ significantly when the constraints are not considered. Figure 4-4b shows the stress distribution when the constraint is omitted and it can be observed that a discrepancy of about 3% compared to unconstrained walls is obtained.

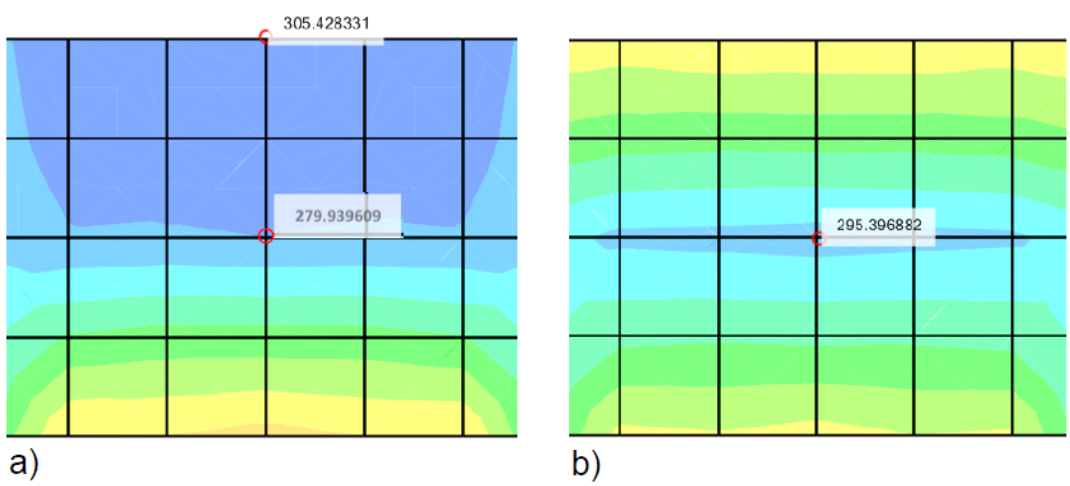

Figure 4-4. Maximum shear in the lintel, a) constrained top and b) unconstrained top

The method proposed by Bogensperger et al. (2010) is used in this analysis. Table 4-6 summarize the procedure based on thickness notation indicated in Figure 4-5.

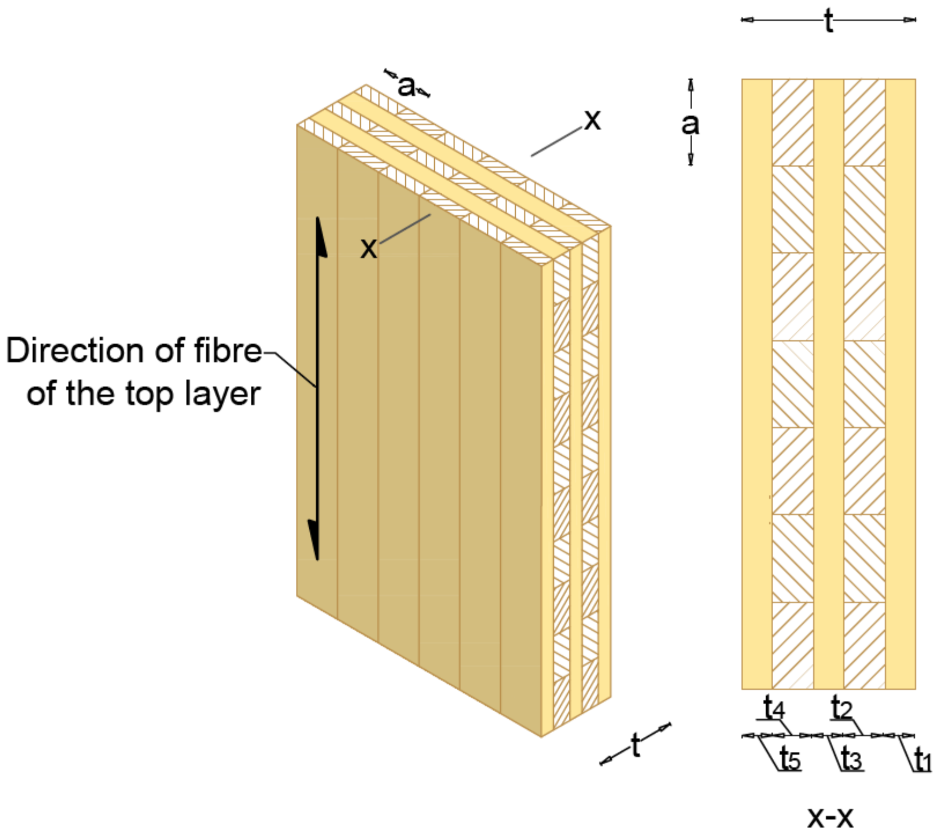

Figure 4-5. Thickness notation for the RVSE model

Table 4-6. RVSE model

# of RVSE	Ideal thickness t_i^*
1	t_1^* =min (2 t1; t2) = 25
2	t_2^* =min (t2; t3) = 18
3	t_3^* =min (t3; t4) = 18
4	t_4^* =min (t4; 2 t5) = 25

Nominal shear stress

The nominal shear stress, τ_0^*, is determined by dividing the maximum shear stress in the lintel by the sum of the ideal thicknesses, using Equation 2-1, presented in Chapter 2:

$$\eta_{RVSEi}^* = \tau_{0,RVSEi}^* = \frac{\eta \cdot \frac{t_i^*}{\sum_i t_i^*}}{t_i^*} = \frac{\eta}{\sum_i t_i^*} = \tau_0^*$$

η, maximum shear stress corresponding to $F12$ in the numerical model.

$$= \frac{305.4}{25 + 18 + 18 + 25} = 3.55\ N/mm^2$$

Real shear stress

The real shear stress (τ_v) is twice the nominal shear stress and is obtained as:

$$\tau_v = 2 \cdot \tau_0^* = 2 * 3.55 = 7.10\ N/mm^2$$

Comparing this value with the shear strength (f_v), one obtains:

$$\frac{\tau_v}{f_v} = \frac{7.10}{7} * 100\% = 1.01$$

Torsional shear stress

The torsional shear stress can be obtained as a function of the nominal shear stress, using Equation 2-3, presented in Chapter 2:

$$\tau_M = 3 \cdot \tau_0^* \cdot \frac{t_i^*}{a} = 3 \cdot 3.55 \cdot \frac{25}{100} = 2.66\ N/mm^2$$

The value is compared to the torsional strength (f_T), which gives:

$$\frac{\tau_M}{f_T} = \frac{3.32}{3.5} = 0.76$$

Based on all the different verifications undertaken above, the lintel beam appears to fail in shear in this example, provided that the hold-downs are not failing before lintel. This check will be presented next.

4.3.2 Hold-down failure

4.3.2.1 Capacity curves

The capacity curve of the walls is defined by the wall's kinematic behaviour as well as the properties of the mechanical devices. The ultimate displacement of the curve is determined based on the ultimate displacement of the first hold-down given in Table 4-2, or failure in the CLT panel. Figure 4-6 shows an example of such capacity curve for wall W1-1 resulting from the pushover analysis. It can be seen from the graph that the wall behaviour is governed by failure in the lintel beam. The continuation of the graph (dashed line) represents the hypothetical behaviour of the wall if the lintel capacity is increased, allowing the three hold-down devices to yield, and the wall to dissipate energy.

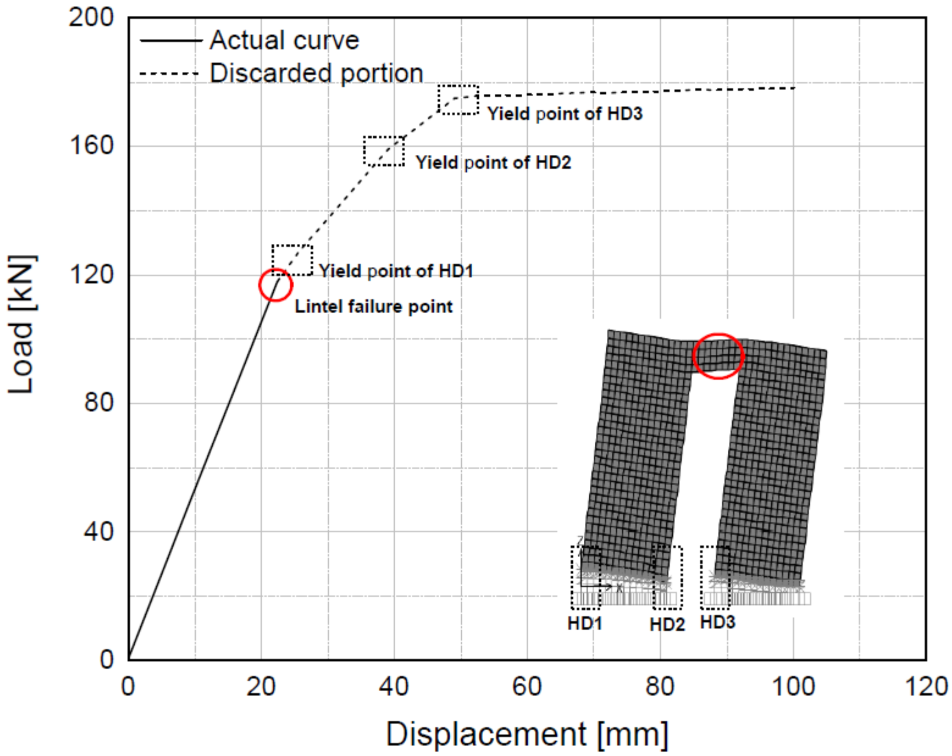

Figure 4-6. Capacity curve of CLT wall W1-1

4.3.2.2 Equivalent Energy Elastic Plastic Principle

The Equivalent Energy Elastic Plastic (EEEP) method, as outlined in the ASTM E2126 standard (ASTM, 2007) was used to derive and compare the properties of the analyzed walls. An example of how the EEEP curve is used to idealize the curves from the pushover analyses can be seen in Figure 4-7. As the pushover curves in this analysis do not exhibit any post-peak descending capacity curve, the maximum load is equal to the peak load. The yield load and the secant stiffness are obtained from the expressions in Equations (4-1) and (4-2), reproduced from the ASTM E2126 standard (ASTM, 2007). The plastic portion (horizontal line) equal to F_{yield} of the idealized curve is selected in such a way that the areas under the two curves is equal.

$$F_{yield} = \frac{-\Delta_{failure} + \sqrt{\Delta_{failure}{}^2 - {}^{2A}/_{K_e}}}{{}^{-1}/_{K_e}} \qquad (4\text{-}1)$$

where:

$$K_e = \frac{0.4F_{failure}}{0.4\Delta_{failure}} \qquad (4\text{-}2)$$

and A is the calculated dissipated energy under the pushover curve.

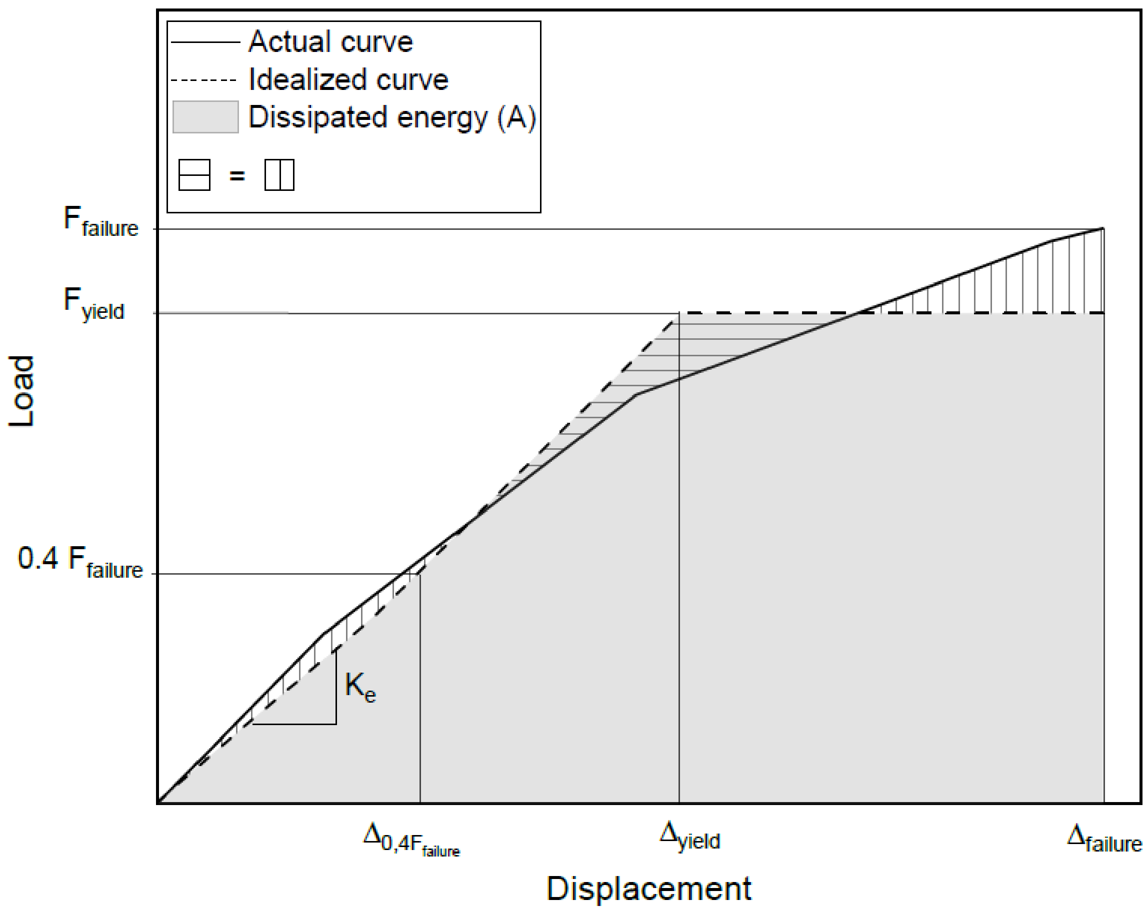

Figure 4-7. Equivalent Energy Elastic Plastic curve principle

The ductility (μ) can be determined by calculating the ratio of the displacement corresponding to failure ($\Delta_{failure}$) to the displacement corresponding to yielding (Δ_{yield}) as shown in Equation (4-3):

$$\mu = \frac{\Delta_{failure}}{\Delta_{yield}} \qquad (4\text{-}3)$$

4.4 Results and discussion

The summary of the results obtained from the non-linear pushover analysis for walls with door opening are presented in Table 4-7 and 4-8 for double and single hold-down configuration, respectively. Included in the tables are the predicted kinematic modes obtained from the elastic analysis (Chapter 3), as well as the inelastic analysis. Also reported in the tables are the mechanical properties obtained from the EEEP curves, the ultimate failure mode and whether the first hold-down has yielded. This check clarifies the reason for having certain amount of ductility in the system, even when the ultimate failure is characterized as failure in the CLT panel.

Tables 4-9 and 4-10 present similar information for the results obtained from the analysis of walls with window openings and consisting of double and single hold-down configuration, respectively.

Table 4-7. Inelastic analyses for CLT walls with door openings for double hold down configuration

Wall id	Predict. Kinem. Elast. mode	Elast. kinem. Mode	Inelast. kinem. mode	Ult. failure	HD1 yielded Yes/No	Δ_{yield} [mm]	$\Delta_{failure}$ [mm]	F_{yield} [kN]	$F_{failure}$ [kN]	K_e [kN/mm]	μ [-]
W1-1	1	1	1	CLT	N	22.4	22.4	118	118	5.3	1.00
W1-2	1	1	1	CLT	N	20.5	20.5	109	109	5.3	1.00
W1-3	1	1	1	CLT	Y	22.1	31.7	144	159	6.5	1.43
W1-4	1	1	1	CLT	Y	21.1	28.1	139	150	6.6	1.33
W1-5	1	1	1	CLT	N	17.7	17.7	125	125	7.0	1.00
W1-6	1	1	1	CLT	N	16.5	16.5	118	118	7.1	1.00
W1-7	1	1	1	CLT	Y	18.8	22.1	170	179	9.1	1.18
W1-8	1	1	1	CLT	Y	17.2	18.3	158	164	9.2	1.06
W2-1	2	2	2	CLT	N	19.1	19.1	92	92	4.8	1.00
W2-2	2	2	2	CLT	N	16.6	16.6	78	78	4.7	1.00
W2-3	1	1	1	CLT	N	19.3	19.3	121	121	6.2	1.00
W2-4	1	1	1	CLT	N	16.5	16.5	100	100	6.1	1.00
W2-5	2	2	2	CLT	N	18.5	18.5	114	114	6.2	1.00
W2-6	2	2	2	CLT	N	16.0	16.0	98	98	6.1	1.00
W2-7	2	2	2	CLT	N	18.4	18.4	147	147	8.0	1.00
W2-8	2	2	2	CLT	N	16.1	16.1	126	126	7.8	1.00
W3-1	1	1	1	HD	Y	41.7	67.2	89	102	2.1	1.61
W3-2	1	1	1	HD	Y	40.9	67.1	91	102	2.2	1.64
W3-3	1	1	1	HD	Y	35.9	59.7	92	102	2.6	1.66
W3-4	1	1	1	HD	Y	35.3	59.6	93	103	2.6	1.69
W3-5	1	1	1	CLT	Y	38.7	58.5	112	127	2.9	1.51
W3-6	1	1	1	CLT	Y	36.6	53.0	110	123	3.0	1.45
W3-7	1	1	1	HD	Y	32.8	52.7	120	139	3.7	1.61
W3-8	1	1	1	HD	Y	32.1	52.2	122	141	3.8	1.63
W4-1	1	1	1	CLT	N	44.6	44.6	104	104	2.3	1.00

W4-2	1	1	1	CLT	N	37.8	37.8	92	92	2.4	1.00
W4-3	1	1	1	CLT	Y	43.3	50.7	138	150	3.2	1.17
W4-4	1	1	1	CLT	N	39.4	39.4	130	130	3.3	1.00
W4-5	2	2	2	CLT	N	40.7	40.7	113	113	2.8	1.00
W4-6	2	2	2	CLT	N	34.8	34.8	100	100	2.9	1.00
W4-7	2	2	1	CLT	Y	40.8	44.5	154	161	3.8	1.09
W4-8	2	2	2	CLT	N	33.8	33.8	132	132	3.9	1.00

Table 4-8. Inelastic analyses for CLT walls with door openings for simgle hold down configuration

Wall id	*Predict. Kinem. mode*	*Elast. kinem. mode*	*Inelast. kinem. mode*	Ult. failure	*HD yielded Yes/No*	*Δ_{yield} [mm]*	*$\Delta_{failure}$ [mm]*	*F_{yield} [kN]*	*$F_{failure}$ [kN]*	*K_e [kN/mm]*	*μ [-]*
W1-1	1	1	1	HD	Y	20.0	36.0	89	90	4.5	1.8
W1-2	1	1	1	HD	Y	19.9	36.1	89	90	4.5	1.8
W1-3	1	1	1	HD	Y	16.6	33.4	90	91	5.4	2.0
W1-4	1	1	1	HD	Y	16.5	33.0	90	91	5.5	2.0
W1-5	1	1	1	CLT	N	18.0	18.0	106	106	5.9	1.0
W1-6	1	1	1	CLT	N	16.3	16.3	97	97	6.0	1.0
W1-7	1	1	1	HD	Y	16.0	29.1	123	124	7.7	1.8
W1-8	1	1	1	HD	Y	15.9	28.3	123	124	7.7	1.7
W2-1	2	2	2	CLT	N	17.9	17.9	70	70	3.9	1.0
W2-2	2	2	2	CLT	N	15.6	15.6	60	60	3.8	1.0
W2-3	1	1	1	CLT	N	19.8	19.8	105	105	5.3	1.0
W2-4	1	1	1	CLT	N	16.3	16.3	84	84	5.1	1.0
W2-5	2	2	2	CLT	N	17.8	17.8	85	85	4.8	1.0
W2-6	2	2	2	CLT	N	14.9	14.9	69	69	4.6	1.0
W2-7	2	2	2	CLT	N	17.5	17.5	112	112	6.4	1.0
W2-8	2	2	2	CLT	N	15.1	15.1	98	98	6.5	1.0
W3-1	1	1	1	HD	Y	29.6	56.6	53	53	1.8	1.9
W3-2	1	1	1	HD	Y	28.3	57.6	53	53	1.9	2.0
W3-3	1	1	1	HD	Y	25.2	51.4	53	53	2.1	2.0
W3-4	1	1	1	HD	Y	23.5	51.2	52	54	2.2	2.1
W3-5	1	1	1	HD	Y	28.3	50.6	72	72	2.5	1.7
W3-6	1	1	1	HD	Y	27.2	50.5	72	72	2.6	1.8
W3-7	1	1	1	HD	Y	23.0	44.1	72	73	3.2	1.9
W3-8	1	1	1	HD	Y	22.3	45.2	73	73	3.3	2.0
W4-1	1	1	1	CLT	N	44.2	44.2	92	92	2.1	1.0
W4-2	1	1	1	CLT	N	37.0	37.0	81	81	2.2	1.0

W4-3	1	1	1	HD	Y	35.4	50.9	103	103	2.9	1.4
W4-4	1	1	1	HD	Y	33.9	48.5	102	103	3.0	1.4
W4-5	2	2	2	CLT	N	40.4	40.4	96	96	2.4	1.0
W4-6	2	2	2	CLT	N	31.3	31.3	78	78	2.5	1.0
W4-7	2	2	2	CLT	Y	39.5	42.9	131	137	3.3	1.0
W4-8	2	2	2	CLT	N	33.9	33.9	117	117	3.4	1.0

Table 4-9. Inelastic analyses for CLT walls with window openings for double hold down configuration

Wall id	***Predict. Kinem. Elast. mode***	***Elast. kinem. Mode***	***Inelast. kinem. mode***	**Ult. failure**	***HD1 yielded Yes/No***	***Δ_{yield} [mm]***	***$\Delta_{failure}$ [mm]***	***F_{yield} [kN]***	***$F_{failure}$ [kN]***	***K_e [kN/mm]***	***μ [-]***
W5-1	1	1	1	CLT	Y	18.4	20.6	193	202	10.5	1.1
W5-2	1	1	1	CLT	N	15.6	15.6	202	202	12.9	1.0
W6-1	1	1	1	CLT	N	28.9	28.9	158	158	5.5	1.0
W6-2	1	1	1	CLT	N	24.6	24.6	157	157	6.4	1.0

Table 4-10. Inelastic analyses for CLT walls with window openings for single hold down configuration

Wall id	***Predict. Kinem. Elast. mode***	***Elast. kinem. Mode***	***Inelast. kinem. mode***	**Ult. failure**	***HD1 yielded Yes/No***	***Δ_{yield} [mm]***	***$\Delta_{failure}$ [mm]***	***F_{yield} [kN]***	***$F_{failure}$ [kN]***	***K_e [kN/mm]***	***μ [-]***
W5-1	1	1	1	HD	Y	14.0	27.3	128	131	9.2	1.9
W5-2	1	1	1	HD	Y	15.0	23.7	176	177	11.7	1.5
W6-1	1	1	1	HD	Y	21.3	37.4	100	102	4.7	1.7
W6-2	1	1	1	HD	Y	23.7	34.1	138	139	5.8	1.4

4.4.1 Effect of HD configuration on the behaviour of walls with door openings

4.4.1.1 Kinematic behaviour

Figure 4-8 presents the effect of the hold-down configuration on the elastic stiffness of the walls. The transition between the observed kinematic mode in the elastic and inelastic ranges is represented by two numbers for each wall. For example “1-1” represent that the wall was in kinematic mode 1 (one centre of rotation) in the elastic range and it remains in that mode in the inelastic range. It can be noted that for all cases involving wall configurations 1 and 3, kinematic mode 1 is the dominant mode in both the elastic and inelastic ranges. This can be attributed to the fact that the stiffness of lintel beam dominates the behaviour in these wall configurations. Where the lintel slenderness is relatively high (Configuration 2), kinematic mode 2 dominates the behaviour. An exception to this are walls W2-3 and W2-4, where the hold-down stiffness and the wall thickness are relatively high.

In general it can be observed that the elastic stiffness is reduced when comparing the results from walls with double to single hold-down configurations. The reduction in the elastic stiffness for walls is about 15 % on average regardless of the wall configuration. The drop is observed to be higher in the configuration where the lintel slenderness is relatively higher than the wall segment slenderness (Configuration 2). It can also be observed that the lamella layup has insignificant effect (less than 6% difference) on the elastic stiffness of the wall for both SH and DH configurations.

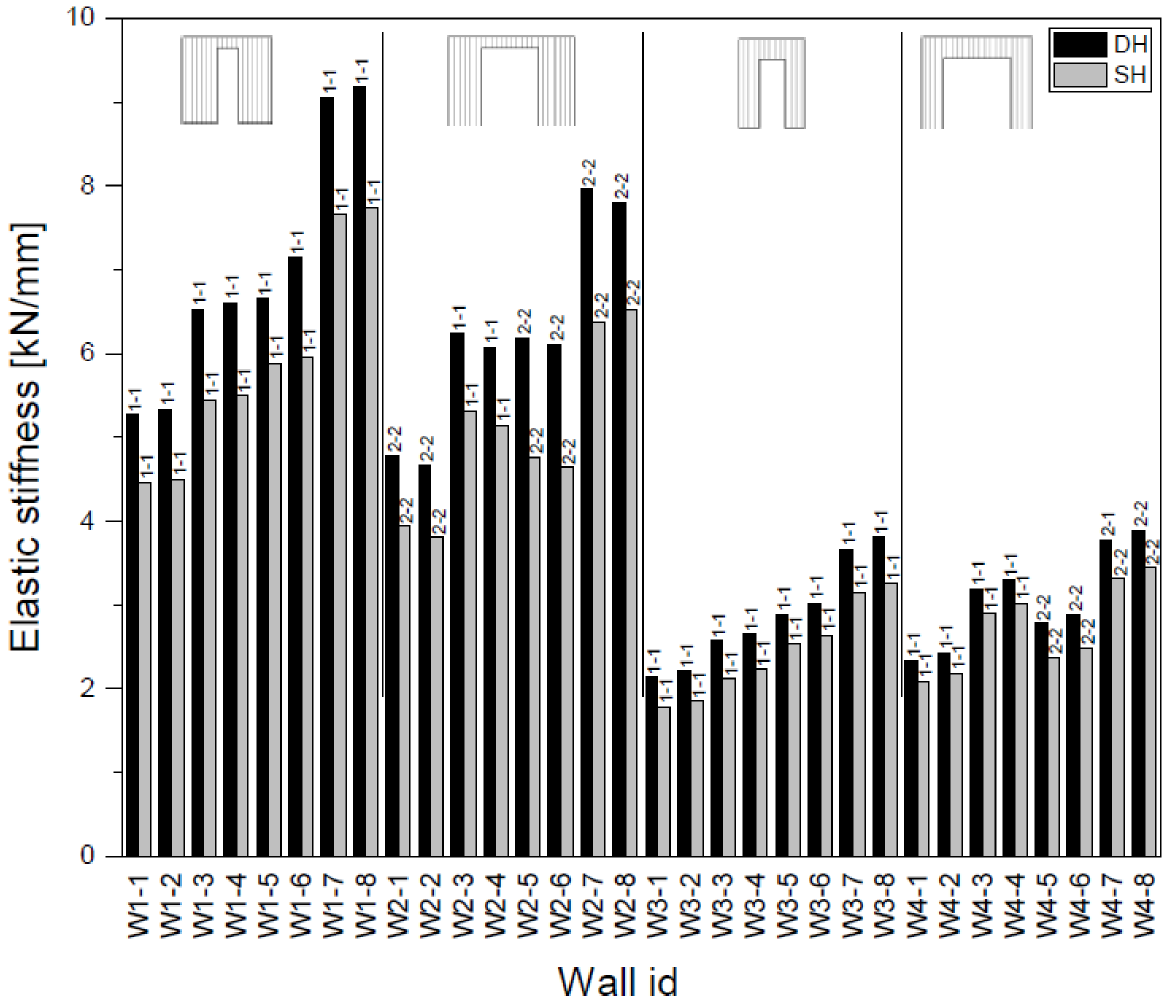

Figure 4-8. Effect of HD configuration on elastic stiffness of the walls (DH VS SH)

Although less frequent, the analysis also reveals the possibility of change in the kinematic mode between two-centre of rotation in the elastic range to one-centre of rotation in the inelastic range. An example of such behaviour is observed in the case of W4-7, with double hold-down configuration.. This result implies that relying on the prediction in the elastic range may not always lead to accurate prediction of the final kinematic mode of the wall. The deformed shape of wall W4-7 is presented in Figure 4-9, including the vertical displacement of HD1 and the reaction values in all the hold-downs. The engagement of HD2 in the inelastic range can be seen in Figure 4-9b.

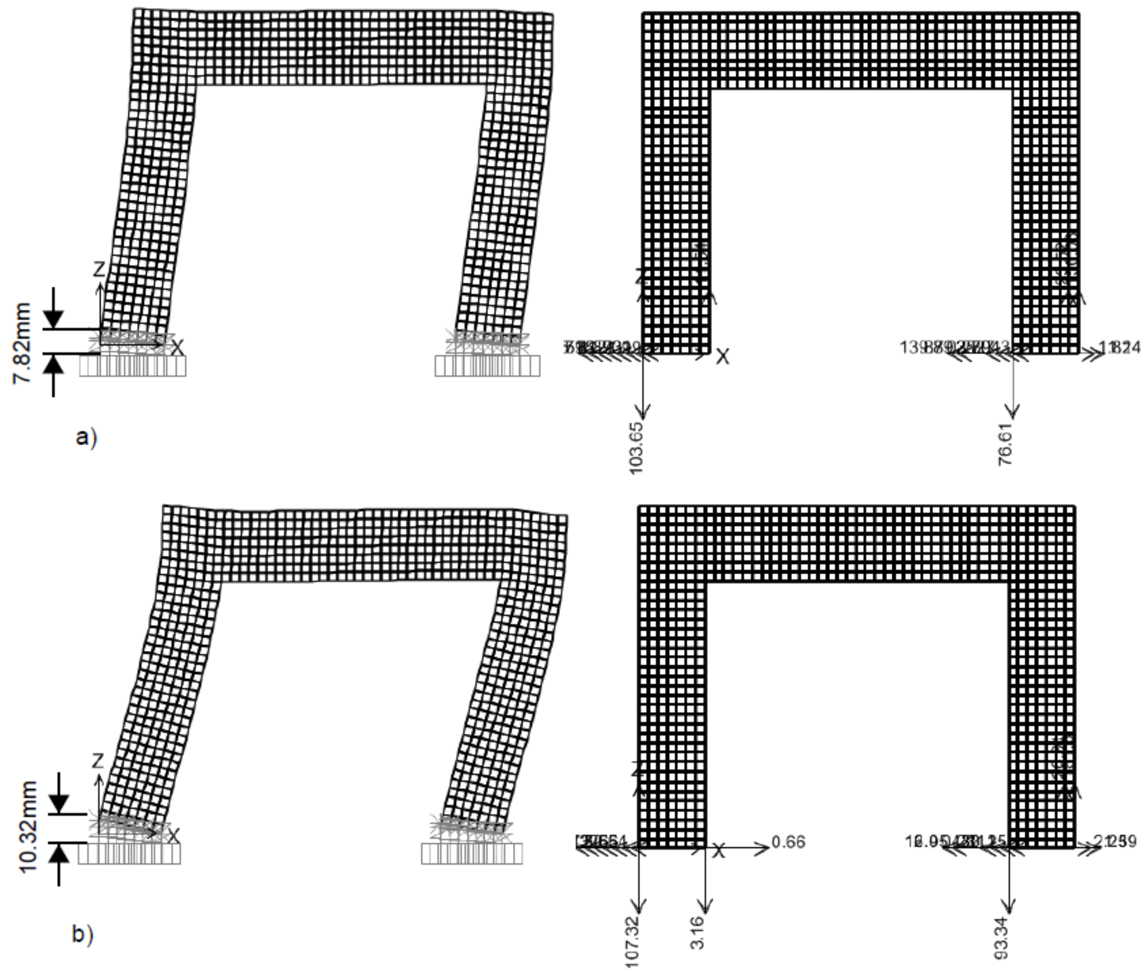

Figure 4-9. Change of kinematic modes: deformed shapes and reactions in a) elastic range and b) inelastic range of wall W4-7

4.4.1.2 Failure Modes

Figure 4-10 presents the strength and failure modes of the various wall configurations investigated. For wall configuration 1, it can be observed that failures in the walls with DH configuration occurred in CLT lintel. It is interesting to note that the failure generally changes to that of the hold-down when SH configuration is used. An exception to this observation is the behaviour of walls W1-5 and W1-6, where failure occurs in CLT due to the decrease in the thickness of horizontal lamellae. Such decrease is due to the reduced total wall thickness from 150 to 100 mm. For wall configuration 2, failure consistently occurred in the CLT lintel beam. As expected, configuration 3 was dominated by hold-down failure. An exception to this generalization is walls W3-5 and W3-6, where the thickness of horizontal lamellae is decreased. In general, failure in wall configuration 4 was dominated by that of the CLT lintel beam, except walls W4-3 and W4-4 with SH, where the increased total wall thickness influenced the failure.

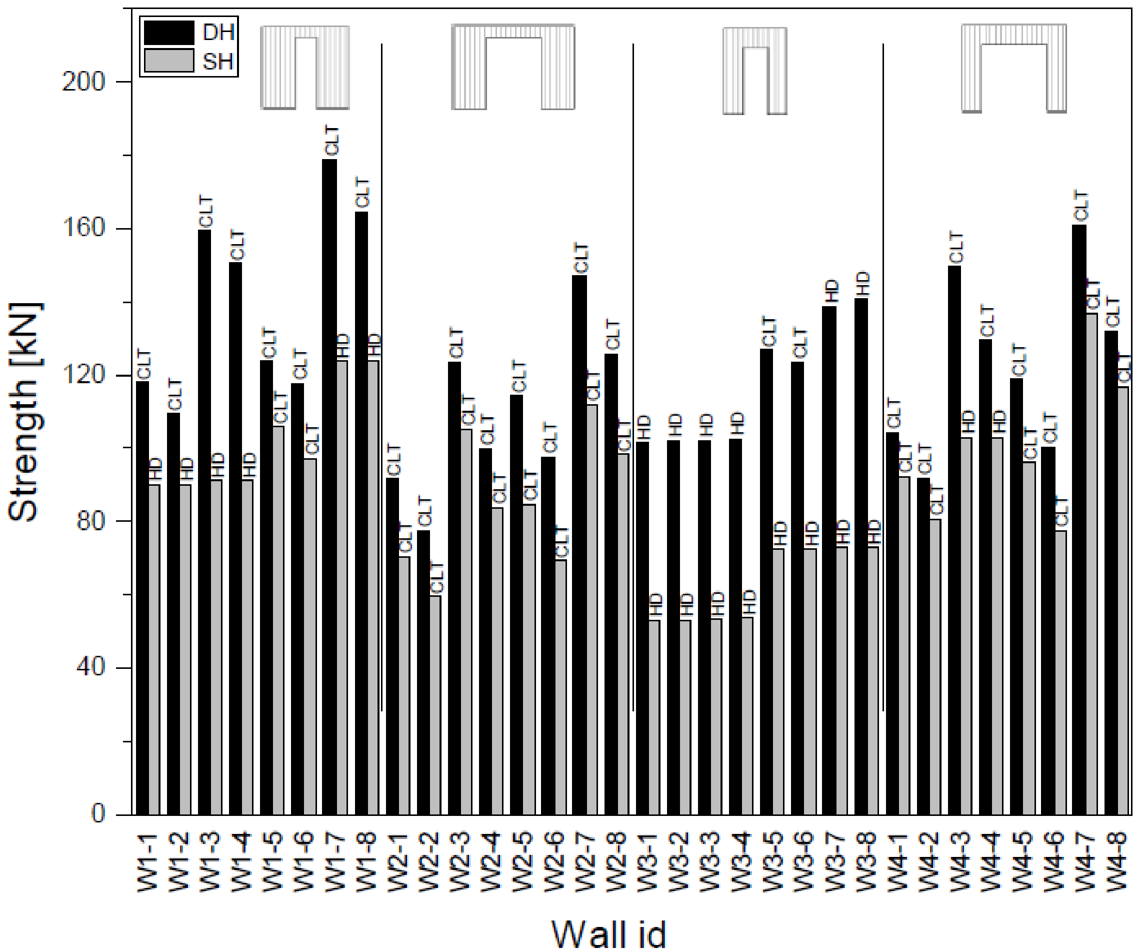

Figure 4-10. Effect of HD configuration on ultimate load of the walls (DH VS SH)

As expected, the results show a decrease in strength when comparing walls with SH to those with DH. The drop is most significant and consistent for wall configuration 3, where only 50% of the strength is obtained for the configurations with SH compared to DH. The drop in the other wall configurations is about 22% on average. An influencing factor on the amount of strength reduction is the layup configuration due to the difference in the torsional strength of the lintel with different lamellae ratio. This effect is mostly pronounced in wall configurations 2 and 4, where the effect is about 15%. This is mainly attributed to the higher lintel slenderness ratios in these wall configurations. For similar reasons, wall configuration 3 is much less sensitive to the lamellae ratio, with a maximum effect of 3%.

4.4.1.3 Global Ductility

Figure 4-11 shows the effect of the hold-down configuration on the global ductility of the walls. Wall configuration 2 only contained brittle failure modes, and as such the behaviour of the wall was not affected by the hold-down configuration or lamella layup. Although the behaviour is less consistent, wall configuration 1 exhibit a very significant improvement in ductility when considering walls with SH configuration. The ductility is observed to increase by approximately 47% on average.

Wall configuration 3 shows a consistently high global ductility for both the SH and DH configurations. This is particularly the case in the SH configuration where the ductility was additionally increased by about 23% relative to the DH configuration. The behaviour in wall configuration 4 is less consistent and generally dominated by brittle behaviour.

No clear tendency can be observed regarding the effect of lamella layup on the ductility, however, the effect is about 5% on average, and as such can be considered relatively insignificant.

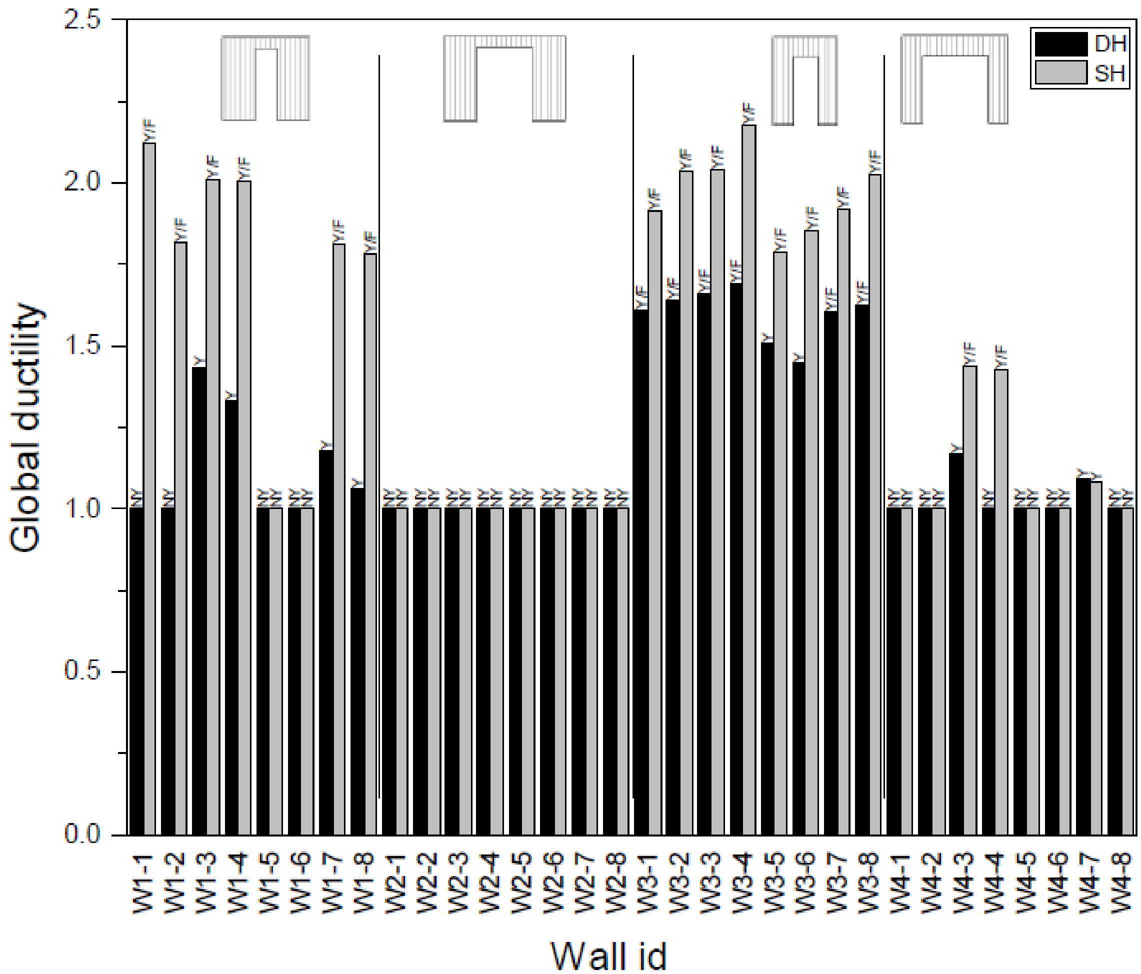

Figure 4-11. Effect of HD configuration on global ductility of the walls (DH VS SH)

4.4.2 Effect of HD configuration on the behaviour of walls with window openings

4.4.2.1 Kinematic behaviour

The effect of hold-down stiffness and configuration on the elastic stiffness of the walls with window openings is presented in Figure 4-12. All configurations exhibited one-centre of rotation and the kinematic mode did not change when moving from elastic to inelastic range. The added stiffness and strength of the bottom parapet meant that the wall behaved as a monolithic wall experiencing rigid body behaviour.

The elastic stiffness was reduced by about 11% on average when comparing walls with SH to DH configuration and by about 5% when considering hold-downs with low capacity compared to those with high capacity (WHT620 to WHT440).

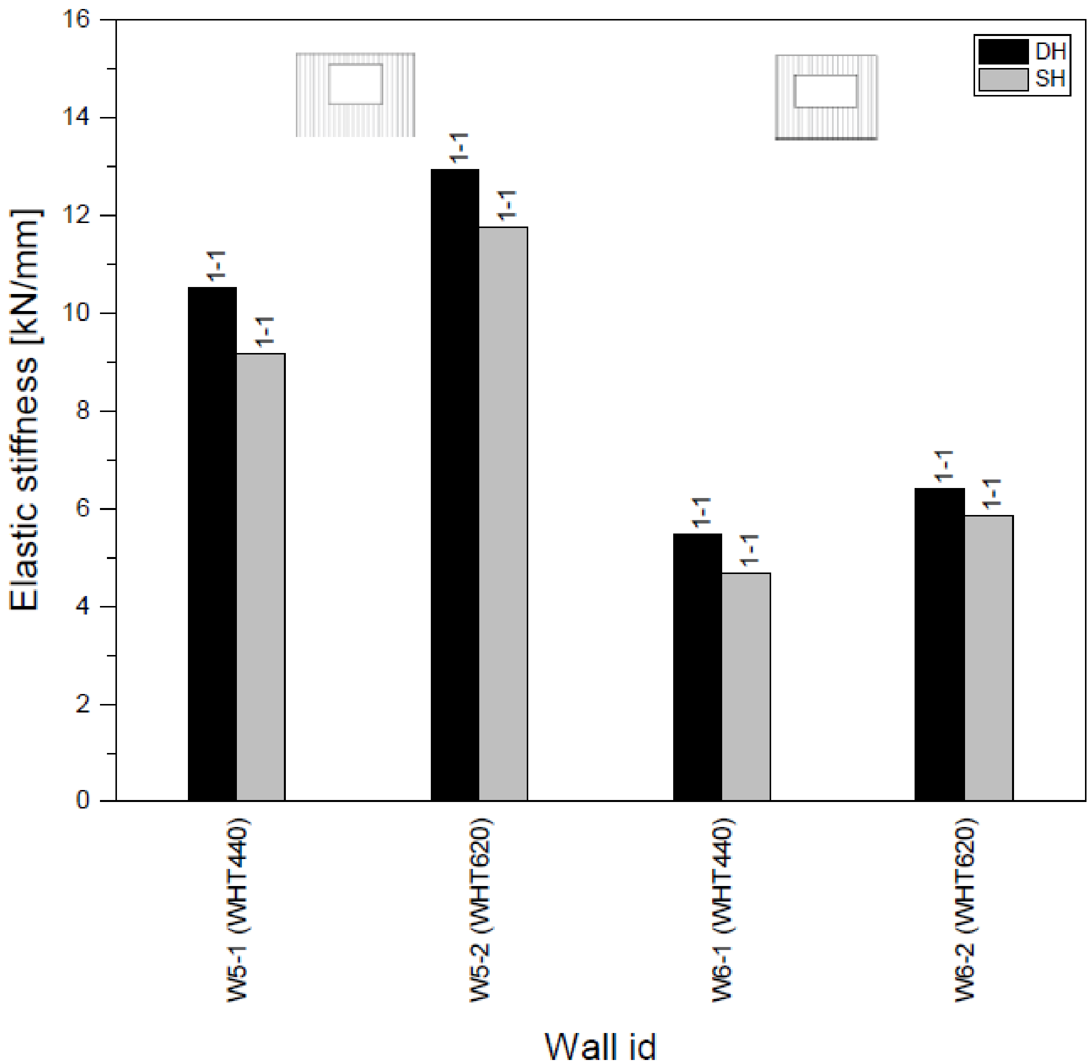

Figure 4-12. Effect hold down stiffness and configuration on elastic stiffness of the walls (DH VS SH)

4.4.2.2 Failure Mode

Figure 4-13 presents the strength of the investigated wall configurations, including the ultimate failure mode observed. In all cases where DH configuration was used, failure occurs in the CLT lintel beam, whereas walls with SH configuration, the failure occurred in hold down.

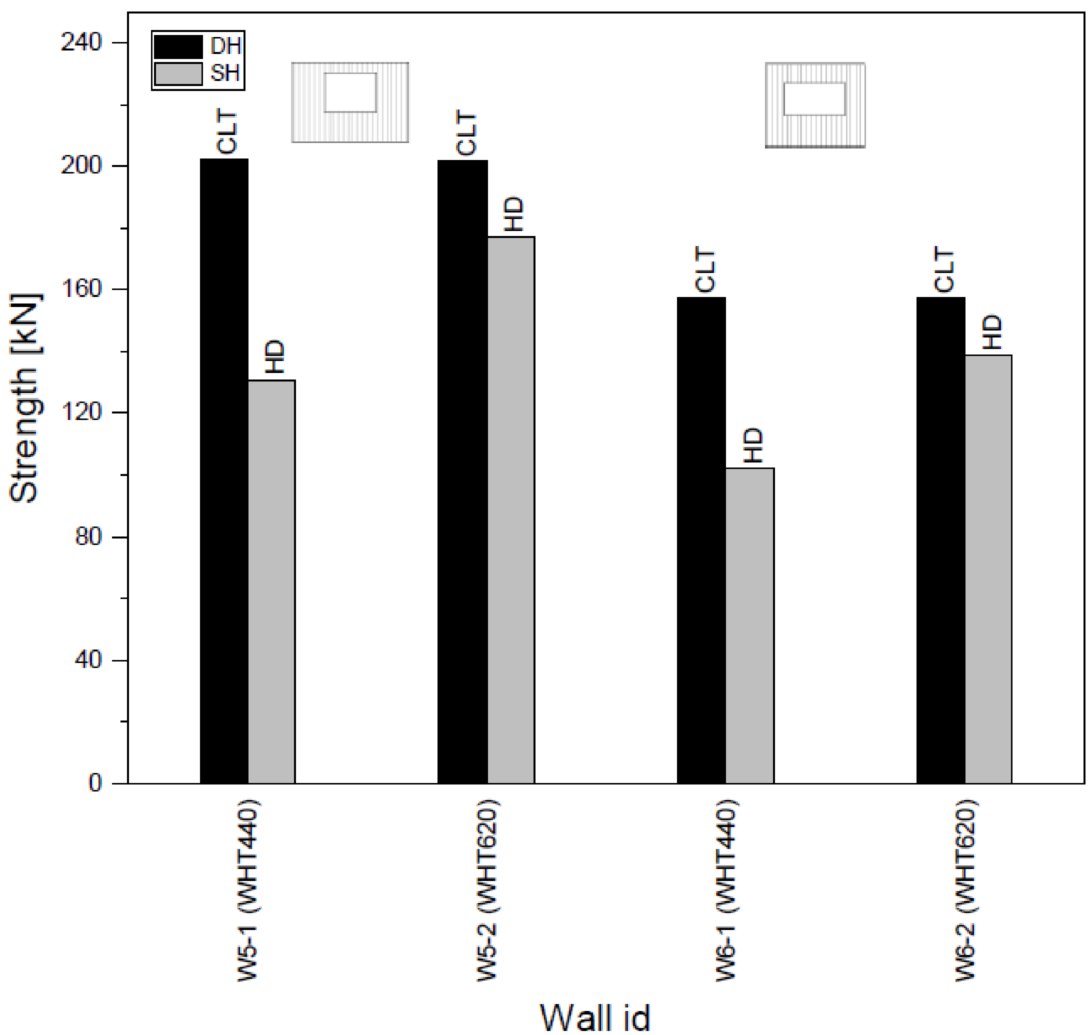

Figure 4-13. Effect of stiffness and hold down configuration on strength of the walls (DH VS SH)

4.4.2.3 Global Ductility

The global ductility of walls with windows is shown in Figure 4-14. It can be observed that using SH configuration consistently leads to an increase in the wall ductility. Increasing the stiffness and strength in the hold-down (WHT440 to WHT620) lead to a decrease in the ductility since these hold-down devices have lower ductility (see Table 4-2).

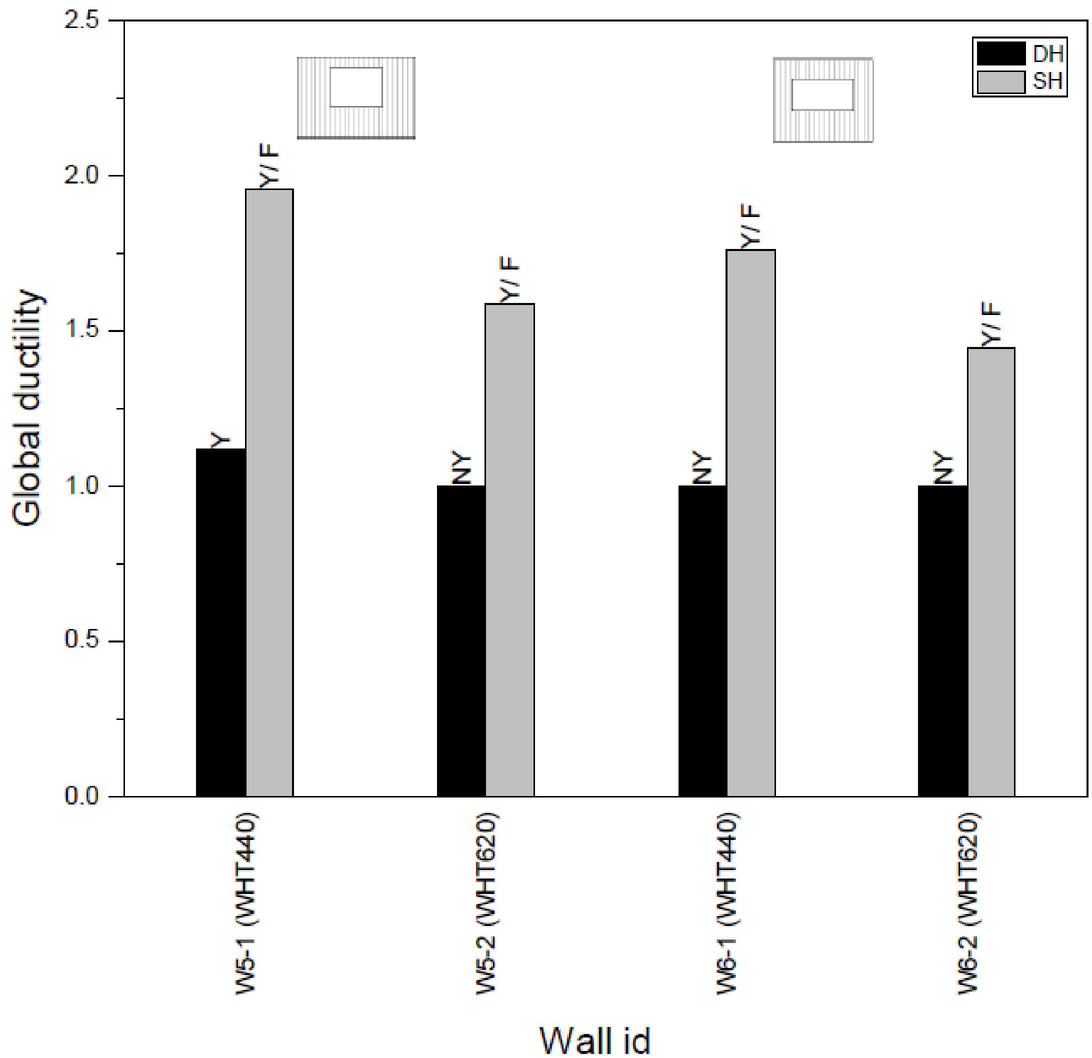

Figure 4-14. Effect of stiffness and hold down configuration on ductility of the walls (DH VS SH)

4.4.3 Comparison between walls with door and window openings

4.4.3.1 Kinematic behaviour

When comparing walls with door openings to those with window openings, it can be observed that the addition of the bottom parapet led in general to a change in the kinematic mode of the walls. As demonstrated in Figure 4-15, the kinematic behaviour generally changed from two-centre of rotation to one-centre of rotation when the bottom parapet is added for both double and single hold down configurations. The elastic stiffness is increased by about 121% and 147%, on average, in the double (figure 4-15a) and single (figure 4-15b) hold-down case, respectively.

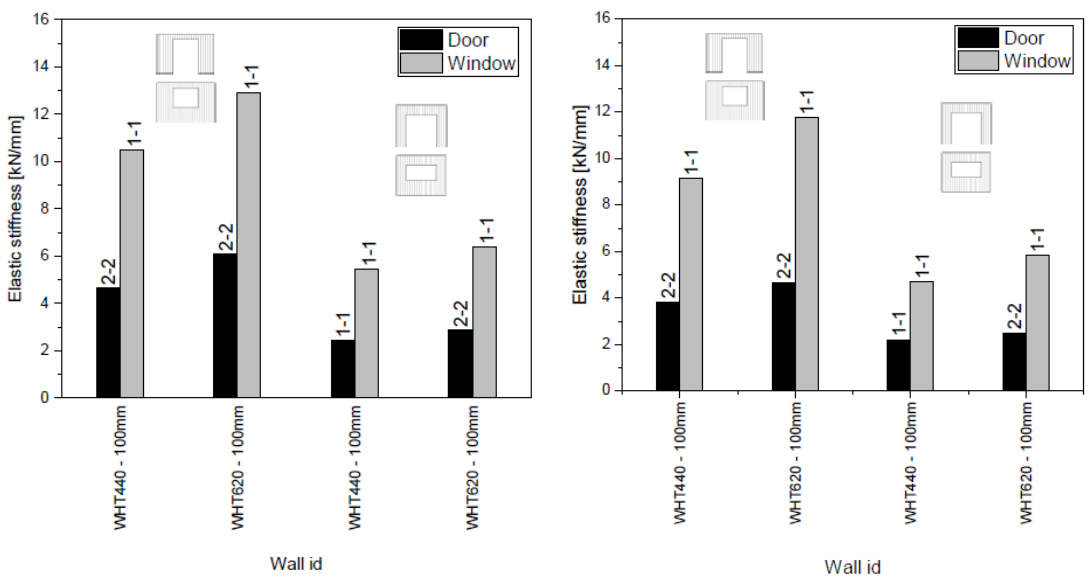

Figure 4-15. Effect of bottom parapet on elastic stiffness of the walls for a) DH configuration and b) SH configuration

4.4.3.2 Failure Mode

The overall strength is increased in all cases when the bottom parapet is introduced in the wall (Fig. 4-16). Walls with window openings also allow for a change in failure mode from the CLT to the hold-down due to the increase in the CLT panel capacity. This is particularly evident in the walls with SH configurations, where the change in failure mode occurred in all wall configurations. However, the bottom parapet has no effect on the failure mode in case of double holdown (figure 4-16-a).

A higher increase in wall strength is observed in wall configurations 2 and 5 compared to configurations 4 and 6. This result may be attributed to the fact that the wall segments in wall configurations 2 and 5 are bending less than those in configurations 4 and 6 due to the relatively higher slenderness ratio of the lintel beam. On average, the wall strength increased by about 98% for DH configuration (figure 4-16-a) and around 94% for SH configuration (figure 4-16-b) due to the effect of the parapet.

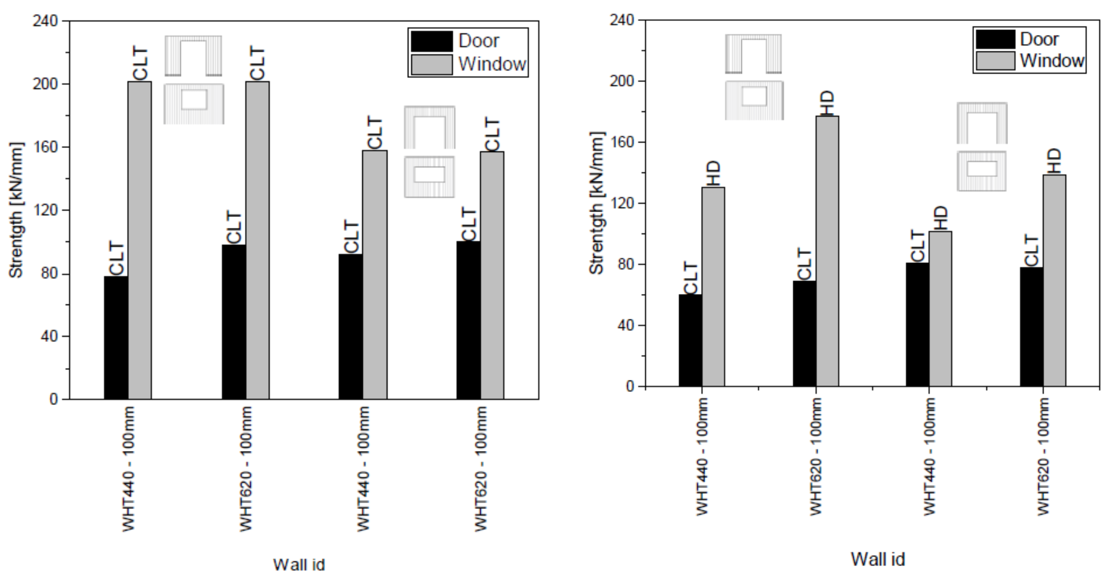

Figure 4-16. Effect of bottom parapet on strength of the walls for a) DH configuration and b) SH configuration

4.4.3.3 Global Ductility

Whether the failure mode changes or not (Fig. 4-16) has a direct impact on the global ductility of the wall when comparing wall configurations with doors and windows. Figure 4-17 shows that having the failure occurring in the CLT, meant that walls with DH configuration were unaffected by the increase in stiffness and strength of the CLT panels (Fig. 17-a). Contrarily the additional of the bottom parapet has a noticeable effect on the global ductility in case of SH configuration which is a consequence of engaging the hold-down (Fig.4-17-b).

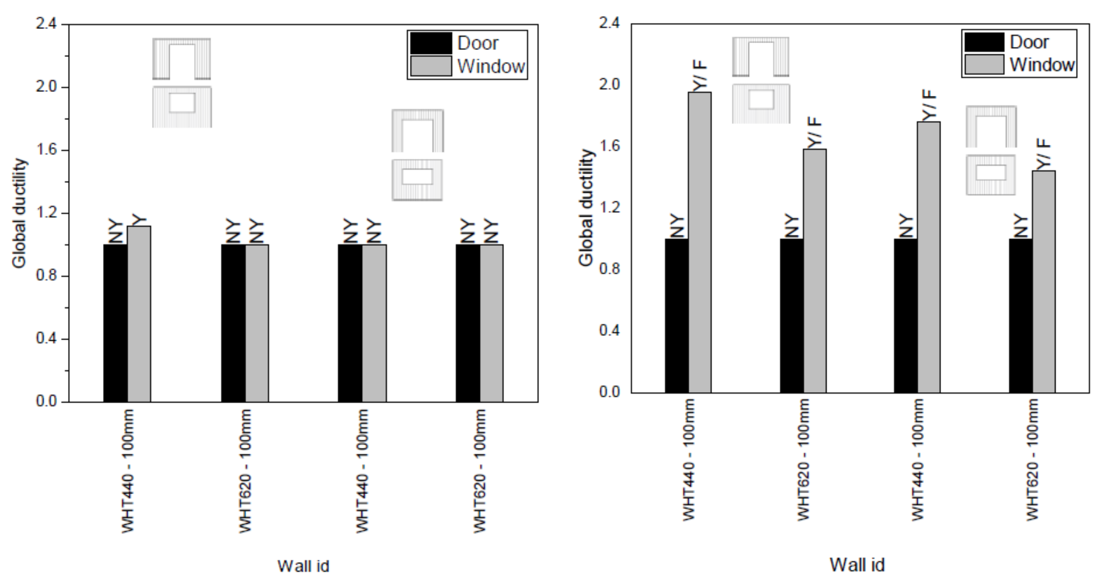

Figure 4-17. Effect of bottom parapet on ductility of the walls for a) DH configuration and b) SH configuration

4.5 Classification Tree Failure Model

This section discusses a method to help with preliminary design and classification of the failure mode in the wall in terms of CLT or hold-down failure. The classification tree is intended to be used in the capacity-based seismic design, where the preferred failure mode can be controlled. It should be noted that the method is limited to the configuration studied, and although the values are representative of the range used in construction, deviation from these assumptions may alter the output of the analysis. As such it is important to present the limitation of the analysis, as shown in Table 4-11.

Table 4-11. Framework of the classification tree model

Characteristic of the wall	***Value***
Wall type	*Centrally placed door opening*
Total wall thickness	*≈100 and 150 mm*
Lamellae ratio	*≈1 or 0.67*
Lintel slenderness	*≈0.67, 1, 2 and 6*
Wall segment slenderness	*≈2, 3.5 and 4*
Hold down stiffness	*≈6500 and ≈13000 N/mm*
Hold down configuration	*single vs double*

Based on the analyzed shearwalls with door opening, the *"rpart" package ("Recursive PARTitioning")* of an open source statistical software were used (R Core Team, 2018) to predict whether each wall configuration analyzed in the inelastic range failed in terms CLT or HD. Each node corresponding to the quantitative factors gives a binary decision corresponding to the failure case observed.

4.5.1 Classification Based on Most Important Parameters

Figure 4-18 presents the classification tree, where different paths are illustrated based on the properties used in the analyses. The first variable selected by the algorithm to construct the classification tree is the lintel beam slenderness. This is done because the lintel beam slenderness is the variable that contributes the most to the reduction of the residual mean deviance (RMD). The classification tree shows that if the lintel slenderness is less than 1.5, the total wall thickness (t) governs the failure mechanism. At this level, when the wall thickness is 150 mm, failure is likely to occur in the hold-downs. However, if the wall thickness is 100 mm, the hold-down configuration will dominate the behaviour. For double hold-down configuration, the hold-down stiffness governs the failure, where for relatively high values failure occurs in the lintel, otherwise failure is expected in the hold-down. In case of SH configuration, the laminate ratio is the governing variable.

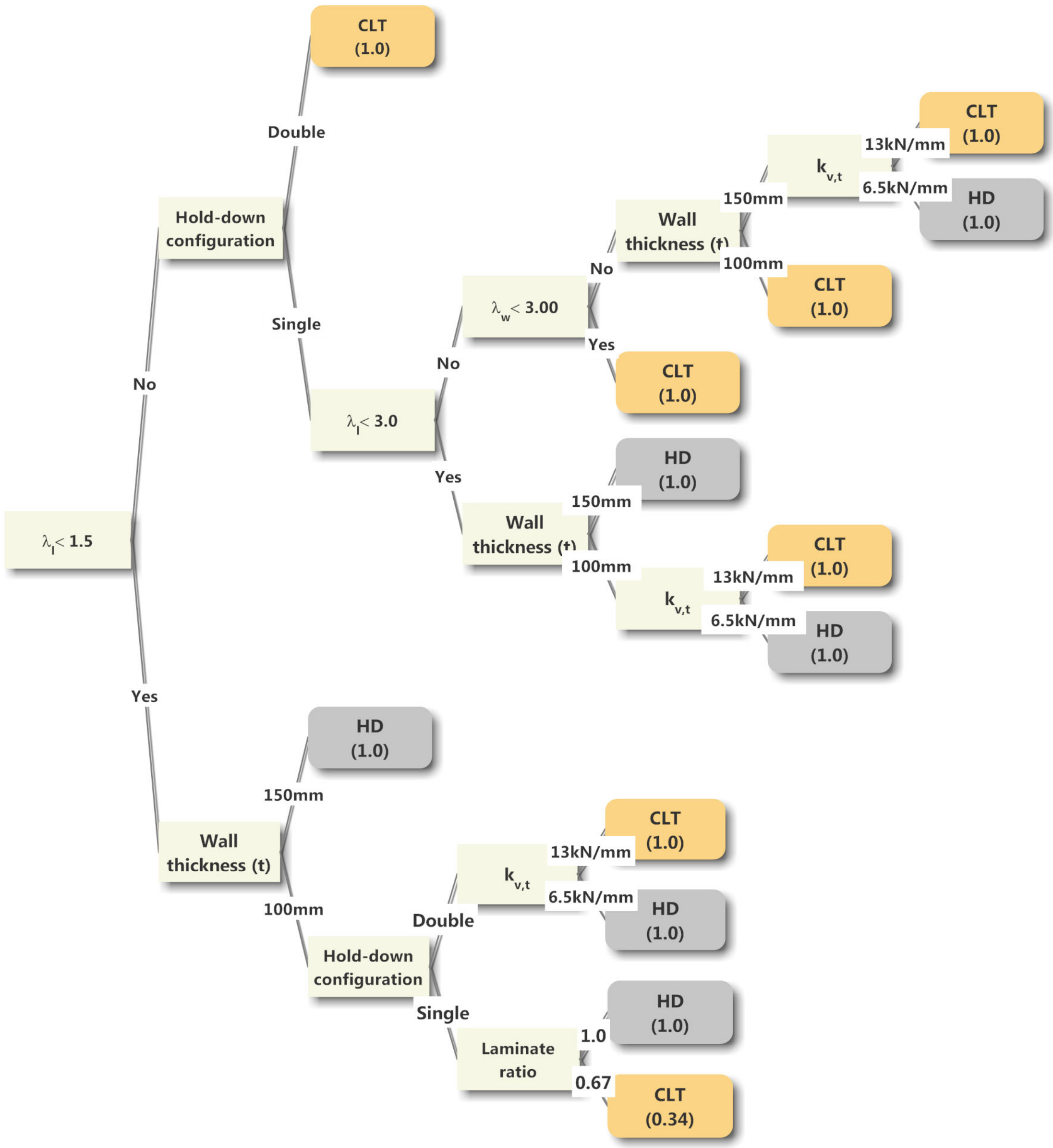

Figure 4-19. Classification tree model failure of CLT shearwalls with door openings in terms of hold-down (HD) or CLT

4.5.2 Accuracy of the model

Table 4-12 shows that the method was successful in predicting all the failure modes using the fitted tree.

Table 4-12. Results of the classification tree model

Actual	**Group**	**Predicted**	
Failure	*Size*	*CLT*	*HD*
CLT	*42*	*42*	*0*
		100%	*0%*
HD	*22*	*0*	*22*
		0%	*100%*

The Residual Mean Deviance (RMD), which is equivalent to the Root Mean Square in a regression analysis, provides an estimate of the accuracy of prediction. The smaller the value, the more precise the prediction. A value of RMD of 0.073 was found for the classification tree which is low and indicates the appropriateness of the model for the analysis cases studied.

References of Chapter 4

ASTM, E2126-07. (2007). Standard Test Methods for Cyclic (Reversed) Load Test for Shear Resistance of Walls for Buildings. West Conshohocken, PA: ASTM International.

Bogensperger, Thomas, Moosbrugger, Thomas, & Silly, Gregor. (2010). *Verification of CLT-plates under loads in plane.* Paper presented at the 11th World Conference on Timber Engineering 2010, WCTE 2010, June 20, 2010 - June 24, 2010, Trentino, Italy.

Casagrande, Daniele, Polastri, Andrea, Sartori, Tiziano, Loss, Cristiano, & Chiodega, Manuela. (2016). *Experimental tests for mechanical characterization of timber buildings connections*.

CSI. (2017). SAP2000 Integrated Software for Structural Analysis and Design. Berkeley, California: Computers and Structures Inc.

EN1995-1-1. (2004). (Eurocode 5) Design of timber structures – Part 1.1: General – Common rules and rules for buildings.: CEN Brussels.

EOTA. (2015). Three-Dimensional Nailing Plate (Angle Brackets and Hold-Downs for Timber-to-Timber or Timber-to-Concrete or Steel Connections) *European Technical Assessment ETA-11/0086*. Charlottenlund, Denmark.

ETA-12/0347. (2017). European Technical Assessment, Solid Wood slab elements to be used as structural elements in buildings, Manufacturer: X-Lam Dolomiti: OIB: Austrian Institute of Construction Engineers, Austria.

R Core Team. (2018). R: A language and environment for statistical computing. Vienna, Austria. R Foundation for Statistical Computing. Retrieved from https://www.R-project.org/.

CHAPTER 5

Equivalent Frame Model

5.1 General

Despite the contributions and advancement in complex numerical analysis methods, the appropriateness of such methods is limited, when considering their use in design practice. Furthermore, the applicability of such complex analysis for multi-storey buildings is also hindered by the high number of degrees of freedom and the complex post-processing analysis. This has prompted the author to investigate the applicability of an equivalent frame model (EFM) as an alternative analysis approach for CLT shearwalls with openings when subjected to lateral loads. This approach has been successfully used for modelling other structural materials, such as concrete and masonry (Tomasevic M., 1978, Brencich et al., 1998, Magenes and Della Fontana, 1998), but its application to CLT is novel.

The proposed equivalent frame model is developed specifically to aid in the analyses of the elastic behaviour of CLT shearwalls with openings. The proposed X-Lam Equivalent Frame model (i.e. X-LEF model) applies to monolithic CLT walls and takes into account the mechanical interaction between wall segments and lintels. The model can easily be adopted to the case of segmented walls by simply considering pinned restraints between the wall segments and lintel. It is noteworthy to mention that the proposed approach represents the first step in the application of the proposed method.

5.2 General Description of the Equivalent Frame Model for CLT Shear Walls

The unique contribution of the proposed model lies in the introduction of orthotropic material behaviour characterizing the CLT panels, as well as flexible mechanical anchors at the base of the CLT walls. The vertical wall segments and lintel beams are represented by 1-D frame elements, with rectangular cross-section, placed at their centre lines (Figure 5-1). The vertical wall segments are attached to a base by means of vertical and horizontal springs, which are connected to horizontal rigid bars at the bottom of the wall segments, simulating the mechanical behaviour of the anchors. The role of the rigid bars is to reflect the actual length of the wall segments as well as the correct location of the mechanical anchors (i.e. hold-down and angle-brackets) along the wall.

The flexible frame elements are assumed to have the same transverse dimensions (i.e. rectangular cross-section) as those of the shear-wall elements (wall segments and lintels). When assigning the material properties of the frame elements, the layout and orientation of the CLT lamellae are required to be taken into account.

Effective moduli of elasticity of the vertical wall segments, $E_{ef,w}$, and lintel beams, $E_{ef,l}$, can be defined through the composite theory by equalizing the axial and in-plane bending stiffness of the CLT cross-sections to the axial and bending stiffness of the corresponding frame element cross-sections, similar to the approach used by Blass and Fellmoser (2004) for solid wood panels. Assuming a linear stress-strain relationship and that plane cross-sections remaining plane, the axial K_A and bending K_B stiffness of the CLT cross sections are calculated by taking into account only the layers parallel to the direction of the stresses, as reported in equations 5-1 and 5-2 for wall segments and lintels, respectively.

$$\begin{aligned} K_{A,w} &= b \cdot \textstyle\sum_i \left(E_{0,i} \cdot t_{v,i}\right) \\ K_{B,w} &= \frac{b^3}{12} \cdot \textstyle\sum_i \left(E_{0,i} \cdot t_{v,i}\right) \end{aligned} \qquad (5\text{-}1)$$

$$\begin{aligned} K_{A,l} &= h_L \cdot \textstyle\sum_j \left(E_{0,j} \cdot t_{h,j}\right) \\ K_{B,l} &= \frac{{h_L}^3}{12} \cdot \textstyle\sum_j \left(E_{0,j} \cdot t_{h,j}\right) \end{aligned} \qquad (5\text{-}2)$$

where $t_{v,i}, t_{h,j}$ represent the thickness of the *i-th* vertical and *j-th* horizontal laminates, respectively, E_0 is the elastic modulus of the laminations in the direction parallel to the grain, b and h_L are the length of the wall segments and the height of the top lintels, respectively. For bottom lintels (i.e. parapet) h_L is replaced by h_C in shearwalls with window openings.

The axial and the bending stiffness for rectangular cross sections of the frame elements are calculated using the effective moduli of elasticity as reported in equations 5-3 and 5-4 for wall segments and lintels, respectively.

$$\begin{aligned} K_{A,frame,w} &= b \cdot t \cdot E_{ef,w} \\ K_{B,frame,w} &= \frac{b^3}{12} \cdot t \cdot E_{ef,w} \end{aligned} \qquad (5\text{-}3)$$

$$\begin{aligned} K_{A,frame,l} &= h_L \cdot t \cdot E_{ef,l} \\ K_{B,frame,l} &= \frac{{h_L}^3}{12} \cdot t \cdot E_{ef,l} \end{aligned} \qquad (5\text{-}4)$$

where t is the thickness of the frame elements taken equal to the total thickness of the CLT panel. Equalizing the expressions of equations 5-1 with the corresponding expressions of equations 5-3, and the expressions of equations 5-2 with those of equations 5-4, the effective moduli for the frame elements, which represent the wall segments and the lintels, can be calculated as in equations 5-5 and 5-6 for wall segments and lintels, respectively.

$$\begin{matrix} K_{A,w} = K_{A,frame,w} \\ K_{B,w} = K_{B,frame,w} \end{matrix} \rightarrow E_{ef,w} = \frac{\sum_i (E_{0,i} \cdot t_{v,i})}{t} \qquad (5\text{-}5)$$

$$\begin{matrix} K_{A,l} = K_{A,frame,l} \\ K_{B,l} = K_{B,frame,l} \end{matrix} \rightarrow E_{ef,l} = \frac{\sum_j (E_{0,j} \cdot t_{h,j})}{t} \qquad (5\text{-}6)$$

The in-plane shear stiffness of the CLT panels is obtained from the product of the total cross section area, including both vertical and horizontal lamellae, and an effective shear modulus of the CLT panels, G^*. The calculation takes into account the effective shear and torsional deformation of all layers, according to the formula given in Bogensperger et al. (2010) and Brandner et al. (2017). Since the frame elements are characterized by the same cross section area as the CLT panel, the effective shear modulus G_{eq} of the frame elements is assumed to be equal to G^*, both for wall segments and lintels, as presented in equation 5-7.

$$G_{ef} = G^* \qquad (5\text{-}7)$$

As reported by Brandner et al. (2017), the effective shear modulus of CLT panels, G^*, can be obtained from equations 5-8 and 5-9 as follows:

$$G^* = \frac{G_{0,mean}}{1 + 6 \cdot \alpha_T \cdot \left(\frac{t_{mean}}{w}\right)^2} \qquad (5\text{-}8)$$

with

$$\alpha_T = p \cdot \left(\frac{t_{mean}}{w}\right)^q \text{and } t_{mean} = \frac{t}{N} \qquad (5\text{-}9)$$

where p and q are equal to 0.53 and -0.79 for a 3-layers panel and equal to 0.43 and -0.79 for a 5-layers, respectively. $G_{0,mean}$ is the in-plane shear modulus of laminations, N is the number of layers in the CLT panel and w is the minimum between: the board width , the distance between two reliefs, or the distance between a relief cut and board edge in the case, where relief cut exist and no edge gluing is provided.

In case of elastic analyses, a linear behaviour of the mechanical anchors can be adopted with a vertical and a horizontal stiffness equal to k_v and k_h, respectively. Due to the contact between the wall panels and the base, the stiffness along the vertical direction is non-linear even in the elastic phase, where stiffness $\left(k_{v,c}\right)$ and $\left(k_{v,t}\right)$ are assumed, when the anchors are subjected to compressive and tensile loads, respectively. When any of the anchors is omitted, the equivalent spring is replaced with a contact (also known as "gap") element with zero-stiffness in tension and a stiffness equal to $k_{v,c}$ in compression (Figure 5-1).

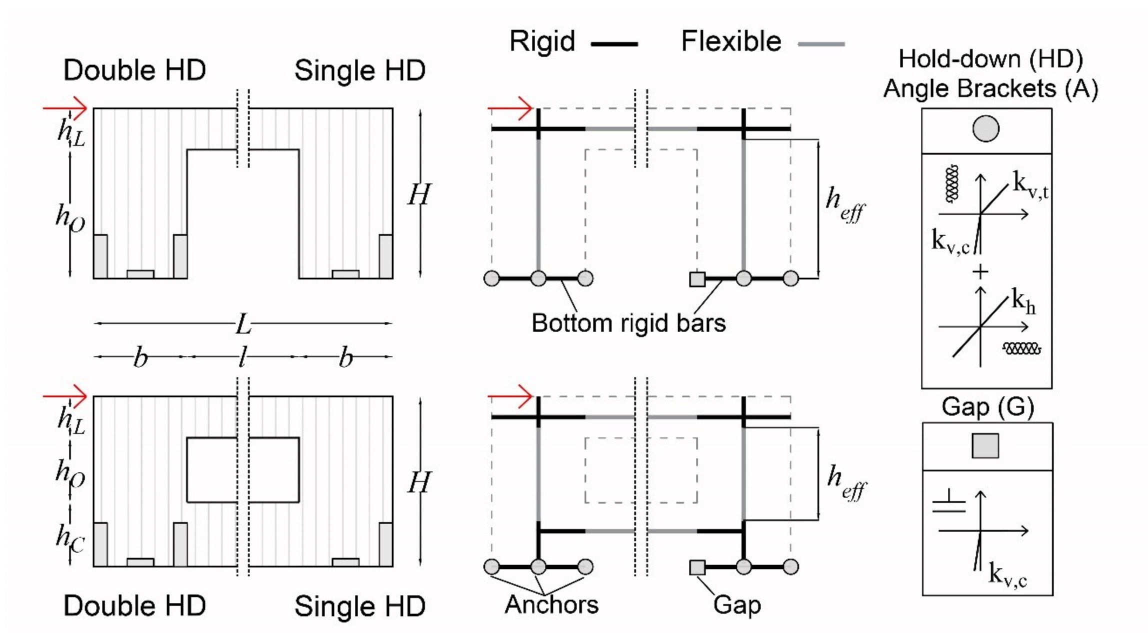

Figure 5-1. Equivalent Frame method for CLT shearwalls with openings

The nodes are considered in the model by limiting the physical length of the frame elements and introducing infinitely rigid zones at the intersection between the wall segments and lintels, as illustrated in Figure 5-2.

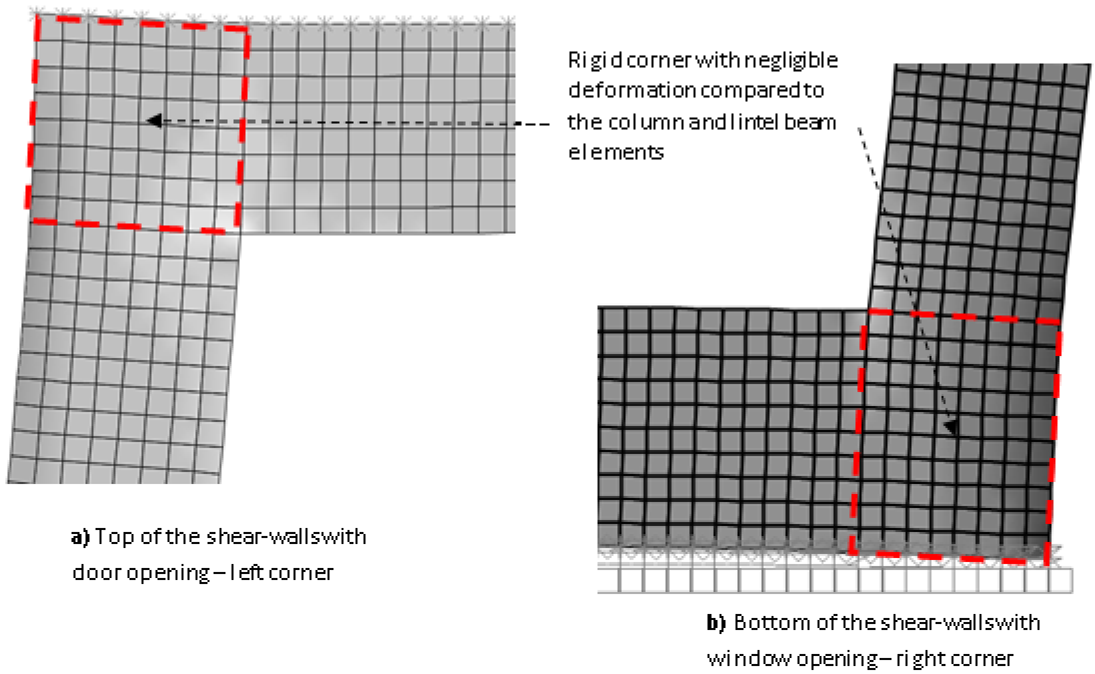

Figure 5-2. Kinematics of the corners in case of 1-storey shearwalls modeled by elastic shell elements

The criterion proposed by Dolce (1991) is adopted in this study to determine the effective height h_{eff} of the wall segments, as shown in equation 5-10.

$$h_{eff} = h' + \frac{1}{3} \cdot b \cdot \frac{H-h'}{h'} \leq H \qquad (5\text{-}10)$$

where b is the length of the wall segments, H is the height of the wall and h' is the distance between the midpoints of the lines connecting the corners of the opening to the wall vertical edges. The lines are limited by an inclination that is less than 30° with horizontal. A graphic representation to determine h' is illustrated in Figure 5-3. This limit for the inclination has not been verified for CLT walls with openings and is a subject of future work. For the lintels, the flexible length l_{eff} is assumed to be equal to the geometrical length l. In Table 5-1, a summary of the geometrical and mechanical parameters of the frame elements (i.e. wall segments, top- and bottom lintels) is reported.

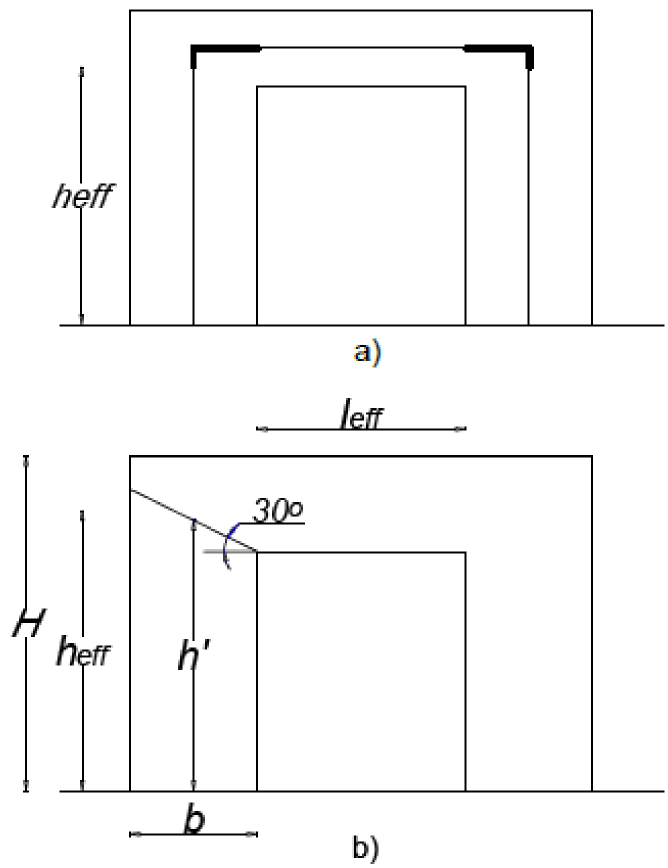

Figure 5-3. Equivalent Frame modeling of 1-storey shearwalls as per Dolce (1991)

Table 5-1. Geometrical dimensions and effective modulus of elasticity and shear modulus of frame elements

Element	Section of frame element	Length of frame element	Effective Modulus of elasticity E of frame element	Effective Shear modulus G of frame element
Wall segments	$b \times t$	h_{eff}	$E_{ef,W}$	G_{ef}
Top Lintel	$h_L \times t$	l_{eff}	$E_{ef,L}$	G_{ef}
Bottom Lintel	$h_C \times t$	l_{eff}	$E_{ef,L}$	G_{ef}

5.3 Numerical analyses

In order to ensure that the proposed model provides mathematically correct output, the wall's lateral stiffness, hold-down tensile load as well as selected internal actions were compared with a 2D model where area elements are adopted. The study addresses cases of both window and door openings assumed to be centrally placed within the wall. The geometry and panel dimension in the analyses were selected based on practical sizes used in construction. A total of twenty-seven (27) configurations with different length-to-width aspect ratios of wall segments and lintels were analyzed, yielding a total of 216 case studies. All analyses were carried out using the commercially available structural analysis software SAP2000 (CSI, 2017).

5.3.1 Geometrical Dimensions and Mechanical Properties of Case Studies

For all configurations, the height of the wall segments $(h_{O,d})$ was taken as $2.4\,m$ for layouts with door openings. The segment below the window (h_C) was taken as $1.0\,m$ whereas the height of the window $(h_{O,w})$ was taken as $1.4\,m$ for all layouts with window openings. Three values of the vertical wall segment width (b) were investigated, namely

$[0.8;\ 1.4;\ 2.8]$ m. The lintel height (h_L) and length (l) were analyzed for values of $[0.4;\ 0.6;\ 0.8]$ m and $[0.8;\ 2.0;\ 3.2]$ m, respectively. The CLT panels consisted of five plies with 20 mm thick laminates, totalling 100 mm in panel thickness. The major direction of the CLT panels was assumed to be along the vertical direction. The MOE of the CLT panels parallel and perpendicular to grain, E_0 and E_{90}, were assumed to be 12.000 MPa and 370 MPa, respectively. The average in-plane shear modulus $G_{0,mean}$ is assumed to be equal to 690 MPa. These values are based on typical values found in the manufacturers' literature (ETA-12/0347, 2017).

The slenderness parameter, representing the ratio of length to width for the lintel and wall segment, is used in the analysis to facilitate the discussion. The slenderness of the wall segments and lintel beam are denoted λ_w and λ_l, respectively, and are defined in Chapter 3, section 3.3.1.

Two layouts for the hold-downs are considered; a double hold-down (DH) configuration, where a hold-down is placed at both ends of each wall segment, or a single hold-down (SH) configuration, where only one anchor per wall-segment is adopted and placed at the ends of the wall. A number of angle brackets n_a along the base of the wall segments were chosen equal to 1, 2 and 3 for a width of the wall segments equal to 0.80 m, 1.8 m and 2.40 m, respectively, as shown in Figure 5-4.

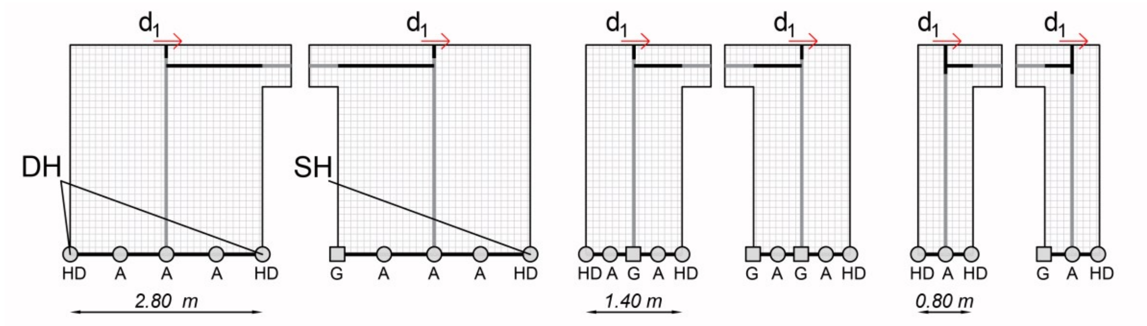

Figure 5-4. Equivalent frame models adopted for the numerical analyses

The hold-down anchors are only considered effective along their main direction such that only the tensile stiffness is considered and the horizontal (shear) stiffness is neglected, as demonstrated by Gavric et al. (2015). Two values of the spring representing the hold-down tensile stiffness reported in Casagrande et al. (2016) were considered, namely $k_{v,t,hd} = 6609\ kN/m\ and\ 13247 kN/m$ for WHT 440 and WHT620 hold-down with 30 and 55 4.0x60 mm nails, respectively.

For the angle brackets, a biaxial behaviour is assumed. The tensile vertical and horizontal stiffness of the spring representing the angle brackets are assumed to be equal to $k_{v.t,a} = 2530\ kN/m$ and $k_{h,a} = 2090\ kN/m$, respectively, as reported in Gavric et al. (2015) for BMF 90 angle bracket with 11 nails.

A summary of the geometrical dimensions and mechanical properties of the cases studied is reported in Table 5-2.

Table 5-2. Geometrical dimensions and mechanical parameters of the case studies

Property	Value
Height of the wall segment for door openings $(h_{O,d})$	*2.4 m*
Height segment below the window (h_C)	*1.0 m*
Height of window opening $(h_{0,w})$	*1.4 m*
Vertical wall segment's width (b)	*0.4 m – 1.8 m -2.4 m*
Lintel length (l)	*0.8 m - 2.0 m - 3.2 m*
Lintel height (h_L)	*0.4 m -0.6 m -0.8 m*
hold-down tensile stiffness $(k_{v,t,hd})$	*6609 kN/m – 13247 kN/m*
Hold-down configuration	*Double (DH)* and *Single (SH)*
Angle brackets vertical tensile stiffness $(k_{v,t,a})$	*2530 kN/m*
Angle brackets horizontal stiffness $(k_{h,a})$	*2090 kN/m*
Number of angle brackets per wall segment	*3 for b=2.8 m* *2 for b=1.4 m* *1 for b=0.8 m*

5.3.2 Load methods

Two different lateral load methods were considered in the analyses. In load method #1, the 2D model and the EFM were subjected to the same lateral displacement d_1 (equal to 20 mm) at the top of both wall segments, resulting in different base shear loads ($V_{b,EFM} \neq, V_{b,2D}$) due to the difference in stiffness between the two models, see Figure 5-5.

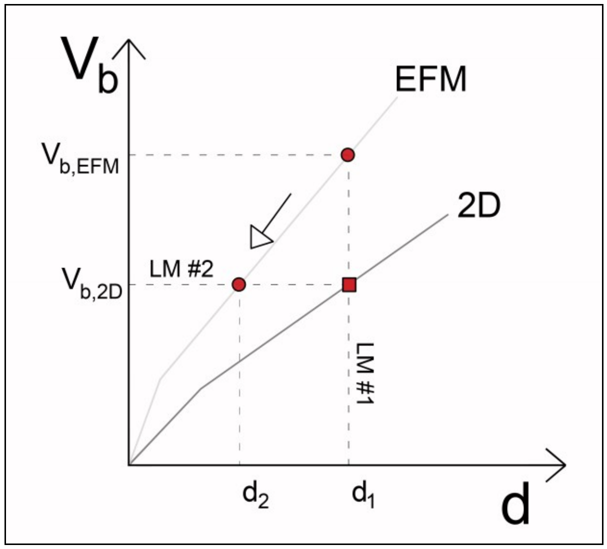

Figure 5-5. Load methods

In load method #2, the 2D model was subjected to the same top displacement d_1 of load method #1, whereas the imposed displacement on the EFM was increased or decreased to d_2 in order to obtain the same base shear of the 2D model, $V_{b,EFM} = V_{b,2D}$. No vertical load was applied in the analyses of the case studies.

It is noteworthy to mention that, in cases where vertical loads are not equal to zero, a non-linear elastic response of the wall is expected due to the elastic non-linear behaviour of mechanical anchors and gap elements. As a result, a non-linear elastic analysis is performed by first applying the vertical load and then increasing the horizontal displacement to the target value. A non-linear relationship between the base shear and the horizontal wall top displacement is expected in this case.

5.3.3 2D Model

The 2D model was developed using four-joints elastic quadrilateral homogenous shell elements available in the SAP 2000 software (CSI, 2017). These elements are able to combine independent membrane and plate behaviour; however, since the analyses were carried out in the 2D plane of the wall, only membrane behaviour was considered in the analysis. A four-point numerical integration formulation is used to determine the shell element stiffness whereas the internal forces are evaluated at the 2-by-2 Gauss integration points and extrapolated to the joints of the element. The membrane behaviour is based on an isoparametric formulation including translational in-plane stiffness components and a "drilling" rotational stiffness for the direction orthogonal to the plane of the element. The in-plane displacements are quadratic.

A systematic reduction in meshing was undertaken until a reasonable result was attained (compared to 25 mm meshing), as reported in Table 5-3. Based on the results of this analysis, 100 mm was used in the 2D model, since this size represented a reasonable balance between accuracy and computation time.

Table 5-3. Base shear values of 2D models for different mesh size

Door opening b=1.4 m; h_L=0.60 m; l=1.4 m	Mesh size		
	100 mm	50 mm	25 mm
Base shear V [kN]	86.4	84.6	83.3
Discrepancy from 25 mm mesh size	3.73%	1.55 %	-

Since homogenous shell elements are adopted, the effective modulus of elasticity of the CLT panels, $E_{ef,2D,v}$ and $E_{ef,2D,h}$, for the vertical and horizontal direction, respectively, need to be implemented to properly consider the contribution of different layers. Similar to the approach presented in Section 5.2 for the frame elements, the values of the effective modulus are determined by equalizing the vertical and horizontal axial stiffness $K_{A,CLT,v}$ *and* $K_{A,CLT,h}$ per unit length of the CLT panels to those of a homogenous shell element in the vertical and horizontal direction $K_{A,2D,v}$ *and* $K_{A,2D,h}$, respectively, as reported in Equations 5-11 to 5-13.

$$\begin{aligned} K_{A,CLT,v} &= \textstyle\sum_i E_{0,i} \cdot t_{v,i}\,; \\ K_{A,CLT,h} &= \textstyle\sum_j E_{0,j} \cdot t_{h,j}\,; \end{aligned} \qquad (5\text{-}11)$$

$$\begin{aligned} K_{A,2D,v} &= E_{ef,2D,v} \cdot t; \\ K_{A,2D,h} &= E_{ef,2D,v} \cdot t; \end{aligned} \qquad (5\text{-}12)$$

$$\begin{aligned} K_{A,2D,v} = K_{A,CLT,v} \; &\rightarrow E_{ef,2D,v} = \frac{\sum_i E_{0,i} \cdot t_{v,i}}{t} \\ K_{A,2D,h} = K_{A,CLT,h} \; &\rightarrow E_{ef,2D,h} = \frac{\sum_j E_{0,j} \cdot t_{h,j}}{t} \end{aligned} \qquad (5\text{-}13)$$

where $t_{v,i}, t_{h,j}$ represent the thickness of the *i-th* vertical and *j-th* horizontal laminates, respectively, and t is the thickness of the shell elements taken equal to the total thickness of the CLT panel. For a 5-layers 100 mm CLT panel with equal layer thickness of 20 mm, and E_0 equal to 12000 MPa, one obtains $E_{ef,2D,v}$ and $E_{ef,2D,h}$ equal to 7200 MPa and 4800 MPa, respectively.

Since the in-plane shear stiffness per unit length of the CLT panels is calculated as the product of the total thickness and the effective shear modulus of the CLT panels, G^*, the effective shear modulus, G_{2D}, of the shell elements are equal to the effective shear modulus of the CLT panels, G^*, both for wall segments and lintels, as presented in Equation 5-14.

$$G_{2D} = G^* \qquad (5\text{-}14)$$

For a 5-layers 100 mm CLT panel, a width of boards w equal to 150 mm and $G_{0,mean} = 690\ MPa$, one obtains $G_{2D} = G^* = 560\ MPa$, using Equation 5-8.

The hold-downs are represented by vertical springs located at the ends of each wall segment whereas the angle brackets are represented by 2-direction springs working along both the vertical and horizontal direction. The tensile stiffness of the hold-down and the angle bracket as well as the horizontal stiffness of the angle brackets were set equal to the values reported in Section 5.3.1. The compressive stiffness of the hold-down and the angle brackets along the vertical direction is represented by a rigid behaviour with stiffness of $k_{v,c} = 10^6\ kN/m$. Vertical gap elements, with stiffness in compression equal to 10^6 kN/m, were placed along the entire base of the wall.

5.3.4 The equivalent frame model

The equivalent frame model was developed using 2-joint frame elements available in the SAP 2000 software (CSI, 2017), which adopts a three-dimensional beam-column formulation including the effects of biaxial bending, torsion, axial deformation, and biaxial shear deformations (Bathe & Wilson, 1976). A rectangular cross section with a shear area factor equal to $\frac{5}{6}$ was chosen. The definition of the geometrical dimensions of frame elements as well as the effective moduli of elasticity and shear modulus are described in

Section 5.2. For a 5-layers 100 mm CLT panel with all the layers having the same thickness equal to 20 mm and E_0 equal to 12000 MPa, the values of $E_{ef,w}$ and $E_{ef,l}$ can be calculated to 7200 MPa and 4800 MPa, respectively, and G_{eq} becomes equal to 560 MPa. The same spring elements used in the 2D models were adopted to the equivalent frame model for the hold-down and the angle brackets.

5.4 Results and discussion

The results from the equivalent frame model was compared with the 2D model based on parameters such as base shear load, tensile load in the hold-downs, and in-plane bending moment at the lateral sections in the lintel beams. The shear force and in-plane bending moment were obtained from the 2D model by means of the "Section Cut" function available in SAP2000 software which integrates the internal forces per unit length of the shell elements for a given cross section.

The discrepancy, ϵ, between the two models was calculated as provided in equation 5-15. Positive values in equation 5-15 indicate that the values obtained from the frame model are higher than those obtained from the 2D model.

$$\epsilon = \left(\frac{resp_{EFM}}{resp_{2D}} - 1\right) \times 100\% \qquad (5\text{-}15)$$

where $resp_{EFM}$ and $resp_{2D}$ are the generic parameters for the EFM and the 2D model, respectively.

All detailed analysis can be found in Appendix B.

5.4.1 Base shear load

Since the base shear load of the EFM and 2D model are the same in load method #2, only load method #1 is considered in the following discussion. The results for the base shear load are provided in Table 5-4 in terms of maximum $|\varepsilon_{BS}|_{max}$ and mean $|\varepsilon_{BS}|_{mean}$ of the absolute values of discrepancies.

The highest value of the absolute error is equal to 12.6%, which was obtained for the case with door openings ($\lambda_w = 3.00; \lambda_l = 5.00$), SH hold-down configuration and hold-down stiffness equal to 6609 kN/m. A discrepancy greater than 10% was only observed in 10.2% of the cases with door openings.

From Figure 5-6, where the data for the errors with hold-down stiffness equal to 13247 kN/m are reported, it can be seen that the discrepancy between the two models as function of the slenderness ratio of the lintel and wall segments does not seem to be significant in cases with window openings (Figure 5-6c and 5-6d). For door openings, the discrepancy seems to increase with increasing lintel slenderness. The lowest values are related to slenderness of the wall segments equal to 0.86, whereas the highest values are related to a slenderness of the wall segments equal to 3.00. Parameters such as hold-down configuration (SH vs DH) and hold-down stiffness did not seem to have a significant effect on the discrepancy between the two models.

Table 5-4. Discrepancies for the Base Shear Load

Opening [-]	**Hold-down** [-]	$\mathbf{k_{v,t,hd}}$ [kN/m]	$\lvert\varepsilon_{BS}\rvert_{mean}$ [%]	$\lvert\varepsilon_{BS}\rvert_{max}$ [%]
Door	Double	13247	5.5	8.8
Door	Double	6609	6.1	10.5
Door	Single	13247	7.1	11.4
Door	Single	6609	7.3	12.6
Window	Double	13247	2.8	6.0
Window	Double	6609	3.0	5.8
Window	Single	13247	3.1	6.1
Window	Single	6609	3.0	5.3

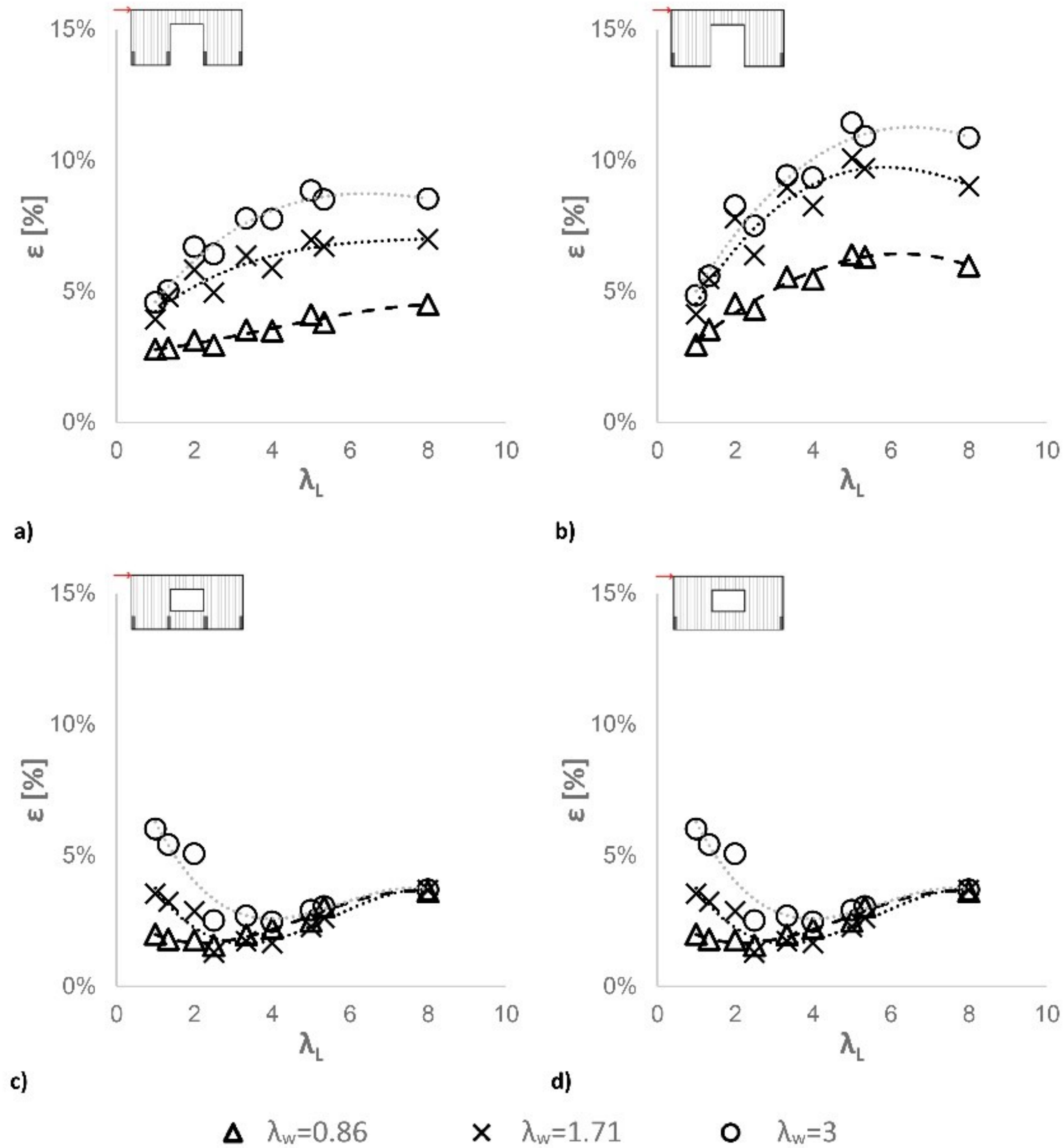

Figure 5-6. Discrepancy for the global stiffness, kv,t,hd = 13247 kN/m: a) Door opening - DH, b) Door opening – SH, c) Window opening – DH and d) Window opening – SH

5.4.2 Tensile Load in Hold-down

The differences found between the proposed X-LEF model and the 2D model with regard to the maximum tensile load in the hold-downs are reported in Table 5-5. The results show that slightly higher values of discrepancies were obtained for load method #2 than load method #1. For load method #1, the maximum discrepancy in terms of absolute value found was 8.7% ($\lambda_w = 3.00; \lambda_l = 3.30; k_h = 6609\ kN/m; Single\ HD$), and 6.1% ($\lambda_w = 0.86; \lambda_l = 8.00; k_h = 13247\ kN/m; Single\ HD$), for configurations with door and window openings, respectively. On the contrary, for load method #2, the maximum discrepancy in terms of absolute value found was 14.2% ($\lambda_w = 3.00; \lambda_l = 5.30; k_h = 6609\ kN/m; Single\ HD$), and 10.4% ($\lambda_w = 0.86; \lambda_l = 8.00; k_h = 13247\ kN/m;\ Single\ HD$), for configurations with door and window openings, respectively. A discrepancy greater than 10% was only observed in 7.4% of the cases with door openings and in only one case with window openings for load method #2.

Figure 5-7 presents the values of error obtained in load method #1, for a hold-down stiffness equal to 13247 kN/m, as function of the lintel and wall segment slenderness. For all cases, no clear trend is observed, and the error range remains relatively consistent.

Table 5-5. Discrepancies for tensile force in the hold-own

			load method #1		load method #2	
Opening	**Hold-down**	**$k_{v,t,hd}$**	$\lvert\varepsilon_{Th}\rvert_{mean}$	$\lvert\varepsilon_{Th}\rvert_{max}$	$\lvert\varepsilon_{Th}\rvert_{mean}$	$\lvert\varepsilon_{Th}\rvert_{max}$
[-]	[-]	[kN/m]	[%]	[%]	[%]	[%]
Door	Double	13247	2.1	5.4	3.7	8.4
Door	Double	6609	2.0	4.3	5.7	12.6
Door	Single	13247	3.2	7.8	4.0	11.4
Door	Single	6609	3.2	8.7	4.6	14.2
Window	Double	13247	0.7	2.8	2.8	6.2
Window	Double	6609	0.9	1.9	3.4	5.8
Window	Single	13247	2.9	6.1	0.9	10.4
Window	Single	6609	1.7	4.4	1.2	4.4

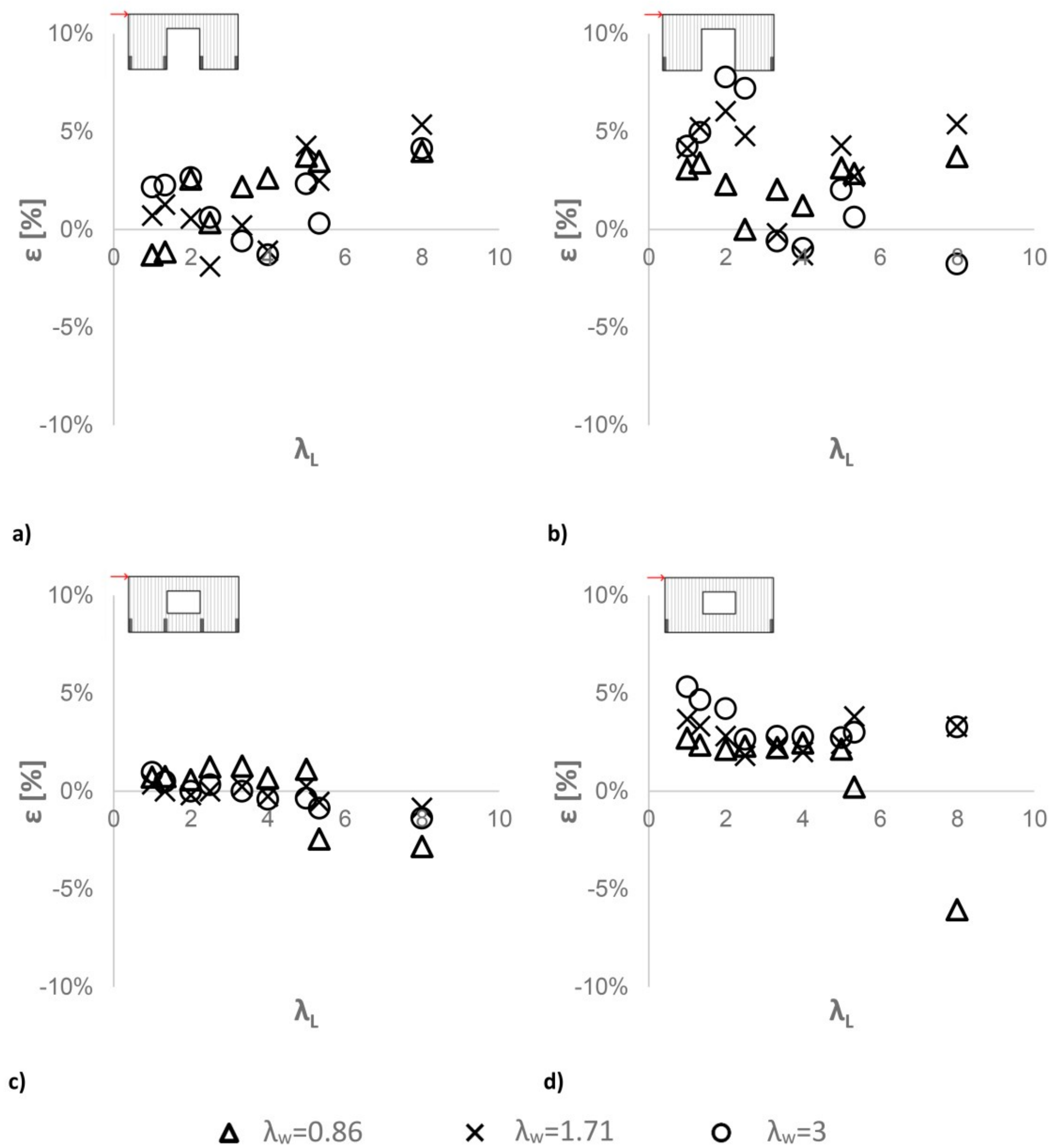

Figure 5-7. Discrepancy for hold-down tensile load, kv,t,hd = 13247 kN/m, in load method #1: a) Door opening - DH, b) Door opening – SH, c) Window opening – DH and d) Window opening - SH,

5.4.3 Shear load and bending moment in the top lintel

The differences in the shear load values obtained for the top lintels are summarized in Table 5-6. The largest error value obtained was equal to 18.7% ($\lambda_w = 1.71; \lambda_l = 5.00; k_h = 6609\ kN/m; Single\ HD$) and 22.9% ($\lambda_w = 0.85; \lambda_l = 8.00; k_h = 6609\ kN/m; Single\ HD$) for walls with door and window openings, respectively, when load method #1 is adopted. For load method #2, a highest absolute value of 8.3% ($\lambda_w = 1.71; \lambda_l = 5.00; k_h = 6609\ kN/m; Double\ HD$) and 26.7% ($\lambda_w = 0.85; \lambda_l = 8.00; k_h = 6609\ kN/m; Single\ HD$) is obtained for walls with door and window openings, respectively.

In both load methods, the differences between the values obtained for different hold-down configurations and stiffness were observed to be insignificant. Comparing the mean of absolute errors, values lower or equal than 10% and 7% are obtained from load method #1, for door and window opening, respectively. On the contrary, in load method #2, absolute mean values of discrepancies of less than 4% are obtained for door opening and no significant variation from load method #1 was observed for window openings.

A discrepancy in terms of absolute values greater than 15% was only observed in 15.7% of the cases with door openings and in 7.4% of cases with window openings for load method #1. For load method #2 all cases give a discrepancy lower than 10% for door openings and for window opening a discrepancy greater than 15% was only observed in 13.9% of the cases.

Figure 5-8 shows an example of the discrepancy obtained in load method #1 for hold-down stiffness equal to 13247 kN/m. Whereas an increasing trend as a function of lintel stiffness is observed for door openings (especially for values between 1 and 6), a decreasing trend is observed in the case of window openings.

Table 5-6. Discrepancies shear load in the lintel

			load method #1		load method #2	
Opening	**Hold-down**	$\mathbf{k_{v,t,hd}}$	$\lvert\varepsilon_{Vl}\rvert_{mean}$	$\lvert\varepsilon_{Th}\rvert_{max}$	$\lvert\varepsilon_{Vl}\rvert_{mean}$	$\lvert\varepsilon_{Th}\rvert_{max}$
[-]	[-]	[kN/m]	[%]	[%]	[%]	[%]
Door	Double	13247	7.7	15.4	3.1	7.4
Door	Double	6609	9.7	18.2	3.8	8.3
Door	Single	13247	9.6	17.1	3.3	5.9
Door	Single	6609	9.5	18.7	3.0	7.4
Window	Double	13247	6.5	20.6	6.3	23.4
Window	Double	6609	6.7	22.1	6.6	25.4
Window	Single	13247	6.9	20.0	6.6	23.7
Window	Single	6609	7.0	22.9	6.9	26.7

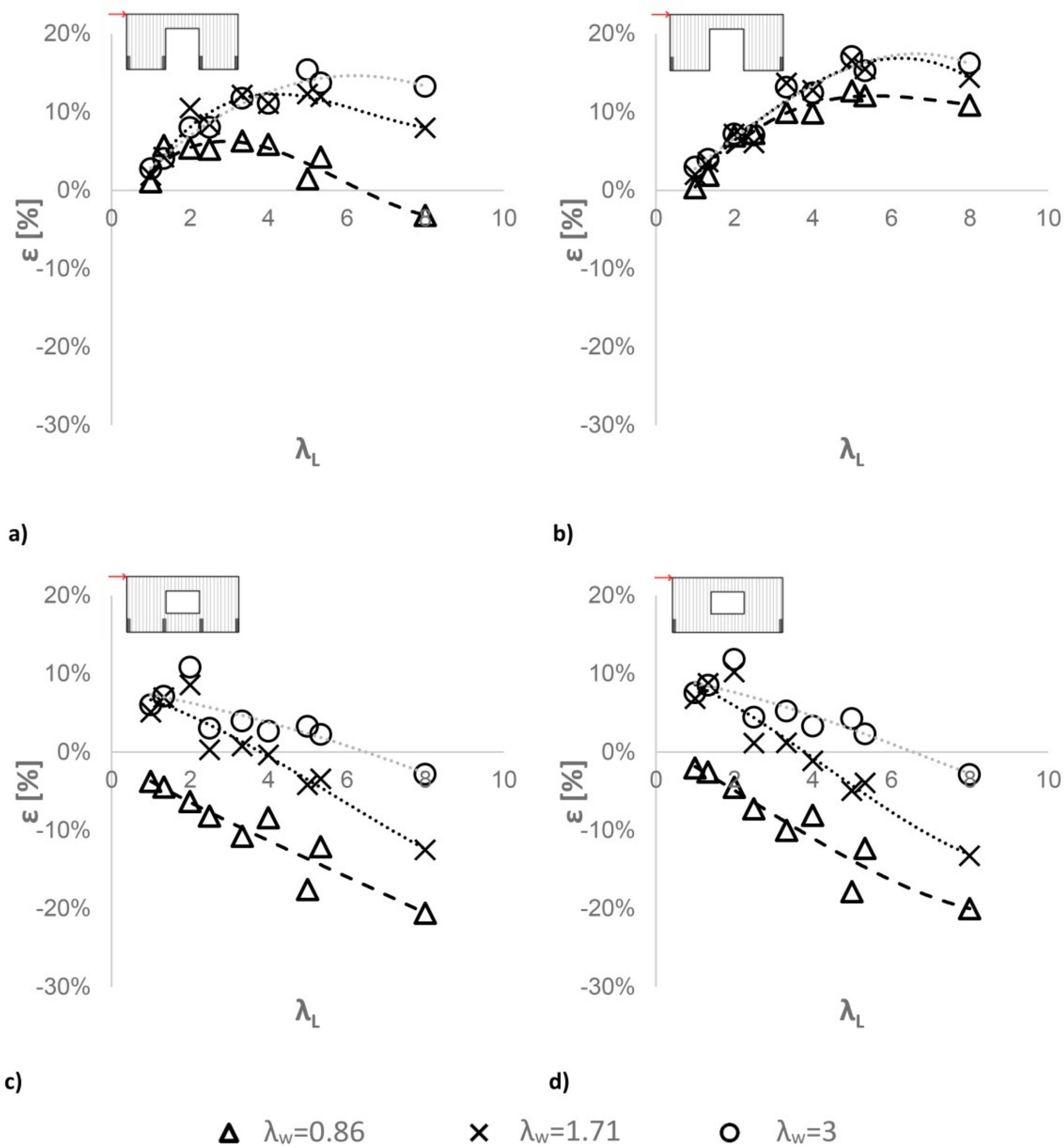

Figure 5-8. Discrepancy for lintel shear load, kv,t, hd = 13247 kN/m, in load method #1: a) Door opening - DH, b) Door opening – SH, c) Window opening – DH and d) Window opening - SH,

The results of discrepancies obtained for the bending moment values in the lintel are presented in Table 5-7. It can be observed that similar to the case for shear in the top lintel, the mean absolute values are higher for load method #1 compared to method #2 for door openings whereas similar values are obtained in case of window openings. The maximum absolute values of discrepancies do not change significantly between the two load methods.

From Figure 5-9, it is seen that, a clear trend is not observed for door openings whereas a decreasing trend in the error is found as a function of lintel slenderness.

For load method #1, an absolute value of discrepancy in bending moment higher than 18% was achieved in the 11.1% and 6.5% of cases for door and window opening, respectively. For load method # 2, only 3.7% and 7.4% of analyzed cases for walls with door and window openings, respectively, were observed to have an absolute value of error higher than 18%.

Table 5-7. Discrepancies of bending moment load in the lintel

			load method #1		**load method #2**	
Opening	**Hold-down**	**$k_{v,t,hd}$**	$\lvert\varepsilon_{Ml}\rvert_{mean}$	$\lvert\varepsilon_{Th}\rvert_{max}$	$\lvert\varepsilon_{Ml}\rvert_{mean}$	$\lvert\varepsilon_{Th}\rvert_{max}$
[-]	[-]	[kN/m]	[%]	[%]	[%]	[%]
Door	Double	13247	12.3	27.0	6.8	23.5
Door	Double	6609	14.8	29.3	8.2	25.3
Door	Single	13247	11.4	18.0	4.0	9.4
Door	Single	6609	12.1	19.6	4.6	13.0
Window	Double	13247	8.3	26.6	7.3	24.2
Window	Double	6609	8.7	29.5	7.8	26.9
Window	Single	13247	7.1	18.9	6.5	22.7
Window	Single	6609	7.6	22.0	7.0	25.9

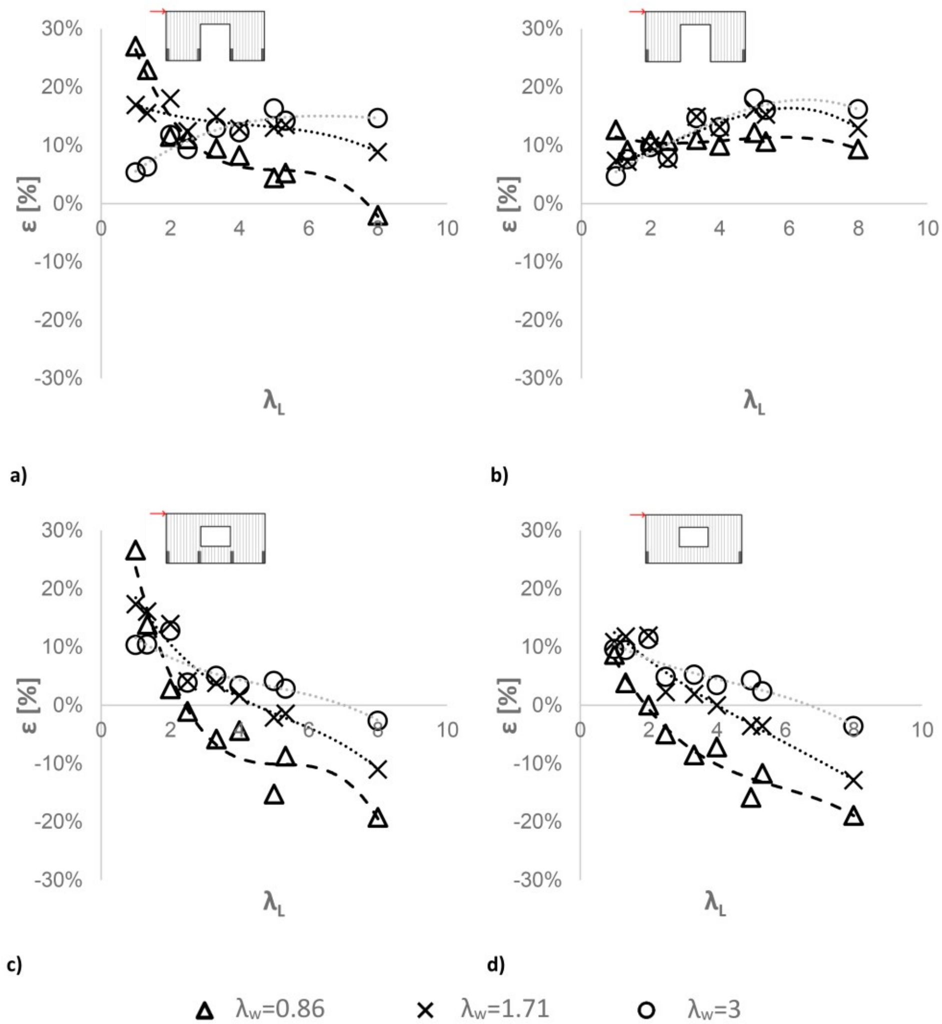

Figure 5-9. Discrepancy for lintel bending moment, kv,t,hd = 13247 kN/m, in load method #1: a) Door opening - DH, b) Door opening – SH, c) Window opening – DH and d) Window opening – SH

5.5 Experimental Validation with Published Shear Wall Test Results

The current research on CLT shearwalls with openings is still at its infancy. The issue is also complicated by the fact that many different configurations are required to cover a variety of design situations. As a minimum, parameters that need to be considered relating to the wall segments and lintel slenderness, as well as connections between the wall and the support (i.e. floor or foundation). In this section an experimental validation with shearwall test results found in literature is presented. The stiffness of two full-scale shear-wall tests are compared to those obtained from the numerical analysis using the EFM procedure.

Two prominent experimental campaigns on CLT shearwall with openings are those by Flatscher et al. (2015) and Ceccotti et al. (2006).

Flatscher et al. (2015) investigated a 3-ply (40V-32H-40V) 112 mm thick CLT shearwall with door opening, subjected to a horizontal monotonic load. The overall wall dimensions were 2.5 m by 2.5 m, and the door opening had dimensions equal to 0.9 m x 2.1 m (Figure 5-10). A vertical uniformly distributed load equal to 20.8 kN/m was applied on top of the wall to simulate gravity loads. A commercially available hold-down connector (HTT22) was used at each end of the wall (denoted in this paper as single hold-down shear-wall configuration). The hold-down was connected to the CLT wall segment using fifteen 4.0x60 mm ring shank nails. Two angle brackets (one at each wall segment) of type AE116 were attached to the walls using fourteen 4.0x60 mm ring shank nails. The stiffness of the angle-bracket in the horizontal ($k_{h,a}$) and the vertical ($k_{v,t,a}$) directions were equal to 2.90 kN/mm and 5.98 kN/mm, respectively. The vertical stiffness of the hold-down $k_{v,t,hd}$ was equal to 8.05 kN/mm. All stiffness values were obtained from experimental tests carried out on the connections and reported in Flatscher et al. (2015). Since no tests were carried out to obtain the horizontal (shear) stiffness of the hold-down $k_{h,hd}$, a value of 3.40 kN/mm, obtained from Gavric et al. (2015) for a similar hold-down (WHT540) and with a similar number of nails, was adopted. The elastic stiffness of the wall K_{ser} (EN26891, 1991), obtained from the full-scale experimental tests and evaluated as secant stiffness between the 10% and the 40% of the maximum horizontal load F_{max} (74.6 kN) as shown in Equation (5-15), was reported to be equal to 3917 kN/m (see Table 5-8).

$$K_{ser} = \frac{0.4F_{max} - 0.1F_{max}}{d_{0.4Fmax} - d_{0.1Fmax}} \qquad (5\text{-}15)$$

A non-linear elastic analysis was carried out on the equivalent frame model of the wall, by first applying the vertical load and then increasing the lateral force up to maximum value of load obtained from the experimental tests. Evaluating the secant stiffness K_{ser} from the experimental test, one obtains a value of 3610 kN/m. This yields a difference between the predicted and test value of -7.8% (Table 5-8).

As part of the SOFIE project, Ceccotti et al. (2006) performed a cyclic full-scale test on 5-ply, 85 mm thick CLT shearwalls with door openings. The wall dimensions were 2.95 m x 2.95 m with a door opening of 1.2 m x 2.2 m (Figure 5-10). The connection to the base consisted of two 90x48x3.0x116 BMF angle brackets attached with sixteen nails and two standard SIMPSON strong tie BMF HTT22 hold-downs with fourteen nails used in a SH hold-down configuration. A uniform gravity load of 18.5 kN/m was applied. No data were found in this paper for the stiffness of the connections and therefore the stiffness of the angle brackets and hold-down were taken from the experimental tests presented by Flatscher et al. (2015), where the same hold-down and angle bracket types were tested. The secant stiffness obtained from the 1st envelope load-displacement curve was equal to 3927 kN/m (Table 5-8).

From the force-displacement curve of the equivalent frame model, the secant stiffness K_{ser} was evaluated to be 3469 kN/mm, yielding a difference between the predicted and test value of -11.6%, see Table 5-8.

Table 5-8. Experimental and EFM data

Parameter	Flatscher et al. (2015)		Ceccotti et al. (2006)	
	Experimental test	**EFM**	**Experimental test**	**EFM**
F_{max} [kN]	74.6	-	100.6	-
$0.1F_{max}$ [kN]	7.46	7.46	10.06	10.06
$d_{0.1Fmax}$ [mm]	Not available	1.1	1.96	1.75
$0.4\ F_{max}$ [kN]	29.84	29.84	40.24	40.24
$d_{0.4Fmax}$ [mm]	Not available	7.30	9.30	10.45
K_{ser} [kN/m]	3917	3610	3927	3469
ε_{Kser}	-7.8%		-11.6%	

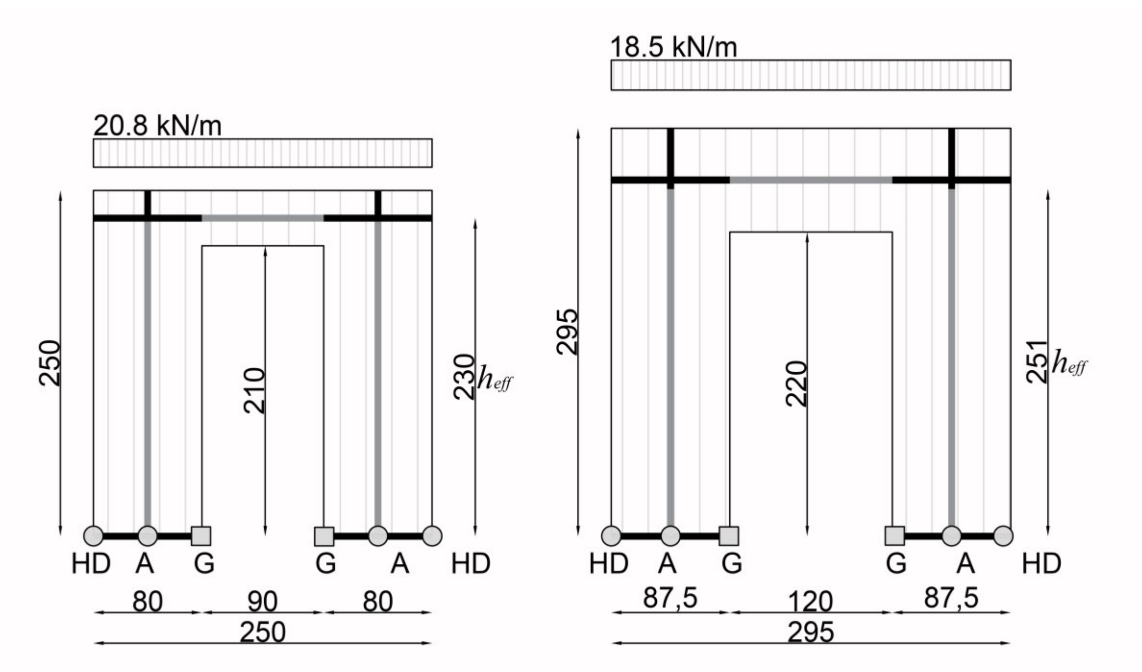

Figure 5-10. Shear-wall specimens used for the experimental validation. All measurements are in [cm]

Although reasonable agreement between the results obtained from the proposed model and experimental testing were found, the comparison is only considered preliminary because of the limited cases.

References of Chapter 5

Bathe, Klaus-Jürgen, & Wilson, Edward L. (1976). *Numerical methods in finite element analysis*. Englewood Cliffs, N.J.: Prentice-Hall.

Blass, Hans Joachim, & Fellmoser, Peter. (2004). *Design of solid wood panels with cross layers*. Paper presented at the Proceedings of the 8th World Conference on Timber Engineering, Lahti, Finnland 2004. Vol. 2.

Bogensperger, Thomas, Moosbrugger, Thomas, & Silly, Gregor. (2010). *Verification of CLT-plates under loads in plane.* Paper presented at the 11th World Conference on Timber Engineering 2010, WCTE 2010, June 20, 2010 - June 24, 2010, Trentino, Italy.

Brandner, Reinhard, Dietsch, Philipp, Dröscher, Julia, Schulte-Wrede, Michael, Kreuzinger, Heinrich, & Sieder, Mike. (2017). Cross laminated timber (CLT) diaphragms under shear: Test configuration, properties and design. *Construction and Building Materials, 147*, 312-327. doi:https://doi.org/10.1016/j.conbuildmat.2017.04.153

Casagrande, Daniele, Polastri, Andrea, Sartori, Tiziano, Loss, Cristiano, & Chiodega, Manuela. (2016). *Experimental tests for mechanical characterization of timber buildings connections*.

Ceccotti, A., Lauriola, M. P., Pinna, M., & Sandhaas, C. (2006). *SOFIE Project - Cyclic tests on cross-laminated wooden panels*. Paper presented at the 9th World Conference of Timber Engineering (WCTE).

CSI. (2017). SAP2000 Integrated Software for Structural Analysis and Design. Berkeley, California: Computers and Structures Inc.

Dolce, Mauro. (1991). Schematizzazione e modellazione degli edifici in muratura soggetti ad azioni sismiche. *L'Industria delle Costruzioni, 25,* 44-57.

EN26891. (1991). Timber structures – Joints made with mechanical fasteners - General principles for the determination of strength and deformation characteristics.

: ISO 6891-1983 (E).

ETA-12/0347. (2017). European Technical Assessment, Solid Wood slab elements to be used as structural elements in buildings, Manufacturer: X-Lam Dolomiti: OIB: Austrian Institute of Construction Engineers, Austria.

Flatscher, G., Bratulic, K., & Schickhofer, G. (2015). Experimental tests on cross-laminated timber joints and walls. *ICE Structure and Buildings*(168(11)), 868–877.

Gavric, Igor, Fragiacomo, Massimo, & Ceccotti, Ario. (2015). Cyclic behaviour of typical metal connectors for cross-laminated (CLT) structures. *Materials and Structures, 48*(6), 1841-1857. doi:10.1617/s11527-014-0278-7

CHAPTER 6

Experimental testing

6.1 General

The main purpose of the experimental campaign is to validate the elastic and in-elastic finite element models presented in Chapters 4 and 5. The test configurations, set-up and key results, including the capacity curves and corresponding kinematic modes are presented in this chapter.

6.2 Configurations

The walls consisted of five-ply CLT panels, manufactured using C24 spruce timber members, totalling 85 mm in thickness. Each lamella (ply) is 17mm thick with a transversal to longitudinal lamella ratio of 0.67. The five walls, initially panels, have been cut out by inserting openings to form three specimens with door opening and two specimens with window opening. To resist the uplift force generated from the wall overturning, two types of hold-down anchors, WHT440 and WHT620, were used (RothoBlass, 2015). These were selected to represent typical anchors found in construction covering a realistic range of stiffness and capacities. Both single (SH) and double hold-down (DH) configurations were investigated, reflecting the two most common design choices. The SH configuration simulates the case where only one hold-down is installed at the two ends of the wall. Similarly, the DH configuration involves the placement of two hold-down at both end of each wall segment. The hold-down brackets were connected to the wall panels using annular-ringed shank nails with a diameter of 4 mm and length of 60 mm. A total of thirty (30) nails where used to connect the WHT440 anchor, while fifty-five (55) nails were used for the WHT620 anchor. The anchors were bolted to the steel foundation using 16 mm bolts grade 8.8.

The geometry of the wall specimens and the hold-down configurations for walls with door and window openings are illustrated in Figure 6-1. All specimens had a total height, H, of 2.6 m. The total wall length, L, for specimens $01-04$ was 1.95 m, while the length of wall 05 was 2.3 m. The height of the openings, whether door or window, is defined as h_O, as shown in Figure 6.1. The opening height depended on the depth of the lintel beam, while the depth of the bottom parapet for walls with window openings, h_C, was kept at 1.1 m. The lintel height, h_L, varied for the different configurations and was set to 600 mm for specimens 01, and 02, 400 mm for specimens 03 and 04, and 300 mm for specimen 05.

The lintel length, l, also varied as a function of the total wall length and the width of the vertical wall segments. The lintel length was 750 mm for specimens 01 and 02, 700 mm for specimens 03 and 04, and 1000 mm for specimen 05.

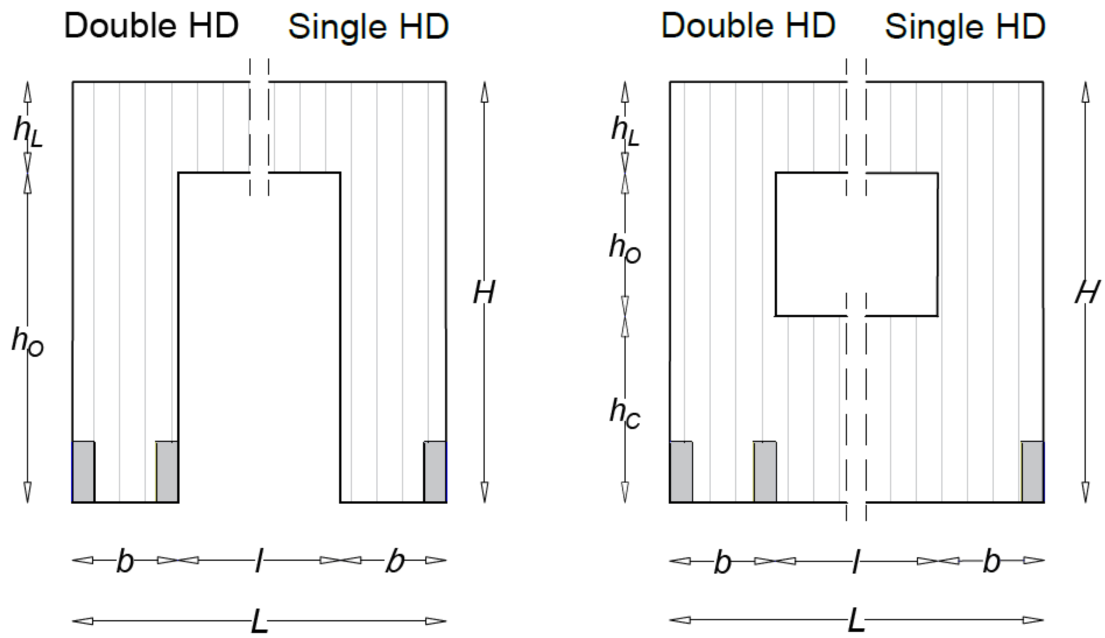

Figure 6-1. Geometric configuration of the tested shearwalls

6.3 Test Set-Up

Figures 6-2a and 6-2b show a schematic and a photograph depicting the full-scale test setup, including the tested CLT shearwall, the rigid steel reaction frame and the steel foundation beam to which the CLT shearwalls were attached. The load was applied on the walls using a horizontal hydraulic actuator with a load capacity of 400kN. The end of the actuator was placed at 140 mm from the top of the walls. The load was applied using a steel dowel, with a diameter of 40 mm, placed between the actuator head and a 25 mm thick steel plate that was attached to the side edge of the CLT panel, as indicated in Figure 6-3a. This system allows free rotation and vertical displacement of the CLT panel and prevents friction forces between the actuator and the specimens from developing. The sliding of the tested walls was prevented by means of steel rod blocking and a steel plate was interlayered between the CLT shearwalls and the steel rod as shown in Figure 6-3b.

The steel plate was designed to prevent any local crushing at the bottom edge of the CLT panels. Following each test, the plate and the blocking were inspected for any damage or failure and it was observed that no local failure due to concentrated stresses was found in any of the tests. It was also confirmed that the sliding of the wall was negligible.

Although the sliding action is very important in describing the overall behaviour of the CLT shearwall, its contribution to the mechanisms investigated in the current study is insignificant. Sliding can be treated separately from the rocking movement and incorporated into the wall behaviour. The out of plane movement of the wall was prevented by using steel guides (Fig.6-2a) and wooden blocks with anti-friction material between the guides and the specimen (Fig. 6-3c). No vertical load was applied to the CLT shearwalls in the current study.

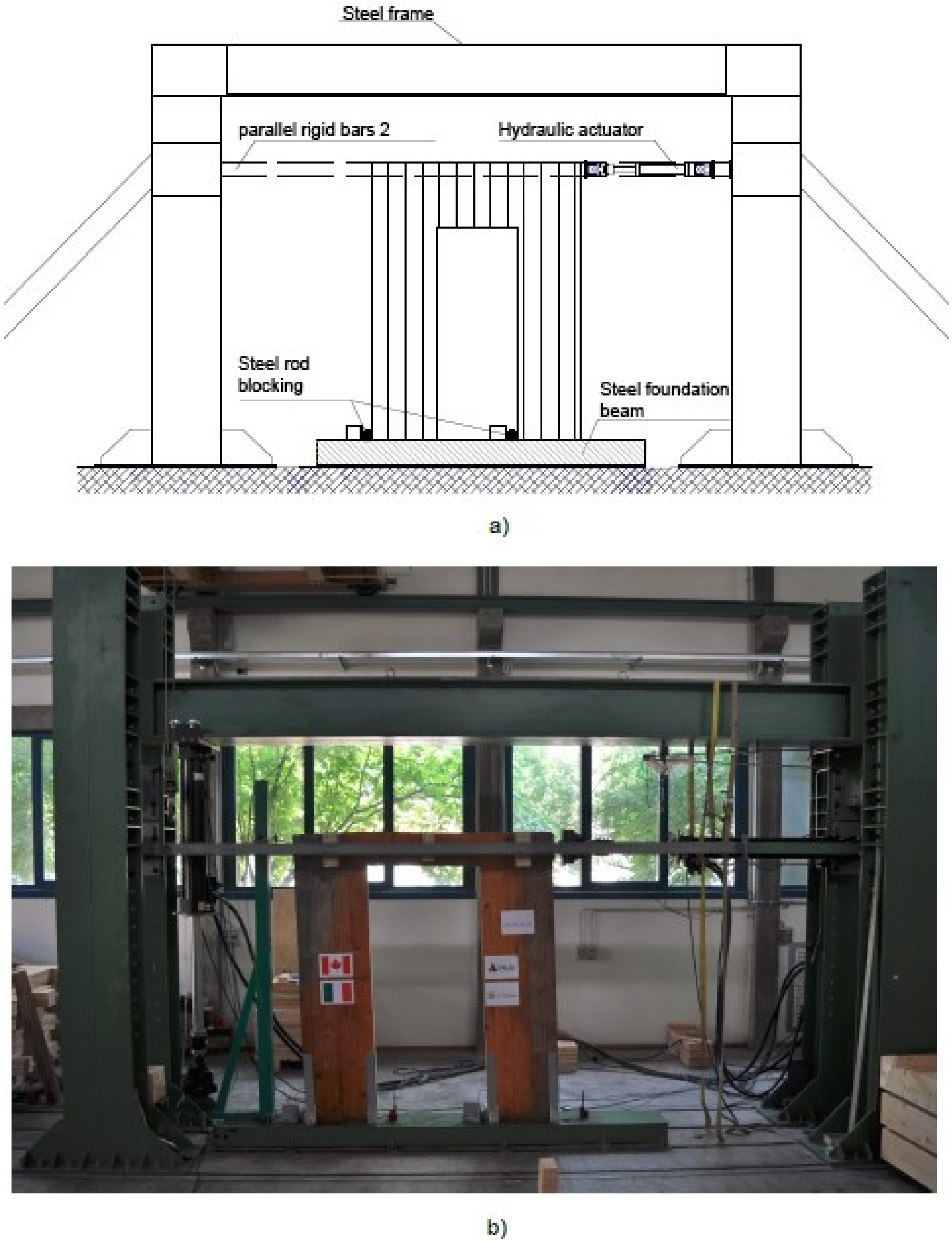

Figure 6-2. Test Set-Up, a) sketch and b) global view of the apparatus

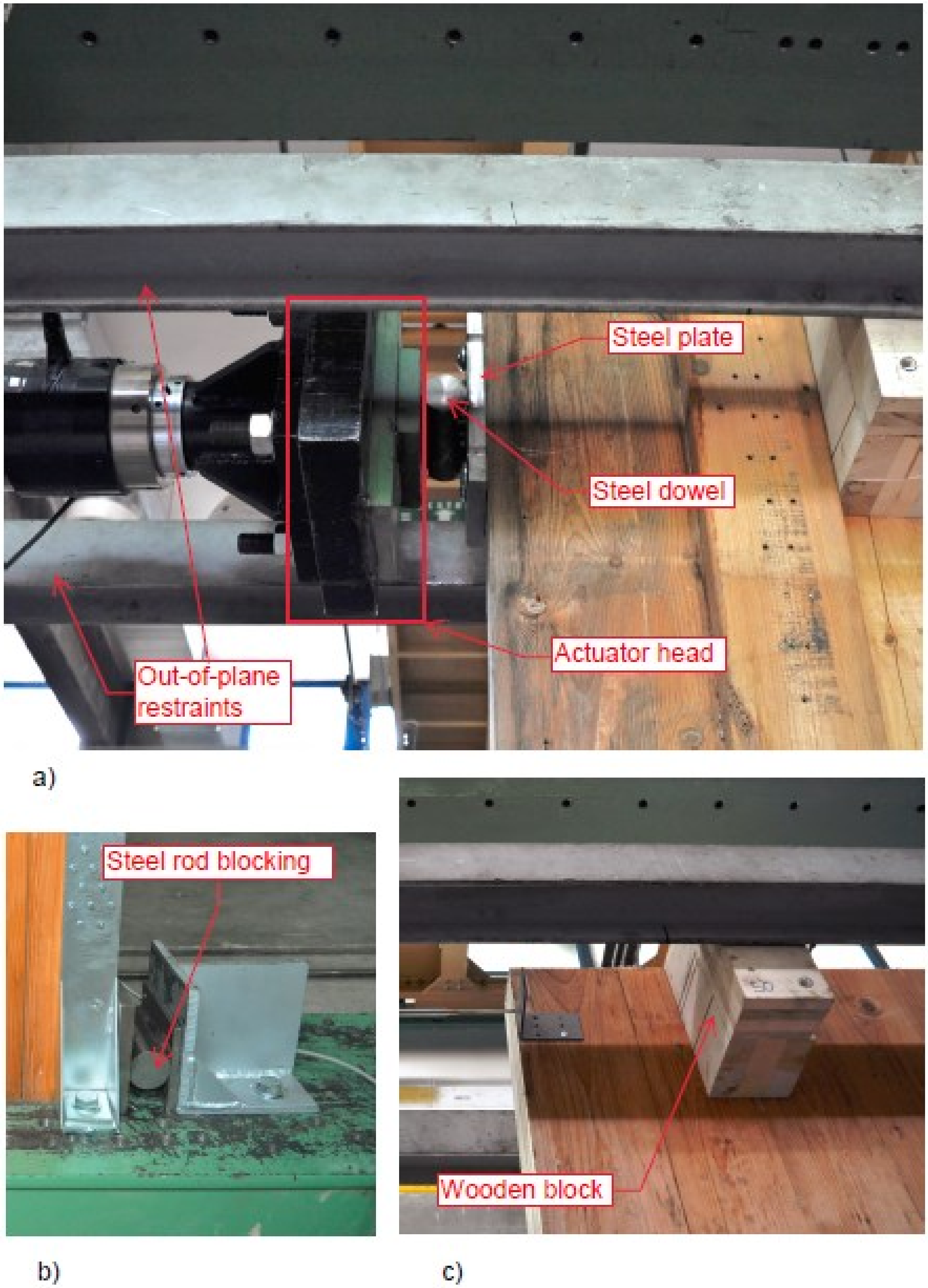

Figure 6-3. a) Out-of-plane guides and steel plate between the specimens and the actuator, b) steel rod for anti-sliding of the walls and c) horizontal movement anti friction device

6.4 Test procedure and instrumentation

The CLT shearwall specimens were tested using the static monotonic loading protocol outlined in the EN 594 standard (EN594, 2011). This standard specifies the test method to be used when determining the racking strength and stiffness of timber frame wall panels. The displacement rate used in the loading was 0.1 mm/s, and the test was terminated when the ultimate failure was achieved, either in the CLT lintel beam or the hold-downs.

Six Linear Variable Differential Transducers (LVDTs), connected to a data acquisition system, were used to measure the horizontal and vertical displacements of the CLT panels, as illustrated in Figure 6-4. LVDT CH0 was placed at the top of the wall and used to measure the total horizontal displacement. CH2 was used to measure any potential sliding displacement at the base of the panel, or rather to ensure that no significant horizontal displacement took place during texting, since such movement was prevented using the steel rod blocking. Four LVDTs, namely CH3, CH4, CH6 and CH7, were used to establish the rocking behaviour of the individual wall segments by measuring the vertical uplift displacement associated with the four hold-downs. The actuator was equipped with a 500kN load cell, which measured the force imparted onto the wall specimen in channel CH5, while the horizontal displacement in the actuator was measured using an internally built LVDT (CH1). The details related to each tested wall can be found in Appendix C.

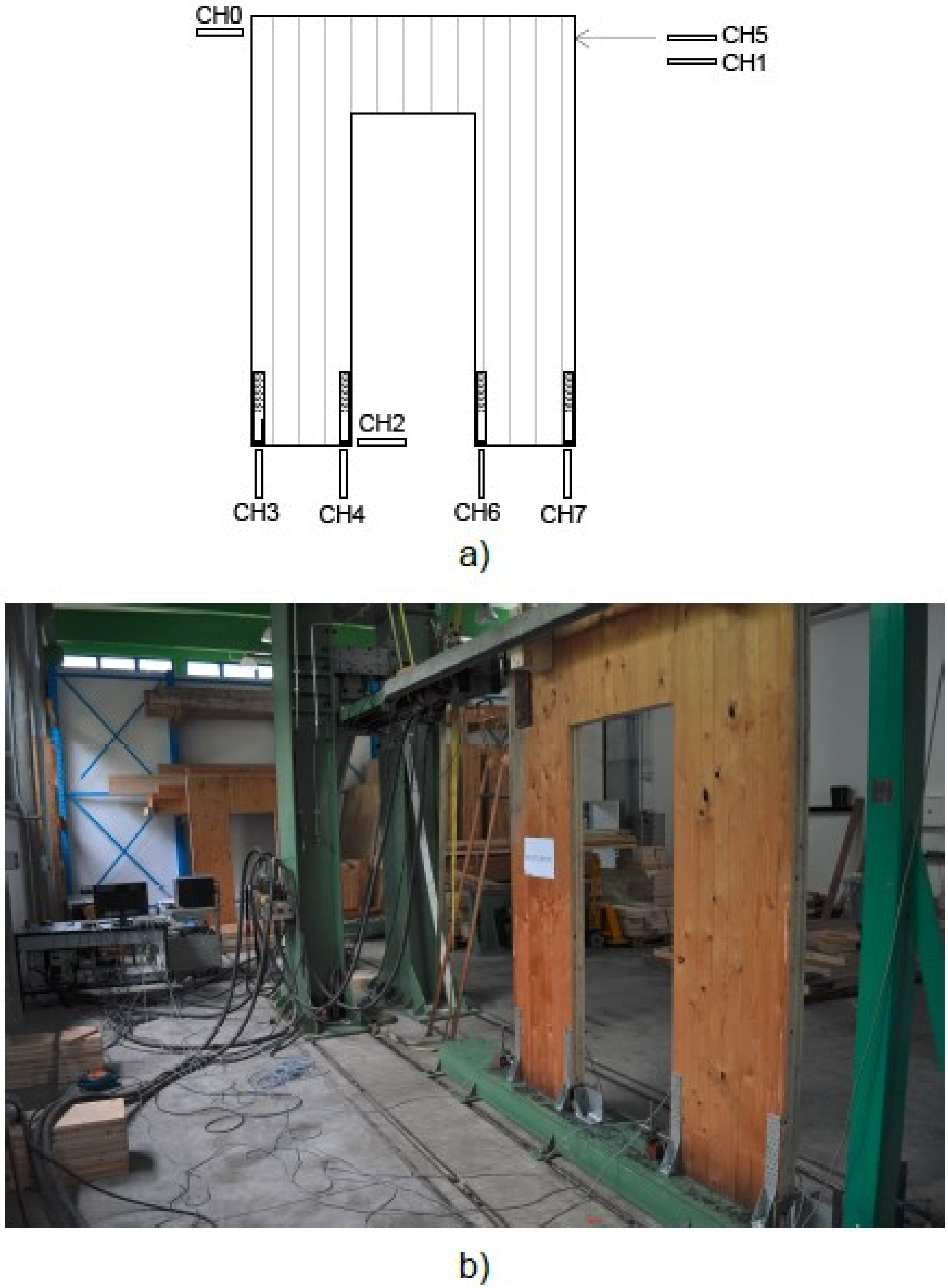

Figure 6-4. Testing instrumentation system, a) sketch of the channels position and b) wiring and data acquisition

6.5 Description of the test specimens

6.5.1 Specimen 01

Specimen 01 consisted of a wall with a total dimension of $1.85 \times 2.60\ m^2$ and with a door opening of dimensions $2.00 \times 0.75\ m^2$. More detailed information about the wall geometry are provided in Figure 6-5a. The wall was fixed to the steel foundation with four WHT440 hold-downs of $440mm$ length and $60mm$ width, as illustrated in Figures 6-5b. The connection between the hold-down and the CLT panel was done through thirty $4.0 \times 60mm$ anker nails. A WHTBS washer of $56mm$ length and $43mm$ width was used on top of the hold-down base (Figure 6-5c). The hold-down was connected to the steel foundation base using an M16 bolt. Photographs depicting the wall system, including the geometry, hold-down configuration and the position of the LVDT instrumentation are presented in Figure 6-6.

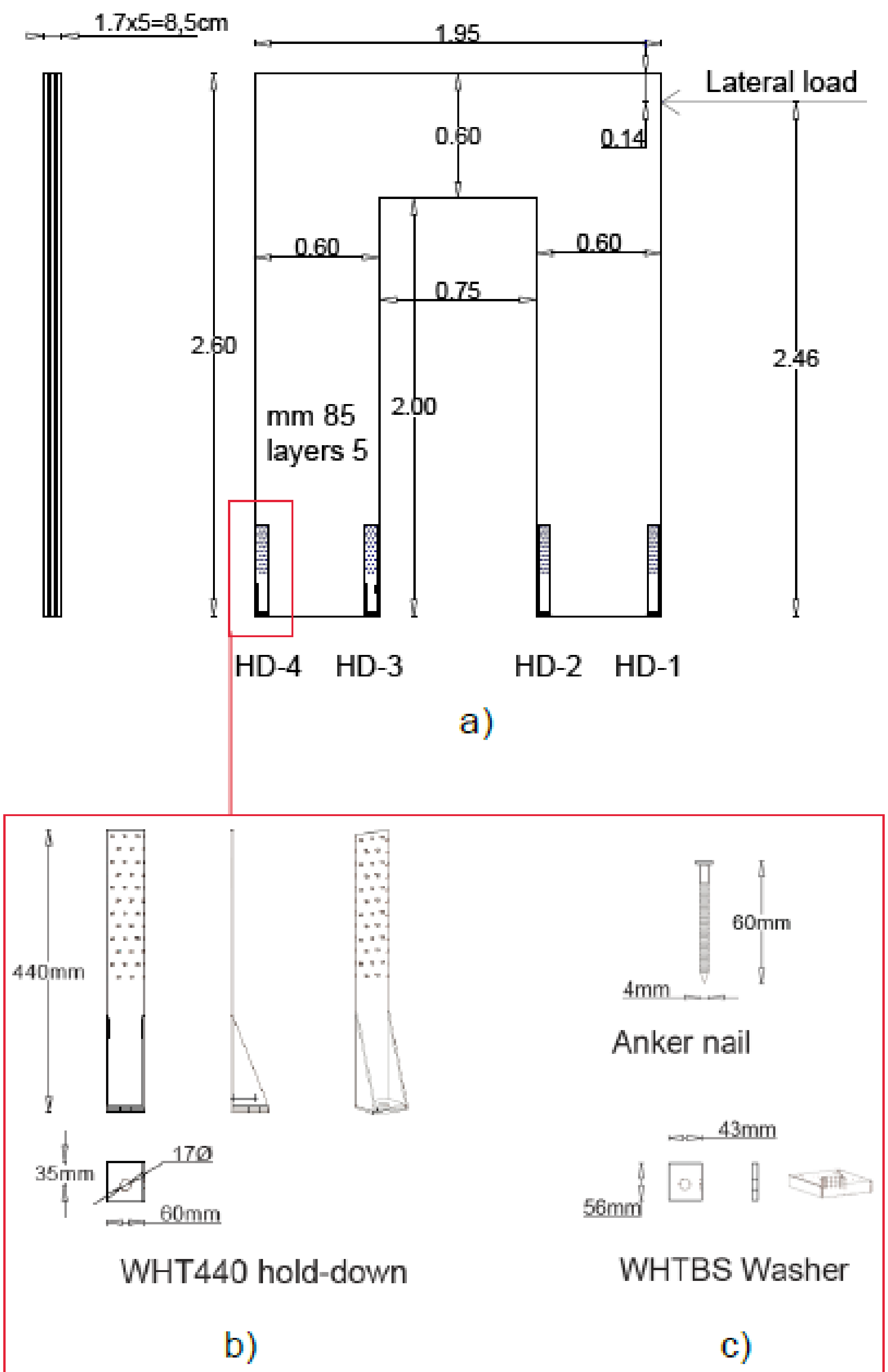

Figure 6-5. Detailing sketch of geometric configuration and connection system of shearwall 01

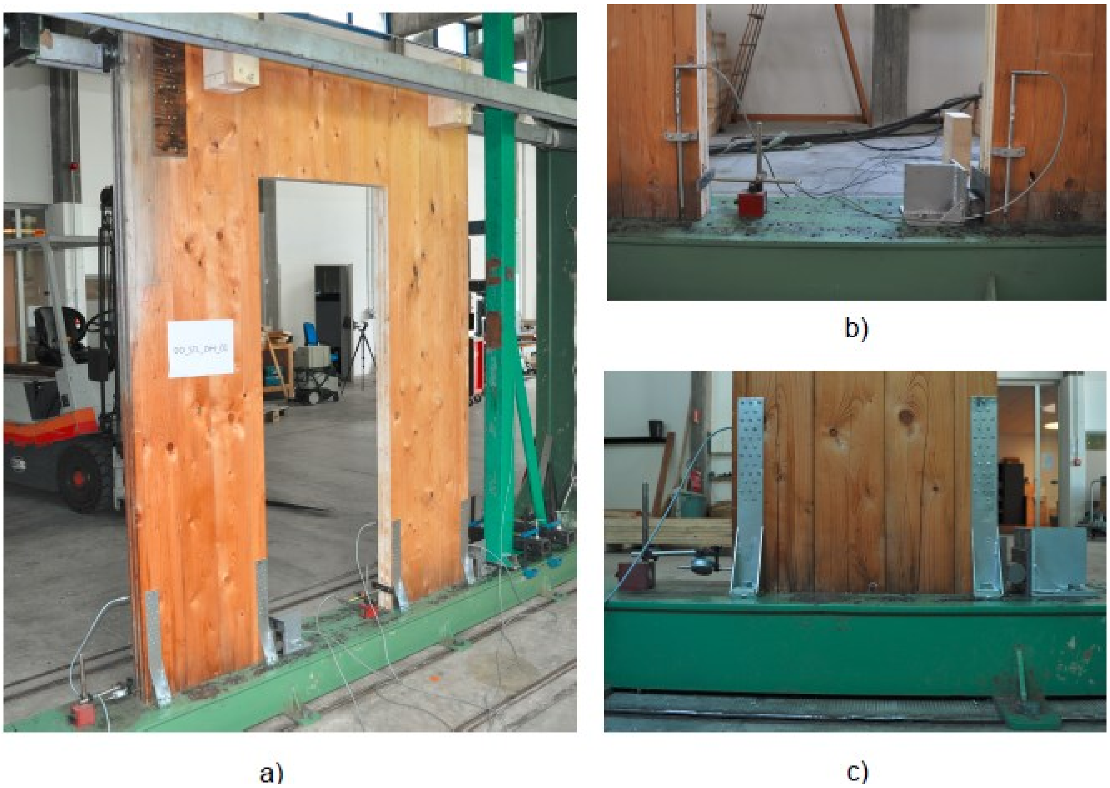

Figure 6-6. Geometric configuration, connection system and monitored displacements of shearwall 02, a) picture of the wall, b) LVDTs placed at the two inner extremities of right and left wall segments and c) zoom in of WHT440 hold-downs connection at the right wall segment of the wall

6.5.2 Specimen 02

Specimen 02 consisted of a wall with door opening, with similar overall wall and opening dimensions as specimens 01. The key difference between the two walls is that whereas specimens 01 had four hold-down anchors, one at each end of the two wall segments, Specimens 02 only has two hold-down anchors, one at each end of the wall (Figure 6-7).

The same type of hold-down connections was used to attach Specimen 02 to the steel base, as that used for Specimen 01, namely WHT440 hold-downs (refer to Figure 6-5b and 6-5c). Photographs depicting the wall system, including the geometry, hold-down configuration and the position of the LVDT instrumentation are presented in Figure 6-8.

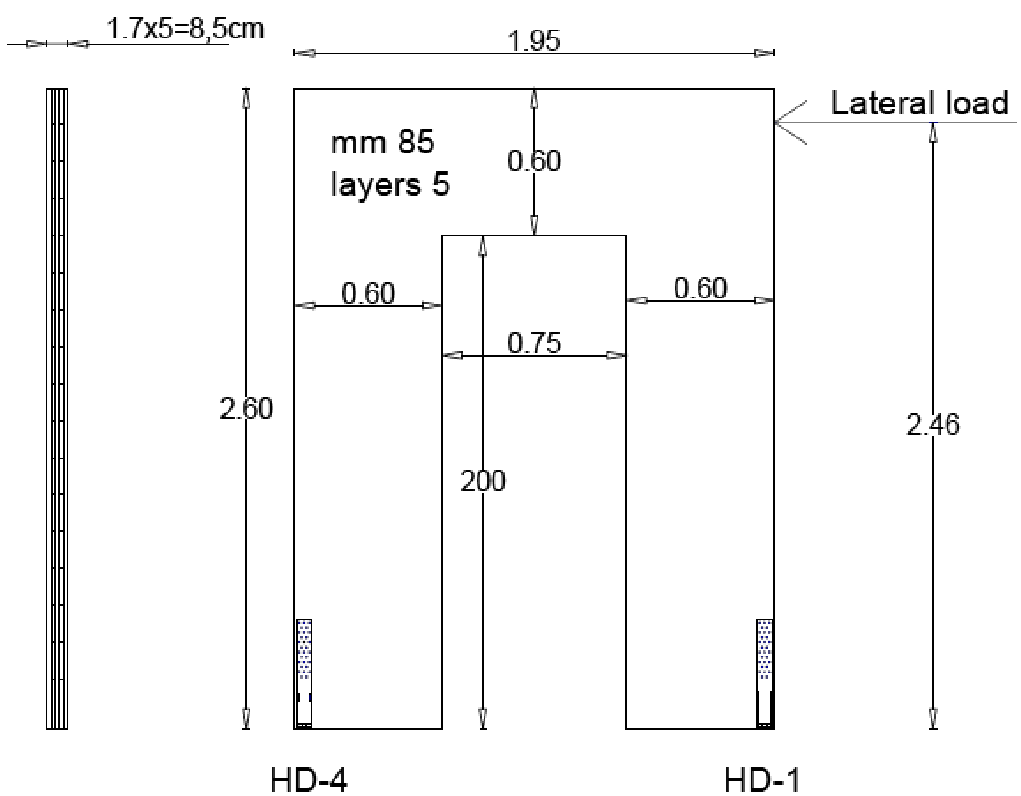

Figure 6-7. Detailing sketch of geometric configuration and connection system of shearwall 02

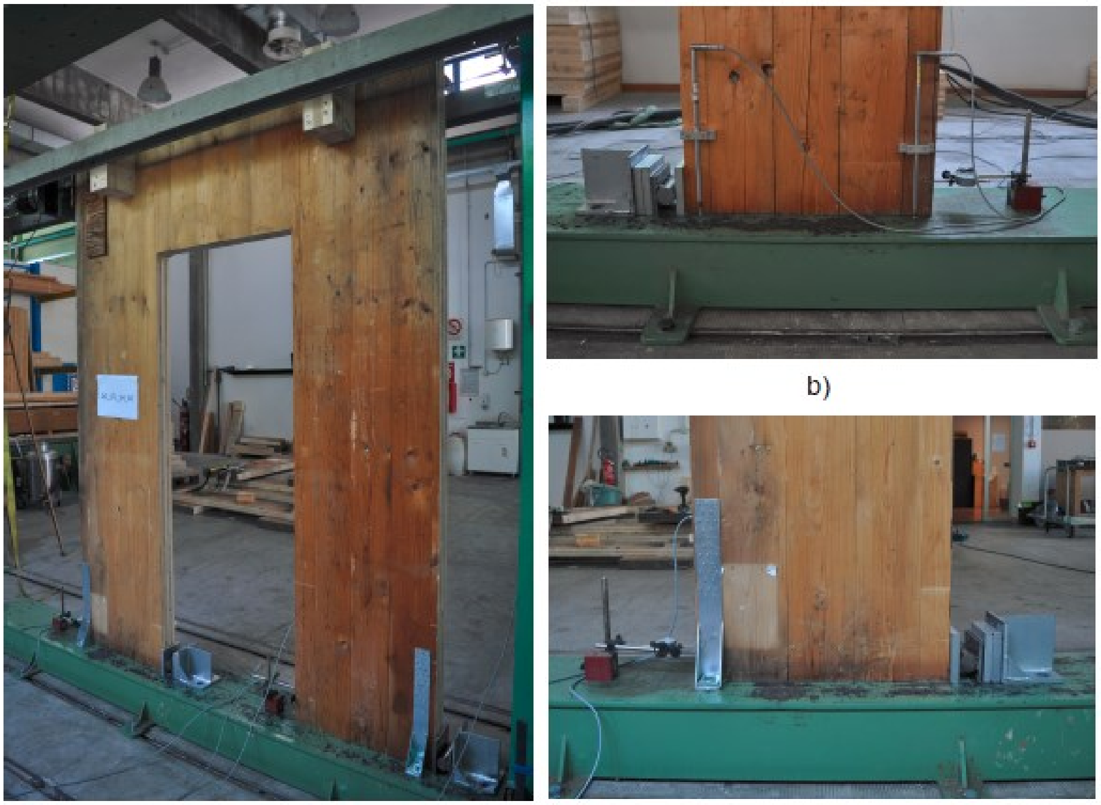

b)

a)

c)

Figure 6-8. Geometric configuration, connection system and monitored displacements of shearwall 01, a) picture of the wall, b) LVDTs placed at the two extremities of right wall segment and c) zoom in of WHT440 hold-down connection at the right wall segment of the wall

6.5.3 Specimen 03

Specimen 03 consisted of a wall with a total dimension of $2.60 \times 1.90\ m^2$ and with a window opening with dimension of $1.10 \times 0.70\ m^2$. More detailed information about the wall geometry are provided in Figure 6-9. The hold-down type and layout are similar to that outlined for Specimen 01 (refer to Figure 6-5b and 6-5c). The wall attachment to the steel foundation is also done in a similar manner as that for Specimen 01. Photographs depicting the wall system, including the geometry, hold-down configuration and the position of the LVDT instrumentation are presented in Figure 6-10.

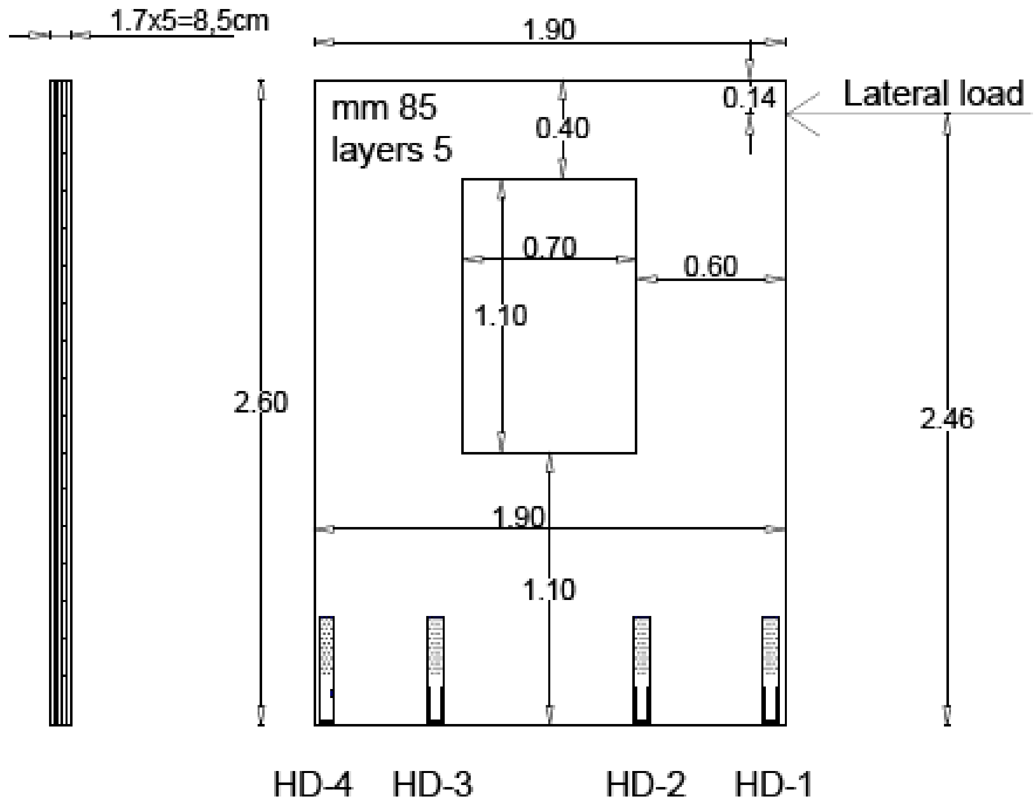

Figure 6-9. Detailing sketch of geometric configuration and connection system of shearwall 03

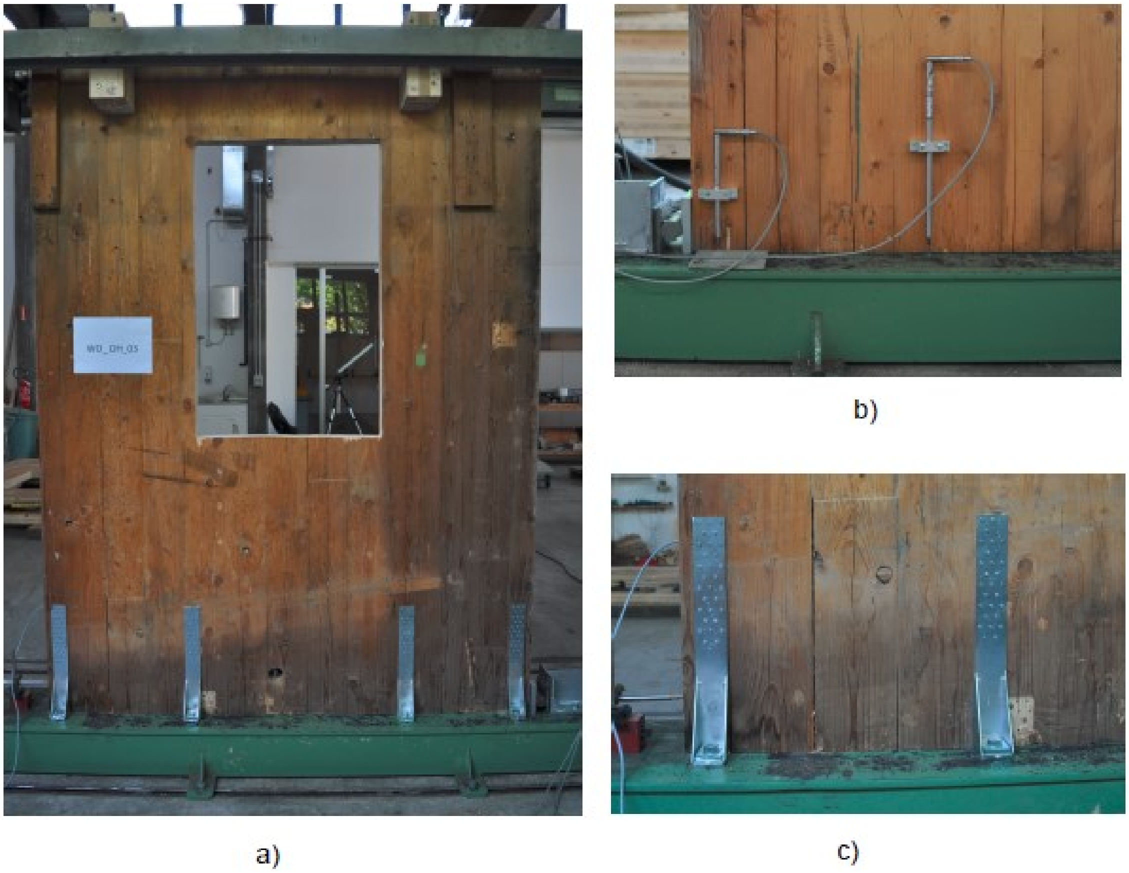

Figure 6-10. Geometric configuration, connection system and monitored displacements of shearwall 03, a) picture of the wall, b) LVDTs placed at the left side of the wall and, c) zoom in of WHT440 hold-down connection at the right side of the wall

6.5.4 Specimen 04

Specimen 04 consisted of a wall with window opening, with similar overall wall and opening dimensions as those of Specimen 03. The key difference between the two walls is that whereas specimens 03 had hold-down anchors at each end of the two wall segments, Specimen 04 only has two hold-down anchors, one at each end of the wall (Figure 6-11). The same type of hold-down connections was used to attach Specimen 04 to the steel base, as that used for Specimen 03, namely WHT440 hold-downs (refer to Figure 6-5b and 6-

5c). Photographs depicting the wall system, including the geometry, hold-down configuration and the position of the LVDT instrumentation are presented in Figure 6-12.

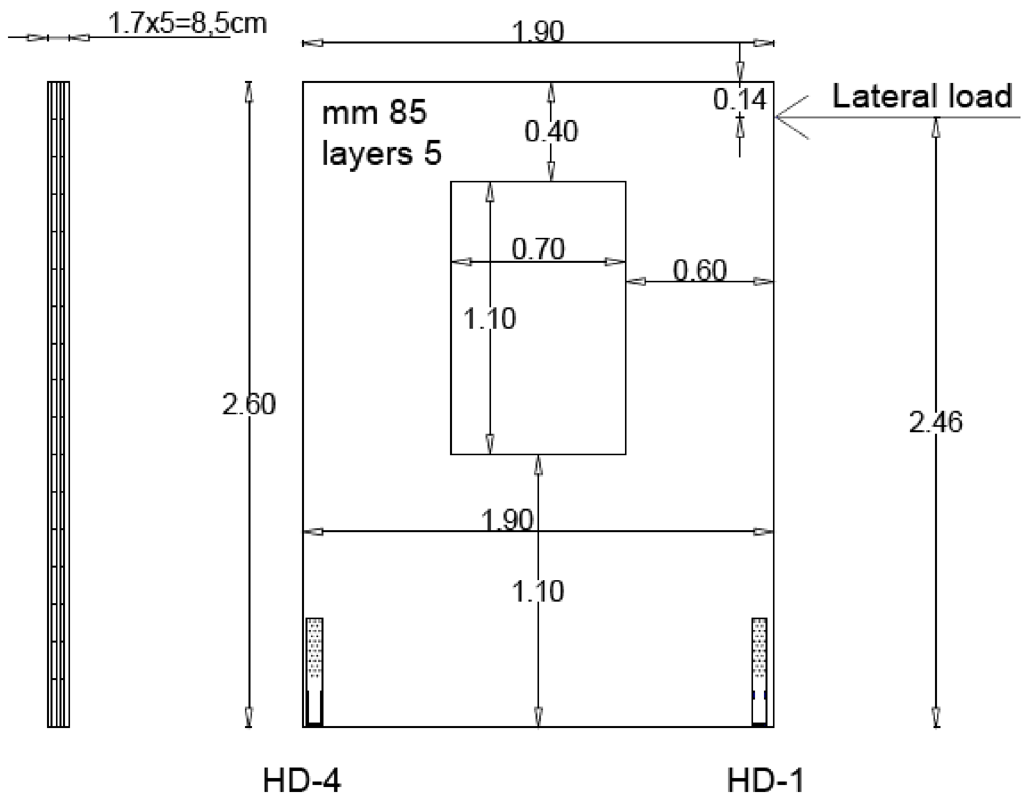

Figure 6-11. Detailing sketch of geometric configuration and connection system of shearwall 04

b)

a) c)

Figure 6-12. Geometric configuration, connection system and monitored displacements of shearwall 04, a) picture of the wall, b) LVDTs placed at the left side of the wall and, c) zoom in of WHT440 hold-down connection at the right side of the wall

6.5.5 Specimen 05

Specimen 05 consisted of a wall with a total dimension of $2.60 \times 2.30\ m^2$ and with a door opening with dimension of $2.30 \times 1.00\ m^2$. More detailed information about the wall geometry are provided in Figure 6-13a. The wall was fixed to the steel foundation with four WHT620 hold-downs of $620mm$ length and $60mm$ width, as illustrated in Figures 6-13b and 6-13c. The connection between the hold-down and the CLT panel was done through fifty-five $4.0 \times 60mm$ anker mails. A WHTBS washer of $56mm$ length and

$43mm$ width was used on top of the hold-down base (Figure 6-13c). The hold-down was also connected to the steel foundation base using an M16 bolt grade 8.8. Photographs depicting the wall system, including the geometry, hold-down configuration and the position of the LVDT instrumentation are presented in Figure 6-14.

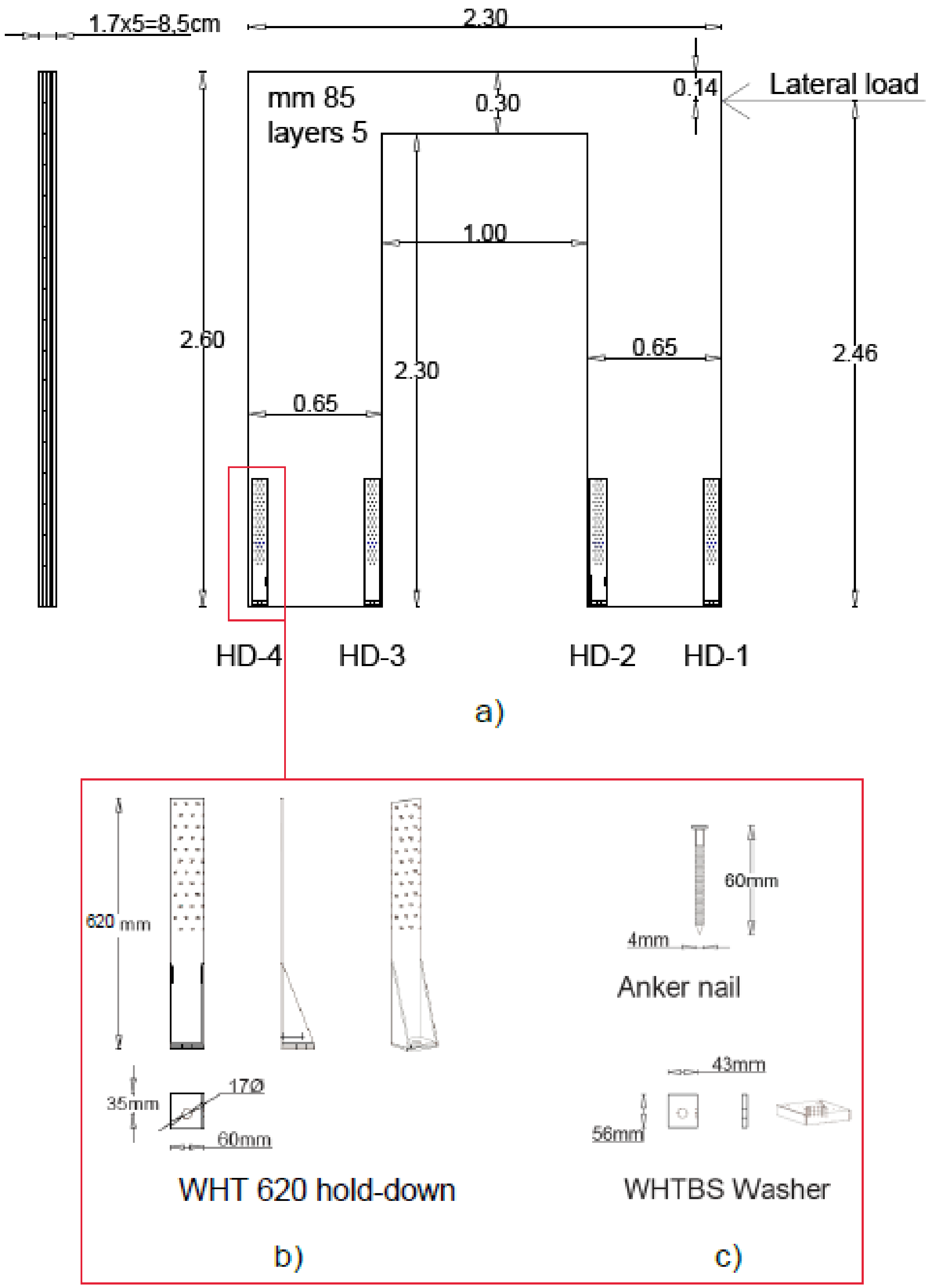

Figure 6-13. Detailing sketch of geometric configuration and connection system of shearwall 05

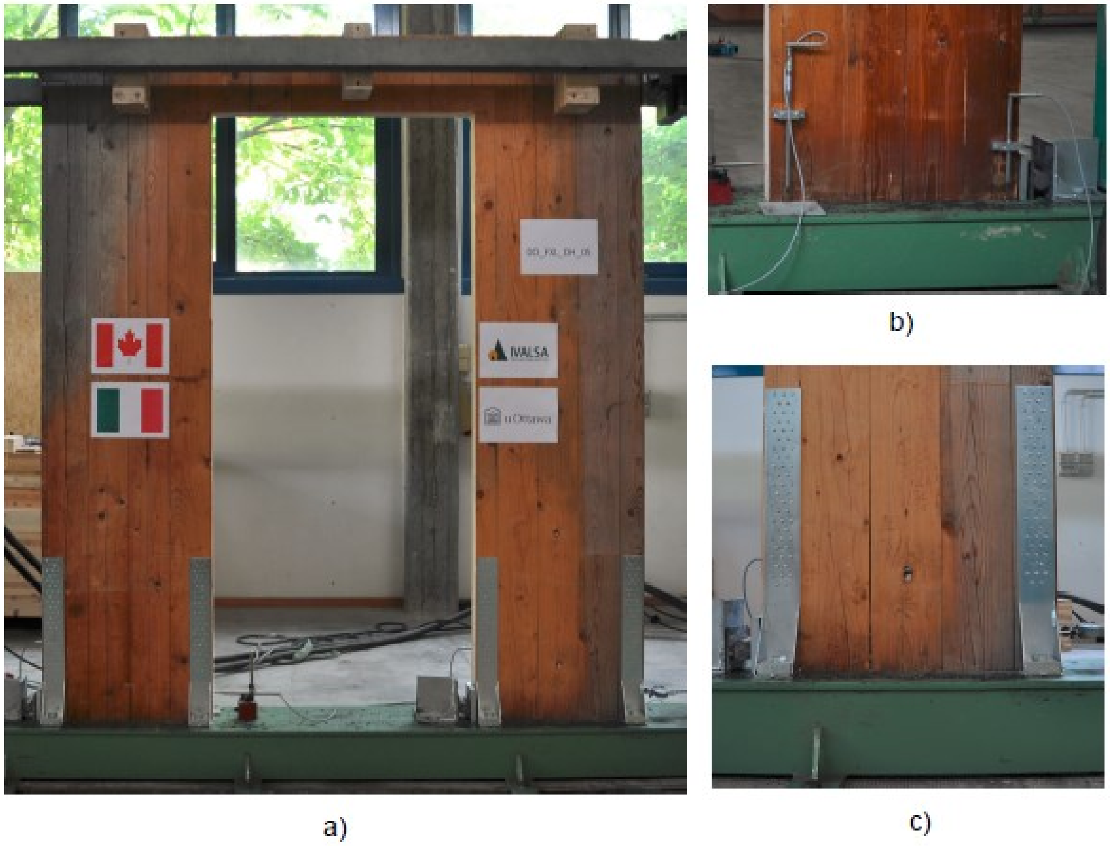

Figure 6-14. Geometric configuration, connection system and monitored displacements of shearwall 04, a) picture of the wall, b) LVDTs placed at the left wall segment and, c) zoom in of WHT620 hold-down connection at the left wall segment

Table 6-1 summarizes the geometrical dimensions of the walls and the mechanical and configuration characteristics of the hold-downs used in the tests.

Table 6-1. Geometrical and mechanical characteristics of the tested shearwalls

ID	Opening	h_L [m]	l [m]	h_O [m]	b [m]	h_C [m]	Lamellae ratio	Hold-down configuration	Hold-down type
01	**Door**	*0.6*	*0.75*	*2.0*	*0.60*	-	*0.67*	*DH*	*WHT440*
02	**Door**	*0.6*	*0.75*	*2.0*	*0.60*	-	*0.67*	*SH*	*WHT440*
03	**Window**	*0.4*	*0.7*	*1.1*	*0.60*	*1.1*	*0.67*	*DH*	*WHT440*
04	**Window**	*0.4*	*0.7*	*1.1*	*0.60*	*1.1*	*0.67*	*SH*	*WHT440*
05	**Door**	*0.3*	*1.0*	*2.3*	*0.65*	-	*0.67*	*DH*	*WHT620*

6.6 Experimental results

This section describes the results obtained from the experimental testing including the overall behaviour of the walls, the failure mechanism observed and a description of the kinematic behaviour of the investigated walls.

6.6.1 Specimen 01

6.6.1.1 Capacity curve

Failure in Wall 01 occurred within approximately 6 minutes, which is reasonably placed within typical ranges of load durations for static loading, i.e. between 2 and 10 minutes. The force-displacement curve obtained from this test can be seen in Figure 6-15. The curve is observed to be linear up to approximately 60 kN, where the graph starts deviating slightly from the linear behaviour. Although the ultimate failure was observed to occur in the hold-down, the overall behaviour of the wall seems fairly brittle. This is expected in those type of structural systems, where there are no joints between the CLT panels that would allow fasteners such as nails and screws to yield and develop energy dissipation through inelastic behaviour. The ultimate load at failure was 96.1kN corresponding to a maximum lateral displacement of 47.6mm.

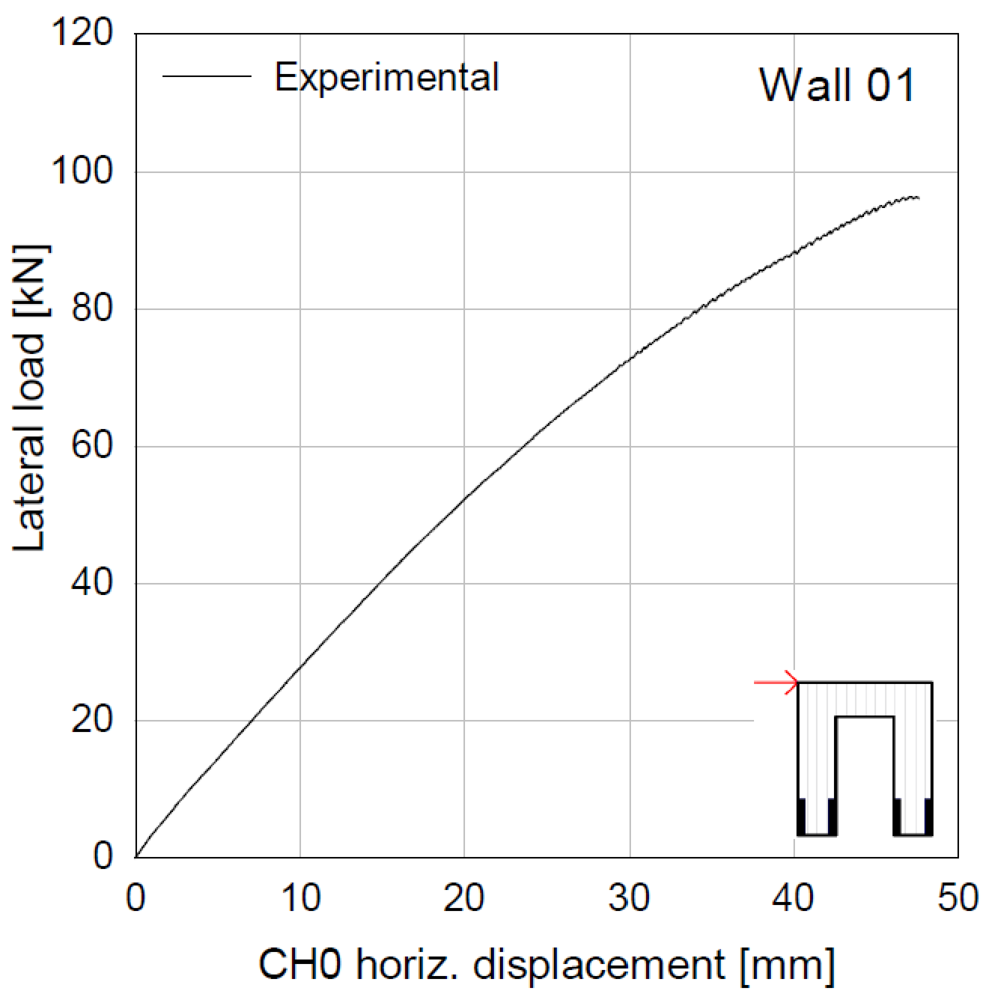

Figure 6-15. Lateral load vs top displacement curve from tested specimen 01

6.6.1.2 Failure Mechanism

The ultimate failure in Specimen 01 occurred in a combination of wood tension failure and failure in the hold-down angle bracket, as shown in Figure 6-16. The rupture in the steel bracket of the most stressed hold-down (HD1) is not a desired failure mode since the nails in the hold-down did not yield. This explains the behaviour observed in the capacity curve, where little to no inelastic energy dissipation was observed in this specimen. Hold-down HD2 (Fig. 6-16e) did not exhibit any significant deformation and the failure of the wood at the first nail row occurred immediately after the rupturing of the steel plate in hold-down HD1. The second wall segment and hold-downs (HD3 and HD4) remained undamaged at the end of the test (Fig. 6-16b).

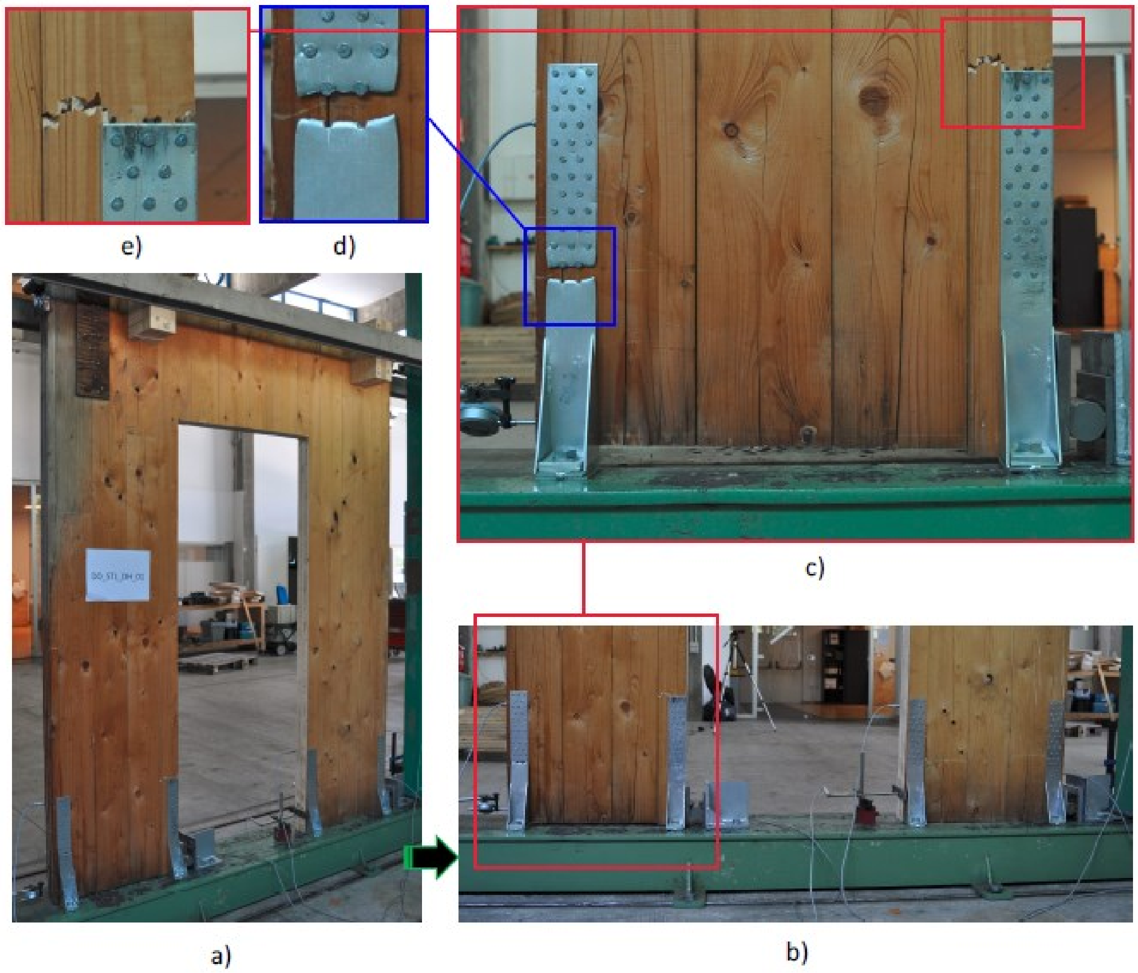

Figure 6-16. Failure mechanism achieved at the end of the test for specimen 01

6.6.2 Specimen 02

6.6.2.1 Capacity curve

Failure in Wall 02 occurred within approximately 6.5 minutes. The force-displacement curve obtained from this test can be seen in Figure 6-17. The curve is observed to be linear up to approximately 40 kN, where the graph starts deviating slightly from the linear behaviour. The ultimate failure was observed to occur in the hold-down, and the overall behaviour especially near the ultimate load seems to exhibit more inelastic behaviour than

Specimen 01. This is due to more engagement of the hold-down anchor (i.e. having two rather than 4 hold-downs). The ultimate load at failure was 60.8kN corresponding to a maximum lateral displacement of 35.1mm. As such both the ultimate load as well as the displacement are significantly smaller than those obtained for Specimen 01.

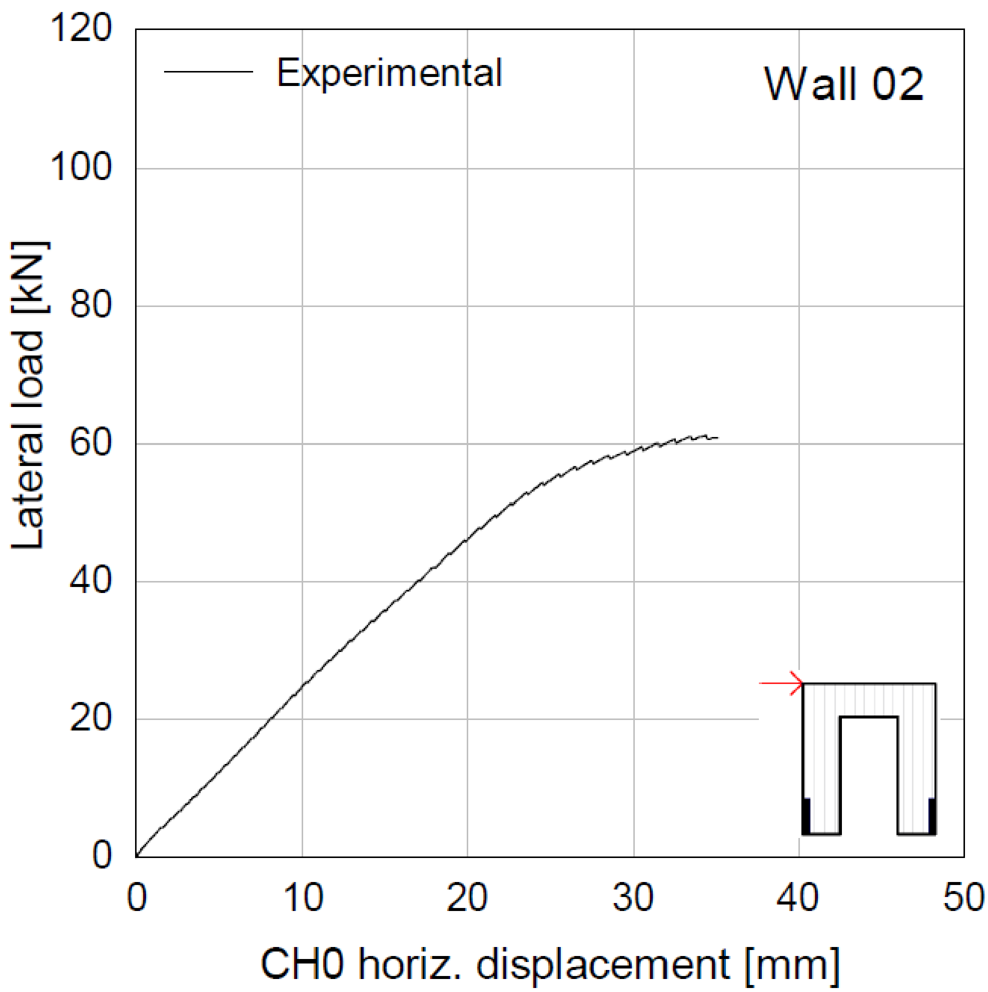

Figure 6-17. Lateral load vs top displacement curve from tested specimen 02

6.6.2.2 Failure Mechanism

The failure in Specimen 02 occurred in the hold-down angle bracket, similar to that observed in hold-down HD1 for specimen 01. The failure mechanism consisted of a rupture of the steel plate of the hold-down as shown in Figure 6-18. The brittle failure can be attributed to the lack of engagement of the nails in the hold-down, resulting in an undesired and brittle failure mode. No CLT wood failure occurred during this test. The second wall segment and hold-down remained undamaged at the end of the test.

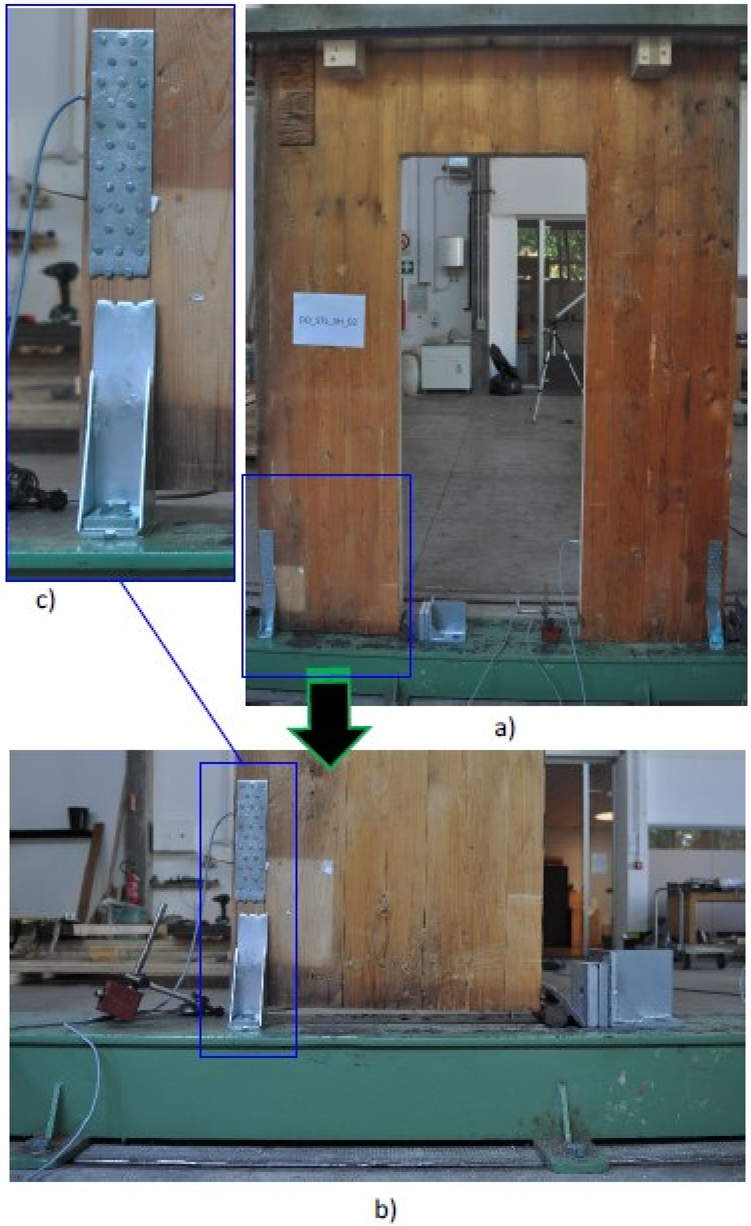

Figure 6-18. Failure mechanism achieved at the end of the test for specimen 02

6.6.3 Specimen 03

6.6.3.1 Capacity curve

Failure in Wall 03 occurred within approximately 7 minutes. The force-displacement curve obtained from this test can be seen in Figure 6-19. The curve is observed to be linear up to approximately 80 kN, where the graph starts deviating slightly from the linear behaviour. The ultimate failure was observed to occur in the hold-down, and the overall behaviour of the wall seems fairly brittle. This is probably attributed to the fact that this configuration had four hold-down anchors, similar in principle to Specimen 01. The ultimate load at failure was 100.4kN, which is significantly higher than Specimen 01 but only slightly higher than Specimen 02. The ultimate lateral displacement was recorded at 34.7mm.

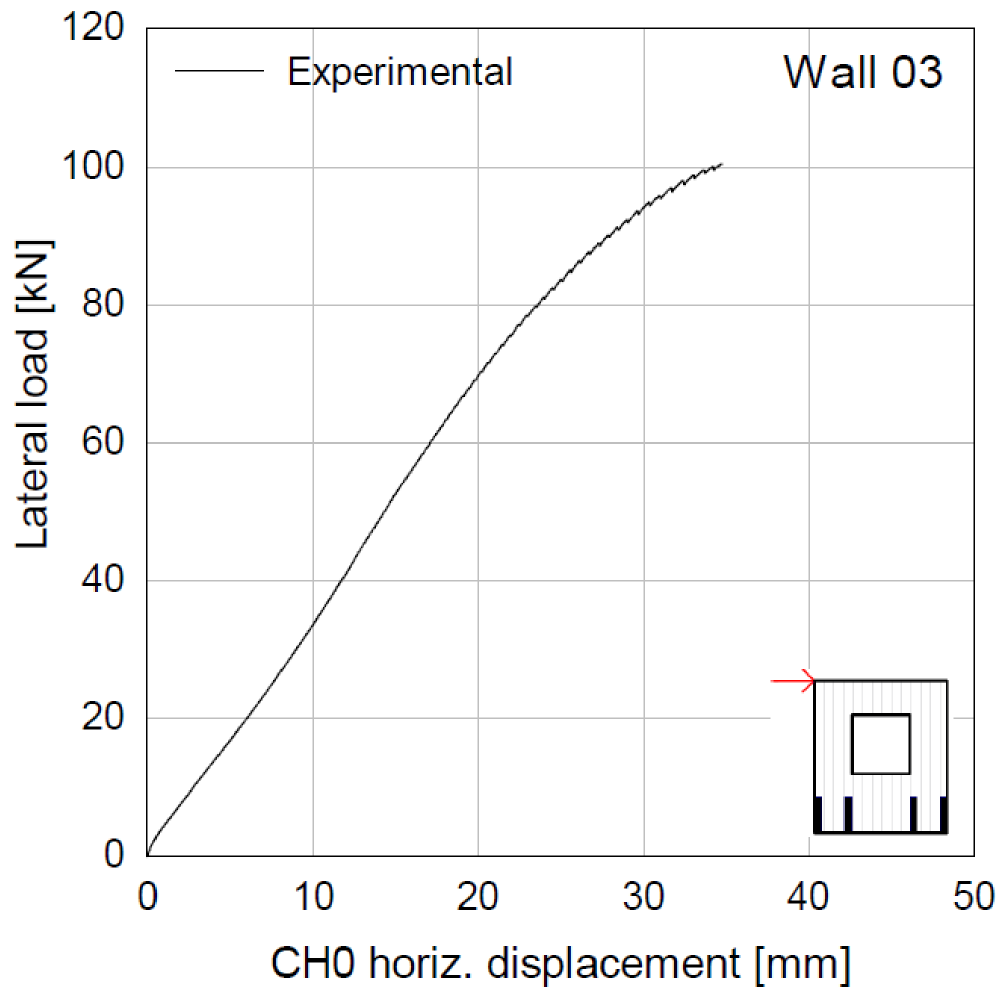

Figure 6-19. Lateral load vs top displacement curve from tested specimen 03

6.6.3.2 Failure Mechanism

The ultimate failure in Specimen 03 occurred in the first and most stressed hold-down angle bracket (HD1), as shown in Figure 6-20. The remaining hold-downs as well as CLT panels showed no damage, and relatively little deformation. The stiffness of the wall due to the presence of four hold-down reduced the overall displacement of the wall. Relatively only small separation can be noticed between the two broken angle plate pieces, likely due to the stiffness of the wall and the contribution of the other hold-down anchorages.

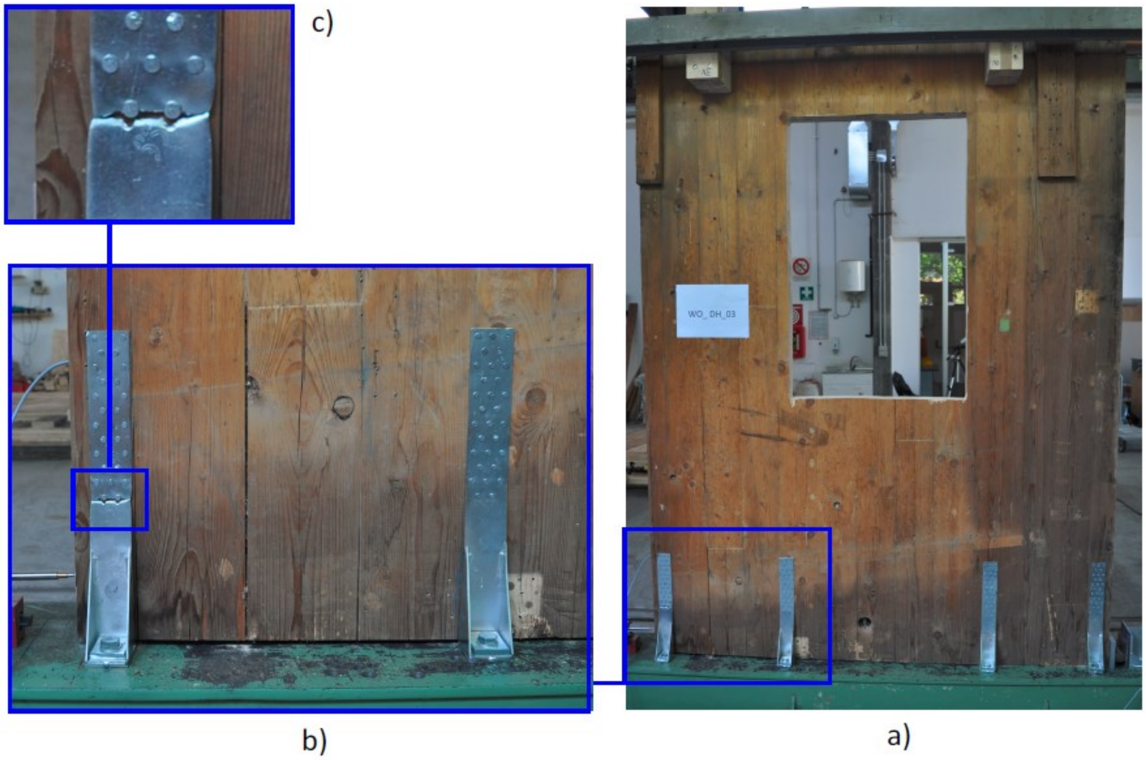

Figure 6-20. Failure mechanism achieved at the end of the test for specimen 03

6.6.4 Specimen 04

6.6.4.1 Capacity curve

Specimen 04 failed occurred within approximately 6 minutes. The force-displacement curve obtained from this test can be seen in Figure 6-21. The curve is observed to be linear up to approximately 50 kN, where the graph starts deviating from the linear behaviour. The ultimate failure was observed to occur in the hold-down, and the overall behaviour especially near the ultimate load seems to exhibit more inelastic behaviour than Specimen 03, probably due to more engagement of the hold-down anchor. The ultimate load at failure was 64.5kN corresponding to a maximum lateral displacement of 33.1mm.

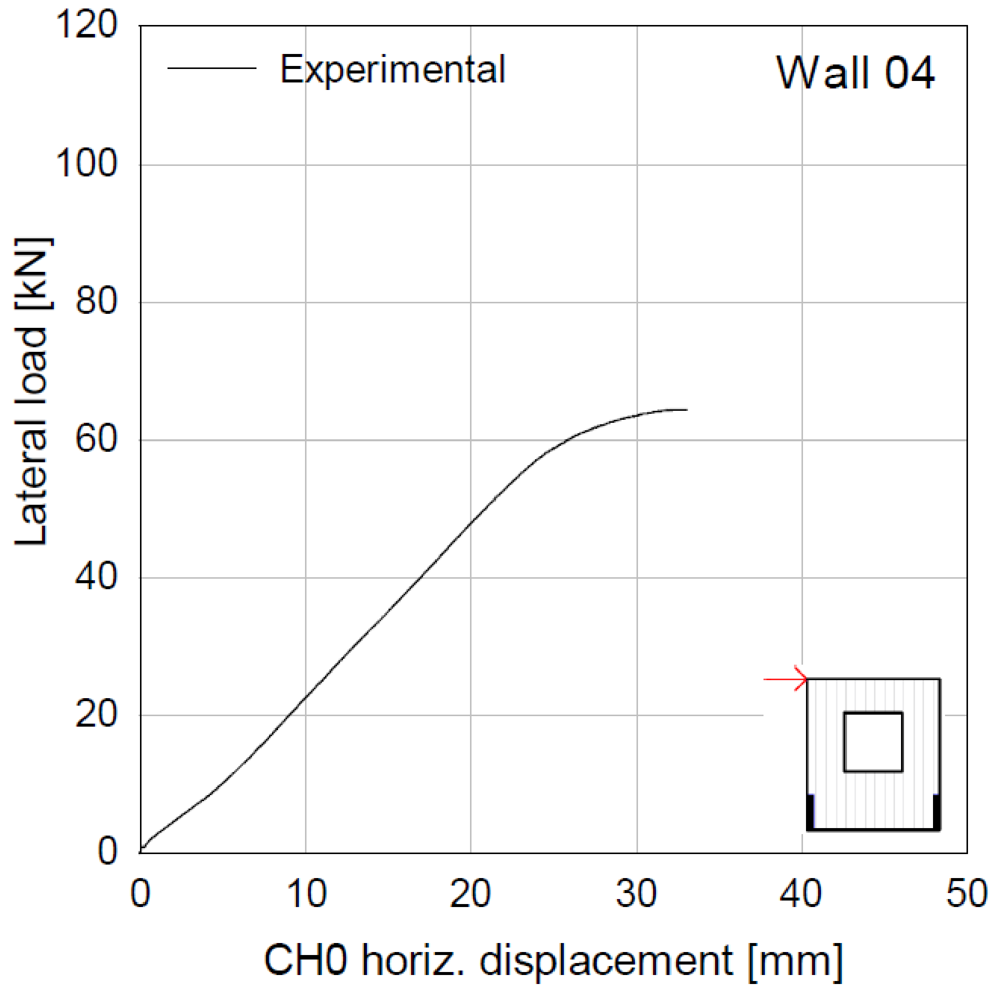

Figure 6-21. Lateral load vs top displacement curve from tested specimen 04

6.6.4.2 Failure Mechanism

The failure mechanism of Specimen 04 was similar to that observed in Specimen 03, where the hold-down plate failed in tension but as can be seen in Figure 6-22, the failure occurred above the bottom nail row. This means that the nails were more engaged in the failure mechanism, although the overall behaviour was governed by the tension failure in the steel strap. More vertical displacement could be observed at the bottom of the wall including the region below the parapet. This is attributed to the number of hold-down (i.e. two) used in this specimen. No failure was observed in the CLT panel.

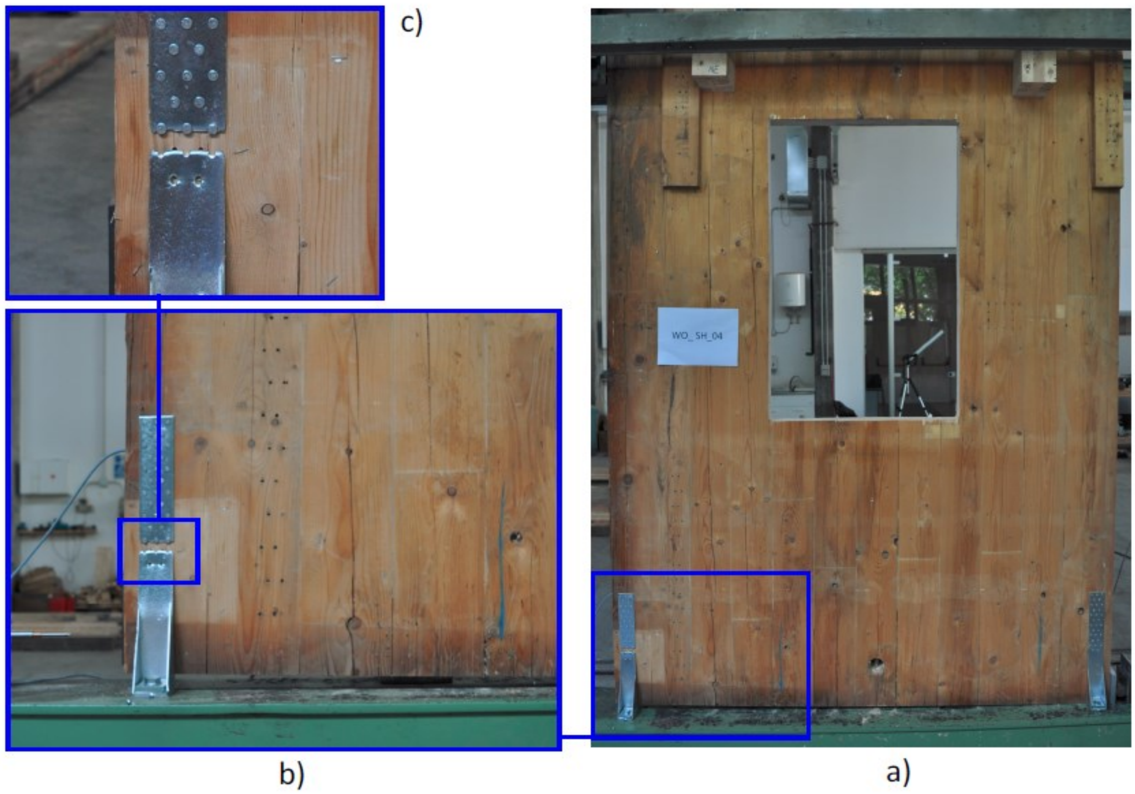

Figure 6-22. Failure mechanism achieved at the end of the test for specimen 04

6.6.5 Specimen 05

6.6.5.1 Capacity curve

Specimen 05 failed within approximately 10 minutes. The force-displacement curve obtained from this test can be seen in Figure 6-23. The curve is observed to be almost linear up to point where the ultimate capacity was reached at 62.2 kN. The overall behaviour of the wall seems brittle, which can be attributed to the fact that failure occurred in the little beam. The maximum lateral displacement of 35.0mm.

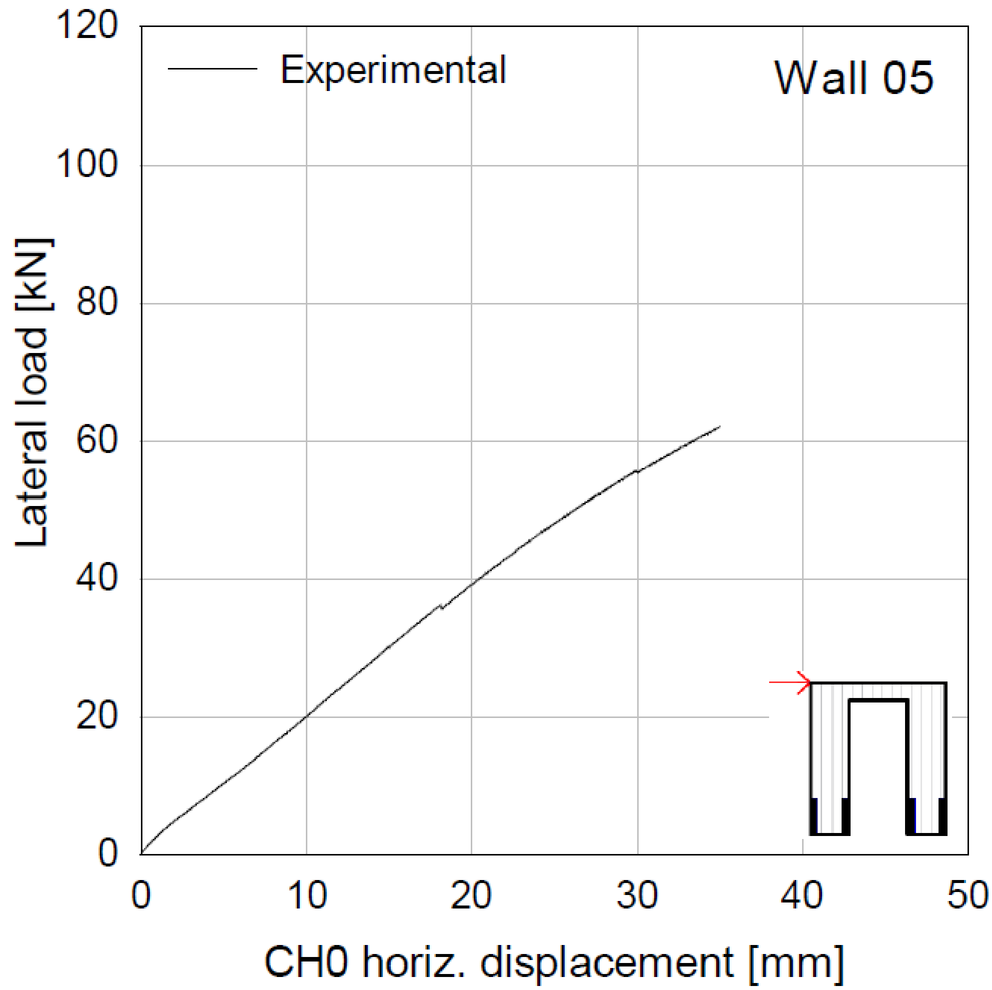

Figure 6-23. Lateral load vs top displacement curve from tested specimen 05

6.6.5.2 Failure Mechanism

The ultimate failure in Specimen 05 was governed by failure in the lintel beam, as shown in Figure 6-24. This explains the behaviour observed in the capacity curve, where linear elastic and brittle curve was observed. It was observed that the lintel beam failed across the beam thickness at the at the top left corner (Figure 6-24c), likely due to shear and bending.

Failure was also observed in the bottom right corner of the lintel beam (Figure 6-24d), which could be attributed to shear failure.

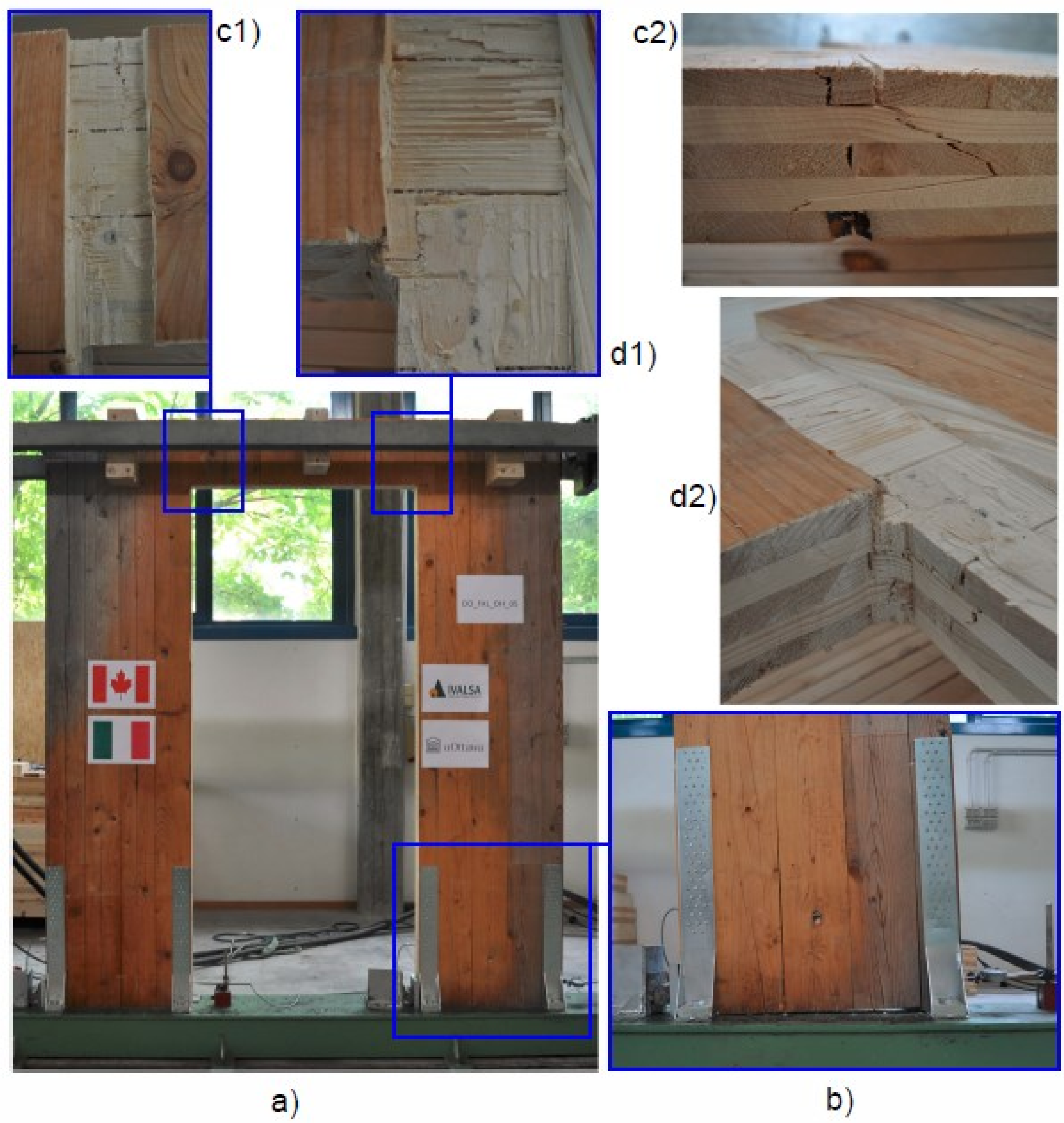

Figure 6-24. Failure mechanism achieved at the end of the test for specimen 05

6.6.6 Equivalent Energy Elastic Plastic curves

The idealized *Equivalent Energy Elastic Plastic* (EEEP) curves for all five specimens are presented in Figure 6-25. Walls 01 and 02 have similar ductility ratios equal to approximatley $\mu = 1.5$. Walls 03 and 04 have comparable ductility ratios of $\mu = 1.24\ and\ 1.15$, respectively. Since wall 05 failed in the CLT panel, the wall behaviour is almost linear brittle and as such no significant ductility was observed.

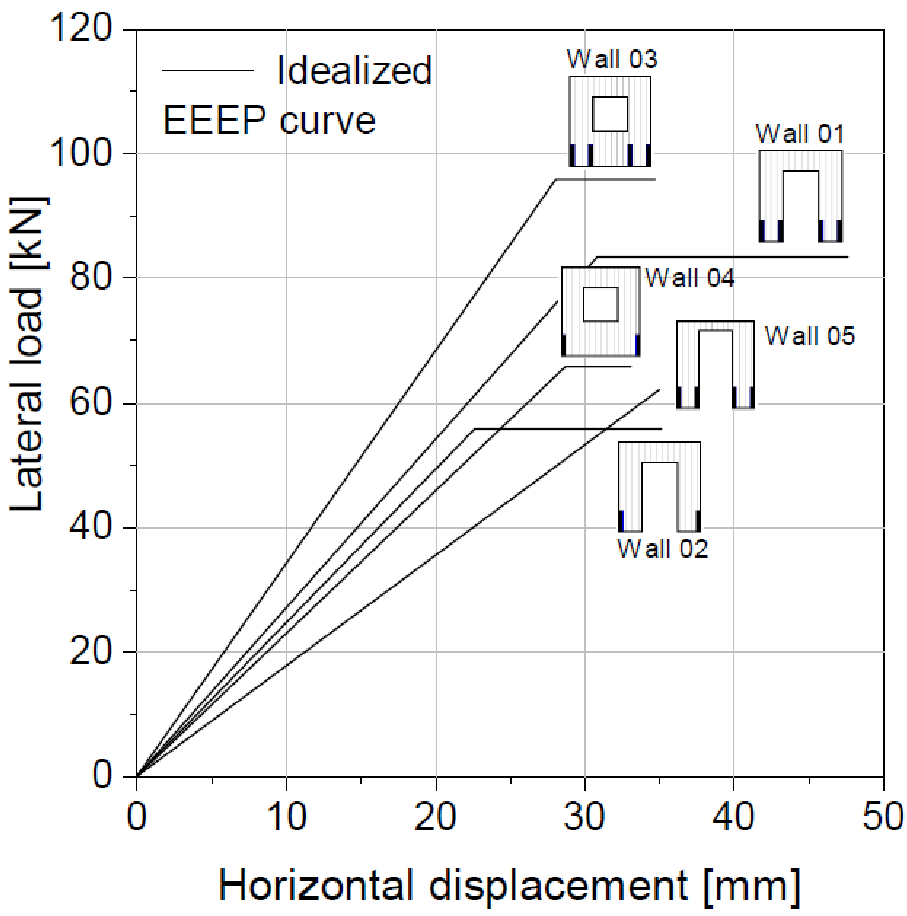

Figure 6-25. Equivalent Energy Elastic Plastic curve of the five specimens

The mechanical properties obtained from the *equivalent energy elastic plastic* curves for each specimen, including the initial stiffness, ultimate and yield force and displacement, as well as ductility ratios are provided in Table 6-2.

Table 6-2. Summary of CLT wall specimens

Specimen id	Ultimate failure	*HD1 yielded Yes/No*	Δ_{yield} *[mm]*	$\Delta_{failure}$ *[mm]*	F_{yield} *[kN]*	$F_{failure}$ *[kN]*	K_e *[kN/mm]*	*μ [-]*
01	*HD*	*Y*	*30.8*	*47.6*	*83*	*96*	*2.7*	*1.54*
02	*HD*	*Y*	*22.6*	*35.1*	*56*	*61*	*2.5*	*1.55*
03	*HD*	*Y*	*28.1*	*34.7*	*96*	*100*	*3.4*	*1.24*
04	*HD*	*Y*	*28.7*	*33.1*	*66*	*64*	*2.3*	*1.15*
05	*CLT*	*N*	*35.0*	*35.0*	*62*	*62*	*2.0*	*1*

6.6.7 Kinematic behaviour

The kinematic behaviour of the walls is an expression of whether the final deformed shape represents one or two points of rotation for the wall. It was observed, based on the deformed shape as well as the sign of the displacements in the LVDT placed near the hold-down locations, that specimens 01, 02, 03 and 04 all exhibited similar kinematic modes, where the wall only had one point of rotation at the hold-down anchor farthest away from the load application point (Figure 6-26a to d). A gap between the bottom of the wall and the supporting steel based was initiated during the tested and was observed at the end of the tests. For specimen 05, the kinematic behaviour was dominated by two points of rotation, as shown in Figure 6-27. Significant bending in the lintel beam could also be observed.

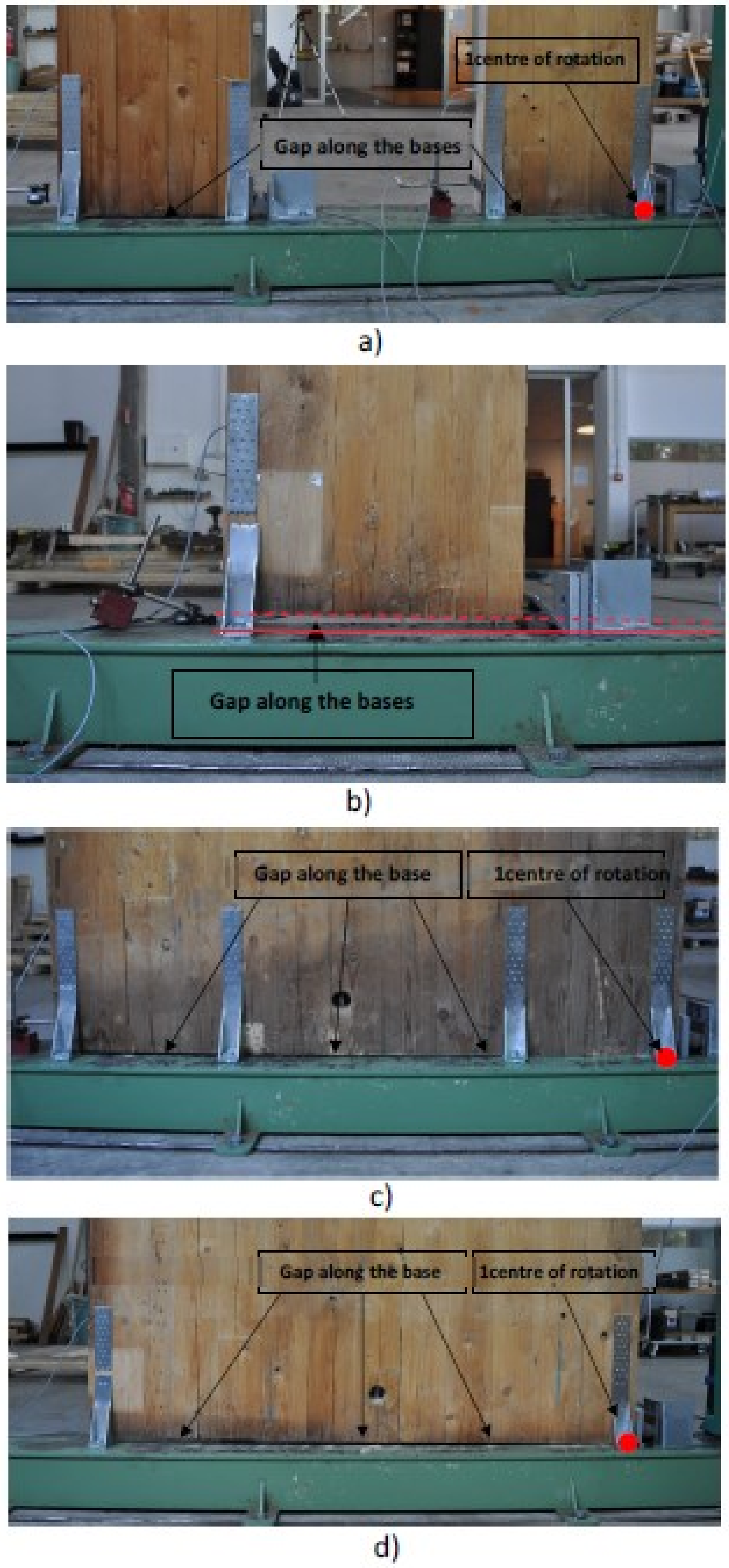

Figure 6-26. Kinematic behaviour of specimens 01, 02, 03 and 04

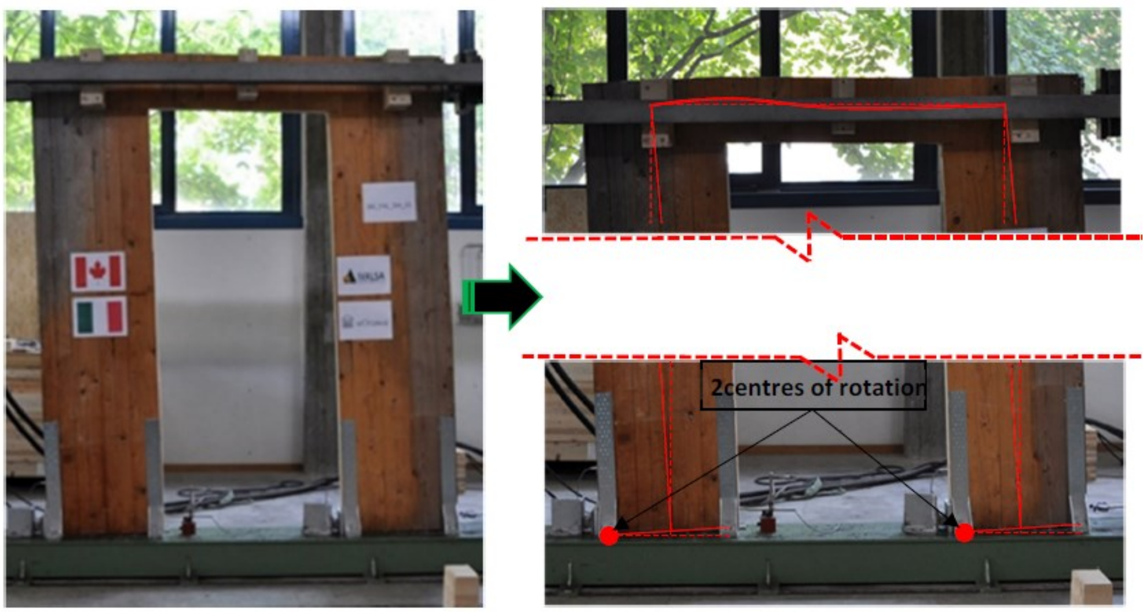

Figure 6-27. Kinematic behaviour of specimen 05

A verification of the observation made about the kinematic behaviour is presented in Figure 6-28, where the vertical displacement of LVDT CH6, placed near hold-down HD2 is presented for all wall specimens. It can be observed that the value of the displacement is positive for wall Specimens 01-04, which indicates that these walls exhibited a single point of rotation. Similarly, a value of almost zero is obtained for the case of Specimen 05, indicating the presence of two centres of rotation.

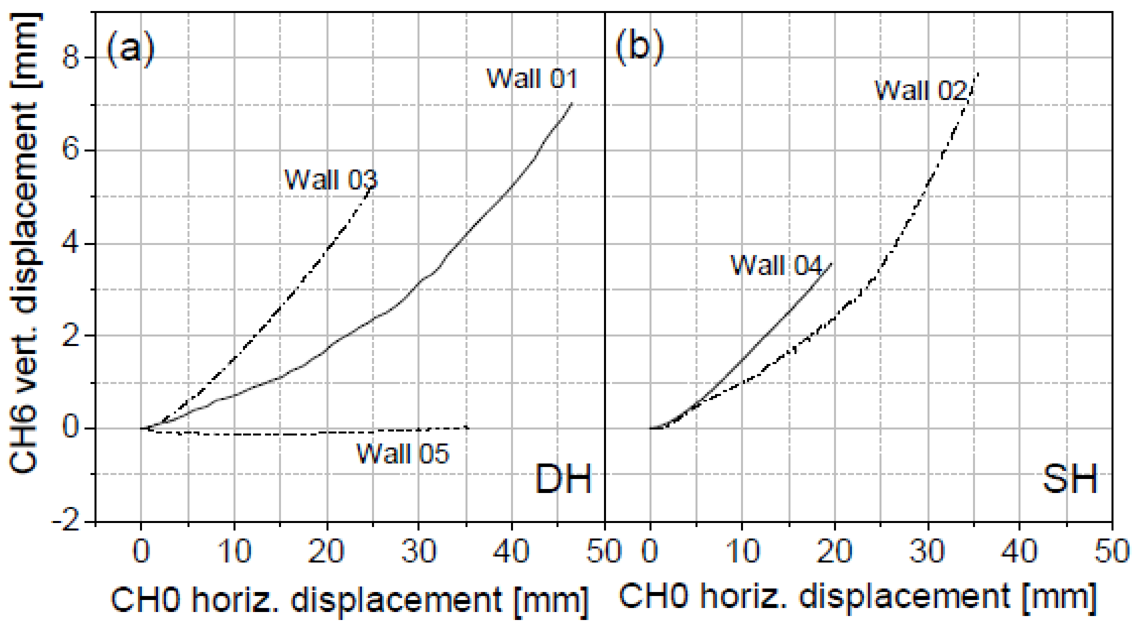

Figure 6-28. Kinematic behaviours of the tested walls with DH (a) and SH (b) configurations

The contribution due to rocking, sliding and panel deformation corresponding to the maximum load is reported in Table 6-3. The rocking and sliding contribution were obtained directly from the measured vertical and horizontal displacements, respectively, whereas the panel deformation contribution was obtained as the difference between the total displacement and those due to rocking and sliding. The results show that although most of the contribution to the wall deformation stems from panel rocking behaviour, the deformation in the CLT panel is significant. This observation seems at odds with previous studies on shearwalls with no openings where panel contribution is much lower compared to the rocking deformation, however, it is important to note that for shearwalls with opening such deformation is likely primarily attributed to lintel bending and shear deformation. This can be seen in wall 05 where the panel contribution is dominating as the lintel is slender compared to the 4 other four test specimens, which were governed by rocking behaviour.

Table 6-3. Deformation contributions of the tested walls

	wall 01	wall 02	wall 03	wall 04	wall 05		average wall 05
					left seg.	right seg.	
Total displ (mm)	47.4	34.4	35.1	32.7	35.0	35.0	35.0
Rocking contr. (%)	51.6	56.9	58.8	79.2	48.3	40.2	44.2
Sliding contr. (%)	7.0	5.2	11.7	6.7	3.4	3.4	3.4
Panel contr. (%)	41.5	37.9	29.5	14.0	48.3	56.4	52.3

6.7 Validation of proposed models against experimental tests from current study

This section contains a comparison between the results from the experimental campaign conducted in the current study and those obtained from the 2D area element model, including the inelastic properties of the connections, as described in Chapter 4, and the EFM as presented in Chapter 5. The comparison with the 2D model is based on the entire wall behaviour and using the capacity curves, whereas the comparison with EFM is primarily based on the elastic stiffness (K_{ser}) obtained from the test capacity curves and the corresponding pushover curves from the model analyses. Comparison between the entire wall behaviour from the test results and the EFM is presented in order to highlight the limitations in the EFM approach. The elastic stiffness is obtained as the secant stiffness between 10% and 40% of the maximum horizontal load $F_{failure}$, in accordance with the EN26891 standard (EN26891, 1991), as presented in Equation 4-2 described in Chapter 4.

The force-displacement curves obtained experimentally for the five tested walls are plotted against the 2D FE model (Chapter 4) and the EFM (Chapter 5), as shown in Figure 5.29 and 6.30, respectively. In general, reasonable agreement between the experimental and modelling results is observed for all walls. It may not be surprising that reasonably good prediction is attained when dealing with rigid CLT panels, where the deformation and failure are limited to that of the hold-down. Even models that don't allow for any flexibility in the CLT panels would likely achieve reasonable level of accuracy in the modeling results. What is unique to CLT walls with openings is that the flexibility of the vertical wall segment and the lintel beam play a significant in the overall wall behaviour and affect the wall stiffness even if failure occurs in the hold-down. The other important aspect of CLT walls with openings is the possibility of the failure occurring in the CLT panel. This is notoriously more difficult to predict due to the greater variability associated with the wood material, as demonstrated in Figure 6-24. As such, the largest deviation between the test results and model prediction is observed in Wall 05, which failed in the lintel beam rather than the hold-down.

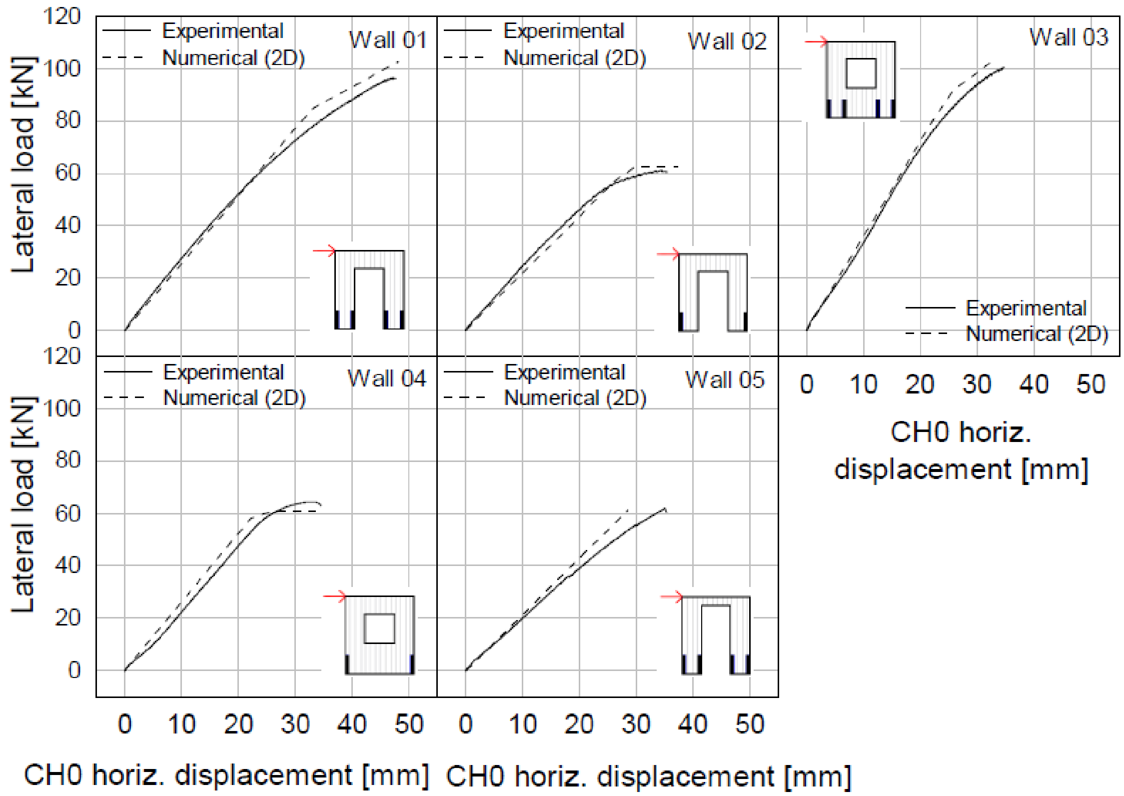

Figure 6-29. Lateral load vs top displacement curve from tests and FE (2D) models

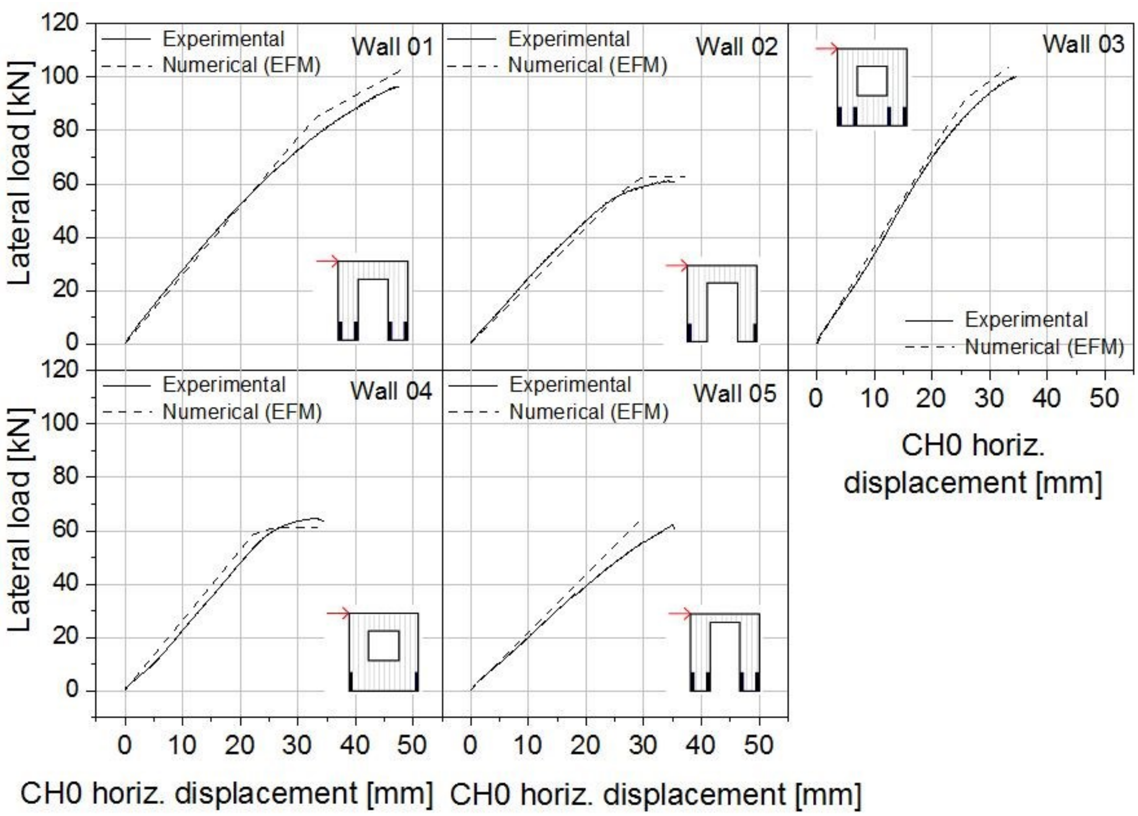

Figure 6-30. Lateral load vs top displacement curve from tests and EFM models

The results show that the EFM is capable of predicting the initial stiffness, ultimate capacity and ductility with reasonable accuracy, especially for walls whose behaviour was dominated by the hold-down behaviour (Walls 01-05). The magnitude of error found here is comparable to that observed when comparing the model to published test results, presented in Chapter 5. The results associated with Wall 5 show the largest discrepancy, which is attributed to the failure occurring in the lintel beam. Clearly more experimental testing and analysis are needed especially for the case where failure occurs in the CLT panel.

References of Chapter 6

ASTM E2126-07, Standard Test Methods for Cyclic (Reversed) Load Test for Shear Resistance of Walls for Buildings, ASTM International, West Conshohocken, PA, 2007, www.astm.org

EN594. (2011). Timber structures — Test methods — Racking strength andstiffness of timber frame wall panels: Ente nazionale italiano di unificazione (UNI).

EN26891. (1991). Timber structures – Joints made with mechanical fasteners - General principles for the determination of strength and deformation characteristics.

: ISO 6891-1983 (E).

RothoBlass. (2015). Wood connectors and timber plates, catalogue of products, RothoBlass SRL. Cortaccia, Italy.

CHAPTER 7

Conclusions and recommendations

7.1 Summary and Conclusions

The principal objective of this research was to study the mechanical and kinematic behaviours of CLT shearwalls with openings. This was done through an integrated experimental and numerical research program investigating the elastic and inelastic performance as well as the kinematic behaviour of CLT shearwalls with openings. The research also proposed an equivalent-frame-model, which allows for simpler and faster analysis and is suitable for design. Five racking tests were performed on full scale CLT walls in order to validate the numerical models as well as the equivalent frame model.

An extensive literature review highlighted the general consensus that rocking mode is the dominant response in CLT shearwalls and that the kinematic behaviour of the CLT shearwalls depends primarily on the mechanical anchors. Studies focussing on the behaviour of CLT shearwalls with openings were found to be very scarce with none specifically investigating the kinematic behaviour and the coupling effect due to the lintel beam .

The investigation of the wall behaviour in the elastic range led to the following conclusions:

- The lintel slenderness and hold-down stiffness have a significant effect on global kinematic behaviour, whereas the wall segment slenderness has little to moderate effect. For all analyzed cases with window opening, only one global kinematic behaviour, consisting of walls with one centre of rotation for the entire wall, was obtained.
- For all studied cases, the ratio of the tensile load in the outermost hold-down resulting from single and double hold-down configurations was observed to be between 1.00 and 1.20 for shearwalls with door openings and between 1.10 and 1.40 for shearwalls with window openings. Generally, the magnitude of the ratio is decreasing with hold-down stiffness and increasing with the lintel height.
- The degree of coupling is found to decrease with increased hold-down stiffness and wall segment width. In the case of one centre of rotation for the entire wall, the degree of coupling increases with the lintel slenderness, whereas when two centres of rotation for each wall segment is obtained, the results show a decreasing tendency of the degree of coupling with increased lintel beam slenderness.
- The total wall thickness is found to have an effect on the kinematic behaviour which can mainly be attributed to the effective thickness of the lamellae in the lintel beam.

The investigation in the inelastic range dealing with the influence of geometrical dimensions of the wall components and mechanical behaviour of hold-down led to the following conclusions.

- Walls with door opening configurations where the lintel and segment slenderness are equal, kinematic mode 1 is the dominant mode in both the elastic and inelastic ranges. Where the lintel slenderness is high relative to the wall segment, kinematic mode 2 generally dominates the behaviour. The analysis also revealed the possibility of change in the kinematic mode between two-centre of rotation in the elastic range to one-centre of rotation in the inelastic range. For walls with window openings, all configurations exhibited one-centre of rotation and the kinematic mode did not change when moving from elastic to inelastic range. The addition of the bottom parapet led in general to a change in the kinematic mode of the walls from two-centre of rotation to one-centre of rotation and increased elastic stiffness significantly.
- For walls with door openings, a significant decrease in strength was observed in walls with single hold-down configuration compared to those with double hold-down. In general, failure in the walls with double hold-down configuration occurred in CLT lintel, while the failure generally occurred in the hold-down when single hold-down configuration is used. When the wall segment was more slender than the lintel beam, failure in the hold-down governed the overall failure mode of the wall, while for wall configurations, where the slenderness of the segment and lintel are equal, the dominant failure mode was in the CLT lintel beam. For wall with window openings, in all cases where double hold-down configuration was used, failure occurred in the CLT lintel beam, whereas walls with single hold-down configuration, the failure occurred in hold down. On average, the wall strength almost doubled due to the effect of the parapet.

- Wall configuration with a slender wall segment compared to lintel shows a consistently high global ductility, particularly in walls with single hold-down configuration. The behaviour in wall configurations where lintel and wall segment slenderness ratio were equal was less consistent and generally dominated by brittle behaviour. For wall with window openings, using single hold-down configuration consistently led to an increase in the wall ductility. Increasing the stiffness and strength in the hold-down led to a decrease in wall ductility since hold-down devices with higher capacity have lower ductility. The additional of the bottom parapet has a noticeable effect for the global ductility in case of single hold-down configuration which is a consequence of engaging the hold-down. No effect of the parapet in case of double hold-down configuration was noticed.

The conclusions drawn from the study on the equivalent frame model are:

- Reasonable fit was observed between the proposed EFM and a detailed 2D area element model when the global elastic stiffness and tensile load in the hold-down was compared. Higher discrepancies were obtained for shear load and bending moment in the lintel beam.
- The model was successfully validated through five full-scale tests on CLT shearwalls with door or window opening as well as two published studies on walls with door openings. The results showed that the EFM is capable of predicting the behaviour in the wall with reasonable accuracy, especially for walls whose behaviour was dominated by the hold-down behaviour. For wall where failure

occurred in the CLT panel (e.g. lintel beam) the model displayed the largest discrepancy.

7.2 Recommendations for Future Work

The numerical model and the proposed equivalent frame model (EFM) were limited in scope to a single wall, where one opening (window or door) is centrally placed. It is suggested that future work expands the proposed model's applicability to multiple storey and non-symmetrical openings, including the presence of both opening types (doors and windows) in the same shearwall.

The experimental campaign in the current study was limited in terms of the number of configurations as well as variation in the geometrical dimensions of the wall segment and lintel beam. There is a need for an extensive experimental campaign to investigate more wall configurations with different lintel beam and wall segment aspect ratios as well as a range of hold-down stiffness and strengths. Ideally, more than one wall and multiple-storey system would be part of the experimental campaign in order to validate the current model or propose more robust models.

Further investigation of the internal distribution of stresses in CLT elements is needed. Failure in the CLT panel is fairly complex and could consist of multiple failure modes. Stress states can be easily found in relatively complex models with shell elements. However, testing at full-scale of wall configurations where the failure occurs in the lintel beam is still lacking. This would significantly help improve model prediction in CLT walls with openings. In addition to varying the overall geometrical parameters of the wall segments and lintel beam, the effect of lamellae ratio on the internal distribution of stresses could be investigated.

The EFM was proven to be a reliable technique to reduce the degrees of freedom generally associated with modeling of CLT shearwalls. The strength of simplicity of such model can be best demonstrated when multiple storeys are considered. Developing a reliable way to extend the current EFM to cover more than one storey by representing the effects of diaphragm and connections between storeys is recommended.

APPENDIX A
Elastic analysis (kinematic modes)

Table A-1. Data set used for the elastic analysis of shear-walls with door openings

Case #	Wall segment flexibility (λ_w)	Lintel flexibility (λ_l)	Shear-wall thickness	Mechanical characteristics of the CLT shearwalls	Hold-downs stiffness	Hold-downs configuration
	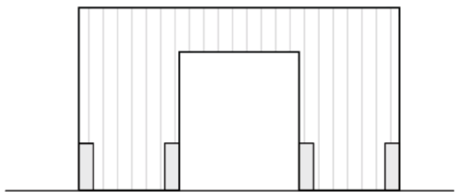			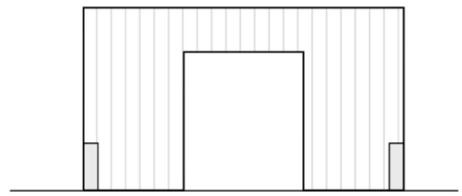		
1	1	2	5-ply * 20mm	E_0 and E_{90}, are assumed to be 12.000 MPa and 500 MPa, respectively. 690 MPA is the value assumed for $G_{0,mean}$	8, 14 and 20 kN/mm	Single (SH) or double hold-down (DH) for each wall segment
2	1	3				
3	1	4				
4	1	5				
5	1	6				
6	1	7				
7	1	8				
8	2	2				
9	2	3				
10	2	4				
11	2	5				
12	2	6				
13	2	7				
14	2	8				
15	3.50	2				
16	3.50	3				
17	3.50	4				
18	3.50	5				
19	3.50	6				
20	3.50	7				
21	3.50	8				
22	1	1				
23	1	1.50				
24	1	2				
25	1	2.50				
26	1	3				
27	1	3.50				

Table A-2. Continued

Case #	wall segment flexibility (λ_w)	Lintel flexibility (λ_l)	Shear-wall thickness	Mechanical characteristics of the CLT shearwalls	Hold-downs stiffness	Hold-downs configuration
28	1	4	5-ply * 20mm	E_0 and E_{90}, are assumed to be 12.000 MPa and 500 MPa, respectively. 690 MPA is the value assumed for $G_{0,mean}$	8, 14 and 20 kN/mm	Single (SH) or double hold-down (DH) for each wall segment
29	2	1				
30	2	1.50				
31	2	2				
32	2	2.50				
33	2	3				
34	2	3.50				
35	2	4				
36	3.50	1				
37	3.50	1.50				
38	3.50	2				
39	3.50	2.50				
40	3.50	3				
41	3.50	3.50				
42	3.50	4				
43	1	0.67				
44	1	1				
45	1	1.33				
46	1	1.67				
47	1	2				
48	1	2.33				
49	1	2.67				
50	2	0.67				
51	2	1				
52	2	1.33				
53	2	1.67				
54	2	2				
55	2	2.33				
56	2	2.67				
57	3.50	0.67				
58	3.50	1				
59	3.50	1.33				
60	3.50	1.67				
61	3.50	2				
62	3.50	2.33				
63	3.50	2.67				

Table A-3. Data set used for the elastic analysis of shearwalls with window openings

Case #	Wall segment flexibility (λ_w)	Top lintel flexibility (λ_l)	Bottom lintel flexibility (λ_l)	Shear-wall thickness	Mechanical characteristics of the CLT shearwalls	Hold-downs stiffness	Hold-downs configuration
	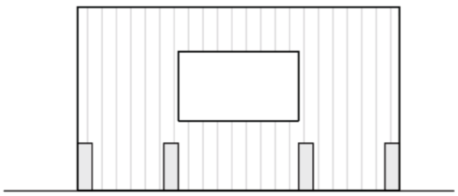				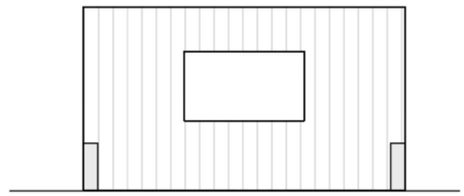		
1	1	2	0.80	5-ply * 20mm	E_0 and E_{90}, are assumed to be 12.000 MPa and 500 MPa, respectively. 690 MPA is the value assumed for $G_{0,mean}$	8, 14 and 20 kN/mm	Single (SH) or double hold-down (DH) for each wall segment
2	1	3	1.20				
3	1	4	1.60				
4	1	5	2				
5	1	6	2.40				
6	1	7	2.80				
7	1	8	3.20				
8	2	2	0.80				
9	2	3	1.20				
10	2	4	1.60				
11	2	5	2				
12	2	6	2.40				
13	2	7	2.80				
14	2	8	3.20				
15	3.50	2	0.80				
16	3.50	3	1.20				
17	3.50	4	1.60				
18	3.50	5	2				
19	3.50	6	2.40				
20	3.50	7	2.80				
21	3.50	8	3.20				
22	1	1	0.80				
23	1	1.50	1.20				
24	1	2	1.60				
25	1	2.50	2				
26	1	3	2.40				
27	1	3.50	2.80				

Table A-4. Continued

Case #	Wall segment flexibility (λ_w)	Top lintel flexibility (λ_l)	Bottom lintel flexibility (λ_l)	Shear-wall thickness	Mechanical characteristics of the CLT shearwalls	Hold-downs stiffness	Hold-downs configuration
28	1	4	3.20	5-ply * 20mm	E_0 and E_{90}, are assumed to be 12.000 MPa and 500 MPa, respectively. 690 MPA is the value assumed for $G_{0,mean}$	8, 14 and 20 kN/mm	Single (SH) or double hold-down (DH) for each wall segment
29	2	1	0.80				
30	2	1.50	1.20				
31	2	2	1.60				
32	2	2.50	2				
33	2	3	2.40				
34	2	3.50	2.80				
35	2	4	3.20				
36	3.50	1	0.80				
37	3.50	1.50	1.20				
38	3.50	2	1.60				
39	3.50	2.50	2				
40	3.50	3	2.40				
41	3.50	3.50	2.80				
42	3.50	4	3.20				
43	1	0.67	0.80				
44	1	1	1.20				
45	1	1.33	1.60				
46	1	1.67	2				
47	1	2	2.40				
48	1	2.33	2.80				
49	1	2.67	3.20				
50	2	0.67	0.80				
51	2	1	1.20				
52	2	1.33	1.60				
53	2	1.67	2				
54	2	2	2.40				
55	2	2.33	2.80				
56	2	2.67	3.20				
57	3.50	0.67	0.80				
58	3.50	1	1.20				
59	3.50	1.33	1.60				
60	3.50	1.67	2				
61	3.50	2	2.40				
62	3.50	2.33	2.80				
63	3.50	2.67	3.20				

A.1 Centres of rotation for 8kN/mm hold-down stiffness

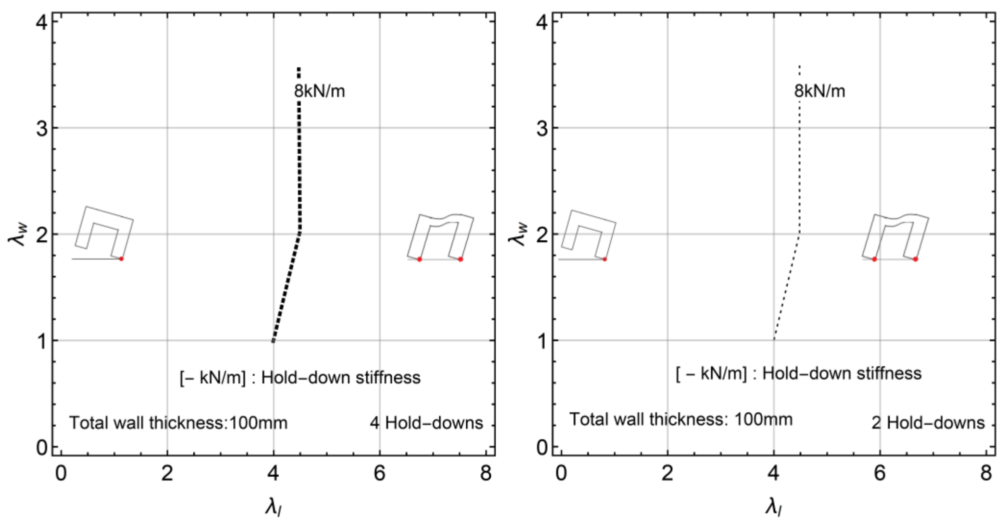

Figure A-1. Global kinematic behaviour for CLT shearwalls for hold-down stiffness of 8kN/mm and total wall thickness of 100 mm

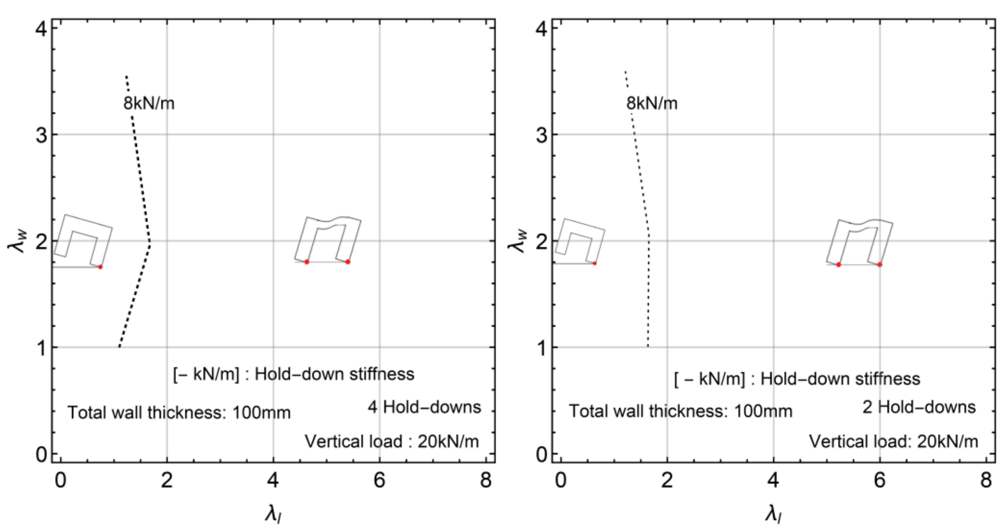

Figure A-2. Global kinematic behaviour for CLT shearwalls with vertical load effect for hold-down stiffness of 8kN/mm and total wall thickness of 100 mm

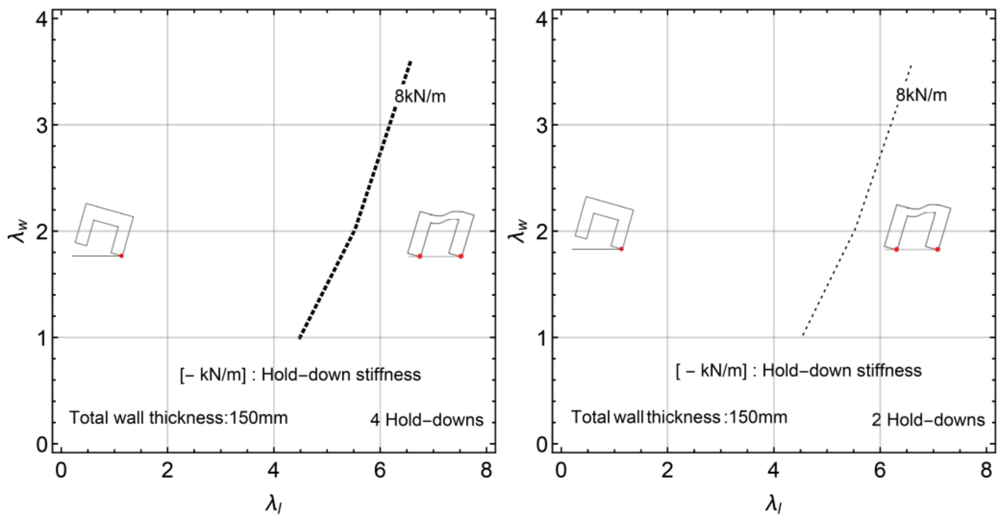

Figure A-3. Global kinematic behaviour for CLT shearwalls for hold-down stiffness of 8kN/mm and total wall thickness of 150 mm

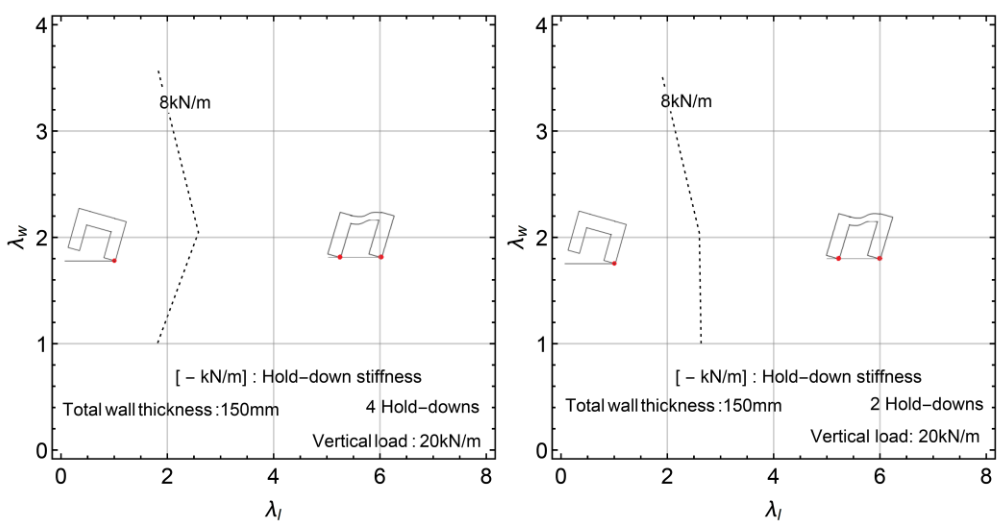

Figure A-4. Global kinematic behaviour for CLT shearwalls with vertical load effect for hold-down stiffness of 8kN/mm and total wall thickness of 150 mm

A.2 Centres of rotation for 14kN/mm hold-down stiffness

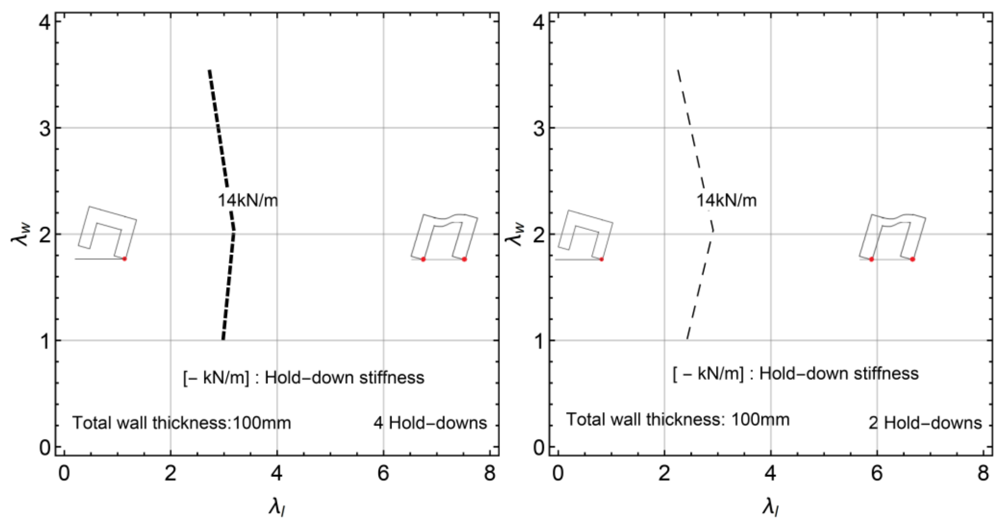

Figure A-5. Global kinematic behaviour for CLT shearwalls for hold-down stiffness of 14kN/mm and total wall thickness of 100 mm

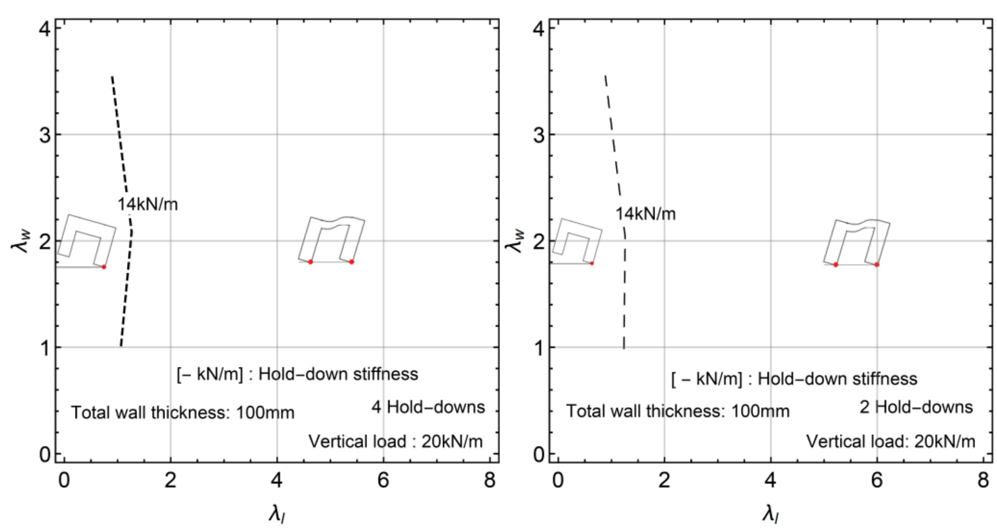

Figure A-6. Global kinematic behaviour for CLT shearwalls with vertical load effect for hold-down stiffness of 14kN/mm and total wall thickness of 100 mm

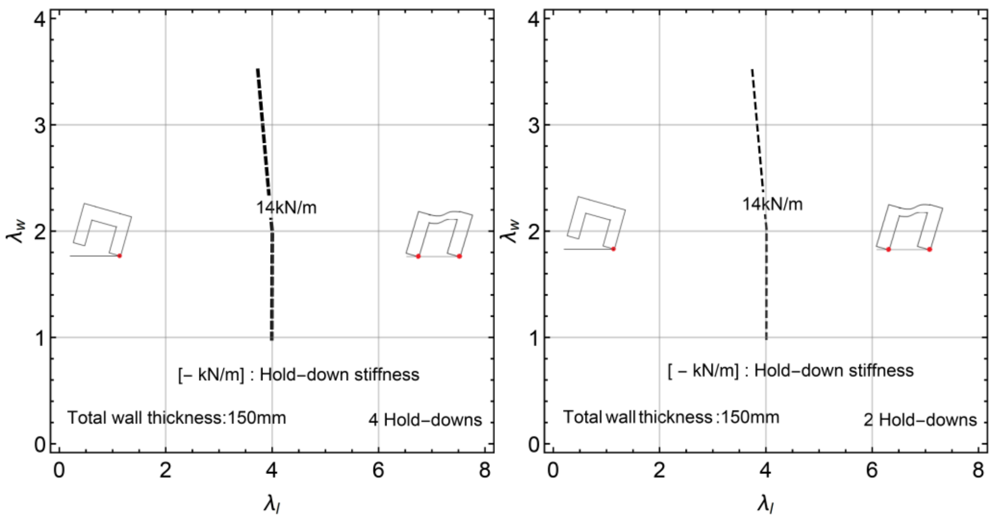

Figure A-7. Global kinematic behaviour for CLT shearwalls for hold-down stiffness of 14kN/mm and total wall thickness of 150 mm

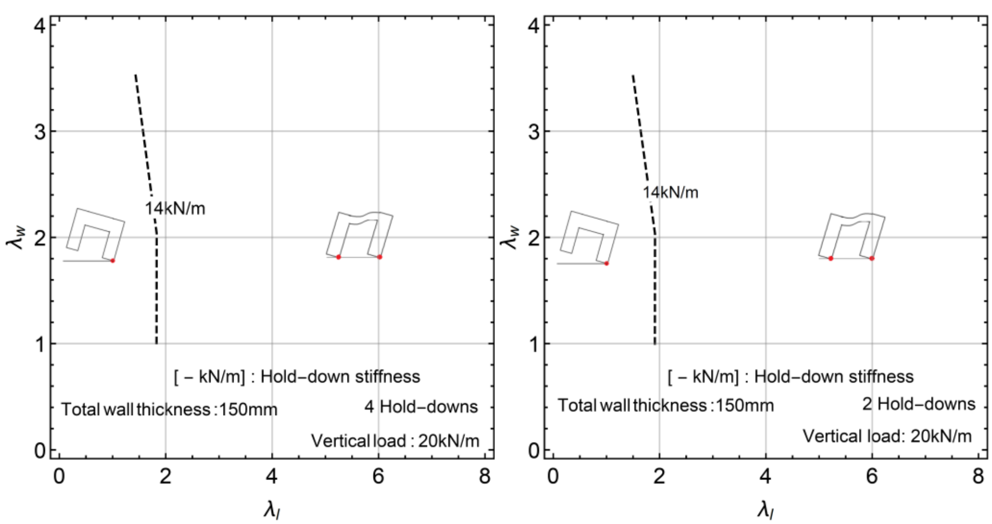

Figure A-8. Global kinematic behaviour for CLT shearwalls with vertical load effect for hold-down stiffness of 14kN/mm and total wall thickness of 150 mm

A.3 Centres of rotation for 20kN/mm hold-down stiffness

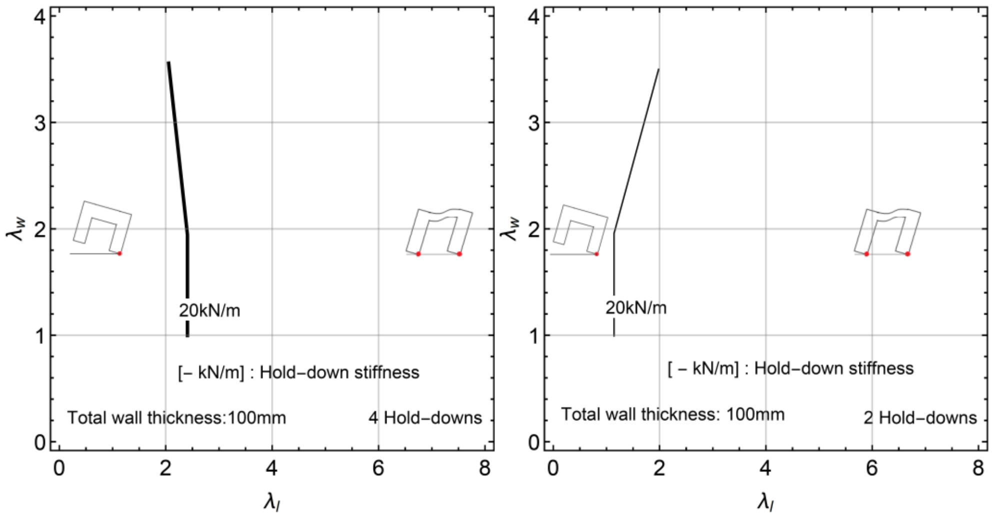

Figure A-9. Global kinematic behaviour for CLT shearwalls for hold-down stiffness of 20kN/mm and total wall thickness of 100 mm

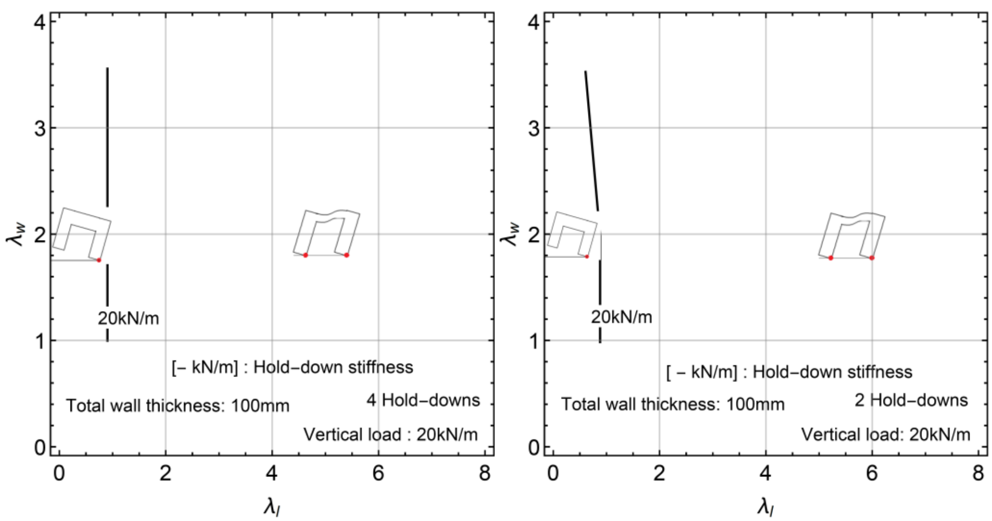

Figure A-10. Global kinematic behaviour for CLT shearwalls with vertical load effect for hold-down stiffness of 20kN/mm and total wall thickness of 100 mm

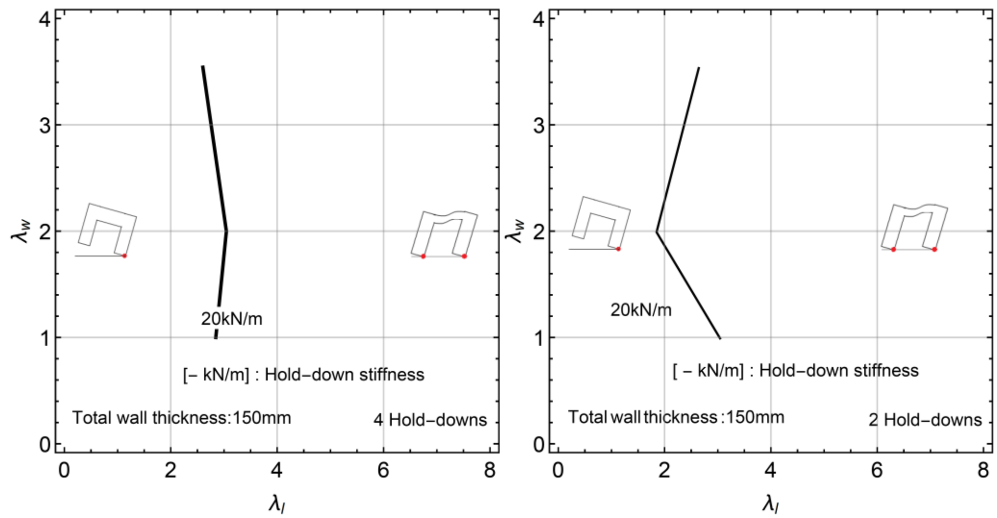

Figure A-11. Global kinematic behaviour for CLT shearwalls for hold-down stiffness of 20kN/mm and total wall thickness of 150 mm

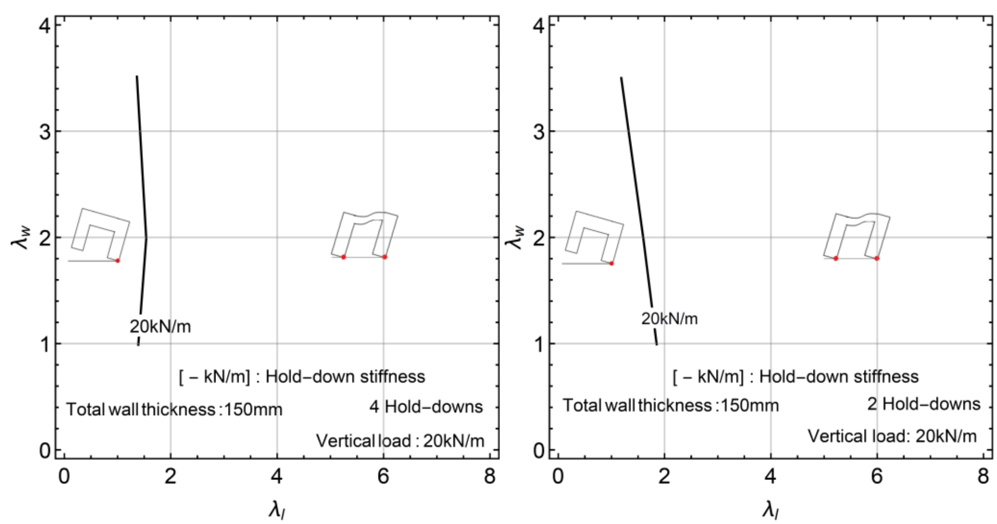

Figure A-12. Global kinematic behaviour for CLT shearwalls with vertical load effect for hold-down stiffness of 20kN/mm and total wall thickness of 150 mm

APPENDIX B
Equivalent Frame Model (EFM)

Table B-1. Data set used for the elastic analysis of shearwalls with door openings

<table>
<tr><th>Case #</th><th>Wall segment flexibility (λ_w)</th><th>Lintel flexibility (λ_l)</th><th>Shear-wall thickness</th><th>Mechanical characteristics of the CLT shearwalls</th><th>Hold-downs stiffness</th><th>Hold-downs configuration</th></tr>
<tr><td colspan="4">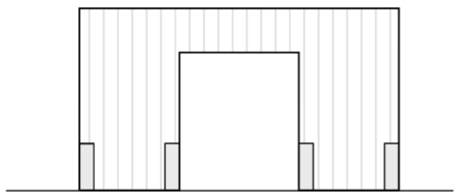</td><td colspan="3">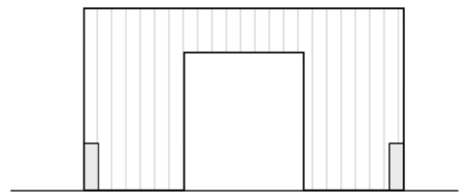</td></tr>
<tr><td>1</td><td>0.86</td><td>2</td><td rowspan="27">5-ply * 20mm</td><td rowspan="27">E_0 and E_{90}, are assumed to be 12.000 MPa and 370 MPa, respectively. 690 MPA is the value assumed for $G_{0,mean}$</td><td rowspan="27">6.622 and 13.247 KN/mm for global kinematic behaviour</td><td rowspan="27">Single (SH) or double hold-down (DH) for each wall segment</td></tr>
<tr><td>2</td><td>0.86</td><td>5</td></tr>
<tr><td>3</td><td>0.86</td><td>8</td></tr>
<tr><td>4</td><td>0.86</td><td>1.33</td></tr>
<tr><td>5</td><td>0.86</td><td>3.33</td></tr>
<tr><td>6</td><td>0.86</td><td>5.33</td></tr>
<tr><td>7</td><td>0.86</td><td>1</td></tr>
<tr><td>8</td><td>0.86</td><td>2.50</td></tr>
<tr><td>9</td><td>0.86</td><td>4</td></tr>
<tr><td>10</td><td>1.71</td><td>2</td></tr>
<tr><td>11</td><td>1.71</td><td>5</td></tr>
<tr><td>12</td><td>1.71</td><td>8</td></tr>
<tr><td>13</td><td>1.71</td><td>1.33</td></tr>
<tr><td>14</td><td>1.71</td><td>3.33</td></tr>
<tr><td>15</td><td>1.71</td><td>5.33</td></tr>
<tr><td>16</td><td>1.71</td><td>1</td></tr>
<tr><td>17</td><td>1.71</td><td>2.50</td></tr>
<tr><td>18</td><td>1.71</td><td>4</td></tr>
<tr><td>19</td><td>3</td><td>2</td></tr>
<tr><td>20</td><td>3</td><td>5</td></tr>
<tr><td>21</td><td>3</td><td>8</td></tr>
<tr><td>22</td><td>3</td><td>1.33</td></tr>
<tr><td>23</td><td>3</td><td>3.33</td></tr>
<tr><td>24</td><td>3</td><td>5.33</td></tr>
<tr><td>25</td><td>3</td><td>1.00</td></tr>
<tr><td>26</td><td>3</td><td>2.5</td></tr>
<tr><td>27</td><td>3</td><td>4.00</td></tr>
</table>

Table B-2. Data set used for the elastic analysis of shearwalls with window openings

Case #	Wall segment flexibility (λ_w)	Top lintel flexibility (λ_l)	Bottom lintel flexibility (λ_l)	Shear-wall thickness	Mechanical characteristics of the CLT shearwalls	Hold-downs stiffness	Hold-downs configuration
		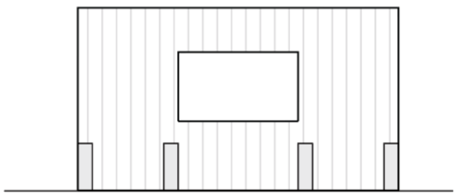			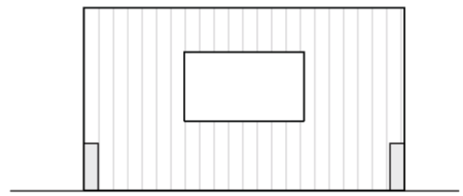		
1	0.86	2	0.80	5-ply * 20mm	E_0 and E_{90}, are assumed to be 12.000 MPa and 370 MPa, respectively. 690 MPA is the value assumed for $G_{0,mean}$	6.622 and 13.247 KN/mm for global kinematic behaviour	Single (SH) or double hold-down (DH) for each wall segment
2	0.86	5	2				
3	0.86	8	3.20				
4	0.86	1.33	0.80				
5	0.86	3.33	2				
6	0.86	5.33	3.20				
7	0.86	1	0.80				
8	0.86	2.50	2				
9	0.86	4	3.20				
10	1.71	2	0.80				
11	1.71	5	2				
12	1.71	8	3.20				
13	1.71	1.33	0.80				
14	1.71	3.33	2				
15	1.71	5.33	3.20				
16	1.71	1	0.80				
17	1.71	2.50	2				
18	1.71	4	3.20				
19	3	2	0.80				
20	3	5	2				
21	3	8	3.20				
22	3	1.33	0.80				
23	3	3.33	2				
24	3	5.33	3.20				
25	3	1.00	0.80				
26	3	2.5	2				
27	3	4.00	3.20				

B.1 Discrepancies of shearwalls with door openings

Figures B.1 to B.28 present the errors between the detailed model and the EFM for both the Displacement and Force control methods.

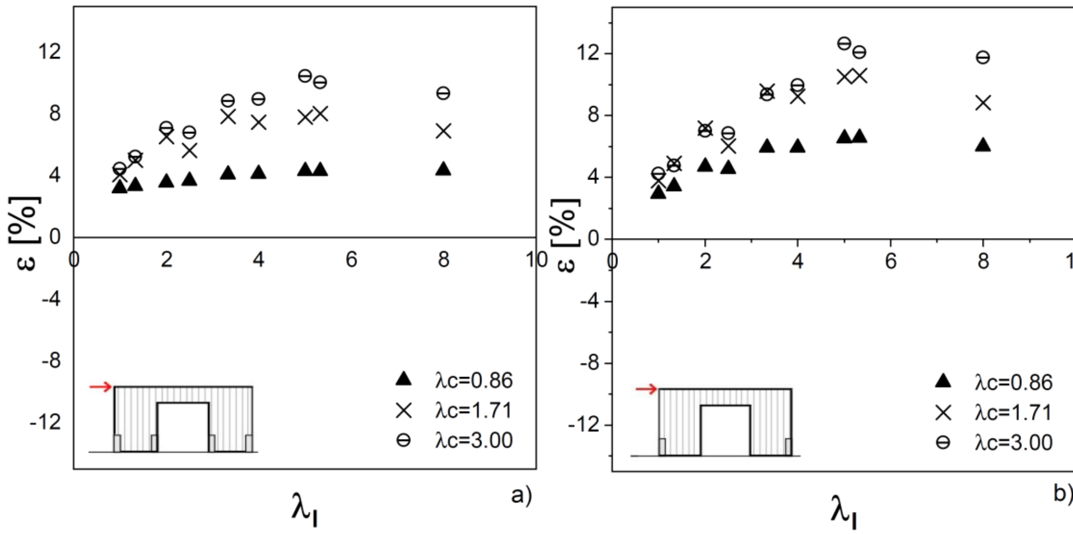

Figure B-1. Discrepancy for the global stiffness, kv,t,hd = 6.622 kN/mm, in load method #1: a) Door opening - DH, b) Door opening – SH

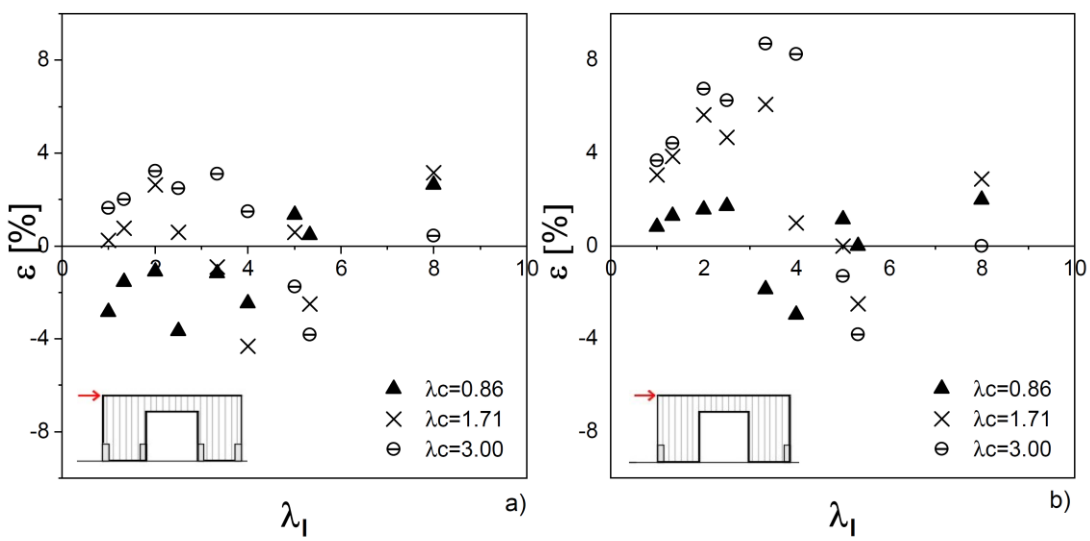

Figure B-2. Discrepancy for hold-down tensile load, kv,t,hd = 6.622 kN/mm, in load method #1: a) Door opening - DH, b) Door opening – SH

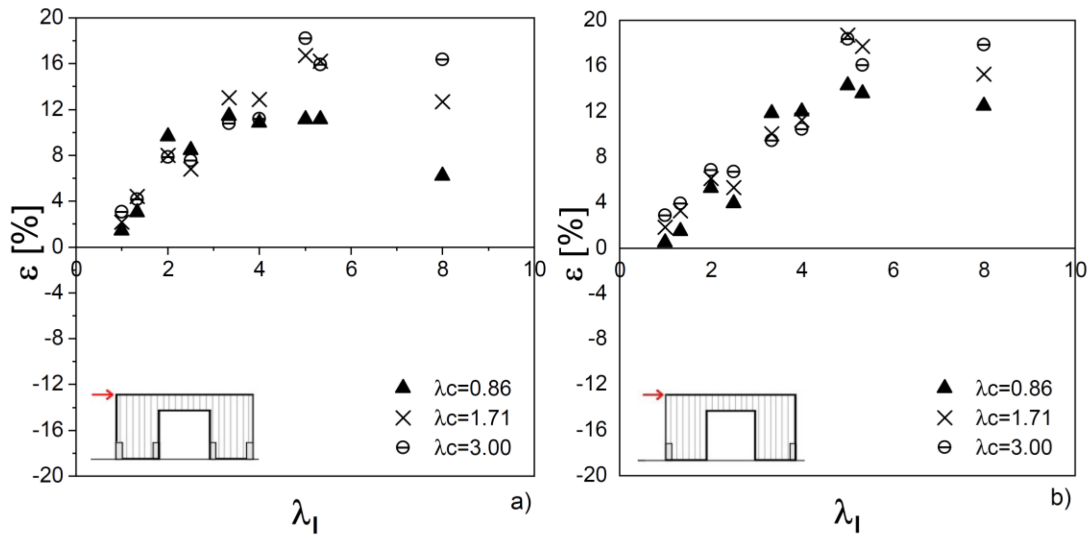

Figure B-3Discrepancy for lintel shear load , kv,t, hd = 6.622 kN/mm, in load method #1: a) Door opening - DH, b) Door opening – SH

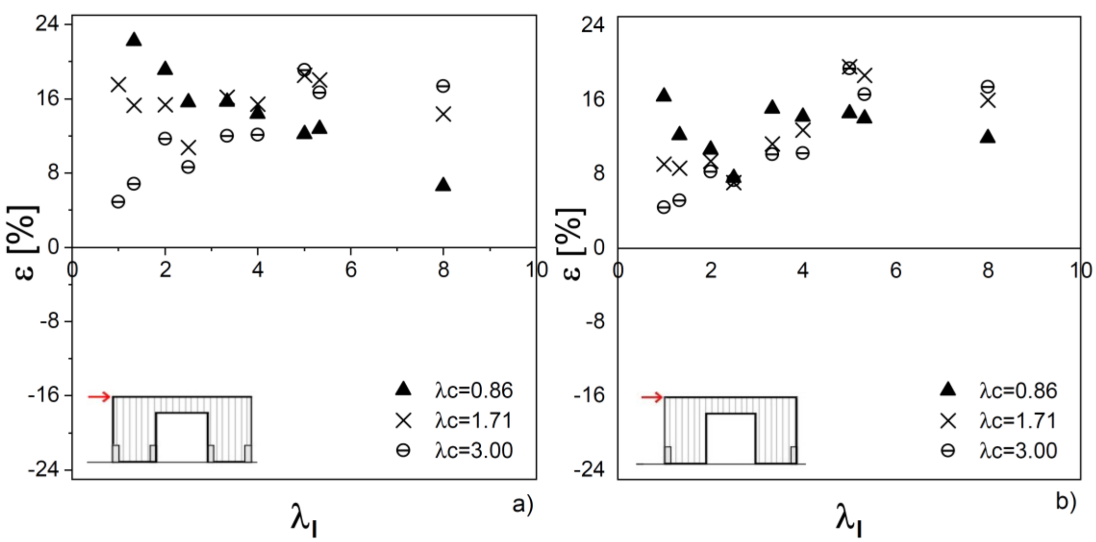

Figure B-4. Discrepancy for lintel bending moment , kv,t,hd = 6.622 kN/mm, in load method #1: a) Door opening - DH, b) Door opening – SH

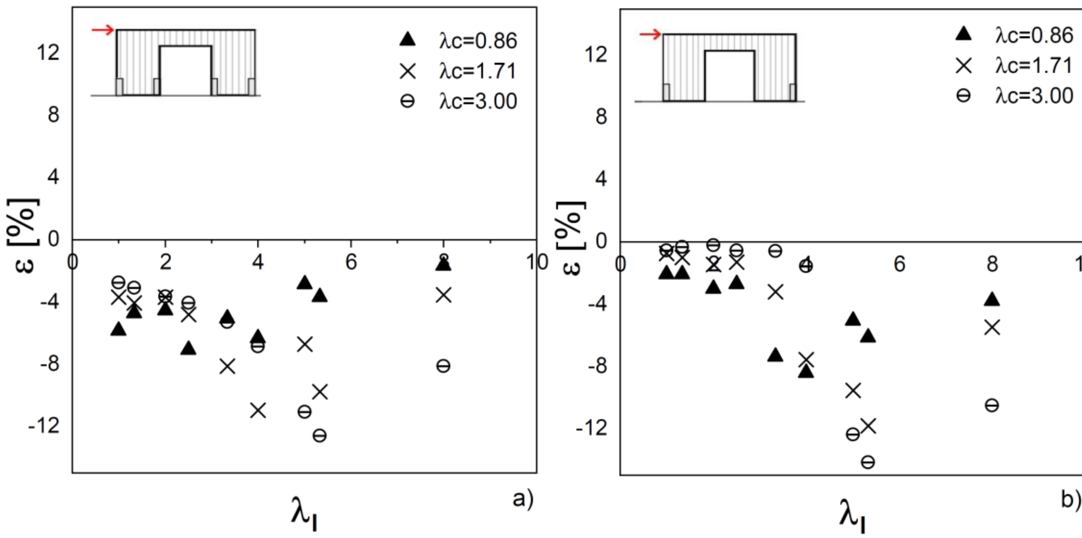

Figure B-5. Discrepancy for hold-down tensile load, kv,t,hd = 6.622 kN/mm, in load method #2: a) Door opening - DH, b) Door opening – SH

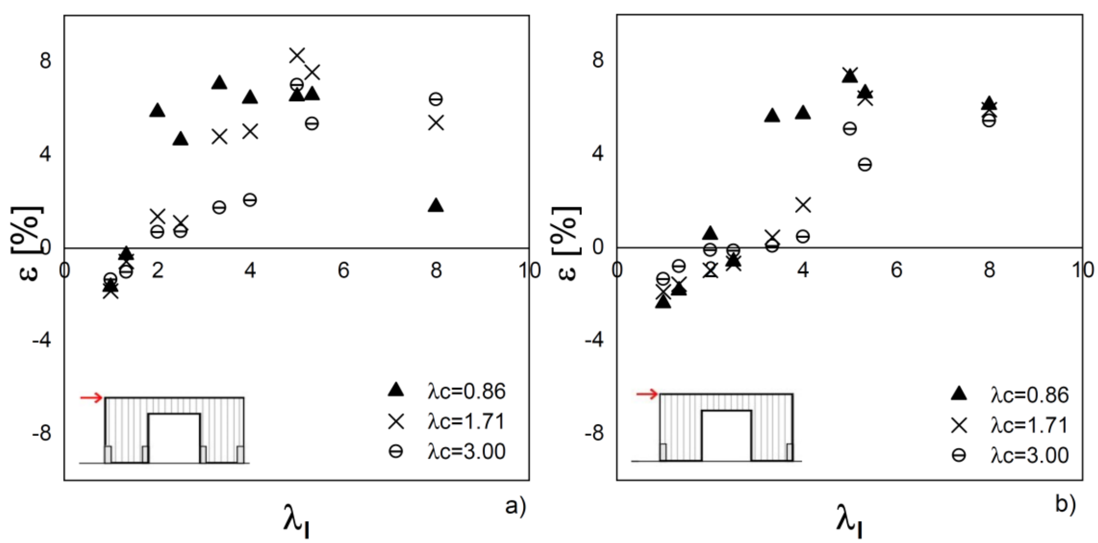

Figure B-6. Discrepancy for lintel shear load , kv,t, hd = 6.622 kN/mm, in load method #2: a) Door opening - DH, b) Door opening – SH

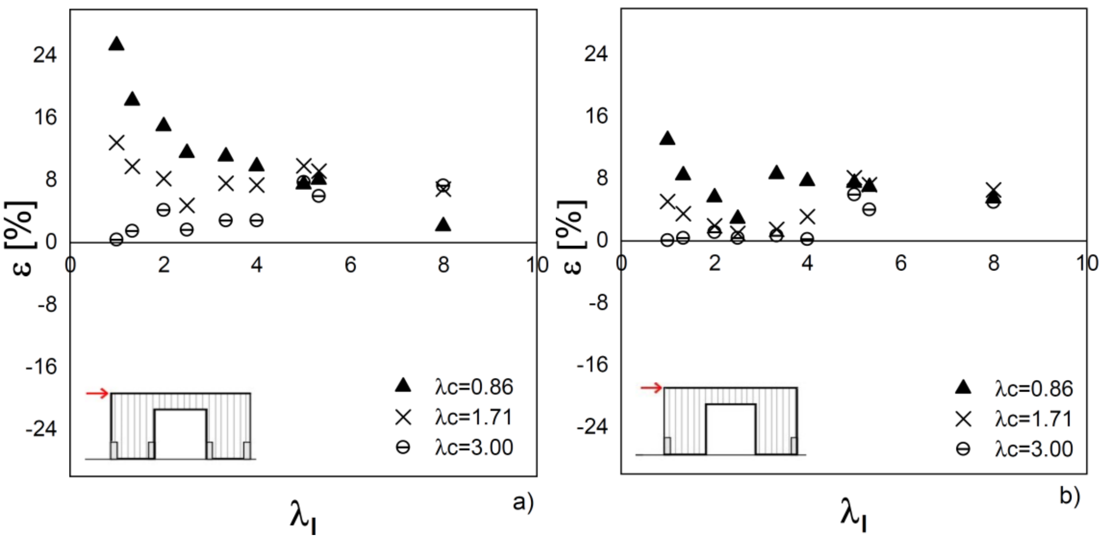

Figure B-7. Discrepancy for lintel bending moment , kv,t,hd = 6.622 kN/mm, in load method #2: a) Door opening - DH, b) Door opening – SH

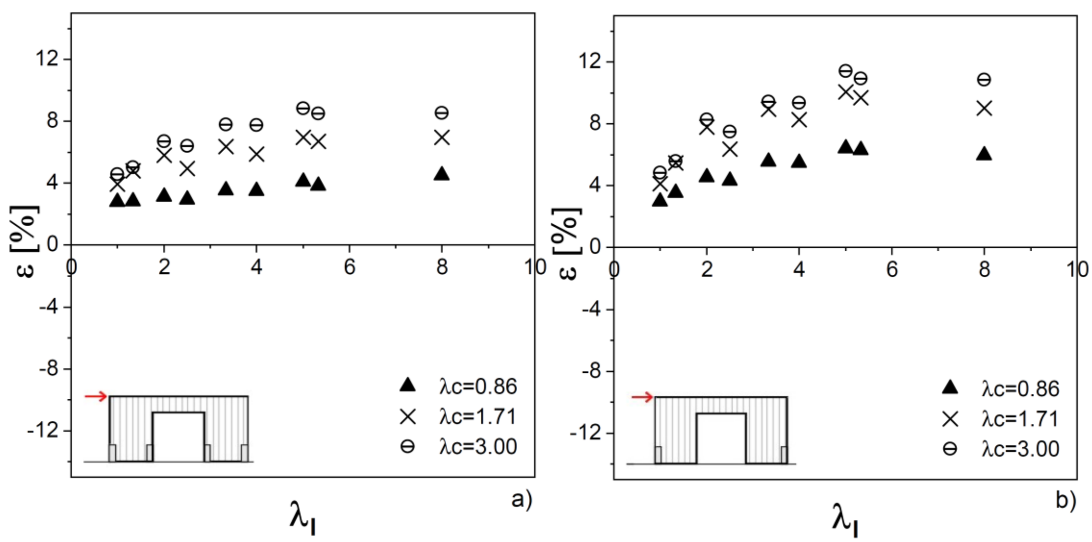

Figure B-8. Discrepancy for the global stiffness, kv,t,hd = 13.247 kN/mm, in load method #1: a) Door opening - DH, b) Door opening – SH

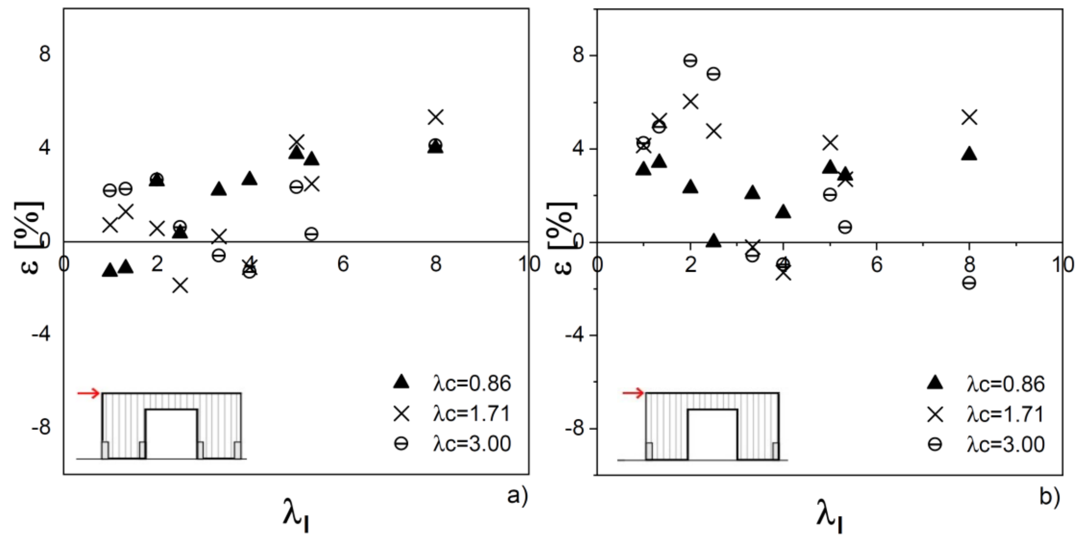

Figure B-9. Discrepancy for hold-down tensile load, kv,t,hd = 13.247 kN/mm, in load method #1: a) Door opening - DH, b) Door opening – SH

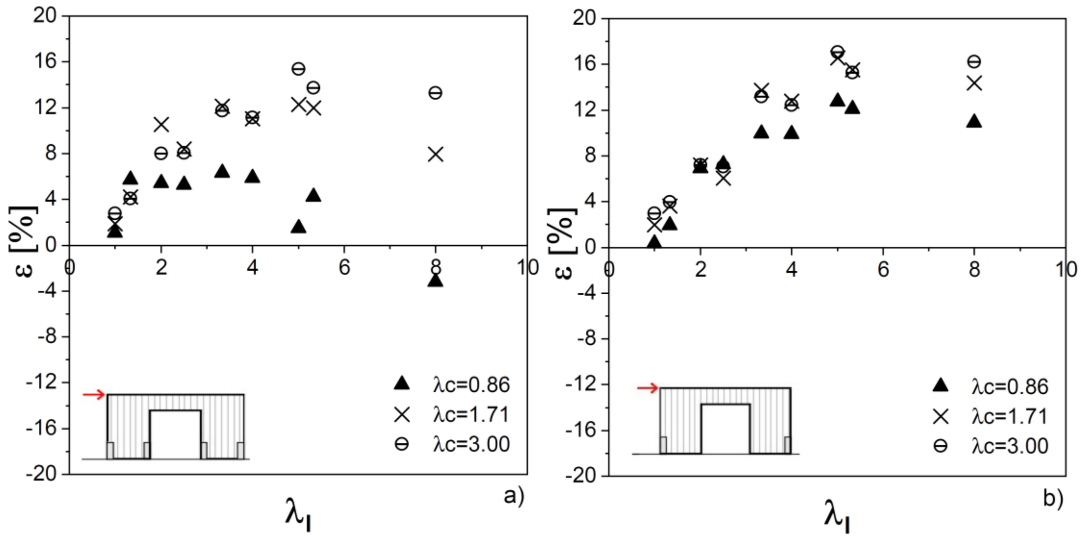

Figure B-10. Discrepancy for lintel shear load , kv,t, hd = 13.247 kN/mm, in load method #1: a) Door opening - DH, b) Door opening – SH

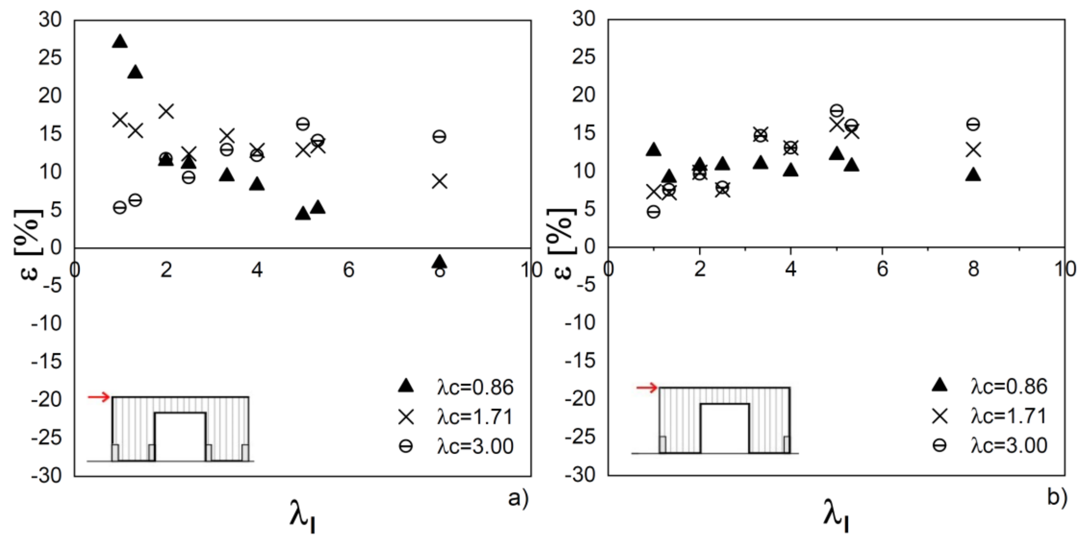

Figure B-11. Discrepancy for lintel bending moment , kv,t,hd = 13.247 kN/mm, in load method #1: a) Door opening - DH, b) Door opening – SH

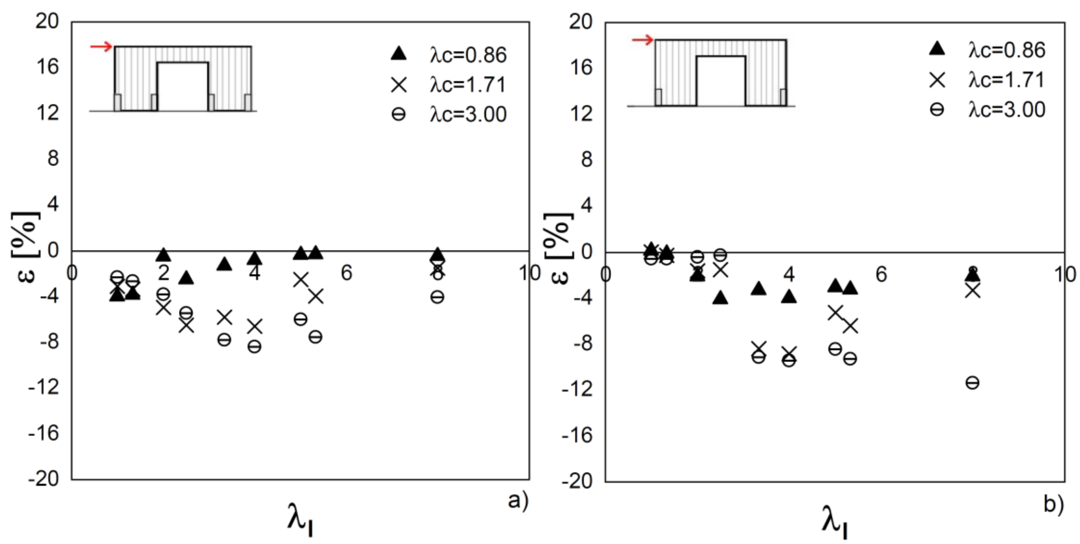

Figure B-12. Discrepancy for hold-down tensile load, kv,t,hd = 13.247 kN/mm, in load method #2: a) Door opening - DH, b) Door opening – SH

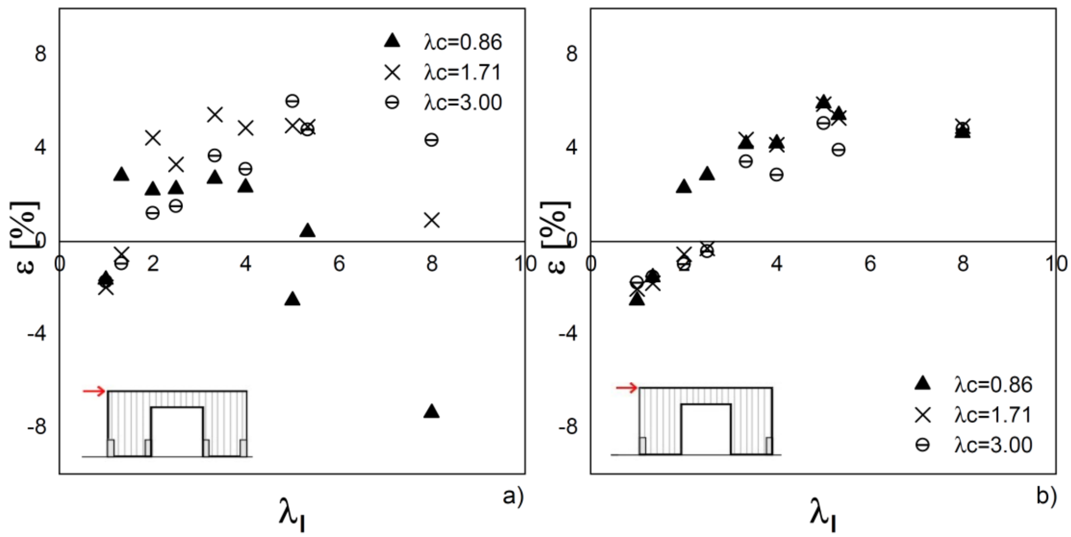

Figure B-13. Discrepancy for lintel shear load , kv,t, hd = 13.247 kN/mm in load method #2: a) Door opening - DH, b) Door opening – SH

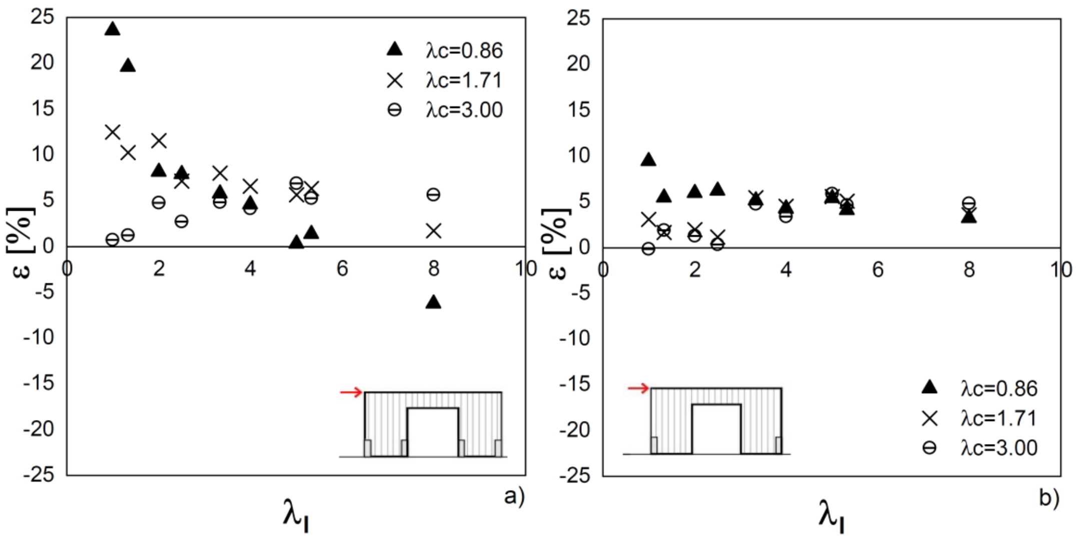

Figure B-14. Discrepancy for lintel bending moment , kv,t,hd = 13.247 kN/mm, in load method #2: a) Door opening - DH, b) Door opening – SH

B.2 Discrepancies of shearwalls with window openings

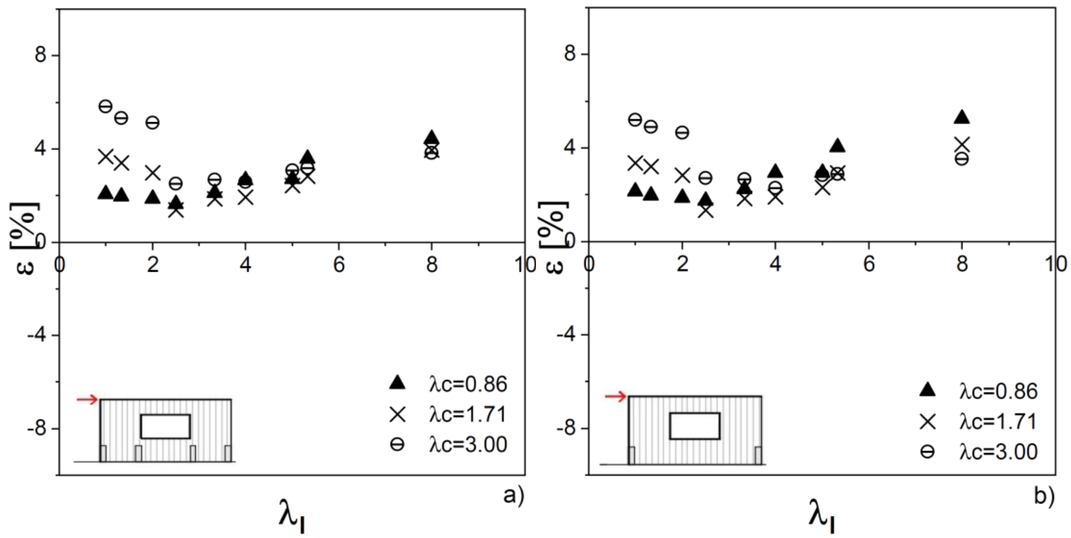

Figure B-15Discrepancy for the global stiffness, kv,t,hd = 6.622 kN/mm, in load method #1: a) Window opening - DH, b) Window opening – SH

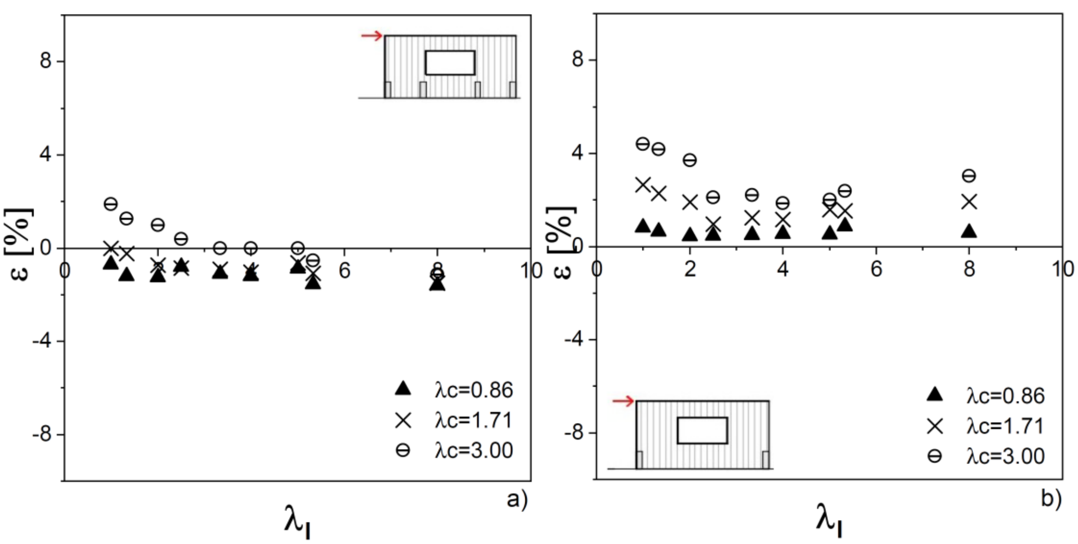

Figure B-16. Discrepancy for hold-down tensile load, kv,t,hd = 6.622 kN/mm, in load method #1: a) Window opening - DH, b) Window opening – SH

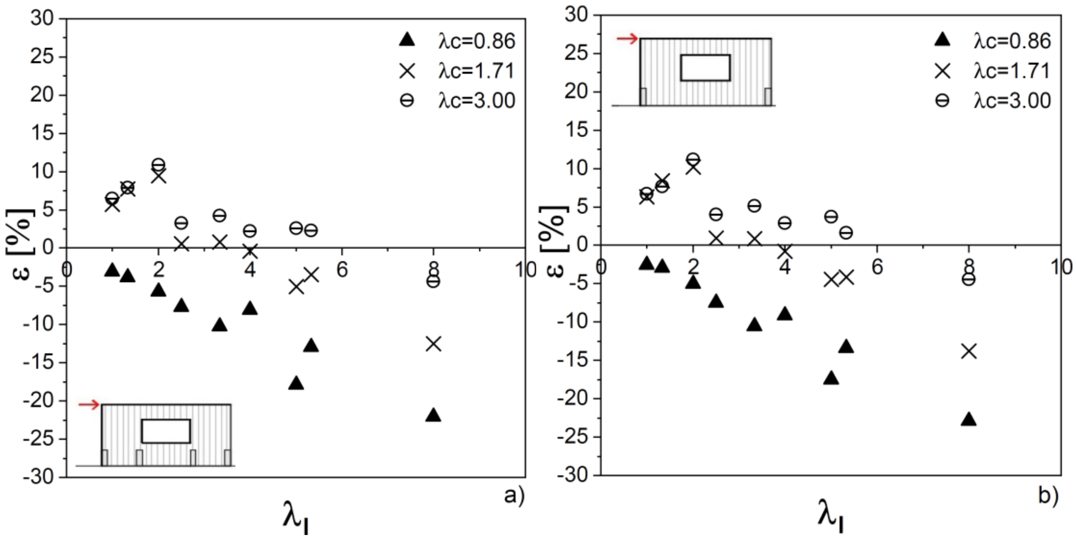

Figure B-17Discrepancy for lintel shear load , kv,t, hd = 6.622 kN/mm, in load method #1: a) Window opening - DH, b) Window opening – SH

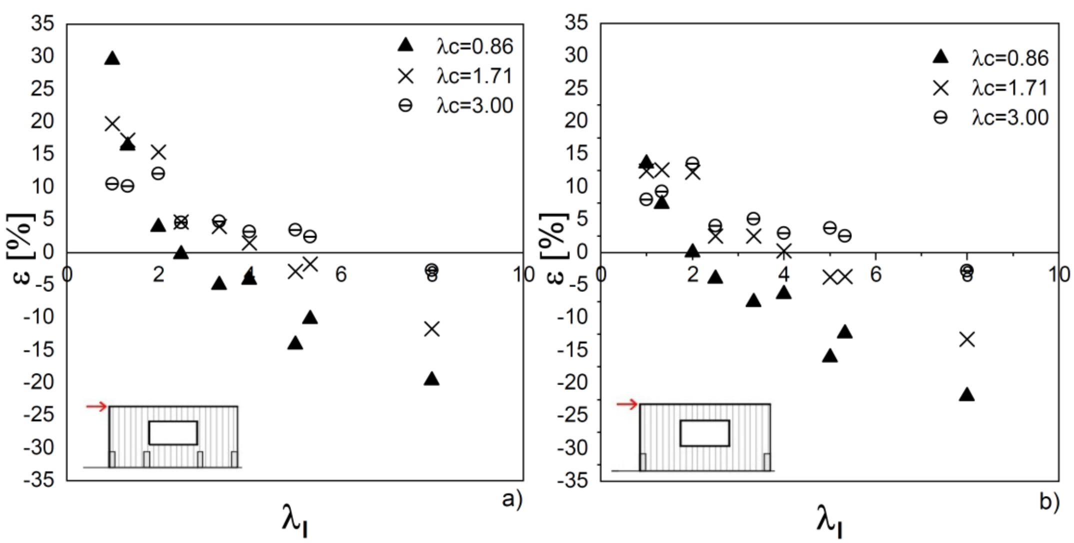

Figure B-18. Discrepancy for lintel bending moment , kv,t,hd = 6.622 kN/mm, in load method #1: a) Window opening - DH, b) Window opening – SH

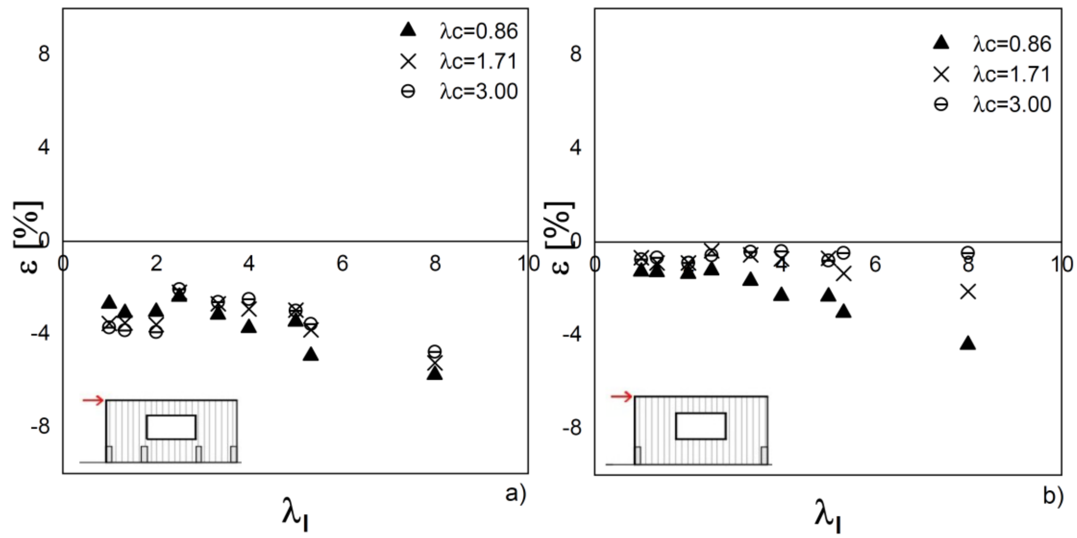

Figure B-19. Discrepancy for hold-down tensile load, kv,t,hd = 6.622 kN/mm, in load method #2: a) Window opening - DH, b) Window opening – SH

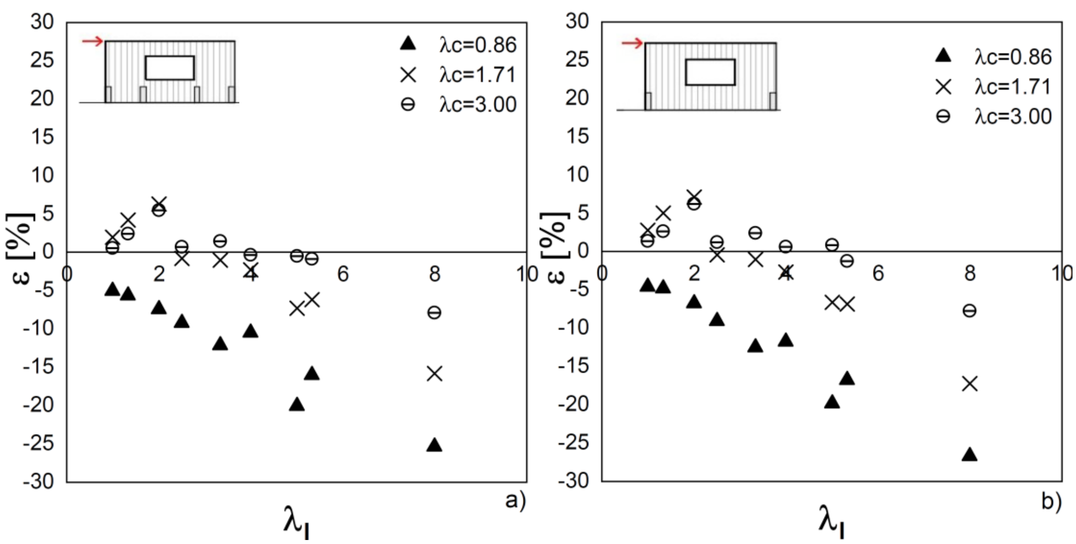

Figure B-20. Discrepancy for lintel shear load , kv,t, hd = 6.622 kN/mm, in load method #2: a) Window opening - DH, b) Window opening – SH

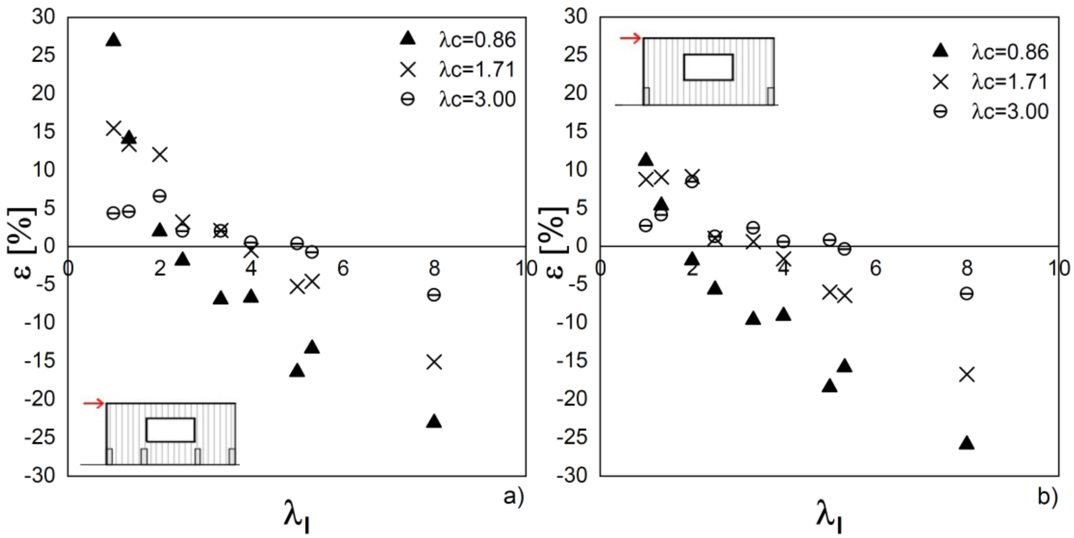

Figure B-21. Discrepancy for lintel bending moment , kv,t,hd = 6.622 kN/mm, in load method #2: a) Window opening - DH, b) Window opening – SH

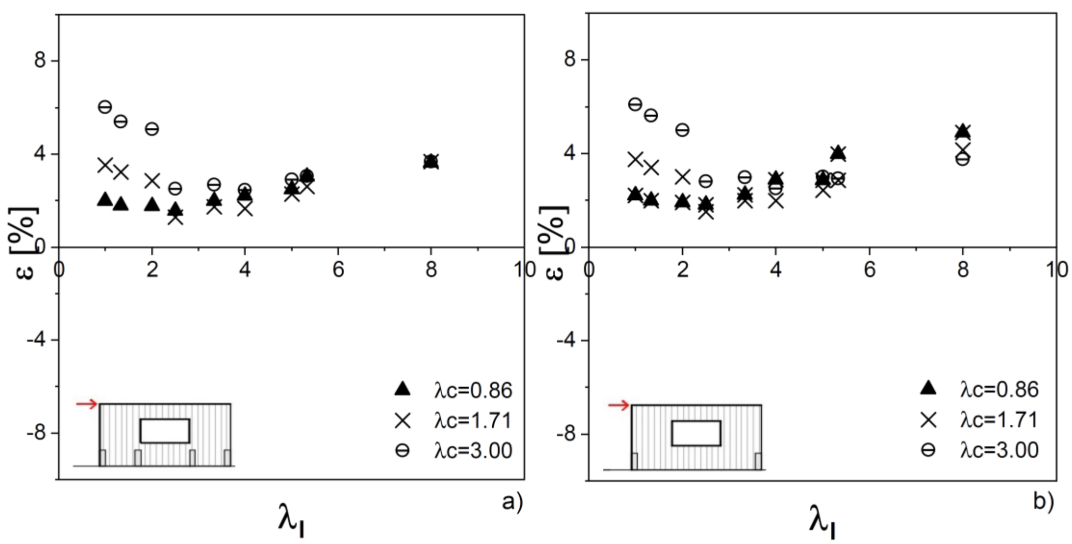

Figure B-22. Discrepancy for the global stiffness, kv,t,hd = 13.247 kN/mm, in load method #1: a) Window opening - DH, b) Window opening – SH

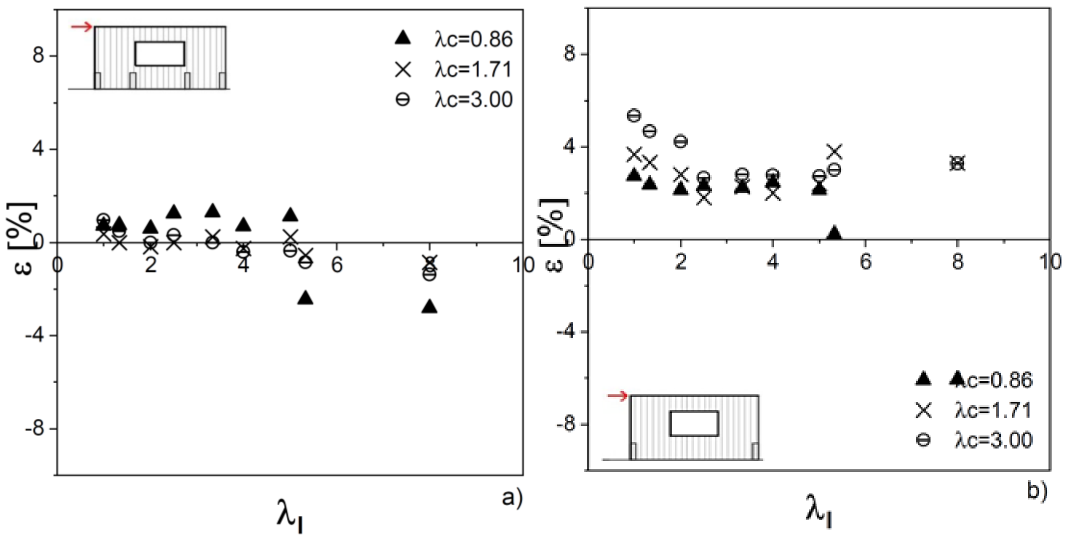

Figure B-23. Discrepancy for hold-down tensile load, kv,t,hd = 13.247 kN/mm, in load method #1: a) Window opening - DH, b) Window opening – SH

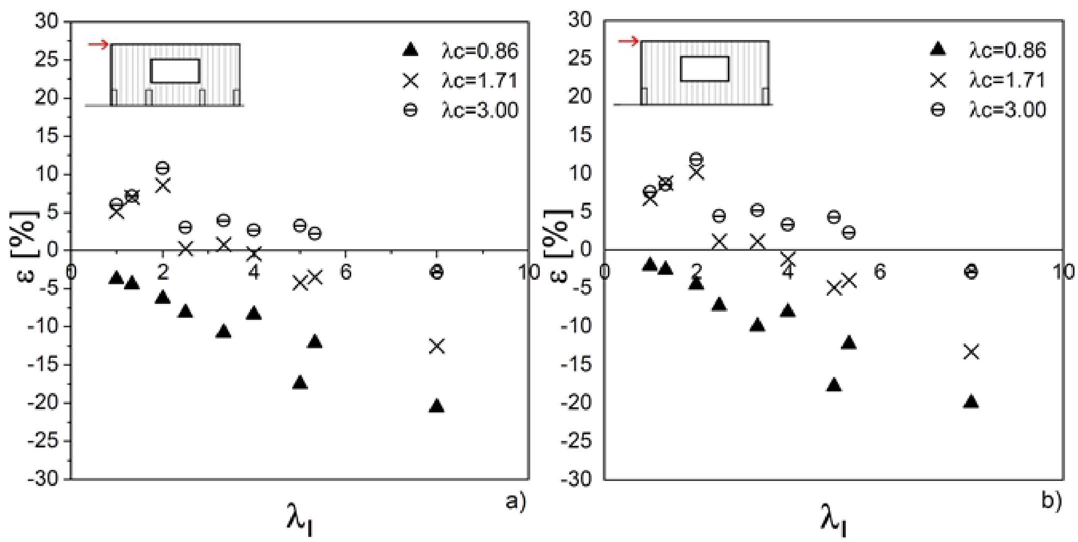

Figure B-24. Discrepancy for lintel shear load , kv,t, hd = 13.247 kN/mm, in load method #1: a) Window opening - DH, b) Window opening – SH

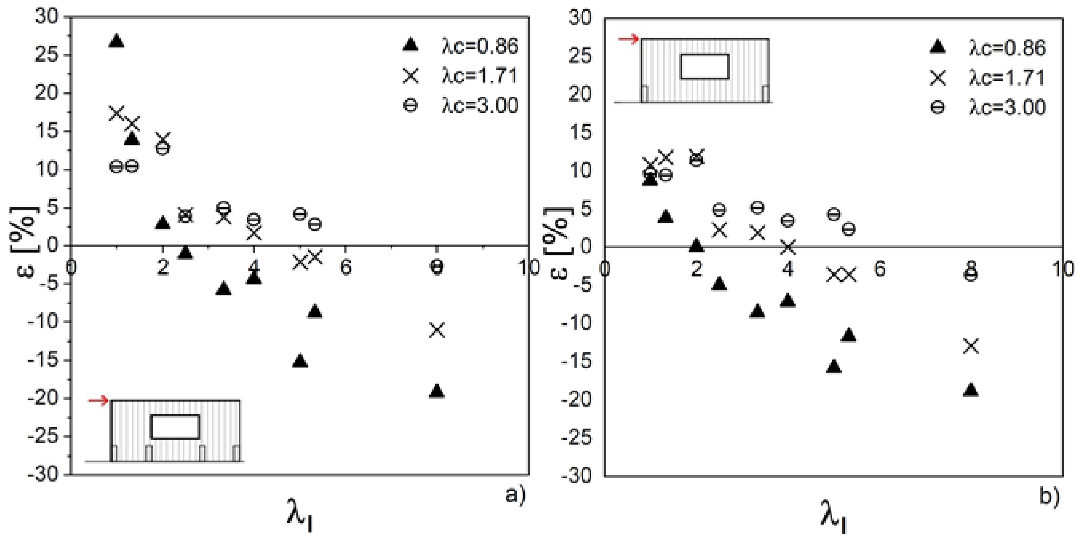

Figure B-25. Discrepancy for lintel bending moment , kv,t,hd = 13.247 kN/mm, in load method #1: a) Window opening - DH, b) Window opening – SH

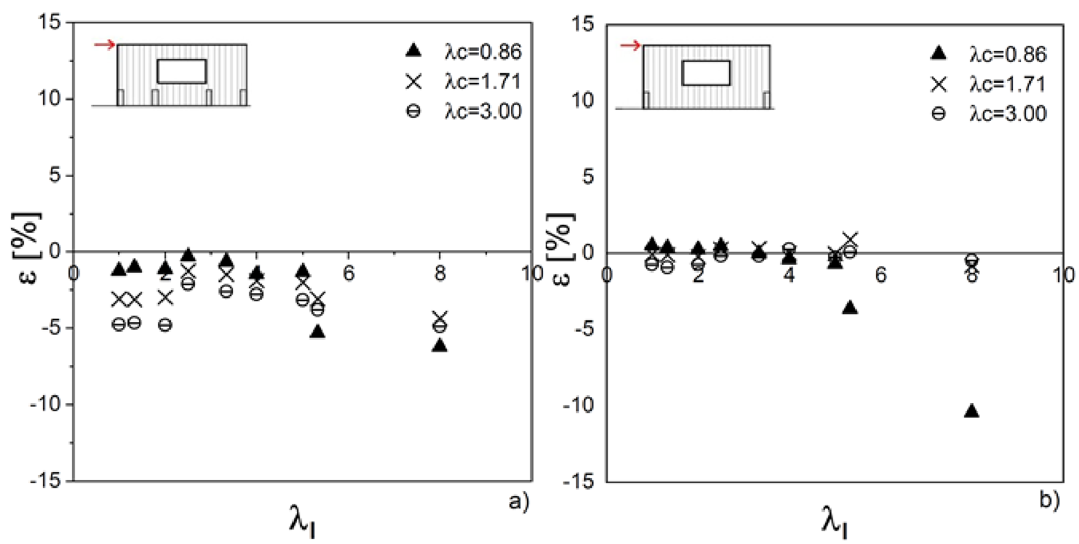

Figure B-26. Discrepancy for hold-down tensile load, kv,t,hd = 13.247 kN/mm, in load method #2: a) Window opening - DH, b) Window opening – SH

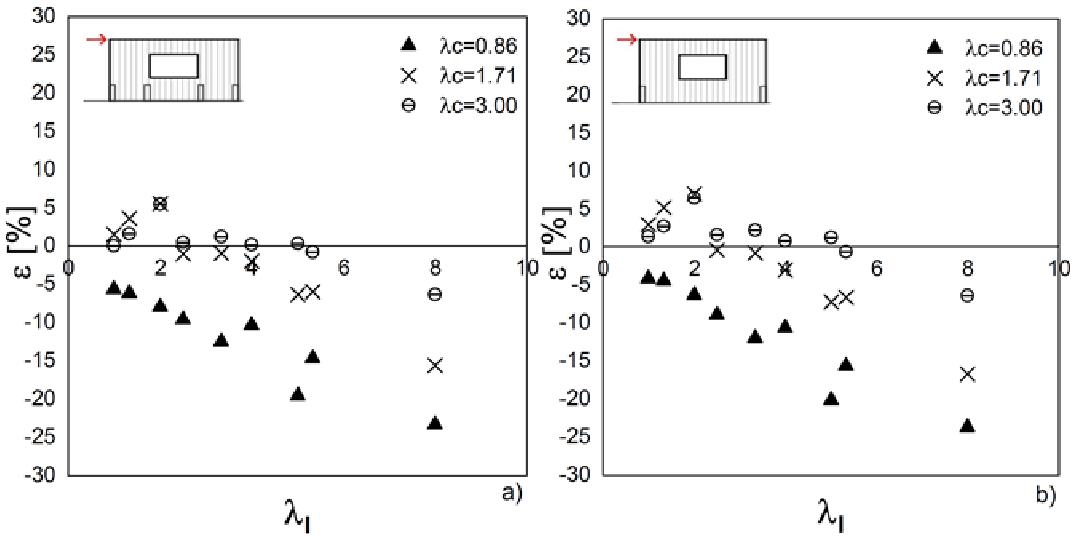

Figure B-27. Discrepancy for lintel shear load , kv,t, hd = 13.247 kN/mm, in load method #2: a) Window opening - DH, b) Window opening – SH

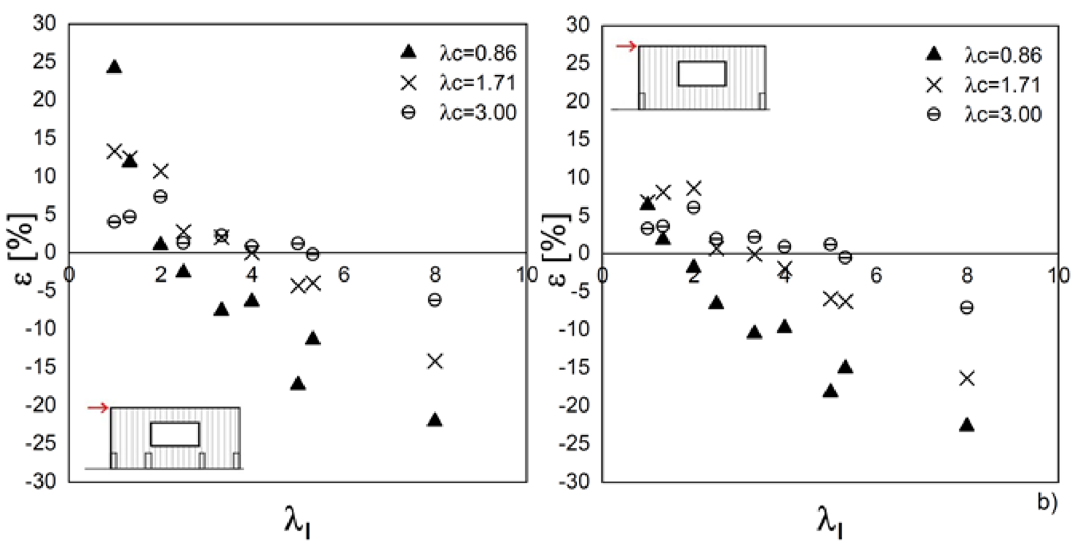

Figure B-28. Discrepancy for lintel bending moment , kv,t,hd = 13.247 kN/mm, in load method #2: a) Window opening - DH, b) Window opening – SH

APPENDIX C
Experimental testing

Test results of specimen 01

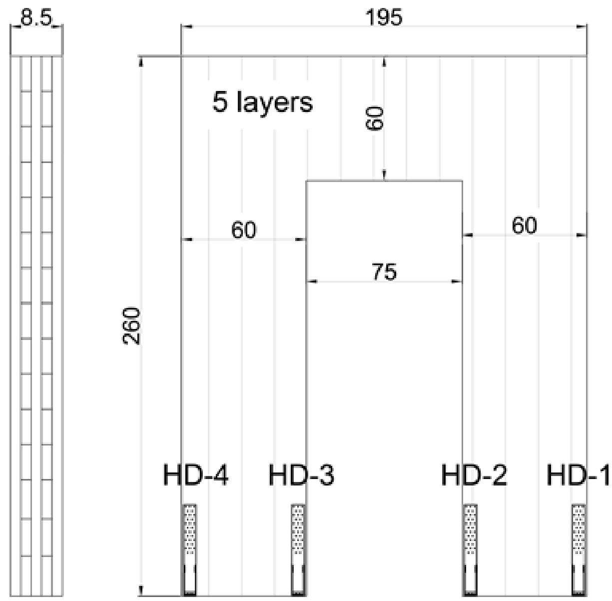

Figure C-1. Geometrical layout of shearwall 1

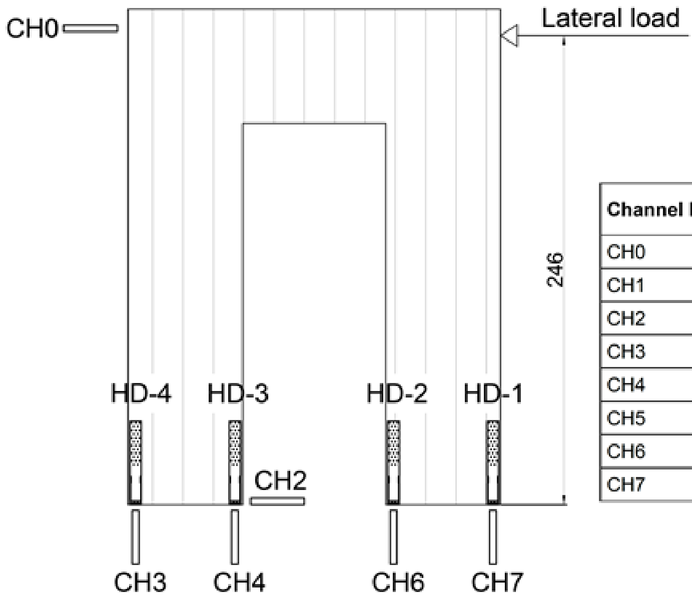

Channel ID	Measured displacement
CH0	Horizontal top wall displacement
CH1	Actuator horizontal displacement
CH2	Bottom slippage
CH3	Vertical displacement of outermost hold-down
CH4	Vertical displacement of innermost hold-down
CH5	Load cell
CH6	Vertical displacement of inner hold-down
CH7	Vertical displacement of outer hold-down

a)

b)

Figure C-2. Measuring device disposition of shearwall 1. Sketch (a) and photo (b)

Table C-1. Geometrical dimensions and mechanical parameters of tested wall 1

Property	**Numerical value**
Strength class of CLT	*C24*
Density	*420* kg/m^3
Total thickness of the shearwall	*85mm*
Number of layers (n)	*5*
Layup configuration	*17+17+17+17+17mm*
Total height of the shearwall (H)	*2.6m*
Total length of the shearwall (L)	*1.95m*
Height of the wall segment (h_O)	*2.0m*
Vertical wall segment's width (b)	*0.6m*
Lintel height (h_L)	*0.6m*
Lintel length (l)	*0.75m*
Lintel slenderness (λ_l)	*1.25*
Wall segment slenderness (λ_w)	*3.33*
hold-down tensile stiffness $(k_{v,t,hd})$	*WHT440 - 6622 kN/m*
Hold-down configuration $[-]$	*Double (DH)*
Nails properties (diameter and length)	$4 \times 60mm$
Number of nails	*30*
Assumed modulus of elasticity E_0	*12000 MPa*
Assumed modulus of elasticity E_{90}	*500 MPa*
Shear modulus	*500 MPa*
Loading protocol	*EN 594 (2011)*
Test duration	*5.82mn*

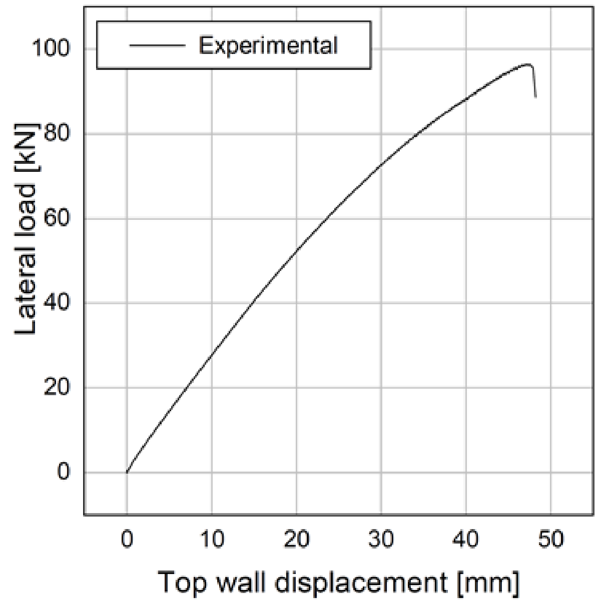

Figure C-3. Entire Force-Displacement curve of the shearwall

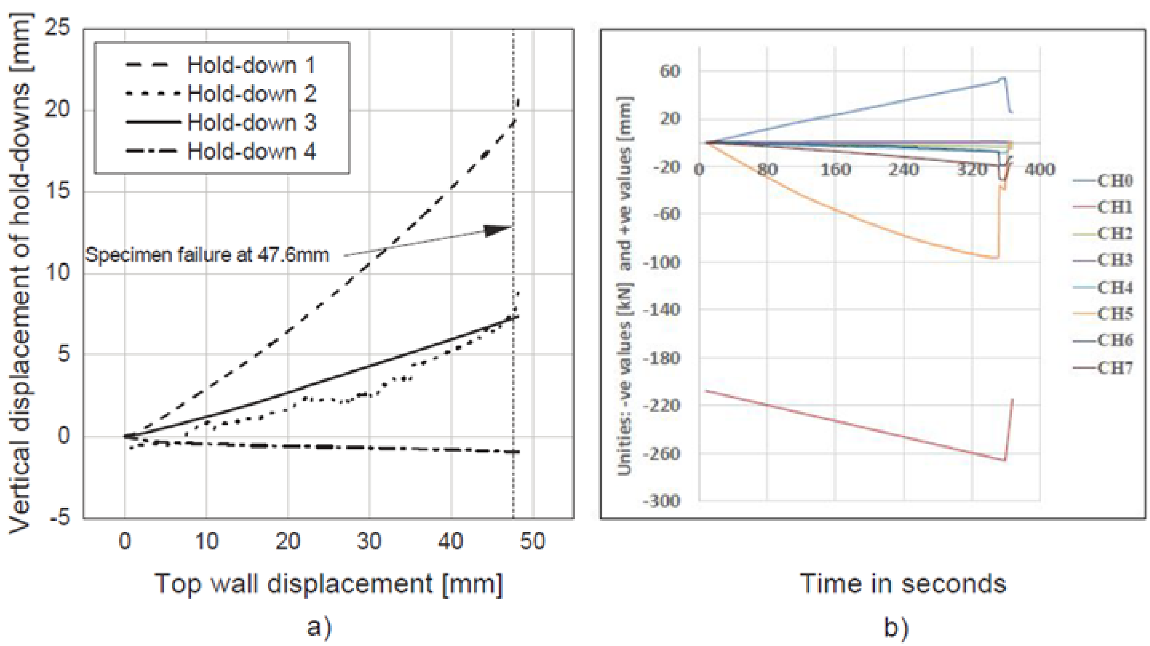

Figure C-4. Data of wall 01: a) displacements of the hold-downs and b) channels' recording

Test results of specimen 02

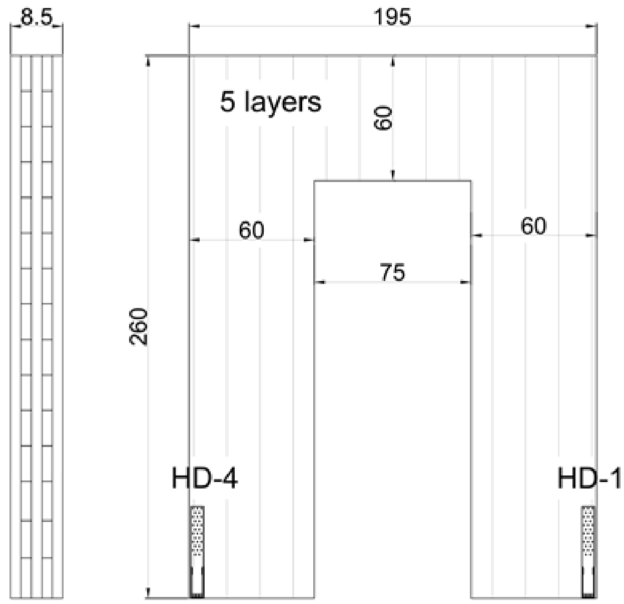

Figure C-5. Geometrical layout of shearwall 2

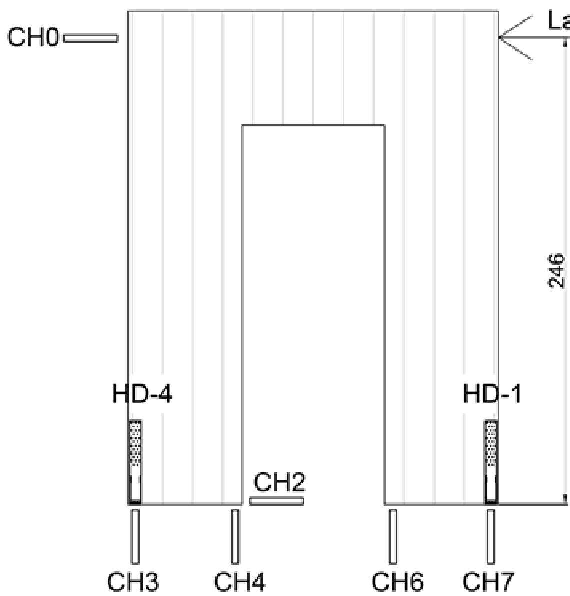

Channel ID	Measured displacement
CH0	Horizontal top wall displacement
CH1	Actuator horizontal displacement
CH2	Bottom slippage
CH3	Vertical displacement of outermost hold-down
CH4	Vertical displacement
CH5	Load cell
CH6	Vertical displacement
CH7	Vertical displacement of outer hold-down

a)

b)

Figure C-6. Measuring device disposition of shearwall 2. Sketch (a) and photo (b)

Table C-2. Geometrical dimensions and mechanical parameters of tested wall 2

Property	Numerical value
Strength class of CLT	*C24*
Density	*420* kg/m^3
Total thickness of the shearwall	*85mm*
Number of layers (n)	*5*
Layup configuration	*17+17+17+17+17mm*
Total height of the shearwall (H)	*2.6m*
Total length of the shearwall (L)	*1.95m*
Height of the wall segment (h_O)	*2.0m*
Vertical wall segment's width (b)	*0.6m*
Lintel height (h_L)	*0.6m*
Lintel length (l)	*0.75m*
Lintel slenderness (λ_l)	*1.25*
Wall segment slenderness (λ_w)	*3.33*
hold-down tensile stiffness $(k_{v,t,hd})$	*WHT440 - 6622 kN/m*
Hold-down configuration	*Single (SH)*
Nails properties (diameter and length)	$4 \times 60mm$
Number of nails	*30*
Assumed modulus of elasticity E_0	*12000 MPa*
Assumed modulus of elasticity E_{90}	*500 MPa*
Shear modulus	*500 MPa*
Loading protocol	*EN 594 (2011)*
Test duration	*6.41mn*

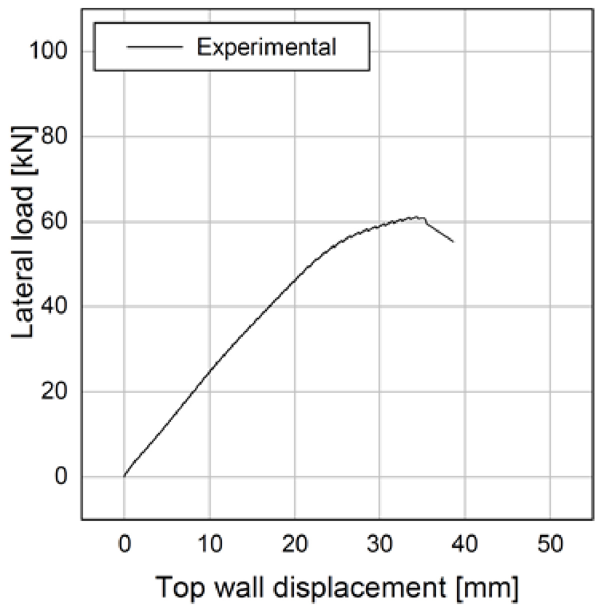

Figure C-7. Entire Force-Displacement curve of the shearwall

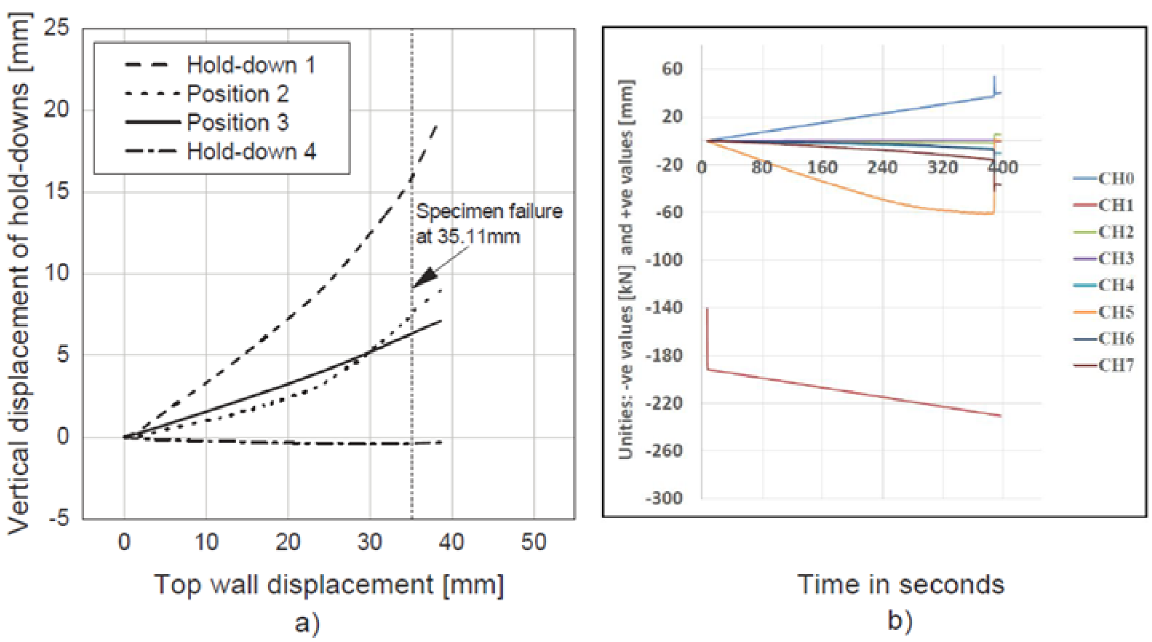

Figure C-8. Data of wall 02: a) displacements of the hold-downs and b) channels' recording

Test results of specimen 03

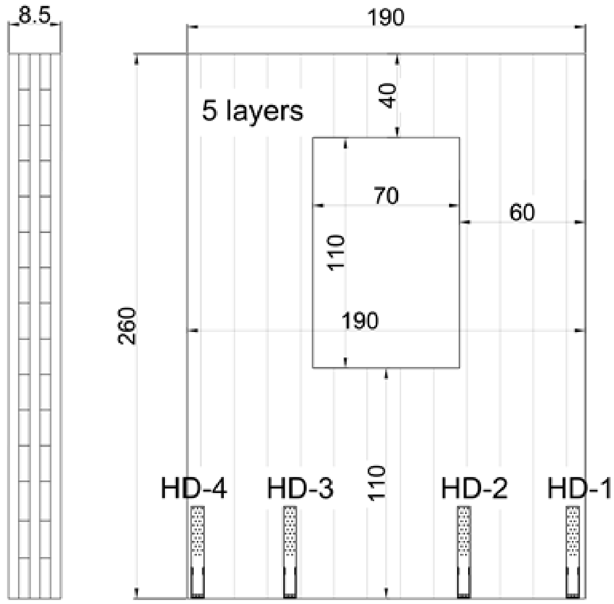

Figure C-9. Geometrical layout of shearwall 3

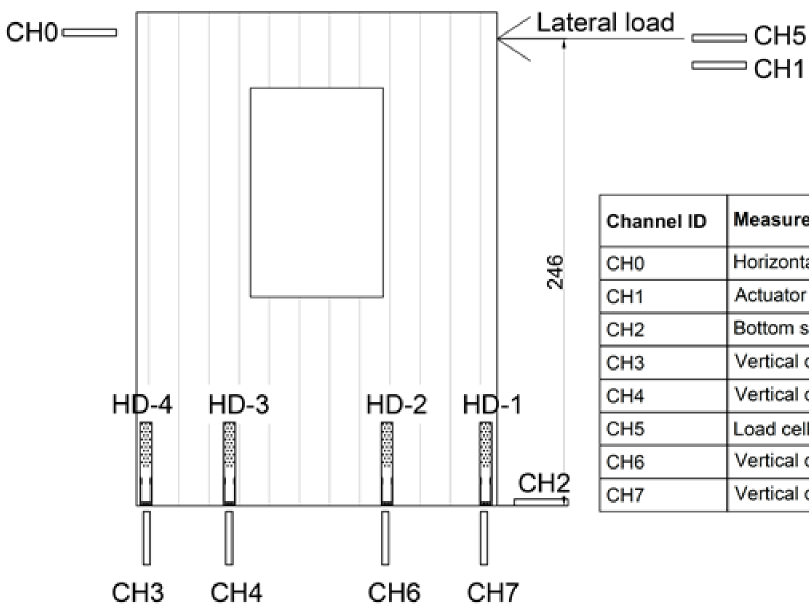

Channel ID	Measured displacement
CH0	Horizontal top wall displacement
CH1	Actuator horizontal displacement
CH2	Bottom slippage
CH3	Vertical displacement of outermost hold-down
CH4	Vertical displacement of innermost hold-down
CH5	Load cell
CH6	Vertical displacement of inner hold-down
CH7	Vertical displacement of outer hold-down

a)

b)

Figure C-10. Measuring device disposition of shearwall 3. Sketch (a) and photo (b)

Table C-3. Geometrical dimensions and mechanical parameters of tested wall 3

Property	**Numerical value**
Strength class of CLT	*C24*
Density	*420* kg/m^3
Total thickness of the shearwall	*85mm*
Number of layers (n)	*5*
Layup configuration	*17+17+17+17+17mm*
Total height of the shearwall (H)	*2.6m*
Total length of the shearwall (L)	*1.90m*
Height of the wall segment (h_O)	*1.10m*
Vertical wall segment's width (b)	*0.60m*
Bottom lintel height (h_c)	*1.10m*
Lintel height (h_L)	*0.40m*
Lintel length (l)	*0.70m*
Lintel slenderness (λ_l)	*1.75*
Wall segment slenderness (λ_w)	*1.83*
hold-down tensile stiffness $(k_{v,t,hd})$	*WHT440 - 6622 kN/m*
Hold-down configuration $[-]$	*Double (DH)*
Nails properties (diameter and length)	$4 \times 60mm$
Number of nails	*30*
Assumed modulus of elasticity E_0	*12000 MPa*
Assumed modulus of elasticity E_{90}	*500 MPa*
Shear modulus	*500 MPa*
Loading protocol	*EN 594 (2011)*
Test duration	*7.05mn*

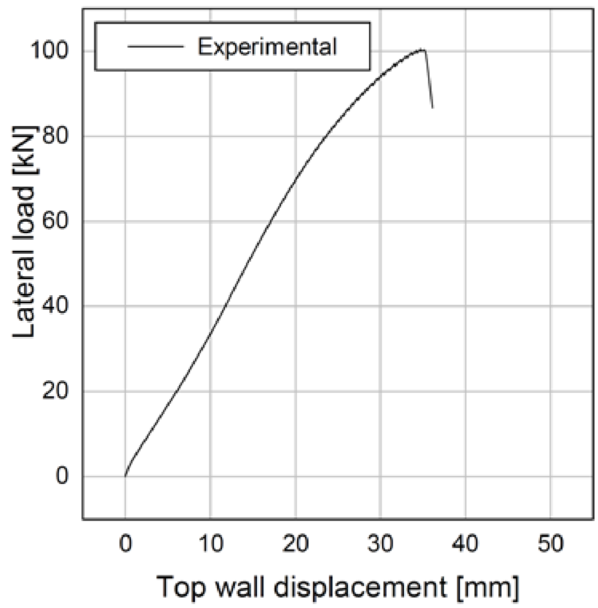

Figure C-11. Entire Force-Displacement curve of the shearwall

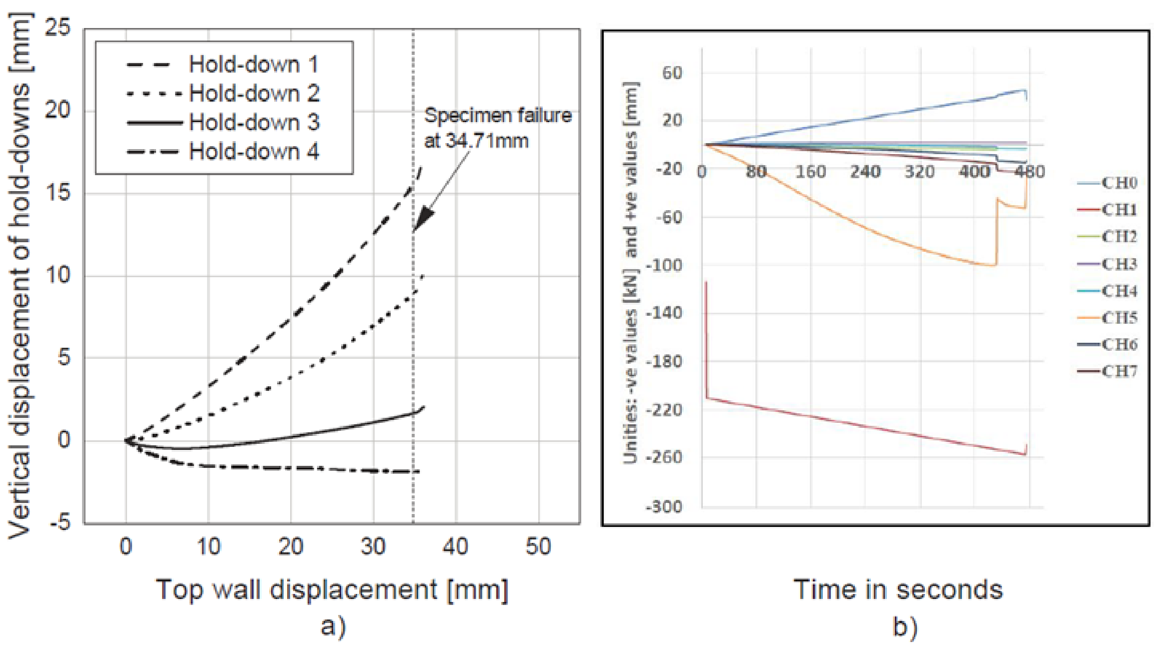

Figure C-12. Data of wall 03: a) displacements of the hold-downs and b) channels' recording

Test results of specimen 04

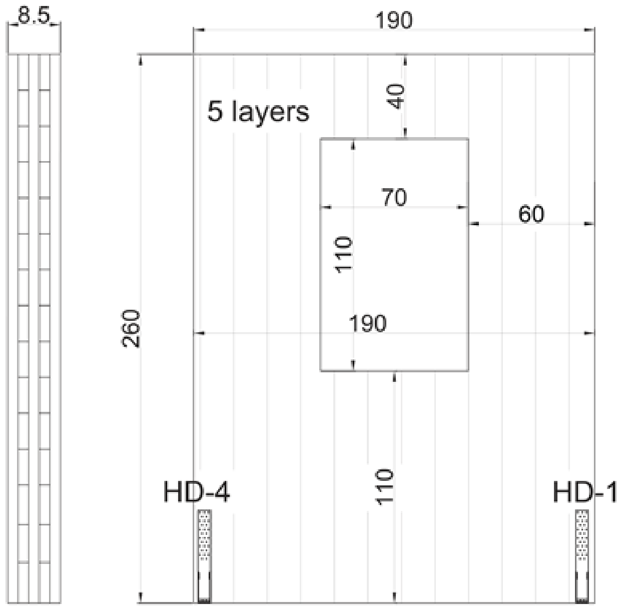

Figure C-13. Geometrical layout of shearwall 4

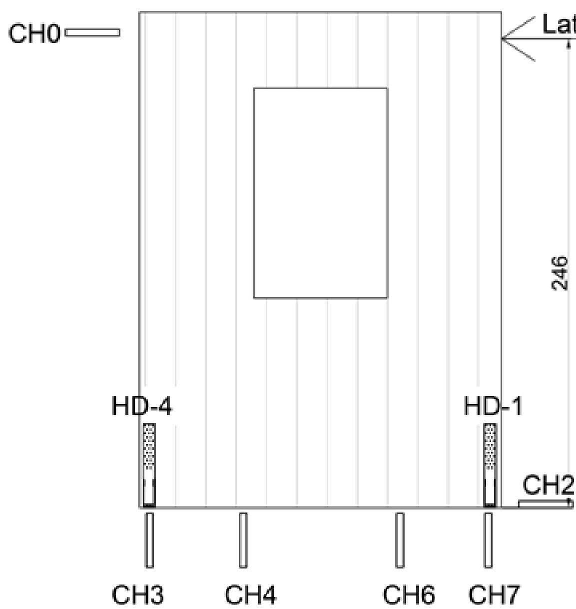

Channel ID	Measured displacement
CH0	Horizontal top wall displacement
CH1	Actuator horizontal displacement
CH2	Bottom slippage
CH3	Vertical displacement of outermost hold-down
CH4	Vertical displacement
CH5	Load cell
CH6	Vertical displacement
CH7	Vertical displacement of outer hold-down

a)

b)

Figure C-14. Measuring device disposition of shearwall 4. Sketch (a) and photo (b)

Table C-4. Geometrical dimensions and mechanical parameters of tested wall 4

Property	Numerical value
Strength class of CLT	*C24*
Density	*420* kg/m^3
Total thickness of the shearwall	*85mm*
Number of layers (n)	*5*
Layup configuration	*17+17+17+17+17mm*
Total height of the shearwall (H)	*2.6m*
Total length of the shearwall (L)	*1.90m*
Height of the wall segment (h_O)	*1.10m*
Vertical wall segment's width (b)	*0.60m*
Bottom lintel height (h_c)	*1.10m*
Lintel height (h_L)	*0.40m*
Lintel length (l)	*0.70m*
Lintel slenderness (λ_l)	*1.75*
Wall segment slenderness (λ_w)	*1.83*
hold-down tensile stiffness $(k_{v,t,hd})$	*WHT440 - 6622 kN/m*
Hold-down configuration $[-]$	*Single (SH)*
Nails properties (diameter and length)	$4 \times 60mm$
Number of nails	*30*
Assumed modulus of elasticity E_0	*12000 MPa*
Assumed modulus of elasticity E_{90}	*500 MPa*
Shear modulus	*500 MPa*
Loading protocol	*EN 594 (2011)*
Test duration	*6.33mn*

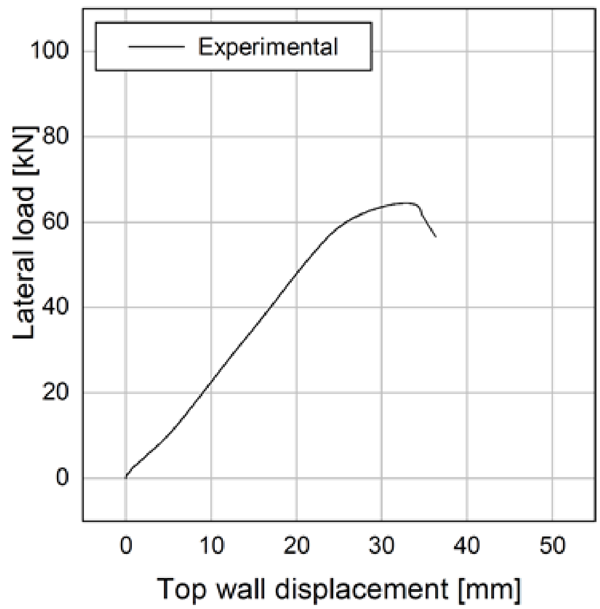

Figure C-15. Entire Force-Displacement curve of the shearwall

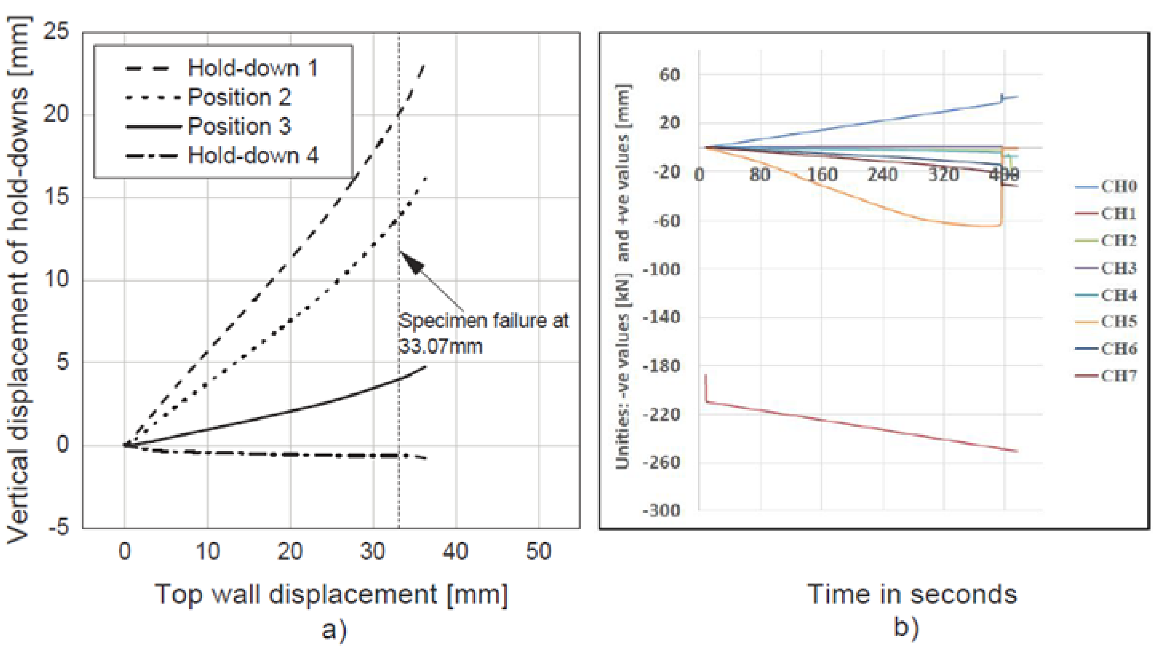

Figure C-16. Data of wall 03: a) displacements of the hold-downs and b) channels' recording

Test results of specimen 05

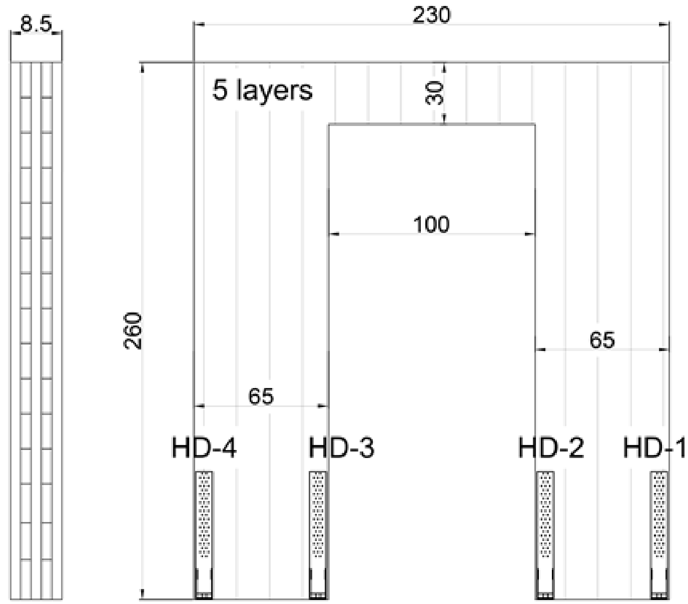

Figure C-17. Geometrical layout of shearwall 5

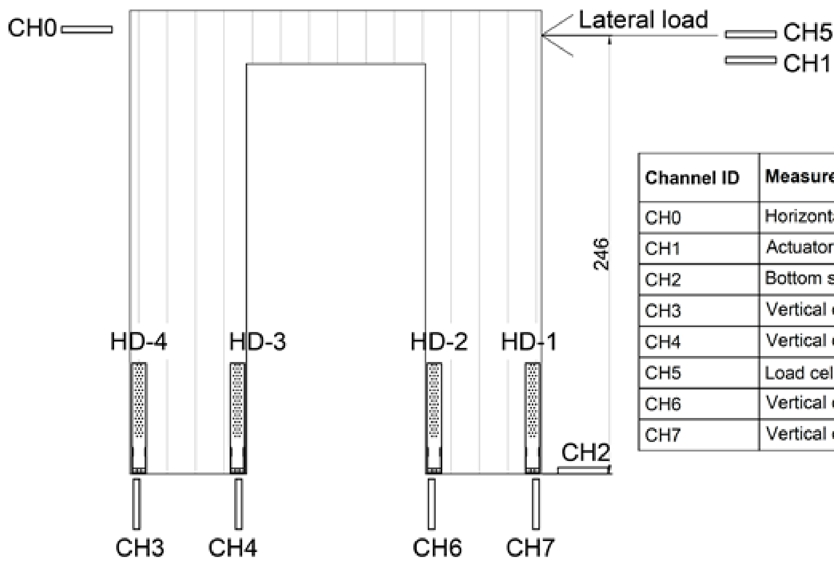

Channel ID	Measured displacement
CH0	Horizontal top wall displacement
CH1	Actuator horizontal displacement
CH2	Bottom slippage
CH3	Vertical displacement of outermost hold-down
CH4	Vertical displacement of innermost hold-down
CH5	Load cell
CH6	Vertical displacement of inner hold-down
CH7	Vertical displacement of outer hold-down

a)

b)

Figure C-18. Measuring device disposition of shearwall 1. Sketch (a) and photo (b)

Table C-5, Geometrical dimensions and mechanical parameters of tested wall 5

Property	**Numerical value**
Strength class of CLT	*C24*
Density	*420* kg/m^3
Total thickness of the shearwall	*85m*
Number of layers (n)	*5*
Layup configuratiom	*17+17+17+17+17mm*
Total height of the shearwall (H)	*2.60m*
Total length of the shearwall (L)	*2.30m*
Height of the wall segment (h_O)	*2.30m*
Vertical wall segment's width (b)	*0.65m*
Lintel height (h_L)	*0.30m*
Lintel length (l)	*1.00m*
Lintel slenderness (λ_l)	*3.33*
Wall segment slenderness (λ_w)	*3.53*
hold-down tensile stiffness $(k_{v,t,hd})$	*WHT440-13247 kN/m*
Hold-down configuration $[-]$	*Double (DH)*
Nails properties (diameter and length)	$4 \times 60mm$
Number of nails	*55*
Assumed modulus of elasticity E_0	*12000 MPa*
Assumed modulus of elasticity E_{90}	*500 MPa*
Shear modulus	*500 MPa*
Loading protocol	*EN 594 (2011)*
Test duration	*10.23mn*

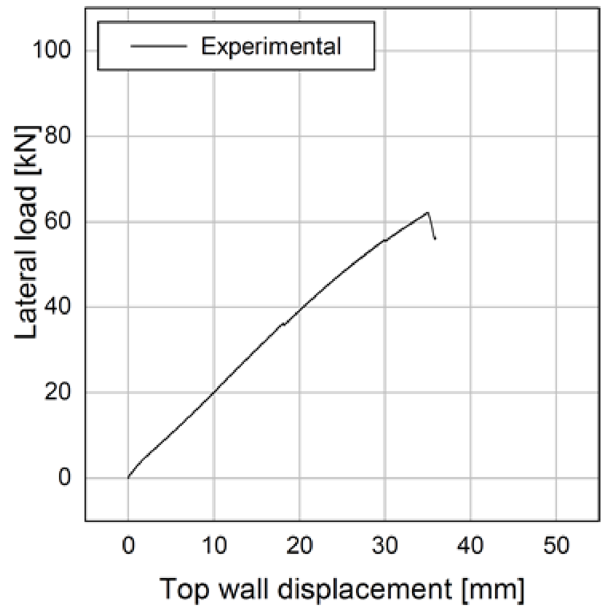

Figure C-19. Entire Force-Displacement curve of the shearwall

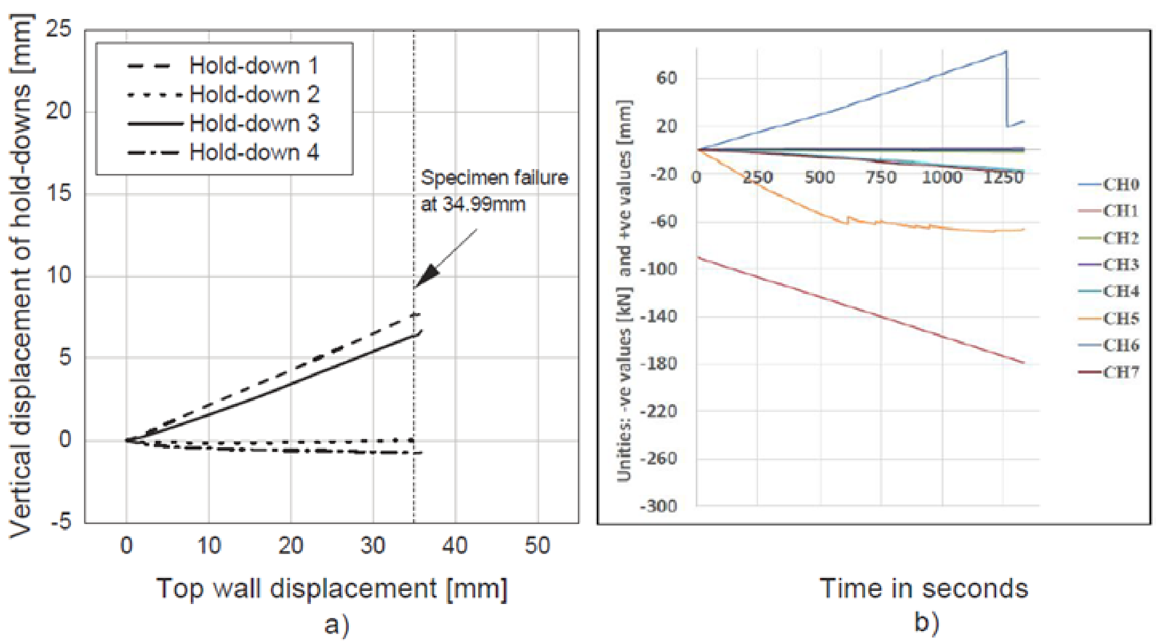

Figure C-20. Data of wall 03: a) displacements of the hold-downs and b) channels' recording